

Spring 5-8-2021

## Design, Synthesis and Evaluation of Novel Inhibitors of Type 5 and 10 17 $\beta$ -Hydroxysteroid Dehydrogenases

Ahmed Morsy  
*University of Nebraska Medical Center*

Tell us how you used this information in this [short survey](#).

Follow this and additional works at: <https://digitalcommons.unmc.edu/etd>

 Part of the [Medicinal and Pharmaceutical Chemistry Commons](#), and the [Molecular Biology Commons](#)

---

### Recommended Citation

Morsy, Ahmed, "Design, Synthesis and Evaluation of Novel Inhibitors of Type 5 and 10 17 $\beta$ -Hydroxysteroid Dehydrogenases" (2021). *Theses & Dissertations*. 513.  
<https://digitalcommons.unmc.edu/etd/513>

This Dissertation is brought to you for free and open access by the Graduate Studies at DigitalCommons@UNMC. It has been accepted for inclusion in Theses & Dissertations by an authorized administrator of DigitalCommons@UNMC. For more information, please contact [digitalcommons@unmc.edu](mailto:digitalcommons@unmc.edu).

**DESIGN, SYNTHESIS AND EVALUATION OF NOVEL INHIBITORS  
OF TYPE 5 AND 10 17 $\beta$ -HYDROXYSTEROID DEHYDROGENASES**

By

**Ahmed Morsy**

A Dissertation

Presented to the Faculty of  
the University of Nebraska Graduate College  
in Partial Fulfillment of the Requirements  
for the Degree of Doctor of Philosophy

Pharmaceutical Sciences Graduate Program

Under the Supervision of Professor Paul C. Trippier

University of Nebraska Medical Center  
Omaha, Nebraska

December 2020

Supervisory Committee:

Howard Fox, M.D., Ph.D.  
Corey Hopkins, Ph.D.  
Joseph Vetro, Ph.D.

## ACKNOWLEDGMENTS

I am thankful to all of the people who contributed to the completion of this dissertation and because of whom the past five years have been filled with motivation and passion for furthering my scientific research and overall knowledge.

I want to extend a thank you to my mentor, Professor Paul C. Trippier, for his continued advice, encouragement, and support throughout my Ph.D. For the motivational words when things were going badly, pushing me onwards when things were going well, supporting my ideas, and the continuous stream of ideas and suggestions. For his advice in my life circumstances that do not relate to the Ph.D. and the helpful reminders that there is life outside of the Ph.D. Without his assistance, this project would not be at the stage it is now, and without his guidance, I will not be at the stage I am in right now in my life.

Besides my mentor, I would like to extend my gratitude towards all of my advisory committee members: Dr. Howard Fox, Dr. Corey Hopkins, and Dr. Joseph A. Vetro for their assistance, encouragement, and suggestions that have improved my dissertation project's quality. I would also like to thank all previous supervisory committees at Texas Tech University Health Sciences Center for assistance and encouragement in the first three years of my Ph.D.

To all the Trippier research group members, both past and present, who made the lab a fun and productive place to be. In particular, a thank you goes to Dr. Nihar Kinarivala and Dr. Bader Huwaimel for helping me to find my feet in the lab, for putting up with an endless stream of questions, and for the never-ending science-related discussions.

To our collaborators, the Penning lab at the University of Pennsylvania and the Frank Gunn-Moore lab at the University of St. Andrews.

To my wife, family, and friends for the continued support and for putting up with the constant ups and downs associated with life in the lab.

Finally, to Texas Alzheimer's Research and Care Consortium-Investigator Grant Program, NIH National Cancer Institute, the Dean for Graduate Studies Stipend, the Bukey Memorial Fund, and Nancy and Ronald Reagan Alzheimer's Scholarship Fund, which all contributed to funding this project.

**ABSTRACT****DESIGN, SYNTHESIS AND EVALUATION OF NOVEL INHIBITORS OF TYPE 5 AND 10 17 $\beta$ -HYDROXYSTEROID DEHYDROGENASES**

Ahmed Morsy, Ph.D.

University of Nebraska, 2020

Supervisor: Paul C. Trippier, Ph.D.

17 $\beta$ -Hydroxysteroid dehydrogenases (17 $\beta$ -HSDs) are essential enzymes in steroid metabolism. More and more evidence points to the pivotal contributions of these enzymes in various other metabolic pathways. Therefore, the latest research results give new insights into the complex metabolic interconnectivity of the 17 $\beta$ -HSDs with human diseases. This dissertation focuses on the metabolic activities of type 5 and 10 17 $\beta$ -HSDs. More specifically, regarding 17 $\beta$ -HSD5 contributions to the progression of prostate cancer (PCa) and 17 $\beta$ -HSD10 aggravation of amyloid-beta (A $\beta$ )-induced toxicity in Alzheimer's disease (AD).

The second leading cause of cancer-related death in males is PCa, with the highest incidence rate of all cancers reported in the U.S. The treatment paradigm is dependent on androgen deprivation therapy (ADT) via surgical or medical castration, targeting the production of androgens, primarily testosterone, in the Leydig cells of the testis. This therapy usually leads to an initial clinical improvement with concomitant suppression of prostate-specific antigen (PSA) levels. However, within 2-3 years, castration-resistant prostate cancer (CRPC) develops in most patients, despite low circulating androgens levels and has more significant metastatic potential. Such adaptations lead to increased intratumoral androgen biosynthesis, along with an increase in tumor responsiveness to circulating castrate levels of androgens. The enzyme 17 $\beta$ -

HSD5 is responsible for androgen biosynthesis, and a significant upregulation of its expression is observed in CRPC patient tumor samples. It plays a vital role in the downstream synthesis of dihydrotestosterone (DHT), the predominant intracellular transcriptional signal to androgen-responsive genes in intact human prostate cells. Hence, the delivery of 17 $\beta$ -HSD5 inhibitor represents a promising therapeutic target to manage CRPC and combat the emergence of resistance to clinically employed therapy. In our lab, we developed a highly potent and selective 17 $\beta$ -HSD5 inhibitor, KV-49g (IC<sub>50</sub> = 70 nM, >2800-fold selectivity over its homologous isoforms). The work described herein continues to elucidate the structure-activity relationship (SAR) around this chemotype in inhibiting 17 $\beta$ -HSD5 activity. Further, we show PCa cells' resistance to newly approved AR antagonists, apalutamide and darolutamide. This resistance was abtained with 24 hours pre-treatment of KV-49g and led to PCa cells death *in vitro*, showing potentiation to AR antagonists' chemotherapeutic effect. Further, we showed that the combination therapy's synergic effect translated to a significant decrease in PSA expression. These results demonstrate a promising therapeutic strategy for treating drug-resistant CRPC that invariably develops in PCa patients following initial treatment with AR antagonists.

The most common form of dementia is AD, affecting an estimated 46.8 million people worldwide in 2015, a number predicted to increase to 74.7 million by 2030 and 131.5 million by 2050. Current therapeutic agents against AD are palliative in nature, managing symptoms without addressing the underlying cause, and thus, disease progression and patient death remain a certainty. Whereas the leading underlying cause for the development of AD was initially thought to be an abnormal deposition of the soluble oligomeric form of A $\beta$ -derived plaques within the brain, the failure of several high-profile therapeutic agents, which were shown to reduce the plaque burden without improving cognition, has recently prompted a shift in focus to disease-modifying therapy. A therapy

that aims to restore a normal target's function that has been compromised by A $\beta$  accumulation, alleviating A $\beta$ -induced toxicity. Soluble A $\beta$  oligomers have been identified in various subcellular compartments, including the mitochondria, where they form a complex with the 17 $\beta$ -HSD10 enzyme resulting in cytotoxicity. The latter suggests two therapeutic approaches that may hold merit in treating AD: disrupting the interaction between the 17 $\beta$ -HSD10 enzyme and A $\beta$ , or directly inhibiting the catalytic activity of the 17 $\beta$ -HSD10 enzyme. AG18051 was identified as a small molecule 17 $\beta$ -HSD10 inhibitor. The work described herein details the synthesis of AG18051 and its analogues to elucidate the SAR around this chemotype. Further, the generation of robust screening assays allowing the catalytic activity of the 17 $\beta$ -HSD10 enzyme to be measured *in vitro* and the neuroprotective effects of 17 $\beta$ -HSD10 inhibitors in ameliorating A $\beta$ -induced toxicity to be assessed. As a result, we have identified more potent compounds than AG18051, with more 'drug-like' structures, that showed significant protection from A $\beta$  toxicity. As such, we now have a number of hit compounds that will form the basis for the generation of subsequent series of derivatives with improved potency, as well as the robust assays required to measure such criteria, potentially leading to the generation of novel therapeutic agents against AD.

## TABLE OF CONTENTS

ACKNOWLEDGMENTS.....	ii
ABSTRACT.....	iv
TABLE OF CONTENTS.....	vii
LIST OF FIGURES.....	x
LIST OF TABLES .....	xii
LIST OF ABBREVIATIONS .....	xiii
CHAPTER 1: INTRODUCTION.....	1
1.1.    PROSTATE CANCER .....	5
1.1.1. INTRODUCTION.....	5
1.1.2. TREATMENT OPTIONS FOR PROSTATE CANCER .....	7
I.    Hormone Therapy.....	8
II.   Targeted Therapy .....	13
III.  Antineoplastic agents .....	15
IV.  Immunotherapy .....	16
1.2.    17 $\beta$ -HYDROXYSTEROID DEHYDROGENASE TYPE 5 (17 $\beta$ -HSD5).....	19
1.2.1. INTRODUCTION TO 17 $\beta$ -HSD5 .....	19
1.2.2. THE CONTRIBUTION OF AKR1C3 TO THE PATHOGENESIS OF CASTRATION-RESISTANT PROSTATE CANCER.....	20
1.2.3. OVEREXPRESSION OF AKR1C3 IS LINKED TO CANCER THERAPIES RESISTANCE.....	22
1.2.4. SUMMARY OF AVAILABLE AKR1C3 INHIBITORS .....	23
1.2.5. MODELING OF AKR1C3 ENZYME AND ITS ISOFORMS .....	26



<b>1.3. ALZHEIMER'S DISEASE .....</b>	<b>28</b>
<b>1.3.1. INTRODUCTION.....</b>	<b>28</b>
<b>1.3.2. OVERVIEW OF THERAPEUTIC APPROACHES TOWARDS ALZHEIMER'S DISEASE .....</b>	<b>29</b>
<b>1.4. AMYLOID-BINDING ALCOHOL DEHYDROGENASE ENZYME (ABAD) .....</b>	<b>34</b>
<b>1.4.1. INTRODUCTION TO ABAD.....</b>	<b>34</b>
<b>1.4.2. THE CONTRIBUTION OF ABAD TO THE PATHOGENESIS OF ALZHEIMER'S DISEASE .....</b>	<b>34</b>
<b>1.4.3. SUMMARY OF AVAILABLE ABAD INHIBITORS .....</b>	<b>38</b>
<b>1.4.4. MODELING OF ABAD ENZYME .....</b>	<b>39</b>
<b>1.5. PURPOSE OF THIS DISSERTATION .....</b>	<b>41</b>
<b>1.5.1. AKR1C3 INHIBITOR DESIGN, SYNTHESIS AND EVALUATION.....</b>	<b>41</b>
<b>1.5.2. ABAD INHIBITOR DESIGN, SYNTHESIS AND EVALUATION.....</b>	<b>41</b>
<b>CHAPTER 2: DESIGN, SYNTHESIS AND EVALUATION OF AKR1C3 INHIBITORS .</b>	<b>42</b>
<b>2.1. INTRODUCTION .....</b>	<b>43</b>
<b>2.2. MATERIALS AND METHODS .....</b>	<b>48</b>
<b>2.3. RESULTS AND DISCUSSION .....</b>	<b>58</b>
<b>2.4. CONCLUSION AND FUTURE DIRECTIONS.....</b>	<b>81</b>
<b>CHAPTER 3: DESIGN, SYNTHESIS AND EVALUATION OF ABAD INHIBITOR.....</b>	<b>82</b>
<b>3.1. INTRODUCTION .....</b>	<b>83</b>
<b>3.2. MATERIALS AND METHODS .....</b>	<b>88</b>
<b>3.3. RESULTS AND DISCUSSION .....</b>	<b>94</b>

3.4. CONCLUSION AND FUTURE DIRECTIONS .....	117
CHAPTER 4: CHARACTERIZATION OF SYNTHESIZED MOLECULES .....	118
REFERENCES .....	164

## LIST OF FIGURES

<b>Figure 1.</b> The conversion between active and inactive steroidal hormones by 17 $\beta$ -HSDs. .....	<b>3</b>
<b>Figure 2.</b> The hypothalamic-pituitary-gonadal axis. ....	<b>6</b>
<b>Figure 3.</b> Structures of a selection of approved hormonal therapy for prostate cancer. .	<b>11</b>
<b>Figure 4.</b> Structures and activities of a selection of AKR1C3 inhibitors. ....	<b>24</b>
<b>Figure 5.</b> Baccharin and its potent and selective analogs.....	<b>25</b>
<b>Figure 6.</b> Comparison of SP1, SP2, and SP3 sub-pockets of four human AKR1C enzymes.....	<b>27</b>
<b>Figure 7.</b> Structures of clinically approved drugs for the treatment of Alzheimer's Disease. .....	<b>30</b>
<b>Figure 8.</b> Summary A $\beta$ -ABAD toxicity mechanisms related to ABAD. ....	<b>36</b>
<b>Figure 9.</b> Structures of a selection of ABAD inhibitors.....	<b>38</b>
<b>Figure 10.</b> Map of interactions between an inhibitor and the ABAD enzyme. ....	<b>40</b>
<b>Figure 11.</b> Metabolic actions of human S9 liver fractions on baccharin and KV-37.....	<b>45</b>
<b>Figure 12.</b> Half-life of lead compounds.....	<b>67</b>
<b>Figure 13.</b> Pharmacokinetic profile of KV-49g in CD-1 mice.....	<b>69</b>
<b>Figure 14.</b> Percentage of cell viability of KV-49g in PCa cell lines. ....	<b>72</b>
<b>Figure 15.</b> Combination effects of KV-49g and ARN or ODM.....	<b>74</b>
<b>Figure 16.</b> Combination of 24 hours pretreatment of KV-49g followed by 72 hours treatment with ARN or ODM in 22Rv1 cells (grown in CSS). ....	<b>76</b>
<b>Figure 17.</b> Combination of 24 hours pretreatment of KV-49g or INDO prior to 72 hours treatment with 12 $\mu$ M of ARN or ODM in 22Rv1 cells (grown in CSS). ....	<b>79</b>
<b>Figure 18.</b> A $\beta$ -ABAD interaction pathology cascade.....	<b>85</b>

<b>Figure 19.</b> Activity map summarizing the minimum pharmacophore for ABAD inhibition.	
.....	<b>105</b>
<b>Figure 20.</b> The effect of A $\beta$ and AG18051 on estradiol levels. ....	<b>109</b>
<b>Figure 21.</b> Neuroprotective effect of AG18051 and 3.8c in ameliorating A $\beta$ -induced toxicity in human SH-SY5Y 'neuron-like' cells. ....	<b>114</b>
<b>Figure 22.</b> AG18051 and 3.8c rescue A $\beta$ -induced mitochondrial dysfunction.....	<b>116</b>

## LIST OF TABLES

<b>Table 1.</b> 17 $\beta$ -HSDs and their relation to diseases .....	<b>4</b>
<b>Table 2.</b> Structure-activity relationship around the baccharin chemotype for AKR1C3 inhibition. ....	<b>60</b>
<b>Table 3.</b> Structure, inhibitory and selectivity properties of prenyl chain analogues. ....	<b>63</b>
<b>Table 4.</b> The IC <sub>50</sub> values of ARN and ODM in the three PCa cell lines. ....	<b>72</b>
<b>Table 5.</b> Optimization of protection reaction conditions to synthesize an N-protected 3.1. ....	<b>96</b>
<b>Table 6.</b> Assessing the activity of AG18051 derivatives by measuring the change in NADH absorbance in the presence of ABAD. ....	<b>102</b>
<b>Table 7.</b> Assessing the potency of AG18051 derivatives in ameliorating A $\beta$ -induced reduction in estradiol levels. ....	<b>110</b>

## LIST OF ABBREVIATIONS

17 $\beta$ -HSD	17 $\beta$ -hydroxysteroid dehydrogenase
ABAD	amyloid-binding alcohol dehydrogenase enzyme
AD	Alzheimer's disease
ADME	absorption, distribution, metabolism, and excretion
ADT	androgen deprivation therapy
AKR	aldo-keto reductase
AML	acute myeloid leukemia
APC	antigen presenting cell
APP	amyloid precursor protein
AR	androgen receptor
ARE	androgen receptor element
ARN	apalutamide
A $\beta$	amyloid-beta
BBB	blood-brain barrier
BOP	benzotriazolyl-oxytris (dimethylamino) phosphonium hexafluorophosphate
Cdk5	cyclin-dependent kinase 5
CI	complex I
CI	combination index
CIV	complex IV
c-Jun	N-terminal kinases
CRPC	castration-resistant prostate cancer
CSS	charcoal-stripped
DHT	dihydrotestosterone

DMAP	4-dimethylaminopyridine
DRI	dose reduction index
DSBs	DNA double-strand breaks
ENZ	enzalutamide
Ep-1	endophilin I
ERAB	endoplasmic reticulum associated amyloid $\beta$ -peptide-binding protein
FDA	food and drug administration
GM-CSF	granulocyte-macrophage colony-stimulating factor
GnRH	gonadotropin-releasing hormone
GSK-3 $\beta$	glycogen synthase kinase-3 $\beta$
HPLC	high-pressure liquid chromatography
HR	homologous recombination
HupA	Huperiza
Ile	isoleucine
INDO	indomethacin
LDH	lactate dehydrogenase
LH	luteinizing hormone
LHRH	luteinizing hormone-releasing hormone
mCRPC	metastatic CRPC
MHB	2-methyl-3-hydroxybutyrate
MPO	multiparameter optimization score
NAD	nicotinamide adenine dinucleotide
nmCRPC	non-metastatic CRPC
NMDA	<i>N</i> -methyl-D-aspartate
NMR	nuclear magnetic resonance

NSAID	non-steroidal anti-inflammatory drug
ODM	darolutamide
PAP	prostatic acid phosphatase
PARP	poly (ADP-ribose) polymerase
PCa	prostate cancer
PD-1	programmed death receptor-1
PK	pharmacokinetic
PSA	prostate specific antigen
ROS	reactive oxygen species
SAR	structure-activity relationship
SCHAD	short-chain 3-hydroxyacyl-CoA dehydrogenase
Prdx-2	peroxiredoxin-2
SDR	short-chain dehydrogenases/reductase
SPR	surface plasmon resonance
S-tetralol	(S)-(+)-1,2,3,4-tetrahydro-1-naphthol
T	testosterone
T-ALL	T-cell acute lymphoblastic leukemia cells
$\Delta^4$ -AD	$\Delta^4$ -androstene-3, 17-dione



## **CHAPTER 1: INTRODUCTION**

## INTRODUCTION

A biochemical reaction involving a nicotinamide adenine dinucleotide ( $\text{NAD}^+$ ) molecule, acting as a hydrogen donor or acceptor to reduce or oxidize an endogenous steroidal compound, plays a critical role in cell health. This reaction occurs in a Rossmann fold of a  $17\beta$ -hydroxysteroid dehydrogenase ( $17\beta$ -HSD) enzyme. It facilitates the interconversion between the active and inactive forms of specific steroidal hormones in their biosynthesis's final steps (Figure 1). Thus, the  $17\beta$ -HSD enzymes play a vital role in cell function by regulating the amount of active steroid available to bind to a particular receptor. A disturbance in these enzymes' usual function is involved in several diseases, especially when a hormonal imbalance is present. The  $17\beta$ -HSD enzymes are mostly  $\text{NAD(P)(H)}$  dependent dehydrogenases/reductases acting on a large, heterogeneous set of substrates including steroids, retinols, prostaglandins, polyols, and xenobiotics.<sup>1</sup>

To date, 15 types of  $17\beta$ -HSD enzymes have been identified (Table 1), and with one exception,  $17\beta$ -HSD type 5 ( $17\beta$ -HSD5), an aldo-keto reductase (AKR), they are all short-chain dehydrogenases/reductases (SDRs).<sup>2</sup> The  $17\beta$ -HSDs share several amino acid sequences containing conserved motifs, such as those within the Rossmann fold, and are generally similar in size (250-350 amino acids). However, the overall homology across the  $17\beta$ -HSDs is low.<sup>3</sup>

Although the name,  $17\beta$ -HSDs, suggests the primary redox activity is at the  $17\beta$ -position of the steroid, we now know that several of the  $17\beta$ -HSDs can convert multiple substrates at multiple sites, such as at the 3-position on the steroid ring,<sup>4</sup> and most have bidirectional capabilities, catalyzing either the oxidative or reductive activity. While the major substrates of  $17\beta$ -HSDs are steroidal hormones, a few are believed to be dedicated primarily to other substrates, such as fatty acids,<sup>5,6</sup> cholesterol,<sup>7</sup> bile acids,<sup>8</sup> or retinoids.<sup>9</sup> Many  $17\beta$ -HSDs are expressed explicitly in patterns across tissues and organs. Others

have specific expression in the cytosol (17 $\beta$ -HSD1), microsomes (17 $\beta$ -HSD3), mitochondria (17 $\beta$ -HSD10), and peroxisomes (17 $\beta$ -HSD4). These observations, along with kinetic studies, have demonstrated that although the enzymes have multifunctional capabilities, most have preferential substrate usage and directionality *in vivo*. For instance, 17 $\beta$ -HSD10 is localized in the mitochondria. Since the mitochondrial matrix is slightly more basic than that of the cytosol, the enzyme plays a role in the metabolism of the estrogenic hormones by unidirectional catalysis, namely the oxidative inactivation of 17 $\beta$ -estradiol.<sup>10</sup>

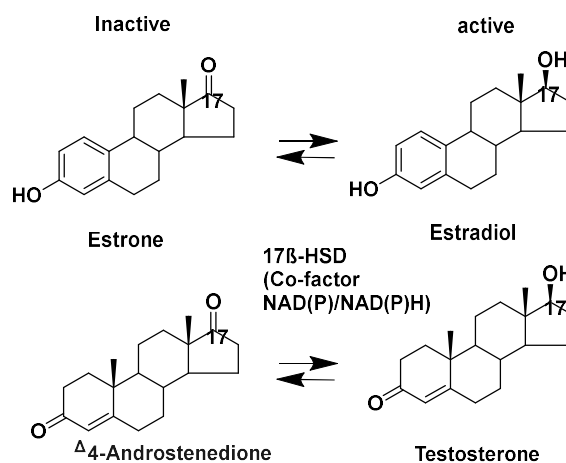


**Figure 1.** The conversion between active and inactive steroidal hormones by 17 $\beta$ -HSDs.

**Table 1.** 17 $\beta$ -HSDs and their relation to diseases

GENE NAME	PATHOLOGY	REFERENCE
<i>HSD17B1</i>	Breast cancer, prostate cancer, endometriosis	11, 12
<i>HSD17B2</i>	Breast, prostate cancer, endometriosis, osteoporosis	11, 13
<i>HSD17B3</i>	17 $\beta$ -HSD3 deficiency, prostate cancer	14
<i>HSD17B4</i>	Perrault syndrome, ovarian cancer, endometriosis	13, 15, 16
<i>HSD17B5</i> (AKR1C3)	Breast cancer, prostate cancer, Leukemia	17-19
<i>HSD17B6</i>	Prostate Cancer	20
<i>HSD17B7</i>	Breast cancer	21
<i>HSD17B8</i>	Polycystic kidney disease	22
<i>HSD17B9</i>	Fundus albipunctatus	23
<i>HSD17B10</i> (ABAD)	Alzheimer's disease, prostate cancer	24, 25
<i>HSD17B11</i>	Prostate Cancer	26
<i>HSD17B12</i>	Breast cancer, ovarian carcinoma	21, 27
<i>HSD17B13</i>	Non-alcoholic fatty liver disease	28
<i>HSD17B14</i>	Breast cancer	29
<i>HSD17B15</i>	Retinitis pigmentosa	30

## **1.1. PROSTATE CANCER**

### **1.1.1. INTRODUCTION**

The success of chemotherapeutic drugs has been hindered mainly by cancer resistance.<sup>31, 32</sup> Cancer cells reprogram themselves to become unaffected by previously effective drugs. Traditional drug development approaches for cancer therapy are transitioning to be more focused on understanding the underlying biological causes of drug resistance and cancer treatments' design to overcome it. Prostate cancer (PCa) is the most frequently diagnosed cancer in men in the US. In 2020, the estimated incidence of PCa exceeded lung cancer and was the second leading cause of mortality in malignant tumors in males.<sup>33</sup>

The typical prostate cell growth mechanism starts from the hypothalamus that releases a luteinizing hormone-releasing hormone (LHRH), which signals the pituitary gland to secrete a luteinizing hormone (LH; Figure 2).<sup>34</sup> The latter then reaches, through blood circulation, the Leydig cells in the testes. These cells then secrete testosterone (T), which is translocated to prostate cells and converted to dihydrotestosterone (DHT).<sup>34</sup> The binding of DHT to the androgen receptor (AR) leads to its activation, acting on androgen receptor elements (AREs) in the nucleus, leading to the release of antigen (PSA), a serine protease produced by prostate cells, commonly used as a marker for PCa proliferation.<sup>34</sup> These AREs also lead to the growth and survival of prostate cells. In PCa, cells' typical growth mechanism is overly activated and leads to cancer progression and tumor formation.<sup>34</sup>

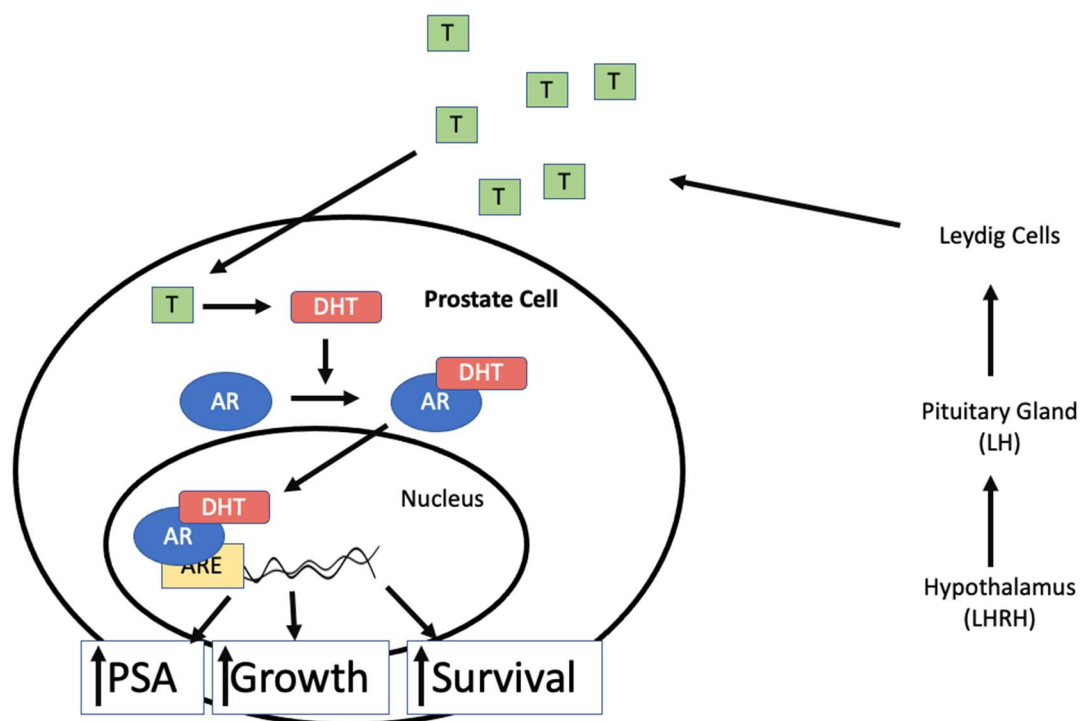


**Figure 2.** The hypothalamic-pituitary-gonadal axis.

Abbreviations: ARE, androgen receptor element; AR, androgen receptor; DHT, dihydrotestosterone; LH, luteinizing hormone; LHRH, luteinizing hormone-releasing hormone; PSA, prostate-specific antigen; T, testosterone.

### 1.1.2. TREATMENT OPTIONS FOR PROSTATE CANCER

Statistics on PCa demonstrate that one man in nine will be diagnosed with the disease in their lifetime, and one man in 41 will die of this type of cancer.<sup>33</sup> As a result, in 2020, the estimated number of deaths due to PCa is 33,330.<sup>33</sup> Besides PSA testing, the clinical stages of PCa are primarily defined by tumor status and whether it is a metastatic or non-metastatic type.<sup>35, 36</sup> Metastasis is commonly identified in regional lymph nodes and bone.<sup>36</sup> The treatment paradigm of PCa is dependent on its type and clinical stage, side effects of the treatment, and overall health of the patient. Active surveillance and watchful waiting strategies are used in the early stages of the disease, where the tumor growth is slow and asymptomatic.<sup>36</sup> It is often used in older men or with men where severe or life-threatening illness is present. As the term suggests, the tumor's active surveillance is achieved by monitoring tumor status through PSA testing and prostate biopsy, determining whether to delay or start treatment.<sup>35</sup> Surgical procedure involving the removal of the prostate and some surrounding lymph nodes is considered the first treatment option for non-metastatic PCa patients.<sup>37</sup> Side effects such as erectile dysfunction and urinary incontinence are expected with surgical procedures.<sup>38</sup> Another treatment option for early-stage PCa is radiation therapy. External-beam radiation therapy that aims to destroy PCa cells is used as a monotherapy or in combination with surgical procedures.<sup>39</sup> Expected short-term side effects are increased urinary urge or frequency, problems with sexual function, problems with bowel function, rectal discomfort or rectal bleeding, and fatigue.<sup>39</sup> Other treatment options are described in detail in the following sections.

## **I. Hormone Therapy**

Hormone therapy, also called androgen deprivation therapy (ADT), is a type of systemic treatment commonly used in advanced PCa and aims to lower T and DHT levels, thereby slowing the growth and progression of a PCa tumor.<sup>37</sup> As described above and in figure 2, the hypothalamus signaling ends by the secretion of T in the circulation. Lowering T or DHT or constraining their access to PCa tumors often makes neoplasms shrink or grow more slowly for a period of time. However, ADT alone does not cure PCa. The decrease in T levels in the circulation sends signals to the hypothalamus and pituitary glands to stimulate T secretion as a positive feedback regulation.<sup>40</sup> The ADT is used in recurrent PCa after surgery or radiation or when metastases have occurred and interventions such as surgery or radiation are not applicable. It can also be used in combination with radiation therapy.

### **LHRH Agonists**

The LHRH agonists such as leuprolide, goserelin, buserelin, and triptorelin, available as a depot injection, act by sustained pituitary overstimulation that eventually downregulates and desensitizes gonadotropin-releasing hormone (GnRH) receptors, causing a decrease in hormone levels.<sup>41</sup> The overall effect of LHRH agonists as an ADT is an initial surge in LH, T, and DHT, which are then suppressed over time.<sup>42</sup> The initial surge in DHT and T stimulates cancer cells' growth and causes a tumor flare in 63% of patients, accompanied by side effects such as libido loss, impotence, hot flashes, and bone pain.<sup>43</sup> Long-term T control with LHRH agonists treatment in PCa patients with a non-metastatic or metastatic type of the disease have been demonstrated to reduce



mortality risk. In 129 patients with metastatic PCa receiving an LHRH agonist, those with high T levels at six months had a 1.33-fold increase in mortality risk.<sup>44</sup>

### **LHRH antagonists**

Another type of ADT is LHRH antagonists that provide a reduction in T levels more quickly than LHRH agonists, with the advantage of avoiding the initial surge in T levels in the circulation.<sup>45, 46</sup> In 2008, the food and drug administration (FDA) approved degarelix, given by monthly injection, to treat advanced PCa. Degarelix represented a safe and effective ADT for one year in patients with PCa without causing a negative impact from testosterone suppression.<sup>47-50</sup> Degarelix, after 14 days, provided a rapid reduction in PSA levels (64% from baseline) and rapid onset of action in the suppression of T (65% from baseline). An oral LHRH antagonist, relugolix, was also approved by the FDA to treat advanced PCa.<sup>50</sup> Relugolix has a lower risk of causing severe cardiovascular side effects, and T production tends to be restored within weeks after treatment rather than months compared to degarelix.<sup>51-54</sup> In a phase III trial, patients with advanced PCa received relugolix or LHRH agonists, leuprolide, for 48 weeks. Relugolix achieved rapid and sustained suppression of testosterone levels that were superior to leuprolide.<sup>52</sup> Common side effects are present with most ADT due to T suppression such as erectile dysfunction, libido loss, hot flashes, gynecomastia, depression, cognitive dysfunction and memory loss, weight gain, sarcopenia, osteopenia, and osteoporosis.<sup>55</sup>

The LHRH modulators usually lead to an initial clinical improvement with a concomitant suppression in prostate PSA levels.<sup>56</sup> Virtually, disease progression occurs in some patients, despite low T levels, leading to the development of a fatal and aggressive form of PCa termed castration-resistant prostate cancer (CRPC), which can metastasize and leads to a decreased overall survival (14–26 months).<sup>57, 58</sup> The AR in CRPC remains activated despite low levels of circulating androgens. Intratumoral androgen biosynthesis,

along with the adaptive changes of the AR, has been the focus in understanding CRPC progression and its therapy resistance over the last decade.<sup>59</sup> The recommended treatment for non-metastatic CRPC (nmCRPC) is orchiectomy and other ADT, described in the following section.<sup>60</sup>

### **Androgen synthesis inhibitors**

Targeting AR signaling, abiraterone acetate (AA; Figure 3), an androgen synthesis blocker, earned FDA approval in 2011.<sup>61</sup> The compound acts by inhibiting the CYP17 enzyme. The CYP17 enzyme acts by catalyzing two key reactions in the production of sex steroids; its 17 $\alpha$ -hydroxylase activity converts pregnenolone into 17 $\alpha$ -hydroxypregnenolone, an essential precursor for androgens, and its 17 $\alpha$ -lyase activity converts the 17 $\alpha$ -hydroxylase products into dehydroepiandrosterone and androstenedione, substrates of testosterone synthesis.<sup>62</sup> Besides being an orally administered agent, the hormone therapy drug provides the advantage of having fewer side effects than antineoplastic therapies. However, AA acts by non-specific inhibition of CYP17 in both gonadal and adrenal steroidogenesis, thereby increasing adrenocorticotrophic hormone levels up to six-fold, which results in mineralocorticoid excess.<sup>63</sup> This imbalance in corticoid hormones can be countered by corticosteroids such as prednisone to prevent serious side effects such as low blood potassium levels, fatigue, fluid retention, hypertensive crisis, and the induction of adrenal insufficiency.<sup>18</sup> In phase III clinical trial, STAMPEDE, AA prolonged overall survival among patients with metastatic CRPC (mCRPC) with concomitant suppression of PSA levels.<sup>64, 65</sup> In the clinic, AA is a first-line treatment option for metastatic PCa and mCRPC.

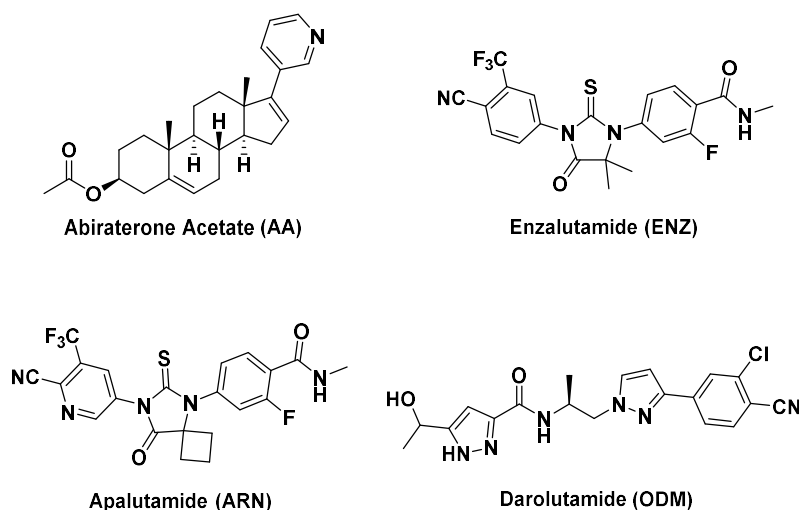


**Figure 3.** Structures of a selection of approved hormonal therapy for prostate cancer.

Another androgen synthesis blocker, Ketoconazole, which inhibits the CYP17 enzyme, has shown clinical efficacy, albeit without survival benefit.<sup>66</sup> Ketoconazole is a synthetic antifungal used off-label as a second-line hormonal treatment for mCRPC since the 1980s.<sup>67, 68</sup> Ketoconazole has shown clinical efficiency before, after, or in combination with chemotherapy.<sup>69-72</sup> The CYP17 inhibitors provide some benefits for CRPC patients but are not curative, and patients often ultimately develop resistance.<sup>73</sup>

### Androgen receptor inhibitors

Another class of compounds that has emerged recently is the AR antagonists, which block AR from continuous activation by DHT. This class functions by inhibiting AR nuclear translocation and subsequent DNA binding. The AR antagonists have the advantage of being orally administered. First-generation drugs included in this class are bicalutamide, flutamide, and nilutamide, and second-generation (Figure 3) are

enzalutamide (ENZ), apalutamide (ARN), and darolutamide (ODM).<sup>74</sup> The AR antagonist ENZ was approved in 2012 and is currently the first-line treatment option for CRPC. The FDA approval was based on the promising effects of ENZ in two phase III clinical trials (AFFIRM and PREVAIL). The results demonstrated significant improvements in survival outcomes and response compared to placebo and have been associated with benefits across all secondary endpoints, including PSA level, soft-tissue response rates, times to PSA progression, radiographic progression-free survival, and first skeletal-related events.<sup>75, 76</sup> The use of ENZ in the clinic has been hindered by patients' resistance<sup>77-79</sup> and dose-limiting CNS seizures, limiting its therapeutic usage.<sup>75, 76</sup> In 2018, another AR antagonist, ARN, was approved.<sup>80</sup> The SPARTAN phase III trial was launched to evaluate the efficacy of ARN in nmCRPC patients at high risk of metastatic disease. The trial enrolled 1,207 patients, and their disease state was defined by PSA doubling time of ten months or less at biochemical progression during ADT, over 70% of patients who had PSA doubling times of six months or less. Patients were randomized to receive ARN or placebo with concurrent ADT and a primary endpoint of metastasis-free survival, defined as the time from randomization to first evidence of distant metastasis or death from any cause within 33 weeks after the last evaluative scan, whichever occurred first, was analyzed. The use of ARN in nmCRPC significantly increased median metastasis-free survival in the treated group (40.5 versus 16.2 months); moreover, overall survival, time to initiate cytotoxic chemotherapy, and second-progression-free survival were longer with ARN compared to the placebo.<sup>81</sup> These findings supported the clinical benefit of ARN and its use in clinic in patients with nmCRPC as well as patients with metastatic hormone-sensitive PCa in combination with ADT.<sup>82</sup> Drug resistance has also been noted with ARN and linked to point mutations in the AR ligand-binding domain<sup>83</sup> and intratumoral androgen biosynthesis mediated by 17 $\beta$ -HSD5.<sup>84</sup> The latest AR antagonist, ODM, was approved for

nmCRPC patients in 2019.<sup>80</sup> Approval was based on the ARAMIS phase III trial that evaluated the effect of ODM in 1,509 patients with nmCRPC.<sup>85</sup> Patients were randomized to receive ODM or placebo and a GnRH analog concurrently or had a previous bilateral orchiectomy, and a primary endpoint of metastasis-free survival was analyzed. The use of ODM increased the median metastasis-free survival in the treated group (40.4 versus 18.4 months). ODM was also associated with benefits regarding all secondary endpoints, including overall survival, time to pain progression, time to cytotoxic chemotherapy, and time to a symptomatic skeletal event.<sup>85</sup> In a recent study, performed in our lab and part of this dissertation work, we were the first to demonstrate the resistance of PCa cell lines to ODM in an *in vitro* study, and it was linked to the intercellular mediation of 17 $\beta$ -HSD5.<sup>84</sup> Details about this study is described in chapter two of this dissertation.

## **II. Targeted Therapy**

In cancer treatment, a targeted therapy refers to cancer drugs designed to interfere with a specific target protein that has a critical role in tumor growth or progression. This type of treatment is the contrast approach of the traditionally known non-selective to neoplasm cytotoxic chemotherapeutics that have been widely used as a cancer therapy in the past decades. The molecular identification of cancer-specific proteins has developed three main types of targeted cancer therapies: 1) monoclonal antibodies, 2) small molecule inhibitors, and 3) immunotoxins. These therapies may be combined with hormone therapy, chemotherapy, or radiotherapy.

To date, only two targeted small molecules, rucaparib and olaparib, have been developed for mCRPC treatment. These compounds exhibit their antineoplastic effect by inhibiting a key enzyme involved in repairing single-strand DNA breaks, named poly (ADP-ribose) polymerase (PARP). In certain types of tumors that carry mutations in the *BRCA1*

and/or *BRCA2* gene, their ability to repair DNA double-strand breaks (DSBs) through the homologous recombination (HR) pathway is lacking.<sup>86</sup> Alternatively, these tumors utilize PARP in the repair of single-strand DNA breaks. Approximately 12% of men with mCRPC harbor a deleterious *BRCA1* or *BRCA2* alteration.<sup>87</sup> Thus, PARP inhibitors can selectively kill *BRCA*-deficient tumor cells lacking HR and have become a focus of therapy for such cancers.<sup>88</sup> In May 2020, the FDA has granted accelerated approval for the orally administered drugs, rucaparib and olaparib for *BRCA*-mutated mCRPC. The FDA has also approved two diagnostic tests (BRACAnalysis CDx and FoundationFocus CDxBRCA) for the qualitative detection of *BRCA1/2* sequence alteration to select patients for the treatment with PARP inhibitors.<sup>89, 90</sup> In 2016, rucaparib was first approved by the FDA for the treatment of patients with deleterious *BRCA*-mutation associated advanced ovarian cancer who have been treated with two or more chemotherapies.<sup>91</sup> The rucaparib approval for mCRPC was based on the TRITON2 phase II trial enrolling 115 patients with *BRCA*-mutated mCRPC that received rucaparib and concomitant GnRH analog or had prior bilateral orchiectomy.<sup>92</sup> Patients showed significant objective response rate in independent radiology review (43.5%; 95% CI, 31.0% to 56.7%; 27 of 62 patients) and investigator assessment (50.8%; 95% CI, 45.2% to 64.1%; 63 of 115 patients) concomitant with significant improvement of PSA response rate (54.8%; 95% CI, 45.2% to 64.1%; 63 of 115 patients).<sup>92</sup> These results supported the efficacy of rucaparib in mCRPC, with a phase III trial currently ongoing to define its clinical benefit in an earlier disease setting among patients with mCRPC (NCT02975934). In 2014, olaparib was first approved for *BRCA*-mutated ovarian cancer, and its approval for mCRPC was based on an investigation in the PROfound phase III trial. In this trial, patients were randomized into two groups, one group taking olaparib and another group taking either ENZ or AA, based on the investigator's choice. Both groups also received a GnRH analog or had prior

bilateral orchiectomy. The results have demonstrated significant longer imaging-based progression-free survival in the olaparib group than the control group (median, 7.4 months versus 3.6 months). A significant benefit was also observed with respect to the confirmed objective response rate and the time to pain progression.<sup>93</sup> In addition, crossed-over patients from the control group showed significant benefit from olaparib treatment in imaging-based progression-free survival. These data granted the FDA approval for olaparib in mCRPC.<sup>93</sup>

### **III. Antineoplastic agents**

The first FDA approved antineoplastic agent for mCRPC was mitoxantrone. The approval was based on improved palliative responses in pain-related measures despite no survival benefit.<sup>94, 95</sup> Mitoxantrone is no longer the first-line treatment option for PCa as other antineoplastic drugs have demonstrated more effectiveness. Docetaxel, a microtubule inhibitor, was the first systemic therapy to demonstrate a survival benefit in mCRPC, was established to be the new standard of care in 2004.<sup>96-98</sup> The FDA approval for docetaxel was based on two phase III trials, the TAX 327 trial and the Southwest Oncology Group 99–16 trial, which proved that the administration of docetaxel provided clear survival benefit.<sup>99, 100</sup> Docetaxel is a first-line therapy for patients with metastatic PCa and mCRPC. Another microtubule inhibitor, cabazitaxel, was also FDA approved for mCRPC.<sup>101</sup> Cabazitaxel is a second-line therapy for docetaxel-treated patients.<sup>102</sup> In a phase III trial, CARD, cabazitaxel treatment improved the median overall survival and median progression-free survival compared to the control group.<sup>103</sup> Other chemotherapies used for PCa treatment based on studies that showed their potential benefits are cisplatin, carboplatin, and etoposide.<sup>104</sup> These drugs are not explicitly FDA approved for PCa

treatment but are listed in the National Comprehensive Cancer Network (NCCN) compendium for PCa.

#### **IV. Immunotherapy**

A treatment for PCa, sipuleucel-T, has been developed based on the concept of antigen-presenting cells (APCs) that trigger T-cells activation, gained FDA approval in 2010.<sup>105</sup> This type of therapy is also called biological therapy where the recombinant antigen protein, sipuleucel-T, is incubated with the patient's isolated APCs *ex vivo*.<sup>106</sup> These cells are then injected into the patient as an immune modulator or vaccine.<sup>107</sup> The antigen-loaded APCs stimulate T-cells that produce chemical messengers such as cytokines, interleukin-12, granulocyte-macrophage colony-stimulating factor (GM-CSF), tumor necrosis factor-alpha, and cytotoxic T-cells.<sup>108</sup> The cytotoxic T-cells are effective in destroying foreign body cells, including cancer cells.<sup>109</sup> The antigen proteins loaded in patient-specific APCs are prostatic acid phosphatase (PAP), an antigen that is highly expressed in most PCa, and GM-CSF.<sup>110</sup> Results from three phase III trials (D9901, D9902A, and D9902B) have sustained the superior overall survival of the treated group.<sup>105, 111, 112</sup> Sipuleucel-T is used as initial therapy for asymptomatic or minimally symptomatic patients with mCRPC. Worth noting, the usual markers of benefit, such as a decline in PSA and improvement in bone or CT scans, are not seen with sipuleucel-T therapy. Therefore, benefits to patients cannot be ascertained using currently available testing.

Another approved immunotherapy PCa treatment is pembrolizumab, which blocks the immune checkpoint receptor programmed death receptor-1 (PD-1). In normal tissue, PD-1 acts as a self-tolerance, surface molecule expressed on an antigen-stimulated T-cell that prevents autoimmune response.<sup>113</sup> When PD-1 receptors are unbound, a normal T-cell immune response occurs. However, when PD-1 binds to its ligands, PD-L1 and PD-



L2, suppression of the immune response is induced by downstream signaling that inhibits T-cells proliferation, cytokine release, and cytotoxicity.<sup>114</sup> Certain tumors abnormally express PD-L1 that binds to PD-1 and suppresses the immune response, allowing tumor cells to avoid immune system attack. Therefore, blockers of the PD-1 receptor represent an attractive approach for tumor eradication.<sup>115</sup> Pembrolizumab was first FDA approved in 2014 for the treatment of patients with unresectable or metastatic melanoma.<sup>116</sup> In 2017, it was granted accelerated approval for “unresectable or metastatic microsatellite instability-high (MSI-H) or mismatch repair (MMR)-deficient solid tumors which have progressed on prior treatment and which have no satisfactory alternative treatment options”.<sup>117</sup> This approval was not just restricted to CRPC patients but included several types of cancer.<sup>118</sup> The use of pembrolizumab is in early clinical evaluation, with on-going trials testing its combination with docetaxel, olaparib, and radiation. The effect of pembrolizumab in two phase I trials showed limited benefit in PSA decline and overall survival rate; thus, its true benefit for CRPC requires further elucidation.<sup>119</sup>

With the advancements in the therapeutic landscape for PCa, a better understanding of the underlying genomic complexity of PCa has improved in the last decade. Clinicians’ ability to stratify patients by risk allowed the recommendation of therapy based on cancer prognosis and patient preference. Initial chemotherapy treatment, at earlier disease stages, can improve survival when compared with ADT. In metastatic PCa, AA and docetaxel provide better treatment options. When nmCRPC occurs, AR antagonists are the selected treatment as they increase patients’ overall survival rate. While in mCRPC, AR antagonists and AA have improved outcomes in patients when compared to hormone therapy. However, mCRPC remains a deadly disease with limited treatment options when resistance occurs, with combination therapy

of AA and ENZ or chemotherapy providing a modest response.<sup>73, 120</sup> In recent years, the molecular mechanisms driving the treatment resistance response in mCRPC are better elucidated. This has fueled the development of novel targeted agents, including PARP inhibitors and immune checkpoints, to treat specific molecular subtypes of mCRPC. Treatment options should be tailored to individual patients accordingly.

## 1.2. 17 $\beta$ -HYDROXYSTEROID DEHYDROGENASE TYPE 5 (17 $\beta$ -HSD5)

### 1.2.1. INTRODUCTION TO 17 $\beta$ -HSD5

The steroidal enzyme 17 $\beta$ -HSD5, also known as AKR1C3 and prostaglandin F<sub>2 $\alpha$</sub>  synthase, belongs to the aldo-keto reductase superfamily of proteins.<sup>121</sup> The enzyme 17 $\beta$ -HSD5, hereto referred to as AKR1C3, has four subtypes that have been identified to date, sharing 84% of amino acid sequence identity but differ in their steroidal substrate stereoselectivities: AKR1C1 (20 $\alpha$ -HSD), AKR1C2 (type-3 3 $\alpha$ -HSD), AKR1C3 (type-2 3 $\alpha$ -HSD), and AKR1C4 (type-1 3 $\alpha$ -HSD).<sup>122, 123</sup> The two enzymes, AKR1C1 and AKR1C2, share >86% sequence identity with AKR1C3 making the selective inhibition of AKR1C3 activity rather challenging.<sup>4</sup> The AKR1C enzymes are soluble monomeric NADPH-dependent oxidoreductases that catalyze the stereospecific interconversion of carbonyl groups and alcohols. The primary action of AKR1C3 *in vivo* is the reduction activity, which converts the weak androgen,  $\Delta^4$ -androstene-3, 17-dione ( $\Delta^4$ -AD) to give T, which can then be converted to DHT by 5 $\alpha$ -reductases type 1 and type 2. AKR1C3 also catalyzes the reduction of 5 $\alpha$ -androstane-3, 17-dione (5 $\alpha$ -Adione) to yield DHT.<sup>124</sup> The activity of AKR1C3 in transforming weak androgens to potent trans-activators of the AR (T, DHT) and the estrogen receptor (17 $\beta$ -estradiol) leads to the pathogenesis of hormone-dependent neoplasms such as PCa and breast cancer.<sup>125</sup> In addition, an increase in the physiological levels of 17 $\beta$ -estradiol alongside a reduction in progesterone levels could contribute to endometrial cancer's pathogenesis,<sup>126</sup> endometriosis,<sup>127</sup> and dysmenorrhea.<sup>125</sup> As a prostaglandin synthase, AKR1C3 reduces the endoperoxide PGH<sub>2</sub> to PGF<sub>2</sub> and converts 11-carbonyl function on PGD<sub>2</sub> to 9 $\alpha$ , 11 $\beta$ -PGF<sub>2</sub>.<sup>128, 129</sup> The increase in PGF<sub>2</sub> leads to the differentiation arrest and proliferation of leukemic blast cells leading to acute myeloid leukemia (AML).<sup>130</sup>

While the activity of AKR1C3 catalyzes the formation of DHT, the actions of the AKR1C1 and AKR1C2 enzymes catalyze the catabolism of DHT to the formation of the pro-apoptotic ligand 5 $\alpha$ -androstane-3 $\beta$ ,17 $\beta$ -diol (3 $\beta$ -Adiol) and the inactive androgen, 5 $\alpha$ -androstane-3 $\alpha$ ,17 $\beta$ -diol (3 $\alpha$ -Diol), respectively.<sup>131, 132</sup> The C4 isoform is a liver-specific subtype that drives the elimination of excess steroid hormones, biosynthesis of bile acids, and xenobiotics' metabolism.<sup>4, 133</sup> Gene profiling studies conducted in clinical prostate tumor tissues have observed a significant decrease in C1 and C2 isoform levels in tumor samples compared to normal prostate specimens.<sup>134</sup> This observation is consistent with the minimal expression of C1 and C2 isoforms in PCa cell lines (PC-3, DU-145, LNCaP, and LAPC-4) compared to the overexpression of the C3 isoform.<sup>131</sup> Given the steroid regulatory functions of the C1, C2, and C4 isozymes, modulation of their activity is undesirable. Hence, one of the most essential considerations in developing an inhibitor of the C3 isoform is to ensure its selective inhibition towards the latter subtype of the enzyme.<sup>4, 131, 135</sup>

### **1.2.2. THE CONTRIBUTION OF AKR1C3 TO THE PATHOGENESIS OF CASTRATION-RESISTANT PROSTATE CANCER**

The activity of AKR1C3 enzyme in the prostate converts 4-androstene-3,17-dione and 5 $\alpha$ -androstane-3,17-dione to T and DHT, respectively, which are potent ligands for the AR, a driving force for PCa development and progression.<sup>125</sup> Reduction of AKR1C3 expression or pharmacological inhibition with indomethacin (INDO; Figure 4), a nonsteroidal anti-inflammatory drug (NSAID) found to have relatively low AKR1C3 activity (IC<sub>50</sub> = 2.3  $\mu$ M, 22-fold selectivity over other isoforms),<sup>136</sup> significantly decreases the levels of T and DHT and PSA.<sup>137</sup> *In vivo*, inhibition of AKR1C3 leads to the reduction of tumor growth in a xenograft model of CRPC.<sup>18, 137</sup> Besides being a primary mediator to the increase in intracrine androgens production in PCa, AR-mediated resistances to

chemotherapeutics is in part due to the co-activation of AR by AKR1C3, stabilizing the AR/AKR1C3 complex and leading up to enhanced transactivation of downstream proliferative signals.<sup>138</sup> Further, AKR1C3 overexpression has recently been correlated to the resistance of PCa to the clinical chemotherapeutic ENZ both *in vitro* and *in vivo*.<sup>77, 79</sup> We have recently reported that AKR1C3 is involved in the acquired resistance of CRPC to novel approved drugs such as ARN and ORN, and that targeting AKR1C3 reserves the drug resistance.<sup>84</sup> The RNA and protein level of AKR1C3 has been reported to be upregulated in CRPC patient tumors and metastatic sites.<sup>139</sup> The protein level of AKR1C3 has been shown to be a promising biomarker in CRPC patients,<sup>137</sup> as its levels were positively correlated with disease progression in 60 human prostate needle biopsies.<sup>140</sup> Further, AKR1C3 plays a crucial role in promoting epithelial-mesenchymal transition and metastasis.<sup>141</sup> In the clinic, AKR1C3 has been shown to be the most upregulated isoform among other AKR enzymes in CRPC patients.<sup>139</sup> Thus, AKR1C3 is a validated target in CRPC, acts downstream in the steroidogenesis pathway, and plays a pivotal role in the pathogenesis and progression of CRPC by catalyzing the production of DHT. Recently, the clinically approved NSAID, INDO, was found to have activity in inhibiting AKR1C3. Although it has a moderate potency and selectivity, it has entered a clinical trial to evaluate its effect in overcoming ENZ resistance in patients with recurrent or metastatic CRPC.<sup>142</sup> Taken together, the enzymatic actions of AKR1C3 increase androgen levels within the prostate leading to the development of CRPC. Thus, inhibition of its activity by small molecules provides a promising approach to overcome the pathogenesis and progression of this devastating form of cancer.

### 1.2.3. OVEREXPRESSION OF AKR1C3 IS LINKED TO CANCER THERAPIES RESISTANCE

In PCa, the keto-reductase activity of AKR1C3 extends to the resistance of cancer cells to therapies. Studies have characterized AKR1C3 as a mediator of resistance of PCa cells to ENZ and AA by providing a source of intratumoral androgens. This resistance has been shown to be reversed by the non-specific AKR1C3 inhibitor INDO.<sup>77, 78</sup> Overexpression of AKR1C3 is also implicated in imparting resistance to finasteride, a 5 $\alpha$ -reductase inhibitor employed for PCa treatment.<sup>143</sup> Further, AKR1C3 as prostaglandin F synthase has been linked to radioresistance in PCa.<sup>144</sup> The augmented PGF<sub>2 $\alpha$</sub>  production causes FP receptor activation and, consequently, mitogen-activated protein kinase signaling that inhibits PPAR $\gamma$  leading to PCa proliferation and resistance to radiation.<sup>145</sup> We have also shown that the resistance to the AR antagonists ARN and ODM has also been linked to the overexpression of AKR1C3 in PCa cell lines.<sup>84</sup>

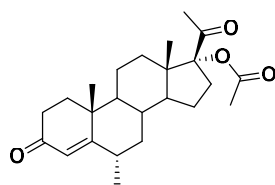
In leukemia, AKR1C3 overexpression leads to the activation of the F<sub>2 $\alpha$</sub>  receptor and downstream mitogen-activated protein kinase cascade due to the overproduction of PGF<sub>2 $\alpha$</sub> .<sup>146</sup> Further, AKR1C3 plays a vital role in inducing myeloid cell proliferation and induction of resistance to differentiation by all-*trans* retinoic acid.<sup>147</sup> One of the most critical resistance mechanisms to the anthracyclines (doxorubicin, daunorubicin, and idarubicin) is the reduction to the less potent C13-hydroxy metabolite (e.g., daunorubicinol and doxorubicinol), and AKR1C3 is the most active enzyme with a confirmed role in anthracycline resistance.<sup>148</sup> The enzyme acts as a phase I biotransformation enzyme that results in chemotherapeutic resistance.<sup>149</sup> A recent study has shown that olaparib synergized daunorubicin antineoplastic activity through its potent inhibition of AKR1C3.<sup>150</sup>

These studies collectively show that the overexpression of AKR1C3 plays a part

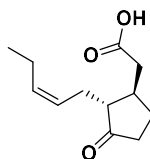
in mediating the resistance of specific tumor cells to cancer therapeutics. A superior therapeutic strategy will be to inhibit the activity of AKR1C3.

#### 1.2.4. SUMMARY OF AVAILABLE AKR1C3 INHIBITORS

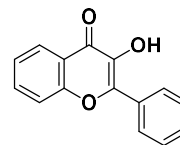
Several synthetic and natural inhibitors of AKR1C3 have been reported, and the reader is directed to referenced reviews that discuss details on the different classes and compounds under investigation.<sup>151, 152</sup> The search for AKR1C3 inhibitors has covered diverse scaffolds: steroids,<sup>125</sup> flavones,<sup>153</sup> jasmonates,<sup>154</sup> NSAIDs, and others (Figure 4).<sup>17, 155</sup> The steroid inhibitors, such as medroxyprogesterone acetate, lack selectivity and stability.<sup>156</sup> Similarly, the Jasmonic acids suffer the same fate of selectivity and potency.<sup>125</sup> Flavonoids such as 2-hydroxyflavone exhibit moderate potency and weak selectivity.<sup>153</sup> The repurposing of NSAIDs exhibits high potency to AKR1C3 and moderate selectivity; however, they did not progress into the clinic. An *N*-naphthylamino benzoate compound and GTX-560 are unique in exhibiting dual activity, AKR1C3 inhibition and antagonizing AR function.<sup>138, 157</sup> The AKR1C3 inhibitor, ASP9521, has been discontinued from clinical trials as no clinical benefit was observed.<sup>158</sup> A recent study by Endo *et al.* has disclosed novel AKR1C3 inhibitors based on the chromene scaffold. Among the synthesized hydroxy-iminochromene carboxamide analogues tested, compound **2j** showed potent inhibitory effects toward AKR1C3. Compared with other inhibitors, the selectivity of compound **2j** toward AKR1C3 was improved.<sup>159</sup> Cinnamic acid derivatives have also been shown to inhibit AKR1C3 with moderate potency and selectivity. The natural product baccharin has an IC<sub>50</sub> of 110 nM and a 500-fold selectivity over AKR1C2 (Figure 5).<sup>160</sup> The scaffold of baccharin presents an attractive one for hit-to-lead optimization studies to understand its structure-activity relationship (SAR) in AKR1C3 inhibition and develop a potent and selective

**Medroxyprogesterone acetate**AKR1C3 IC<sub>50</sub> = 280 nM

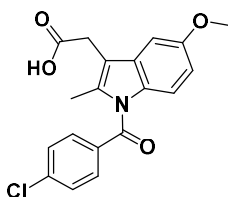
C3/C2 selectivity = 5

**Jasmonic acid**AKR1C3 IC<sub>50</sub> = 24 μM

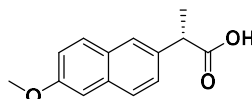
C3/C2 selectivity = 0.71

**2-hydroxyflavone**AKR1C3 IC<sub>50</sub> = 0.3 μM

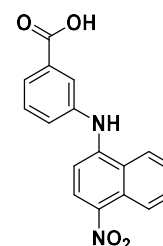
C3/C2 selectivity = 157

**Indomethacin**AKR1C3 IC<sub>50</sub> = 100 nM

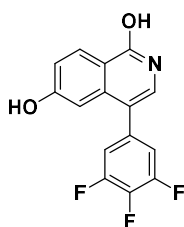
C3/C2 selectivity = 365

**S-Naproxen**AKR1C3 IC<sub>50</sub> = 50 nM

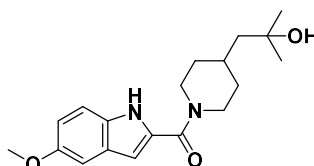
C3/C2 selectivity = 56

**N-naphthylamino benzoate**AKR1C3 IC<sub>50</sub> = 60 nM

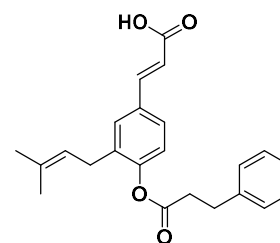
C3/C2 selectivity = 249

**GTX-560**AKR1C3 IC<sub>50</sub> = 0.77 μM

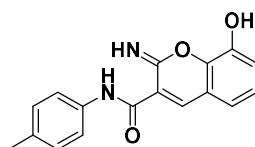
C3/C2 selectivity = Not determined

**ASP9521**AKR1C3 IC<sub>50</sub> = 0.12 μM

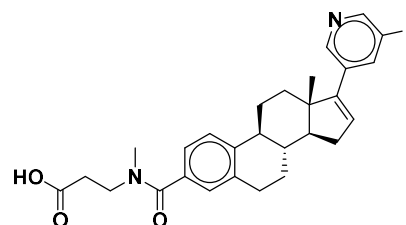
C3/C2 selectivity = &gt;100

**Baccharin**AKR1C3 IC<sub>50</sub> = 110 nM

C3/C2 selectivity = 500

**Compound 2j**AKR1C3 IC<sub>50</sub> = 27 nM

C3/C2 selectivity = &gt;300

**BAY1128688**AKR1C3 IC<sub>50</sub> = Not disclosed

C3/C2 selectivity = Not disclosed

**Figure 4.** Structures and activities of a selection of AKR1C3 inhibitors.



AKR1C3 inhibitor as a treatment approach for CRPC. Previous work in our lab has studied the SAR of baccharin and identified two highly potent and selective inhibitors, KV-49a and KV-49g, with both showing an  $IC_{50}$  of 70 nM and >2500-fold selectivity over the C2 isoform (Figure 5).<sup>161</sup>

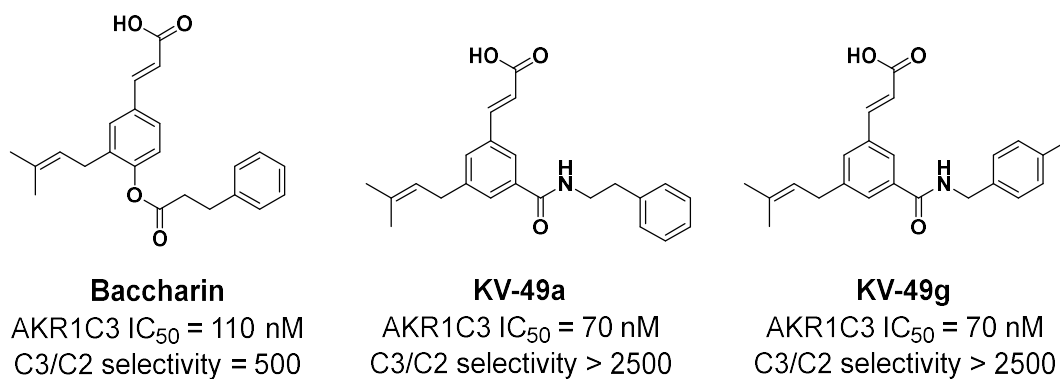


**Figure 5.** Baccharin and its potent and selective analogs.

### 1.2.5. MODELING OF AKR1C3 ENZYME AND ITS ISOFORMS

The crystal structures of AKR1C3 in complex with various inhibitors, the cofactor NADP<sup>+</sup> and substrates such as <sup>Δ</sup>4-AD and PGD<sub>2</sub> have been described.<sup>144, 162-164</sup> The protein structure is composed of a classical triphosphate isomerase (TIM) barrel motif consisting of an alternating arrangement of eight  $\alpha$ -helices interspersed with eight  $\beta$ -helices and capped with three flexible loops.<sup>165</sup> The enzymatic active site of AKR1C enzymes can be dissected into five compartments, namely an oxyanion site, a steroid binding channel, and three subpockets; SP1, SP2, and SP3 (Figure 6).<sup>125</sup> The oxyanion site is conserved among all AKR1C isoforms and consists of the Tyr55 and His117 catalytic residues and NADP<sup>+</sup> cofactor. The steroid channel consists of Trp227 and Leu54. The three subpockets comprise the following amino acid residues; SP1 (Ser118, Asn167, Phe306, Phe311, and Tyr319), SP2 (Trp86, Leu122, Ser129, and Phe311), and SP3 (Tyr24, Glu192, Ser221, and Tyr305).<sup>18</sup> The catalytic residues that form a hydrogen bond by accommodating an oxygen atom of a carboxylic acid, ketone, or hydroxyl functional groups on substrate molecules line encompasses the oxyanion site. This observation provided the basics for the rational design of AKR1C inhibitors, as the pharmacophoric component should comprise a carboxylate or ketone moiety.<sup>161</sup> The steroid channel, conserved in all AKR1C isoforms, is a large, elongated pocket that functions to orient the substrate properly to govern the stereochemical specificity of enzyme catalysis, an indispensable component for dehydrogenase activity. Studies have focused on the active sites of AKR1C enzymes, with the primary differences among the four subtypes being in the SP pockets. The C3 isoform contains a unique Phe306 and Ser129 active binding site, and its SP1 pocket exhibits a larger and more flexible pocket than other subtypes.<sup>166</sup> The amino acid residue Leu306 of C1 and C2 isoforms and the Val306 of AKR1C4 show lower

flexibility than Phe306 of C3; thus, the C3 isoform can accommodate a diverse variety of ligands and is exploited for the rational design of isoform selective inhibitors. Compounds that occupy more space in the SP1 pocket may have higher potency and substrate selectivity. Another difference between C3 and the other three isoforms is the SP2 pocket is the spatial difference in the amino acid at position 311 leads to a larger cavity in C3, and Ser129 also provides the potential for hydrogen bonding with the ligands.<sup>125</sup>

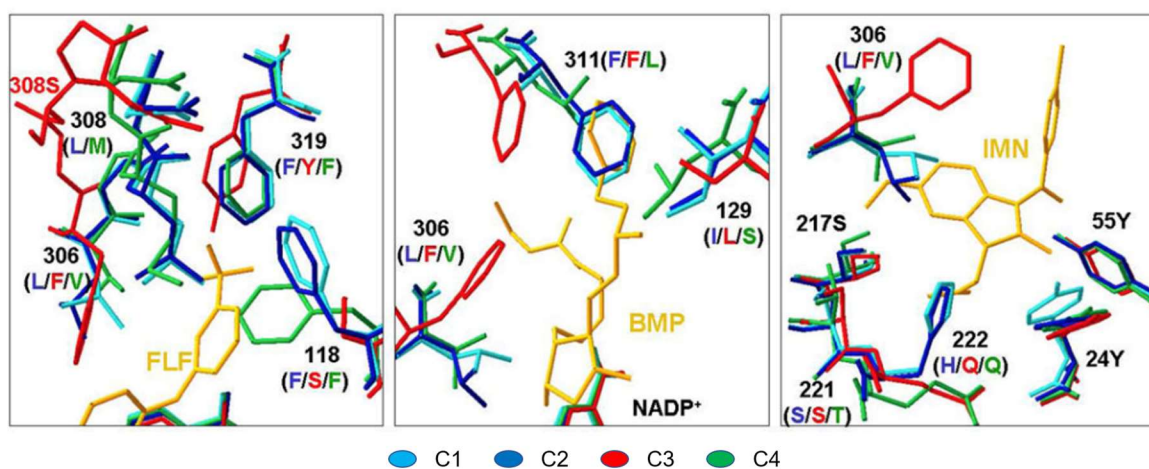


**Figure 6.** Comparison of SP1, SP2, and SP3 sub-pockets of four human AKR1C enzymes.<sup>125</sup>

## 1.3. ALZHEIMER'S DISEASE

### 1.3.1. INTRODUCTION

The most common form of dementia, Alzheimer's disease (AD), discovered by Alois Alzheimer in 1906, was the fifth leading cause of death in 2018, showing an increased death toll by 146.2% between 2000 and 2018.<sup>167</sup> An estimated 5.8 million Americans are currently living with AD and this number is projected to rise to 14 million by 2050.<sup>167</sup> To this date, no disease-modifying therapy or cure exists for this devastating disease. Since its discovery, scientists have overcome several challenges and gained tremendous knowledge of the disease progression with the anticipation of promising approaches for a breakthrough therapy.

Three main pathologies contribute to AD progression, amyloid-beta ( $A\beta$ ) oligomers, tau tangles, and neuroinflammation.<sup>168-170</sup> Approximately 15-20 years before AD symptoms appear,  $A\beta$  protein starts accumulating between neurons, followed by tau protein breakage from microtubules and tangle formation, causing neuronal damage that leads to the initiation of neuroinflammation.<sup>171</sup> Amyloid precursor protein (APP) is a transmembrane protein sequentially cleaved by the aspartate proteases  $\beta$ - and  $\gamma$ -secretase leading to the formation of  $A\beta$  peptide (1–42) and a degenerated C-terminus.<sup>172-174</sup> The normal function of the  $A\beta$  protein is not yet determined. Its soluble peptides aggregate to form oligomers that are toxic to neurons and plaques that deposits between synapses disrupting their connections.<sup>175, 176</sup> Tau protein is a microtubule stabilizer that contributes to axon stability and overall neuronal function.<sup>177</sup> Tau breaks off microtubules and is hyperphosphorylated by kinases such as cyclin-dependent kinase 5 (Cdk5) and glycogen synthase kinase-3 $\beta$  (GSK-3 $\beta$ ).<sup>178</sup> Tau tangles then aggregate intracellularly, causing neurotoxicity.<sup>179</sup> Neuroinflammation in AD is the marker for the damage caused

by A $\beta$  and tau, which further contributes to neuronal dysfunction.<sup>180</sup> The disturbed function of astrocytes and microglia, two components of glial cells, in the AD brain expose neurons to further damage leading to brain deterioration.<sup>181</sup>

### **1.3.2. OVERVIEW OF THERAPEUTIC APPROACHES TOWARDS ALZHEIMER'S DISEASE**

Strategies that search for treatments to combat the neurotoxicity caused by A $\beta$  and tau can be divided into three main approaches.<sup>168</sup>

1. Reduction of A $\beta$  or tau aggregations and accumulation in the brain. This is approached by  $\beta$ -secretase inhibitors,  $\gamma$ -secretase modulators,<sup>182</sup> and immunotherapy against A $\beta$  and tau.<sup>183</sup>
2. Stabilizing the function of existing neurons. This symptomatic approach modulates neurotransmitters and their receptors, improving neuronal health and normal downstream mechanisms.<sup>184</sup>
3. A wide range of targets termed "sensitive targets" are vulnerable to A $\beta$  and tau toxicity. These targets are membrane receptors,<sup>185</sup> cellular and mitochondrial targets.<sup>186, 187</sup> Upon A $\beta$  and tau accumulation, the target function is disturbed, leading to neuron dysfunction. This approach aims to restore normal target function and regain neuron health.

Despite these three distinct approaches, a treatment for AD has proven to be elusive, and FDA approved treatments only provide symptomatic relief. Five approved AD drugs act by modulation of neurotransmitters in the brain (Figure 7). Four of which are acetylcholinesterase inhibitors (tacrine<sup>188</sup>, donepezil<sup>189</sup>, rivastigmine,<sup>190</sup> and galantamine<sup>191</sup>). These drugs act by inhibiting the cholinesterase enzyme action that breaks down acetylcholine, thereby sustaining the latter's action in cholinergic synapses.

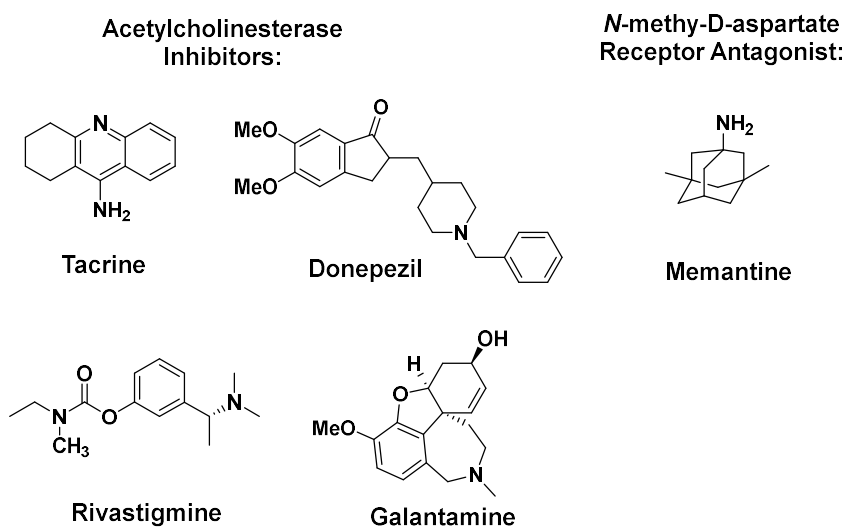


**Figure 7.** Structures of clinically approved drugs for the treatment of Alzheimer's Disease.

Cholinesterase inhibitors have been shown to improve cognition, daily and global function significantly, and some behavioral manifestations of AD, compared with placebo treatment.<sup>192</sup> Moreover, in a meta-analysis of 26 studies, they have provided an overall benefit in stabilizing cognition, function, behavior, and global clinical change.<sup>193</sup> The use of cholinesterase inhibitors has been demonstrated to reduce the risk for nursing home placement, thus reducing healthcare costs and reducing caregivers' stress and time devoted to patients.<sup>194-196</sup> The fifth of the FDA approved AD therapies is the N-methyl-D-aspartate (NMDA) channel blocker memantine. By blocking the  $\text{Ca}^{2+}$  channel in an NMDA receptor and trapping it in the open conformation, memantine leads to decreased intracellular calcium.<sup>197</sup> The blockade of current flow through channels of NMDA receptor-operated ion channels reduces the effects of excitotoxic glutamate release. Moreover, the elevation of  $\text{Ca}^{2+}$  levels and induction of neuronal death have been the central mechanistic hypothesis of AD for many years.<sup>198</sup> In clinical trials, memantine has shown significant

improvement in clinical symptoms and functional activities.<sup>199-201</sup> Meta-analysis on the efficacy of memantine for AD treatment has revealed that its monotherapy is useful in improving cognitive functions and behavioral disturbances in patients with AD. In addition, superiority was noted in its combination therapy with cholinesterase inhibitors compared with the latter's monotherapy.<sup>202</sup>

Despite their benefits in improving symptoms, these FDA approved treatments provide no benefits in slowing the disease's progression. In a post-hoc analysis of DOMINO-AD trial, patients who were randomized to discontinue donepezil therapy were twice as likely to enter a nursing home after one year as were individuals who continued treatment with donepezil; however, this effect lost statistical significance after three years. Moreover, starting memantine treatment had no effect, either as a monotherapy or in combination with donepezil, at any point in the trial.<sup>203</sup> This study and others acknowledge the lack of efficacy of cholinesterase inhibitors, NMDA antagonist, or their combination in benefiting AD patients in their disease progression or delaying the time of death.<sup>201, 204, 205</sup> Thus, urges for a disease-modifying therapy and strategies discussed above have focused on identifying a new therapy. For a detailed discussion of these strategies' current and emerging targets, the reader is directed to the referenced review published by our group.<sup>168</sup> Nonetheless, most of these therapies that reached clinical trials have shown no benefit in slowing the disease's progression. For instance, drugs that fall under the first of the three approaches stated above, such as the  $\beta$ -secretase inhibitors that reached phase III trials in 2019, have been all discontinued for inefficacy or toxicity.<sup>206</sup> The  $\gamma$ -secretase modulator trials have been stopped due to serious adverse effects and diminished efficacy.<sup>207</sup> Trials using antibodies, aducanumab, and crenezumab were halted as preliminary data from trials suggested that the primary endpoint would not be met.<sup>206</sup> Tau immunotherapy clinical trials were promising; however, results were disappointing in

slowing the progression.<sup>208</sup> One of the significant factors contributing to these trials' failure has been donated to treatment timing, i.e., patients at mild to moderate stage might be too late for protein aggregation reducing therapies, as neuronal damage is extensive and irreversible.<sup>168</sup> The criteria for AD diagnosis fail to define disease state before symptoms occur. It is widely accepted that disease onset may occur 15–20 years before clinical symptoms appear. Biomarkers play increasingly important roles in AD drug development, diagnostic confirmation, and support of disease modification. Thus, with an accurate and sensitive biomarker, the disease can be diagnosed early enough for therapeutic intervention.<sup>209-212</sup> The second approach that modulates neurotransmitter signaling has the smallest number of candidates currently in trials, 12 agents out of a total of 121 agents. Despite some success, these therapies have no impact on the disease's biological causes and cell death in AD patients.<sup>206</sup> The third approach, drugs with a disease-modifying effect, is currently the most attractive candidate in AD research.<sup>213</sup> This kind of treatment approach has only been studied recently. Over the past five years, there has been an increase in the number of disease-modification treatment candidates in clinical trials.<sup>206, 214</sup> The AD research in the last decade has been largely focused on identifying biomarkers, a more accurate diagnosis, and disease-modifying therapy that changes AD's biology and produces neuroprotection.

An early event in AD pathogenesis and synaptic loss is mitochondrial dysfunction occurring in neurons caused by A $\beta$  accumulation inside the mitochondrial neurons.<sup>215, 216</sup> Oxidative damage and synaptic degeneration lead to neuron dysfunction and cognitive decline.<sup>217, 218</sup> An emerging mitochondrial target for AD is the most well-characterized of the A $\beta$  binding proteins, 17 $\beta$ -HSD10, also known as amyloid-binding alcohol dehydrogenase (ABAD).<sup>219</sup> The enzyme 17 $\beta$ -HSD10, hereto referred to as ABAD, plays a role in A $\beta$  toxicity by forming protein-protein interaction with A $\beta$ , potentiating its toxicity.<sup>219</sup>



Moreover, studies have demonstrated that ABAD is overexpressed in the same areas of the brain most affected by AD, the cerebral cortex and hippocampus, in both AD patients and transgenic mAPP/ABAD mouse models of AD.<sup>220</sup> More details about ABAD are discussed later in this chapter.

## **1.4. AMYLOID-BINDING ALCOHOL DEHYDROGENASE ENZYME (ABAD)**

### **1.4.1. INTRODUCTION TO ABAD**

The mitochondrial enzyme ABAD, also known as endoplasmic reticulum associated amyloid  $\beta$ -peptide-binding protein (ERAB) and short-chain 3-hydroxyacyl-CoA dehydrogenase (SCHAD), is a multifunctional protein that acts as a vital energy regulator by oxidizing and reducing substrates with an  $\text{NAD}^+$  molecule as a co-factor.<sup>24, 221</sup> Moreover, it catalyzes the third step of mitochondrial oxidation converting 3-hydroxyacyl-CoA in the presence of  $\text{NAD}^+$  to 3-ketoacyl-CoA, NADH, and  $\text{H}^+$ .<sup>222</sup> The enzyme facilitates the catabolism of isoleucine, in which it catalyzes the conversion of 2-methyl-3-hydroxybutyryl-CoA (MHB) to 2-methylacetoacetyl-CoA.<sup>223</sup> The activity of ABAD has a role in sex steroid and neurosteroid metabolism due to its  $3\alpha$ - and  $17\beta$ -hydroxysteroid dehydrogenase activity.<sup>224, 225</sup> Estradiol, a substrate for ABAD, plays a vital function in the mitochondrial system, and its levels are an essential determinant of neuronal survival.<sup>226</sup> Physiological levels of estradiol in the mitochondria perform a critical role as an antioxidant and calcium regulator, a fundamental determinant of neuronal survival.<sup>227</sup>

### **1.4.2. THE CONTRIBUTION OF ABAD TO THE PATHOGENESIS OF ALZHEIMER'S DISEASE**

Higher prevalence and incidence of AD occurs in women, two-thirds of AD patients are female, and studies show that women exhibit greater senile plaque deposition than men.<sup>228</sup> The role of ABAD is to maintain the balance of estradiol/estrone in neurons.<sup>226</sup> However,  $\text{A}\beta$ -ABAD interaction disrupts this balance and leads to a reduction in the levels of estradiol. Thus, leading to an increase in ROS levels, DNA fragmentation, and apoptosis.<sup>229</sup> Two other ABAD substrates have been identified to date: peroxiredoxin-2 (Prdx-2), which functions as an antioxidant and is inactivated in AD.<sup>230</sup> Second, endophilin-

1 (Ep-1), a member of a family of proteins that are responsible for synaptic vesicle endocytosis mitochondrial function, and receptor trafficking.<sup>231</sup> Its activity has been shown to be diminished in AD.<sup>232</sup> The ABAD enzyme interacts with A $\beta$ , binding in the nanomolar range, and enhancing A $\beta$  toxicity.<sup>233</sup> Moreover, it is shown to be overexpressed in the cerebral cortex and hippocampus of AD patients and mAPP/ABAD mice models of AD.<sup>220</sup> Several reports suggest the A $\beta$ -ABAD interaction links A $\beta$  toxicity with the mitochondrial dysfunction apparent in AD.<sup>226, 229, 232, 234</sup> Through its interaction with ABAD, A $\beta$  induces a conformational change in the enzyme structure, thereby inactivating normal enzymatic turnover and ultimately resulting in neuronal apoptosis.<sup>235, 236</sup> Inhibition of the A $\beta$ -ABAD interaction would be expected to offer a neuroprotective effect from A $\beta$  toxicity.<sup>227</sup> A decoy peptide that encompasses the region in ABAD known as the L<sub>D</sub> loop, where A $\beta$  binds and induces its toxicity, has been shown to reduce expression of Prdx-2 and Ep-1, both of which are elevated in AD patients and murine models of AD.<sup>220</sup> Further, the small molecule inhibitor of ABAD, AG18051, has been shown to restore the level of estradiol to normal, subsequent to A $\beta$  injury in SH-SY5Y cells.<sup>227</sup> This data indicates that inhibition of the A $\beta$ -ABAD protein-protein interaction protects mitochondria and neurons from A $\beta$  mediated toxicity and may represent a novel target for AD drug discovery. We have summarized A $\beta$ -ABAD toxicity mechanisms in a recent review article (Figure 8).<sup>24</sup>

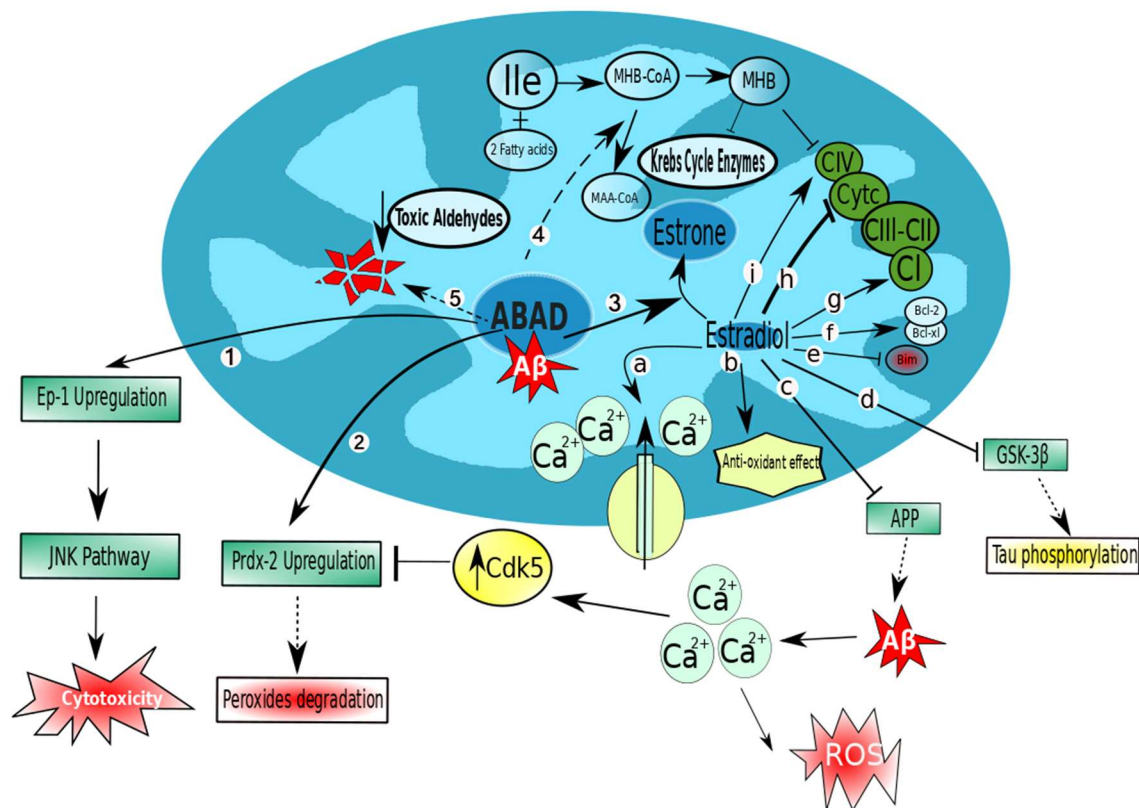


**Figure 8.** Summary A $\beta$ -ABAD toxicity mechanisms related to ABAD.

“1) Upregulation of Ep-1 by ABAD activates the c-Jun N-terminal kinases (JNK) pathway, which leads to cytotoxicity. 2) Upregulation of Prdx-2, which is responsible for the degradation of peroxides, by ABAD. However, due to elevated levels of Cdk5, elevated Prdx-2 is deactivated, which leads to peroxide accumulation. 3) Conversion of Estradiol to Estrone is upregulated with complex interaction leading to reduced estradiol levels in the mitochondria. Estradiol has remarkable effects on neuron protection (a-i). a) Deactivation of estradiol leads to the inability of the mitochondria to sequester  $\text{Ca}^{2+}$  ions from the cytosol. This effect is induced by A $\beta$ , leading to the accumulation of  $\text{Ca}^{2+}$  ions in the cytosol, which results in Cdk5 activation. The accumulation of  $\text{Ca}^{2+}$  ions in the cytosol also leads to reactive oxygen species (ROS) generation. b) Estradiol increases the antioxidants' production by increasing glutathione levels, decreasing oxidative DNA damage in the mitochondria. c) Estradiol reduces (APP) processing, decreasing A $\beta$  levels and concomitantly its aggregation into plaques. d) Estradiol induces the phosphorylation of GSK-3 $\beta$ , which inactivates the enzyme and reduces tau phosphorylation. e) and f) Estradiol functions to enhance the downregulation of pro-apoptotic proteins (e.g., Bim) and the expression of anti-apoptotic proteins (e.g., Bcl-2 and Bcl-xL). g) and i) Estradiol exert an effect on the electron transport chain by increasing the expression of some complexes in the mitochondrial respiratory chain, including complex I (CI) and IV (CIV). h) Estradiol has been shown to prevent the mitochondrial release of cytochrome c, which activates the caspase cascade in the cytoplasm leading to apoptosis. 4) Participation of

ABAD in the final degradation steps of the amino acid isoleucine (Ile) is inhibited by A $\beta$  binding, which leads to the accumulation of 2-methyl-3-hydroxybutyrate (MHB). The latter has toxic effects in inhibiting Krebs cycle enzymes and CIV activity. 5) Toxic aldehydes that accumulate in the mitochondria are degraded by ABAD. This degradation is inhibited by A $\beta$  binding.”<sup>24</sup> Abbreviations: ABAD, Amyloid-binding Alcohol Dehydrogenase; A $\beta$ , Amyloid Beta; APP, Amyloid Precursor Protein; CI, Complex I; CII, Complex II; CIII, Complex III; CIV, Complex IV; CytC, Cytochromes complex; Ep-1, endophilin-1; JNK, Jun N- Terminal Kinase; Ile, Isoleucine; GSK-3 $\beta$ , Glycogen Synthase Kinase-3 $\beta$ ; MAA-CoA, 2-Methylacetoacetyl-coenzyme A; MHB, 2-methyl-3-hydroxybutyrate; MHB-CoA, 2-methyl-3-hydroxybutyryl-Coenzyme A; Prdx-2, peroxiredoxin-2; ROS, Reactive Oxygen Species.

### 1.4.3. SUMMARY OF AVAILABLE ABAD INHIBITORS

Inhibitors of ABAD are in nascent development, with four main classes of compounds being investigated (Figure 9).<sup>24</sup> The fused pyrazole compound class has the most potent inhibitor to date, AG18051 ( $IC_{50}$  = 92 nM; Figure 9).<sup>24, 235, 237</sup> A compound library of AG18051 derivatives were discovered in 2005 and have never been investigated further in their ability to inhibit ABAD activity, and no pharmacophore has been identified.<sup>237</sup> Secondly, a steroidal compound class that lacks selectivity and potency with the most potent identified steroidal compound RM-532-46 as a reversible ABAD inhibitor ( $IC_{50}$  = 0.55  $\mu$ M; Figure 9).<sup>25</sup> The third class is derived from the FDA approved immunosuppressant frentizole (Figure 9). As a hit compound, frentizole had an  $IC_{50}$  of 200  $\mu$ M and studying its SAR has developed a benzothiazole urea analog with a chlorine substituted benzothiazole ring, a urea linker, and a *para*-hydroxy moiety on the terminal phenyl ring, with an adjacent chlorine ( $IC_{50}$  = 1.67  $\mu$ M).<sup>238, 239</sup> Finally, the fourth class of compounds is designed based on the region of ABAD, where A $\beta$  binds, L<sub>D</sub> loop. These inhibitors aim to inhibit A $\beta$ -ABAD interaction without affecting enzyme activity. One compound, VC15, has shown an  $IC_{50}$  of 4.4  $\mu$ M (Figure 9).<sup>240</sup>

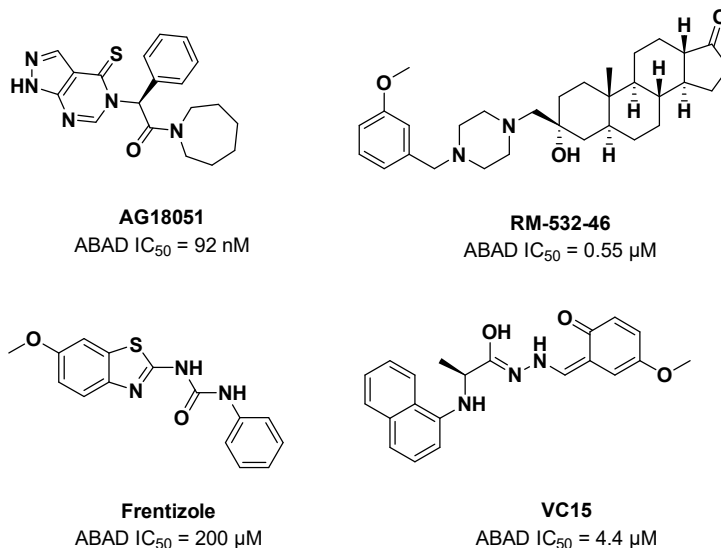


**Figure 9.** Structures of a selection of ABAD inhibitors.

#### 1.4.4. MODELING OF ABAD ENZYME

The crystal structure of ABAD in complex with AG18051 and the cofactor NAD<sup>+</sup> has been described. This demonstrated that the inhibitor occupies the substrate binding pocket and forms a covalent adduct with the cofactor within the active site of ABAD (PDID: 1U7T).<sup>235</sup> The protein structure is composed of the classical Rossmann fold of 17 $\beta$ -HSD enzymes. The molecular mass of ABAD is 108 kDa, consisting of 261 amino acids, that is encoded by the gene *HSD17B10* located at chromosome Xp11.2.<sup>241</sup> The binding of A $\beta$  to ABAD induces conformational changes in the enzyme structure, thereby inactivating normal enzymatic turnover and ultimately resulting in neuronal apoptosis, these findings were supported by surface plasmon resonance (SPR) and nuclear magnetic resonance (NMR) studies.<sup>220, 242</sup> X-rays crystal structure studies of the A $\beta$ -ABAD complex revealed that protein-protein interaction directly links to A $\beta$  toxicity.<sup>243</sup> Crystal structures of the interaction of ABAD with its substrates (fatty acids and hydroxysteroids) support the proposed physiological and pathological relevance to AD progression.<sup>244</sup> Besides the covalent adduct that AG18051 exhibits when binding to ABAD, other interactions are also noted; hydrophobic interactions (black wavy lines, hydrogen bonding (black dashed lines), and  $\pi$ - $\pi$  interactions (green wavy lines) with ABAD (Figure 10).<sup>24</sup> The binding of AG18051 to ABAD is described in chapter three of this dissertation.

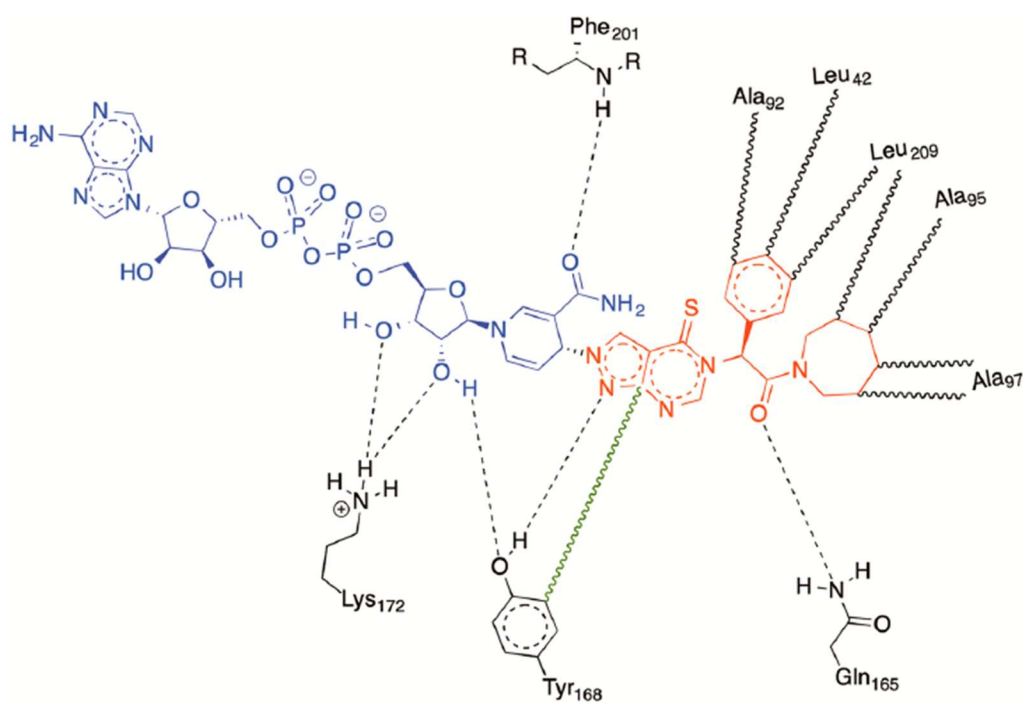


**Figure 10.** Map of interactions between an inhibitor and the ABAD enzyme.<sup>24</sup>



## **1.5. PURPOSE OF THIS DISSERTATION**

### **1.5.1. AKR1C3 INHIBITOR DESIGN, SYNTHESIS AND EVALUATION.**

To date, no specific AKR1C3 inhibitor has been successfully marketed, despite the critical role of the AKR1C3 enzyme in the progression of several types of cancer. Our lab has designed the most potent and selective AKR1C3 inhibitors of this chemotype identified to date, KV-49a and KV-49g. However, the SAR of these molecules is not fully elucidated. This dissertation aims to continue our lab's effort to define the SAR of these molecules, contributing to designing an optimum AKR1C3 inhibitor as a potential treatment for CRPC. The further aim of this work is to investigate the pharmacokinetics (PK) properties of these lead compounds. Moreover, continue investigating these molecules' activity in halting PCa cell progression and studying their effect as potentiators to chemotherapies approved for CRPC.

### **1.5.2. ABAD INHIBITOR DESIGN, SYNTHESIS AND EVALUATION.**

Small molecule inhibitors for ABAD have mainly been ignored. This dissertation investigates the SAR of AG18051 in inhibiting ABAD activity. A novel synthetic route for AG18051 is needed and is the focus of the work of this dissertation, as the known synthetic route is low-yielding and long.<sup>237</sup> The original route consists of a ten-step synthesis, and the route's complexity increases when aiming to design a variety of derivatives. Investigating the potency of synthesized inhibitors *in vitro* AD assays will provide a valuable contribution to understanding the significance of ABAD inhibition in AD. Moreover, developing a robust screening assay will facilitate the screening of the designed molecules.

## **CHAPTER 2: DESIGN, SYNTHESIS AND EVALUATION OF AKR1C3 INHIBITORS**

## 2.1. INTRODUCTION

Given the close correlation between overexpression of AKR1C3 and proliferation of cancer, a great deal of research on AKR1C3 inhibitors has been performed in recent years. The types of inhibitors reported in recent years include cyclopentane derivatives and hormone analogues that are derived from AKR1C3 catalytic substrates, natural products, NSAID analogues, metal complexes, sulfonylureas, and others.<sup>125, 152, 157, 159, 161, 164, 245-248</sup> To date, no compound has been progressed as a potential AKR1C3 inhibitor from discovery to market. Indeed, most of these inhibitors are still in need of substantial medicinal chemistry optimization. Because of the high homology between isoforms of the AKR1C family, the selective regulation of AKR1C enzymes poses challenges for the design and synthesis of inhibitors. Considering the role of C1 and C2 in the prostate to mediate the inactivation of the potent androgen DHT, when targeting CRPC, pan AKR1C enzyme inhibitors can have conflicting and detrimental pharmacological effects.

One of the major limitations in AKR1C3 inhibitor development into the clinic is poor selectivity. The typical steroidal inhibitors medroxyprogesterone acetate and steroid lactone possess low selectivity to AKR1C3 and also inhibit AKR1C4. Steroid lactone is an estrogen derivative having a lactone on the D ring of the steroid and shows a mid-nanomolar IC<sub>50</sub> value, but its inhibitory activity for other AKR1C isoforms has not been investigated. The NSAIDs, such as flufenamic acid derivatives, possess high potency and moderate selectivity towards AKR1C3, while INDO analogs possess low potency and selectivity profile. The nature of the metabolism of fatty acids and their high binding rate of albumin hinders the use of long-chain polyunsaturated fatty acid AKR1C3 inhibitors in the clinic. Cinnamic acid derivatives such as baccharin have a good AKR1C3 inhibitory activity and selectivity, but the ester bond in its structure is metabolically unstable, and the

activity and selectivity of the product after hydrolysis is decreased. Thus, these limitations have made the design and synthesis of selective inhibitors challenging. Two compounds were tested in clinical trials. The first drug, ASP9521, was tested in a small phase I-IIb clinical trial for CRPC and despite being well tolerated, it lacked efficacy.<sup>158, 249</sup> The second compound, BAY1128688, has entered phase II clinical trial for the treatment of endometriosis, but was recently terminated on account of the hepatotoxicity because of the nonspecific inhibition of AKR1D1.<sup>250</sup> Thus, no AKR1C3 selective inhibitors have been clinically applied, although many AKR1C3 inhibitors have been reported.

Cinnamic acid derivatives have been shown to exhibit inhibition activities for AKR isozymes bearing selectivity toward AKR1C3. Baccharin, a cinnamic acid derivative, is a natural product extracted from honeybee propolis and has been shown to potently and selectively inhibit AKR1C3 with an  $IC_{50}$  of 110 nM and selectivity of 500-fold over AKR1C2.<sup>160</sup> This discovery has made baccharin a promising hit to develop a new series of potent and specific inhibitors against AKR1C3. We have adopted this natural product scaffold and previous work in our lab has reported the synthesis and a preliminary SAR for AKR1C3 inhibition.<sup>79, 161, 251</sup> The dihydrocinnamoyloxy moiety of baccharin has been reported as a pharmacophoric structure for AKR1C3 inhibition, and other groups have synthesized potent AKR1C3 inhibitors based on this scaffold.<sup>252</sup> However, the hydrolytic liability due to the presence of an ester linkage made these analogues unsuitable for drug discovery. The hydrolysis of the ester leads to the formation of a metabolite will result in the revocation of the compound potency towards AKR1C3 inhibition.<sup>79</sup> Our lab has previously reported the rapid hydrolysis of baccharin *in vitro*, yielding the phenol drupanin which exhibits an  $IC_{50}$  of 15  $\mu$ M (Figure 11).<sup>79</sup> Baccharin was readily hydrolyzed, while the amide-based inhibitor, KV-37, displayed remarkable stability and half-life of >240 minutes.

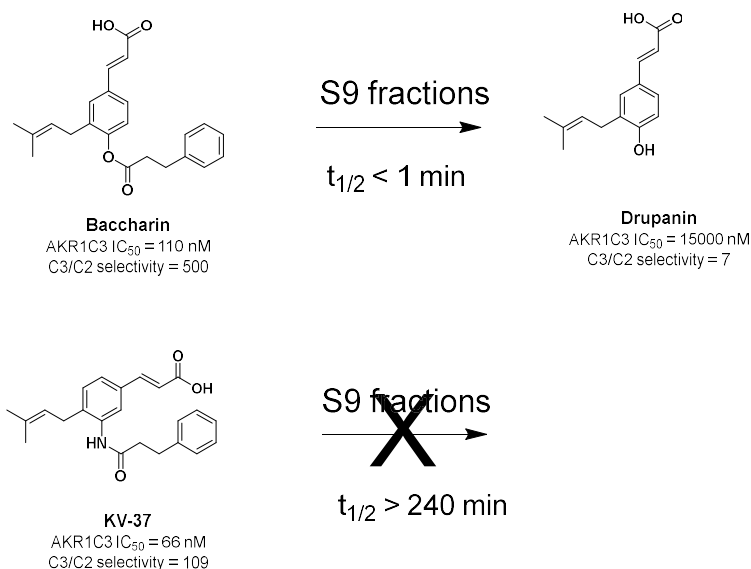


**Figure 11.** Metabolic actions of human S9 liver fractions on baccharin and KV-37.

Our prior studies have reported the design, synthesis, and evaluation of potent AKR1C3 inhibitors bearing a more stable amide bioisostere. First-generation inhibitor KV-37 has demonstrated high synergistic drug interaction in combination with ENZ, superior to that seen with INDO. Moreover, mechanistic studies reveal that KV-37 causes apoptotic cell death in ENZ-resistant PCa cell lines with a consequent reduction in PSA levels. This activity was further confirmed with *in vivo* studies that have shown significant reduction in tumor growth without observable toxicity.<sup>79</sup> The activity of KV-37 was also evaluated in AML cell lines and showed a 6-fold potentiation of etoposide and a 10-fold potentiation of daunorubicin antineoplastic effect.<sup>251</sup> The selectivity over C1 and C2 remained relatively low (109-fold). Continued efforts in our lab have identified second-generation, highly isoform-selective AKR1C3 inhibitors, KV-49a and KV-49g.<sup>161</sup> The two inhibitors possessed >2800-fold selectivity for AKR1C3 inhibition, with inhibitory potency retention in the nanomolar range (70 nM). Furthermore, these compounds provided >100-fold

potentiation to daunorubicin and cytarabine across a panel of AML cell lines and in primary patient-derived T-cell acute lymphoblastic leukemia cells (T-ALL).<sup>161</sup>

The aim of this chapter of the dissertation is to primarily continue the effort in our lab in the design, synthesis, and evaluation of AKR1C3 inhibitors this can be summarized in the following points:

1. Continuing the effort to explore the SAR of our hit scaffold, more specifically, explore the role of the prenyl chain in active compounds. Based on molecular docking done in our lab, we hypothesis that steric bulk at a fixed length from the central phenyl ring fills a unique open SP2 pocket in the AKR1C3 enzyme that is not present in other family members and will account for the high selectivity and potency of our developed compounds.
2. Scaling up the synthesis of KV-49a and KV-49g for *in vivo* studies. The first-generation inhibitor, KV-37, with an amide bioisostere, showed considerable improvement in *in vitro* PK ( $t_{1/2}$  = >240 minutes). However, it suffered from limited *in vivo* half-life. With the second-generation compounds, we hypothesize that the contraction of the linker chain between the amide bond and the terminal phenyl ring will increase the steric hinderance around the amide bond, making it more difficult to be cleaved by peptidases and improving the *in vivo* half-life and other PK properties.
3. Evaluating the effect of lead inhibitors, KV-49a and KV-49g, in PCa cell lines. More specifically, potentiating the effect of the recently approved PCa agents ARN and ODM. We hypothesis that AKR1C3 expression will correlate to the resistance of PCa cells to the recently approved agents and this resistance can be countered by AKR1C3 inhibition using our lead compounds.

Taken together, the experiments are designed to investigate these hypotheses to contribute to the SAR that leads to optimization of potency, selectivity, and PK optimization around the hit compound. Providing a 'drug-like' inhibitor for *in vivo* study.

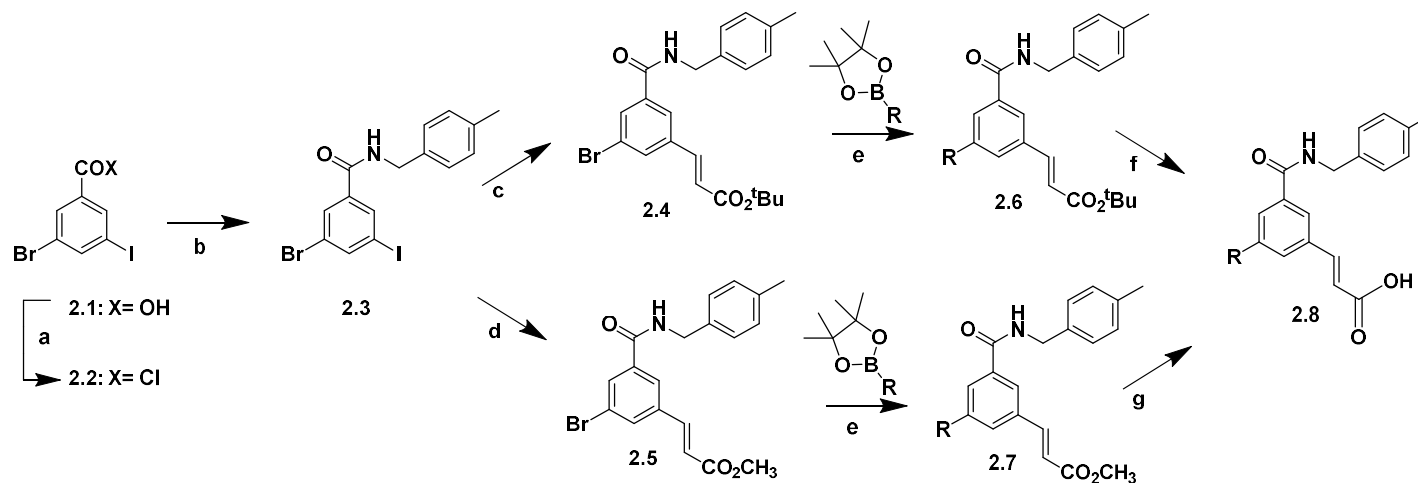
## 2.2. MATERIALS AND METHODS

A detailed account of chemistry procedures and characterization ( $^1\text{H}$  and  $^{13}\text{C}$  NMR and HRMS) is provided in Chapter four. The following sections describe the experiments used throughout this dissertation pertaining to synthesis of prenyl chain analogues, enzyme activity assay, cell culture, cell viability assays, western blotting,  $\text{IC}_{50}$  value determination, statistical analyses, quantification of the degree of synergism, and pharmacokinetic evaluation of AKR1C3 inhibitors.

### *Synthesis of Prenyl Chain Analogues*

We first aimed to scale-up the synthetic route that affords KV-49g. The synthetic route established in our lab for the synthesis of KV-49g (Scheme 1, c) was employed. Commercially available 3-bromo-5-iodobenzoic acid (**2.1**) was used as the common starting material for the synthesis of retroinverted amide linkage analogues. Conversion of **2.1** to its acid chloride **2.2** followed by amide coupling using 4-methylbenzylamine, yielded the amide intermediate **2.3** (98%). Utilizing the increased reactivity of iodine over bromide in **2.3**, it was coupled with *tert*-butylacrylate using the Mizoroki-Heck reaction<sup>253</sup> which chemoselectively yielded intermediate **2.4** (44%), followed by Suzuki-Miyaura cross-coupling reaction<sup>254</sup> with an appropriately substituted boronic acid pinacol ester installed side chain prenyl intermediate **2.6** (75%), that was subsequently refluxed with chromatography grade silica to hydrolyze the *tert*-butyl ester to afford the final compounds **2.8** (30%). The overall yield of this multi-step synthetic route was  $\approx 10\%$ . An alternative synthesis was then employed to improve this yield to obtain KV-49g in larger quantities for *in vivo* studies. In this synthesis (Scheme 1, d), we utilized methyl acrylate instead of *tert*-butylacrylate in the Mizoroki-Heck reaction to afford methylester-protected intermediate **2.5** (49%). Subsequent Suzuki-Miyaura reaction with a prenyl boronic acid



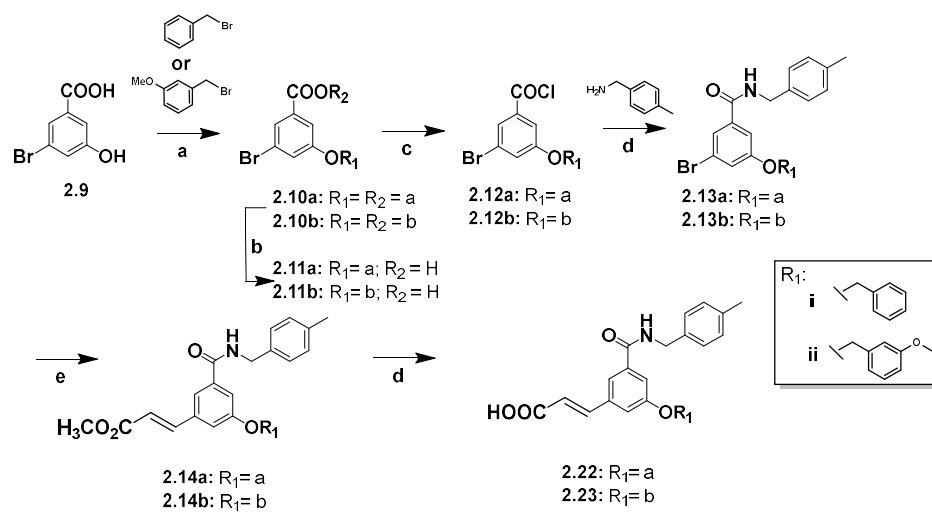


**Scheme 1.** Synthesis of prenyl chain derivatives.

**Reagents and conditions:** (a)  $\text{SOCl}_2$ , PhMe, reflux, 99%; (b) 4-methylbenzylamine, DMAP,  $\text{NEt}_3$ , DCM, 40 °C, 98%; (c) *tert*-butyl acrylate,  $\text{Pd}(\text{OAc})_2$ ,  $\text{P}(\text{Ph})_3$ ,  $\text{NEt}_3$ , PhMe, 110 °C, 37%; (d) methyl-butyl acrylate,  $\text{Pd}(\text{OAc})_2$ ,  $\text{P}(\text{Ph})_3$ ,  $\text{NEt}_3$ , PhMe, 110 °C, 54%; (e)  $\text{Pd}(\text{dppf})\text{Cl}_2$ ,  $\text{Cs}_2\text{CO}_3$ , DMF, appropriately substituted boronic acid pinacol ester, 90 °C; (f)  $\text{SiO}_2$ , PhMe, reflux, 30%; (g) NaOH, THF, quantitative.

pinacol ester was then employed to afford side chain intermediates **2.7** (73%). The intermediate was then hydrolyzed using sodium hydroxide<sup>255</sup> to obtain final compound **2.8** (95%). We found that the alternative synthesis provided a higher final compound yield than the original synthesis used in our lab, with an overall yield of  $\approx 35\%$ . This alternative route has helped scaling up the synthesis to produce higher quantities of final compounds with a 25% increase in yield.

To modify the prenyl side chain of the parent scaffold baccharin to the 1,3,5 *meta*-substituted pattern, the alternative synthetic route discussed above was employed. A detailed account of each compound synthesis and characterization (<sup>1</sup>H and <sup>13</sup>C NMR and HRMS) is provided in Chapter four. Ether analogues **2.22** and **2.23** were synthesized using 3-bromo-4-hydroxybenzoic acid as starting material which was reacted with benzyl bromide or 3-methoxy benzyl bromide with DIPEA as a base to install the ether side chain. After activating the carboxylic acid to an acid chloride, a reaction sequence of amide formation followed by Mizoroki-heck reaction and methyl-butyl ester hydrolysis afforded final compounds (Scheme 2).



**Scheme 2.** Synthesis of ether derivatives.

**Reagents and conditions:** (a) DIPEA, 150 °C; (b) KOH, MeOH, reflux; (c)  $\text{SOCl}_2$ , PhMe, reflux; (d) DMAP,  $\text{NEt}_3$ , DCM, 40 °C; (e) methyl-butyl acrylate,  $\text{Pd}(\text{OAc})_2$ ,  $\text{P}(\text{Ph})_3$ ,  $\text{NEt}_3$ , PhMe, 110 °C; (d)  $\text{SiO}_2$ , PhMe, reflux, 30%.

### ***Enzyme Activity Assay***

The enzyme activity screen for all compounds was performed in collaboration with the Penning lab at the University of Pennsylvania, as previously described.<sup>161</sup> The dehydrogenase activities of AKR1C isozymes were determined by measuring the UV absorption of NADH formation at 340 nm using a Beckman DU-640 spectrophotometer. A typical assay solution contained 100 mM potassium phosphate pH 7.0, 2.3 mM NAD<sup>+</sup>, 3.0 mM (S)-(+)-1,2,3,4-tetrahydro-1-naphthol (Sigma-Aldrich, CAS Number 529339), and 4% acetonitrile (v/v). The mixtures were incubated at 37 °C for 3 minutes followed by adding a serial dilution of AKR1C1, AKR1C2, AKR1C3 or AKR1C4 solution to a final volume of 1 mL to initiate the reaction. After continuously monitoring for 5 minutes, the increase in UV absorption was recorded using different concentrations of an enzyme to calculate the initial velocity and determine the specific activity of the enzyme.<sup>161</sup>

### ***Metabolic Stability Testing of AKR1C3 inhibitors***

The stability testing experiments were performed in collaboration with the Noelle Williams lab at the University of Texas Southwestern Medical Center. The two lead compounds, KV-49a and KV-49g (2 mM solution in DMSO), were incubated with male CD-1 murine liver S9 fractions containing a NADPH-generating system for 0 to 240 minutes at 37 °C. Reactions were quenched with 0.5 mL (1:1) of methanol/IS (IS; final conc. = 50 ng/mL). Samples were vortexed for 15 seconds, incubated at room temperature for 10 minutes, and spun for 5 minutes at 2,400 rpm. The supernatant (1 mL) was then transferred to an eppendorf tube, clarified by centrifugation for 5 minutes at 13,200 rpm at 4 °C, and transferred to an HPLC vial for analysis by Qtrap 4000 mass spectrometry using the following parameters: Ion Source/Gas Parameters: curtain gas = 50, collisional activated dissociation = low, ion spray voltage = 4,500, temperature = 700, nebulizing gas

GS1 = 70, drying gas GS2 = 70. Buffer A: water and 0.1% formic acid; Buffer B: Methanol + 0.1% formic acid; flow rate 1.5 mL/min; column Agilent C18 XDB column, 5 mm packing 50 x 4.6 mm size; 0-1.5 minutes 97% A, 1.5-2.0 minutes gradient to 100% B, 2.0-3.5 minutes 100% B, 3.5-3.6 minutes gradient to 97% A, 3.6-4.5 minutes 97% A; IS: tolbutamide (transition 271.2 to 91.2). Ion transitions followed were 364.276 [M-H] to 243.2 for KV-49a and 364.172 [M-H] to 104.9 for KV-49g.

### ***Pharmacokinetic evaluation of AKR1C3 inhibitors***

The PK *in vivo* experiments were performed in collaboration with the Noelle Williams lab at the University of Texas Southwestern Medical Center. To evaluate the PK properties of KV-49g, 21 female CD-1 mice were dosed intraperitoneal with 20 mg/kg. 0.2 ml/mouse formulated with 5 % DMSO, 5 % Cremaphor, 90% D5W (5% Dextrose in water). Whole blood was collected in a syringe coated with acid citrate dextrose. Plasma was processed from whole blood by centrifugation at 10,000 rpm for 10 minutes. Also collected was brain which was gently washed with 1x PBS to remove residual circulating blood. Then tissue was weighed and snap frozen in liquid nitrogen. For Standards and QC's (Bioreclamation LLC, lot number MSE284936), 98  $\mu$ L & 98.8  $\mu$ L of blank plasma was added to an eppendorf and spiked with 2  $\mu$ L & 1.2  $\mu$ L of initial standard (Warfarin). Note that 100  $\mu$ L of plasma was mixed with 200  $\mu$ L of methanol containing 0.15% formic acid and 12.5 ng/mL warfarin. The samples were vortexed for 15 seconds, incubated at room temperature for 10 minutes, and spun at twice at 13,200 rpm in a standard microcentrifuge. The supernatant was then analyzed by LC-MS/MS as described above to test the stability of the AKR1C3 inhibitors. Brain tissues were homogenized in 3x volume of PBS (x - weight of the tissue). For the standards and QC'S 98  $\mu$ L & 98.8  $\mu$ L of pooled blank brain was added to an eppendorf and spiked with 2 & 1.2  $\mu$ L of initial standard. Standards 's, QC's & samples

of 100  $\mu$ l were then mixed with 200  $\mu$ l of methanol containing 0.15% formic acid and 12.5 ng/ml warfarin. The samples were vortexed for 15 seconds, incubated at room temperature for 10 minutes and spun twice at 13,200 rpm in a standard microcentrifuge. The supernatant was then analyzed by LC-MS/MS.

### **Cell Culture**

The cell lines 22Rv1 and LNCaP (ATCC catalog numbers CRL-2505 and CRL-1740, respectively) were cultured in RPMI 1640 media (Fisher Scientific, catalog number 10131035) supplemented with 10% FBS, 100 U/mL penicillin, and 0.1 mg/mL streptomycin. LNCaP1C3 cells overexpressing AKR1C3 were generated by stable transfection of AKR1C3 plasmid as previously described.<sup>143</sup> All cell lines were authenticated via short tandem repeat analysis and tested for mycoplasma using the MycoAlert mycoplasma detection kit as per the manufacturer's instructions (Texas cancer cell repository) in May 2017, showing no contamination. Where indicated, cells were also cultured in charcoal-stripped (CSS) media prepared by supplementing RPMI 1640 without phenol red (Fisher Scientific, catalog number 11835030) with charcoal-stripped FBS (ThermoFisher Scientific, catalog number 12676011). All cells were maintained at 37 °C in a humidified incubator with 5% carbon dioxide. All compounds were diluted to 20 mM solution in DMSO and were serially diluted in cell culture media for cell treatments to a final concentration range of 0.01 to 100  $\mu$ M, maintaining the final DMSO concentration at less than 1%. Compounds used in the experiments were ENZ (Fisher Scientific, catalog number 501013979), INDO (Fisher Scientific, catalog number AAA1991006), ARN (VWR catalog number 75837196), and DARO (Fisher Scientific, catalog number 501873532).<sup>84</sup>

### ***Cell Viability Assays***

Cells were seeded at a density of 10,000 cells/well in 96-well plates and were incubated in either normal media or CSS media. For pretreatment experiments, cells were treated with AKR1C3 inhibitor, KV-49g or INDO, for 24 hours followed by the addition of ENZ, ARN or ODM and incubated for a further 72 hours. Cell viability was determined by the CellTiter 96 AQueous One Solution Cell Proliferation assay (MTS; Promega, catalog number G3580) as described previously.<sup>251</sup> No intrinsic absorbance was noted with ENZ, ARN, ODM, KV-49g, or INDO in the MTS assay.<sup>84</sup>

### ***Western Blotting***

Cells were washed once with PBS and lysed with RIPA buffer (Thermofisher Scientific, catalog number 89901). Proteins were quantified via BCA assay (Thermofisher Scientific, catalog number 23221) and then were resolved by SDS258 PAGE on 4–20% Tris-Glycine gradient gels (BioRad). After transfer to nitrocellulose membranes, blocking was conducted for 1 hour in Tris260 buffered saline (10 mM Tris-HCl, 100 mM NaCl, pH 7.5) containing 0.1% Tween-20 (TBST) and 1% BSA. Samples were probed overnight at 4 °C with anti-AKR1C3 (Sigma-Aldrich, CAS number A6229; mouse mAb, 1:500), anti-PSA (Cell Signaling Technology, catalog number 5877S, rabbit mAb, 1:1000), or anti- $\beta$ -actin (Sigma-Aldrich, CAS number A5441, mouse mAb, 1:1000), followed by incubation with anti-mouse (Sigma-Aldrich, CAS number SAB4600224) or anti-rabbit (Perkin-Elmer, catalog number NEF812001EA) secondary antibody (1:2000) horseradish peroxidase conjugate for 2 hours, and bands were quantified by densitometry using ImageJ software.<sup>84</sup>

### ***IC<sub>50</sub> Value Determination and Statistical Analyses***

For enzyme assays, the inhibitory potency for each compound was calculated by our collaborators at the Penning lab and represented by IC<sub>50</sub> values and measured as described before.<sup>155, 157, 256</sup> The IC<sub>50</sub> values of baccharin and baccharin analogues were determined by measuring their inhibition of the NADP<sup>+</sup>- dependent oxidation of S-tetralol catalyzed by AKR1C3 or AKR1C2. The concentrations of S-tetralol used in this assay for AKR1C3 and AKR1C2 were 165  $\mu$ M and 15  $\mu$ M, respectively, which were equal to the  $K_m$  value for each enzyme isoform to make a direct comparison of IC<sub>50</sub> values. The IC<sub>50</sub> value of each compound was acquired from a single experiment with each inhibitor concentration run in quadruplicate and directly calculated by fitting the inhibition data to an equation  $[y = (\text{range}) / [1 + (I / \text{IC}_{50})^S] + \text{background}]$  using Grafit 5.0 software. In this equation, “range” is the fitted uninhibited value minus the “background” and “S” is a slope factor. “I” is the concentration of the inhibitor. The equation assumes that y decreases with the increasing “I”. *For cell viability assays*, experiments were repeated at least thrice, and the statistical significance was calculated using the Student *t* test. A *P* value of <0.05 was considered statistically significant. IC<sub>50</sub> values were calculated by GraphPad prism software version 9.0.

### ***Quantification of the Degree of Synergism***

To quantify the degree of synergism, the results of the pretreatment experiments were analyzed by CompuSyn software (Paramus, NJ) based on the median-effect principle or “Chou–Talalay” method.<sup>257</sup> The method is based on the median-effect equation that encompasses the Michaelis–Menten, Hill, Henderson–Hasselbach, and Scatchard equations to provide combination and dose reduction indices.<sup>258</sup> The combination index (CI) and dose reduction index (DRI) values were calculated at a



constant ratio of a chemotherapeutic to AKR1C3 inhibitor at 50% cytotoxic effect ( $F_a = 0.5$ ). CompuSyn software was used to generate the CI and DRI values.  $CI < 1$ , synergism;  $CI > 1.1$ , antagonism; and  $CI = 1.1$ , additive.<sup>258</sup>

## 2.3. RESULTS AND DISCUSSION

### *Prenyl side chain modification*

The established SAR for baccharin outlined in table 2 has demonstrated that derivative **2.15**, the ester chain moved to the *meta* position relative to the acrylate, showed enhanced AKR1C3 inhibitory potency ( $IC_{50} = 0.088 \mu M$ ).<sup>251</sup> Further, improved potency was observed when the ester moiety was replaced with the amide bioisostere, derivative **2.16** ( $IC_{50} = 0.066 \mu M$ ).<sup>251</sup> Rearrangement of the substituents on the central ring to adopt a 1,3,5 substitution pattern greatly enhanced the selectivity for AKR1C3 inhibition over the highly related AKR1C1, 1C2, and 1C4 isoforms, as compared to baccharin. Compound **2.17** displayed inhibitory potency similar to that of baccharin with a 1.5-fold increase in selectivity over AKR1C2, and the selectivity over other AKR isoforms also increased.<sup>161</sup> The following structural change has introduced the most potent and selective derivative of baccharin developed in our lab, retroinversion of the amide to afford KV-49a, demonstrated an  $IC_{50}$  of 70 nM and isoform selectivity >2800-fold over AKR1C2, an increase of 5.6-fold as compared to baccharin. Selectivity over the other isozymes, AKR1C1 and AKR1C4, increased by 1.5 and 7-fold, respectively, when compared to baccharin.<sup>161</sup> Reduction of the carbon spacer length to a methyl group, along with substitution with methyl at the 4-position on the benzyl side chain, KV-49g, further increased the inhibitory potency when compared to baccharin ( $IC_{50} = 70 \text{ nM}$ ).<sup>161</sup> Molecular docking studies done in our lab allowed us to understand the molecular interactions that accounted for KV-49g superior selectivity and provided design parameters for further optimization through chemical derivative synthesis. The docking conformation of KV-49g within the AKR1C3 protein results in pi-pi stacking interactions between aromatic amino acids TYR216, TRP227 and PHE311, and aromatic constituents of the inhibitor which accounts for the enhanced affinity. Further, retro-inversion of the amide functionality within

the compound results in strong hydrogen bond formation between the amide carbonyl and TYR55 and HIS177 residues. In the designed all-*meta* substituted inhibitors, binding of the carboxylic acid takes place to the TRP227 residue and not the SER118, thus accounting for the increased selectivity of this structural scaffold. Further lead optimization by the addition of an electron withdrawing substituents is predicted to increase potency. This is predicted to occur by hydrogen bond accepting groups in this region of the molecule generating further binding interactions to the AKR1C3 TRP24 residue. Optimization of compound selectivity is also predicted by occupying the SP2 pocket of the enzyme by a steric bulk group that will account for hydrophobic interactions.

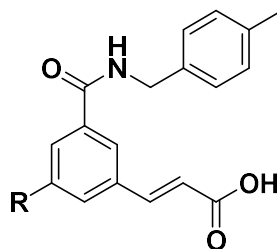
**Table 2.** Structure-activity relationship around the baccharin chemotype for AKR1C3 inhibition.<sup>161</sup>

Compound	Structure	IC <sub>50</sub> (μM)		Fold Selectivity 1C2:1C3
		AKR1C3	AKR1C2	
Baccharin		0.100	51.0	510
2.15		0.088	23.0	261
2.16		0.066	7.2	109
2.17		0.130	94.0	723
KV-49a		0.070	39% inhibition at 200 μM	>2800
KV-49g		0.070	66% inhibition at 200 μM	>2800

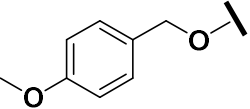
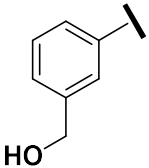
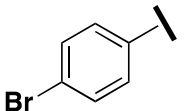
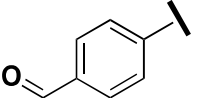
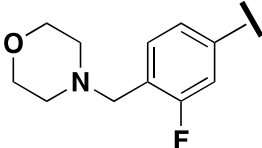
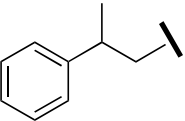
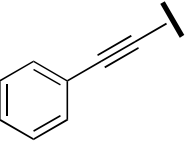
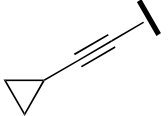
To explore the role of the prenyl chain in active compounds, 15 derivatives were explored (Table 3). Delays in compounds screening at the Penning lab due to the current pandemic affected our efforts in synthesizing more compounds. The base scaffold of our synthesis was our lead candidate KV-49g, as it possessed the highest potency and selectivity, moreover, enhanced 'drug-like' PK profile. We hypothesized that a steric bulk at a fixed length from the central phenyl ring fills a unique open pocket in the AKR1C3 enzyme, thus accounting for the high selectivity of our developed compounds. Evaluating the library of compounds have demonstrated that removal of the prenyl side chain (**2.18**) completely abrogated activity. Replacement of the prenyl side chain with an allyl group (**2.19**) resulted in loss of isoform selectivity and potency. Substitution of the prenyl with either a *cis* or *trans* pentene side chain, compound **2.20** and **2.21**, respectively, resulted in equipotent analogous but reduced selectivity. The ether analogues with phenyl and 4-methoxymethyl benzene (**2.22** and **2.23**) suffered a significant loss in selectivity over AKR1C2 and decrease in inhibition potency. Replacement of the prenyl chain with a 3-hydroxymethylphenyl moiety (**2.24**) reduced AKR1C3 inhibitory potency as well as selectivity. While the 4-bromophenyl analogue (**2.25**) was generally well tolerated, maintaining the inhibition potency when compared to KV-49g and retained moderate selectivity over the AKR1C2 isoform. This suggested that an electron withdrawing substitution on a benzyl ring side chain retains the potency of the inhibitor. In order to explore if a dipole-dipole interaction may be present between, aldehyde functional group was explored. The potency of the inhibitor was reduced with the replacement of the prenyl with a 4-methylbenzaldehyde moiety (**2.26**), suggesting that a polar group in close proximity to the benzene ring to have stronger binding. The replacement with a 4-(2-fluoro-4-methylbenzyl)morpholine moiety (**2.27**) also reduced potency and selectivity, suggesting that a polar bulky side chain affects the inhibitor binding to the enzyme.

Substitution with a side chain that contains an alkyne linker and one phenyl ring or a cyclopropane (**2.28**, **2.29** or **2.30**) resulted in decreased potency and selectivity, suggesting that the rigidity of the alkyne linker hinders the phenyl or the cyclopropane ring from forming hydrophobic interactions. Whereas biphenyl (**2.31**) substitution resulted in the identification of the most potent inhibitor in this class ( $IC_{50} = 50$  nM). The compound retained selectivity against AKR1C1 and AKR1C2 isoforms but lower selectivity towards AKR1C4. This supports our hypothesis that steric bulk at a fixed length from the central phenyl ring fills a unique open pocket in the AKR1C3 enzyme that is not present in other family members and the presence of the biphenyl side chain increases the hydrophobic (pi-pi stacking) interactions. However, the increase in length from the central phenyl ring with a steric bulk as in compound **2.32** with a tolyl-carbazole moiety decreased potency and slightly lowered selectivity towards AKR1C3.

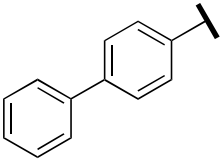
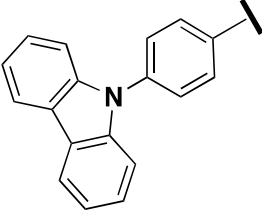
Further work is ongoing to fully probe the SAR of this class. As a preliminary SAR for the compounds discussed above, a phenyl side chain with an electron withdrawing group retains potency and a chain length from the central phenyl with at least three carbons is required to reach into the open pocket.

**Table 3.** Structure, inhibitory and selectivity properties of prenyl chain analogues.

Compound	Structure	IC <sub>50</sub> (μM)				Fold selectivity vs isoforms		
		AKR1C1	AKR1C2	AKR1C3	AKR1C4	C1	C2	C4
Baccharin		187	51	0.10	21	1870	510	210
KV-49g		No inhibition at 200 μM	66% inhibition at 200 μM	0.07	145	>2800	>2800	2042
2.18	Br	5% inhibition at 100 μM	22% inhibition at 100 μM	0.29 ± 0.03	39.8 ± 1.3	>359	>359	143
2.19		N.D.	88	0.26 ± 0.01	N.D.	N.D.	400	N.D.
2.20		80.9 ± 5.1	15.8 ± 2.5	0.08 ± 0.012	25.4 ± 3.1	1079	211.24	339
2.21		34% inhibition at 100 μM	39.4 ± 9.1	0.11 ± 0.0069	69.6 ± 11.0	>929	366.07	647
2.22		N.D.	28.8 ± 5.9	0.16 ± 0.0243	6.5 ± 0.6	N.D.	163	N.D.

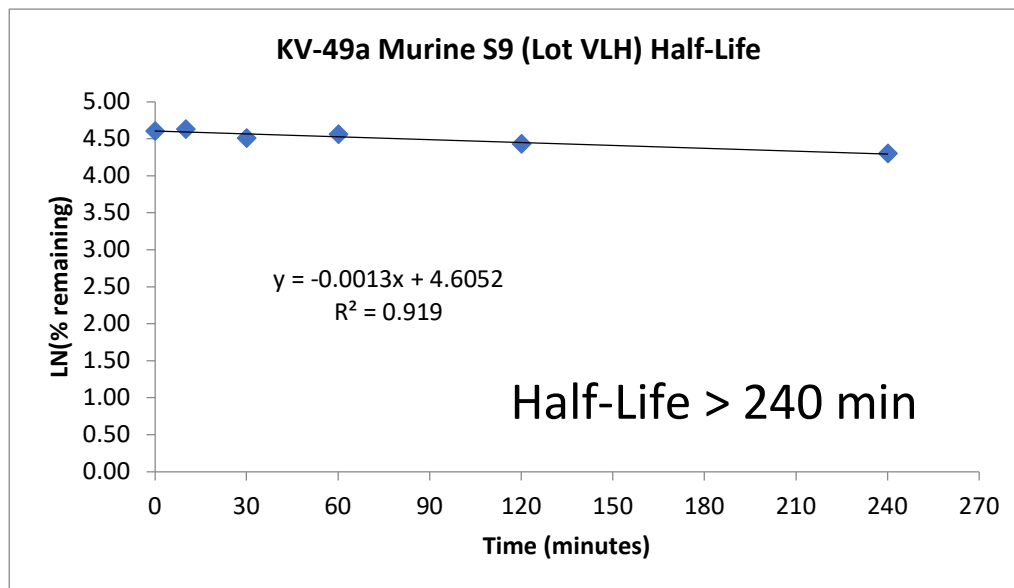
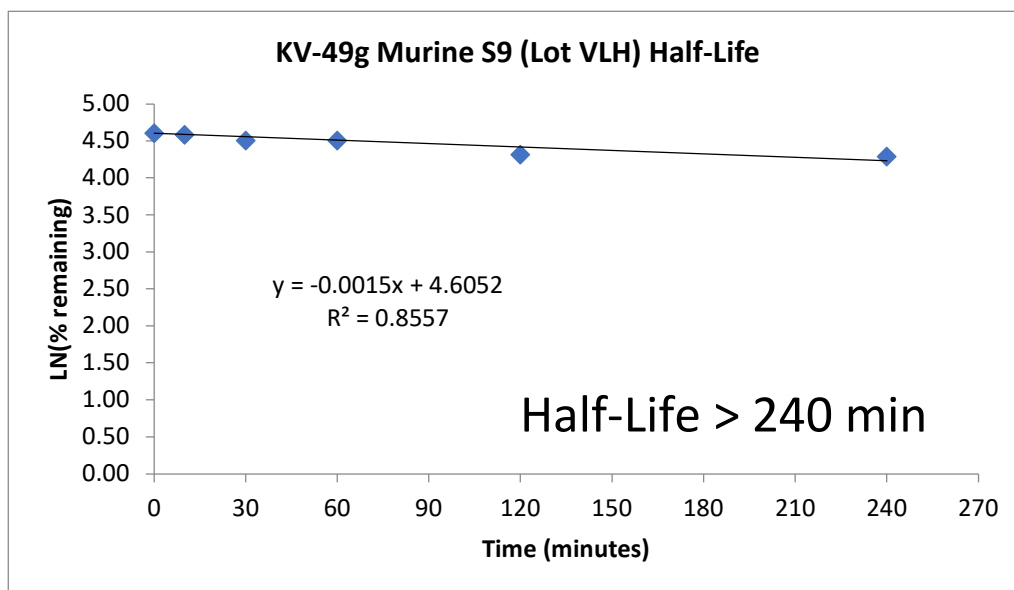
2.23		N.D.	18	$0.29 \pm 0.0141$	N.D.	N.D.	62	N.D.
2.24		N.D.	40 % inhibition at 100 $\mu$ M	$0.33 \pm 0.0143$	N.D.	N.D.	>300	N.D.
2.25		N.D.	$25.1 \pm 6.7$	$0.094 \pm 0.0035$	N.D.	N.D.	267.97	N.D.
2.26		36% inhibition at 100 $\mu$ M	31% inhibition at 100 $\mu$ M	$0.243 \pm 0.03$	$25.5 \pm 3.55$	>411	>411	104
2.27		N.D.	$5.1 \pm 0.6$	$0.330 \pm 0.1053$	N.D.	N.D.	15.49	N.D.
2.28		N.D.	$155.4 \pm 70.7$	$0.880 \pm 0.08$	N.D.	N.D.	176.61	N.D.
2.29		N.D.	$11.1 \pm 3.1$	$0.180 \pm 0.01$	N.D.	N.D.	62.18	N.D.
2.30		N.D.	$36.8 \pm 9.6$	$0.480 \pm 0.0389$	N.D.	N.D.	76.84	N.D.



<b>2.31</b>		31% inhibition at 100 $\mu$ M	$28.5 \pm 4.8$	$0.050 \pm 0.0039$	$2.4 \pm 0.146$	>620	568	48
<b>2.32</b>		$35.7 \pm 5.5$	$30.5 \pm 2.8$	$0.143 \pm 0.0149$	$10.5 \pm 3.10$	249	213	73

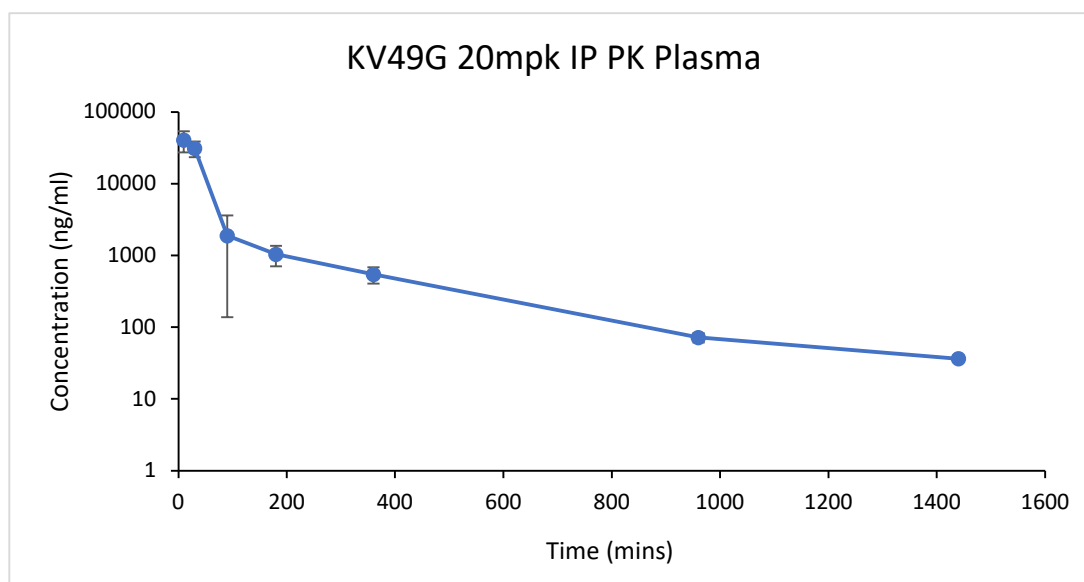
***Evaluation of pharmacokinetic properties of selected lead compounds***

The hit compound baccharin is highly metabolically labile, undergoing rapid hydrolysis to yield the phenol drupanin, which exhibits an AKR1C3 IC<sub>50</sub> of 15  $\mu$ M and only seven-fold selectivity over AKR1C2.<sup>259</sup> To compare the hydrolytic stability of lead compounds, we collaborated with Noelle Williams lab at the University of Texas Southwestern Medical Center for metabolic stability testing of our synthesized compounds. Baccharin and the two lead compounds, KV-49a and KV-49g, were subjected to incubation with mouse S9 fractions in the presence of phase I co-factors from 0-240 minutes. Aliquots were withdrawn and analyzed by LC-MS at various time points. As expected, baccharin was readily hydrolyzed ( $t_{1/2}$  = <1 min), and upon analysis of the mass transitions and fragmentation patterns, it was observed that baccharin was cleaved at the ester site and transformed to the corresponding phenol, (*E*)-3-[4-Hydroxy-3-(3-methyl-2-butenyl) phenyl]acrylic acid (drupanin). While the amide bioisostere, KV-49a and KV-49g, displayed remarkable stability and half-life of >240 minutes (Figure 12).

**A****B**

**Figure 12.** Half-life of lead compounds.  
A) KV-49a B) KV-49g incubated with murine liver S9 fractions.

We then scaled up the synthesis for the lead compound KV-49g for *in vivo* studies. The analysis of the PK properties of the lead compound *in vivo* (CD-1 mice) has demonstrated a more 'drug-like' pharmacokinetic profile suitable for initiating proof-of-concept potentiation effect in mice. The peak plasma concentration ( $C_{\max}$ ) was determined to be 40.5  $\mu\text{g/mL}$ , and  $T_{\max}$ , AUC,  $V_z/F$ , and  $CL/F$  were calculated (Figure 13). *In vivo* PK data in CD-1 mice of KV-49g demonstrated a more 'drug-like' PK profile with  $t_{1/2} > 240$  minutes and improved plasma concentration. Such PK properties of KV-49g are suitable for initiating proof-of concept potentiation effect in T-ALL PDX mice. We hypothesize that the improvement in *in vivo* half-life and other properties, compared to hit compound baccharin, is due to the substitution to an amide bioisostere and the linker chain's contraction between the amide bond and the terminal phenyl ring. Removing a methylene group and modifying from an ethyl linker to a methyl linker increases steric hinderance around the amide bond, making it more difficult to be cleaved by peptidases.



$t_{1/2}$ (min)	237
$C_{max}$ ( $\mu\text{g/mL}$ )	40.5
$T_{max}$ (hr)	0.17
AUC (h.ng/mL)	39,914
$V_z/F$ (mL/Kg))	2839
$CL/F$ (mL/min)	8.2

**Figure 13. Pharmacokinetic profile of KV-49g in CD-1 mice.**

### ***KV-49g Counters PCa Cell Resistance to Chemotherapeutics***

Significant upregulation of the androgen biosynthetic pathway enzyme AKR1C3 is observed in CRPC primary patient tumor samples.<sup>18</sup> The enzyme produces DHT, the predominant intracellular transcriptional signal to androgen-responsive genes in intact human prostate cells.<sup>260</sup> Overexpression of AKR1C3 has been shown to enhance human PCa resistance to a variety of chemotherapeutics.<sup>78, 79</sup> Hence, the delivery of a pharmacological AKR1C3 inhibitor represents a promising therapeutic strategy to manage CRPC and combat the emergence of resistance to clinically employed therapeutics.<sup>251</sup> Our program to discover structurally novel AKR1C3 inhibitors,<sup>259</sup> led to the synthesis of AKR1C3 inhibitor, KV-37, which potentiated the chemotherapeutic effect of ENZ *in vitro*,<sup>79</sup> and the development of KV-49g, the most potent and selective AKR1C3 inhibitor of this chemotype ( $IC_{50} = 70$  nM, >2800-fold selectivity).<sup>161</sup> This inhibitor demonstrated activity as a chemotherapeutic potentiator in the hematological malignancies AML and T-ALL, both of which overexpress AKR1C3.<sup>19, 147</sup>

In this section, we report that elevated AKR1C3 expression in PCa cell lines confers resistance to the recently approved AR antagonists, ARN and ODM. While the structural similarity of ARN with ENZ would suggest this was to be expected, the widely divergent chemotype of ODM may have been hoped to be free from AKR1C3-mediated resistance; unfortunately, this is not the case. Gratifyingly, 24 hours pretreatment of high AKR1C3 expressing PCa cells with our highly potent and selective AKR1C3 inhibitor, KV-49g, abolishes ARN and ODM resistance, leading to increased rates of PCa cell death and a significant decrease in PSA expression, a biomarker directly correlated to the severity of the disease. Additionally, KV-49g provides more substantial potentiation effect than INDO. The clinically approved agent INDO, a compound that possesses relatively low AKR1C3 activity ( $IC_{50} = 2.3$   $\mu$ M, 22 fold selectivity),<sup>136</sup> is currently the subject of a

clinical trial to evaluate its effect in overcoming ENZ resistance in treating patients with recurrent or metastatic CRPC.<sup>142</sup>

Resistance to ARN was noted shortly after its approval and associated with AR gene mutation, *AR* F877L.<sup>83</sup> However, the overall frequency of detected mutations in resistant subjects suggests that *AR* F877L is not the most common contributor to *de novo* or acquired resistance, suggesting a different mechanism of resistance development predominates.<sup>261</sup> At the time we published this research, to the best of our knowledge, it was the first report of resistance to ODM in PCa. To determine the baseline effect of ARN and ODM in a range of PCa cell lines expressing variable levels of AKR1C3, we employed three PCa cell lines; LNCaP (AKR1C3 null), 22Rv1 (AKR1C3 expressing),<sup>79</sup> and LNCaP cells overexpressing AKR1C3, generated by stable transfection of AKR1C3 plasmid as previously described (termed LNCaP1C3).<sup>143</sup> Each cell line was cultured either in normal conditions using RPMI media or in androgen-deprived conditions using CSS media. Our lab has previously reported that LNCaP, 22Rv1 and LNCaP1C3 cells cultured in CSS media overexpress AKR1C3 as a mechanism to counter the androgen-deprived conditions of CSS.<sup>79</sup> The IC<sub>50</sub> values of ARN and ODM in the three PCa cell lines were directly compared (Table 4). Increasing IC<sub>50</sub> values were observed directly correlated to the increased expression of AKR1C3; 11 µM in LNCaP cells, 77 µM in 22Rv1 cells and 101 µM in LNCaP1C3 cells. Moreover, when AKR1C3 expression was induced further using CSS media, the IC<sub>50</sub> values of ARN increased; LNCaP < 22Rv1 < LNCaP1C3 cells which were calculated to be 42, 203 and 134 µM, respectively. Similarly, when the IC<sub>50</sub> values of ODM in PCa cells were calculated, a direct correlation to AKR1C3 expression was observed, 16 µM in LNCaP cells, 46 µM in 22Rv1 and 100 µM in LNCaP1C3 cells. Again, when AKR1C3 expression was further induced by culture in CSS media, increased IC<sub>50</sub> values were noted; 31, 74 and 175 µM in LNCaP, 22Rv1 and LNCaP1C3 cells,

respectively. These data strongly correlate the expression of AKR1C3 in PCa cells to the development of resistance to both ARN and ODM chemotherapeutics.

**Table 4.** The IC<sub>50</sub> values of ARN and ODM in the three PCa cell lines.

Chemotherapeutic	LNCaP		22Rv1		LNCaP1C3	
	RPMI	CSS	RPMI	CSS	RPMI	CSS
ARN	11	42	77	203	101	134
ODM	16	31	46	74	100	175

IC<sub>50</sub> is shown in  $\mu\text{M}$  concentration. RPMI media: imitate normal conditions. CSS media (Charcoal stripped serum media): imitate androgen-deprived conditions/CRPC conditions.

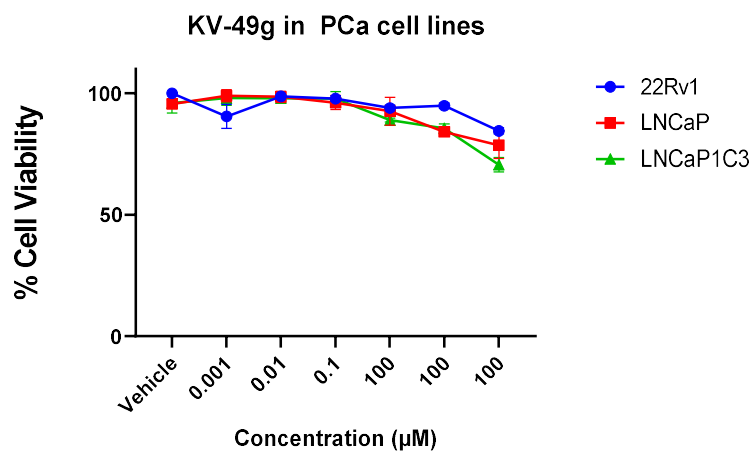


**Figure 14.** Percentage of cell viability of KV-49g in PCa cell lines.



To evaluate the effect of our AKR1C3 inhibitor KV-49g to resensitize these cell lines to the action of ARN and ODM, we first screened for its inherent antineoplastic effect. Consistent with our previous findings,<sup>161</sup> KV-49g did not induce cytotoxicity up to 100  $\mu$ M in any of the cell lines (Figure 14). We previously demonstrated 24 hours pretreatment of AKR1C3 inhibitor in PCa cell lines, followed by chemotherapeutic, resulted in significant synergistic effects,<sup>79, 161</sup> and this same strategy was applied herein. In LNCaP cells, no significant difference was observed between pretreatment of AKR1C3 inhibitor and either ARN or ODM alone due to the low expression of AKR1C3 (Figure 15A and 14C). In LNCaP1C3 cells, with extremely high expression of AKR1C3, a significant potentiation effect was observed upon 24 hours pretreatment of AKR1C3 inhibitor compared to ARN or ODM alone (Figure 15B and 14D). Concentrations of KV-49g as low as 0.1  $\mu$ M potentiated 1  $\mu$ M of ARN, resulting in a 35% decrease in cell viability. A similar synergistic effect was seen with 1  $\mu$ M of KV-49g and 10  $\mu$ M of ODM. A dose-response relationship was observed. These data clearly support that inhibiting AKR1C3 as a therapeutic strategy to counter resistance to ARN and ODM.

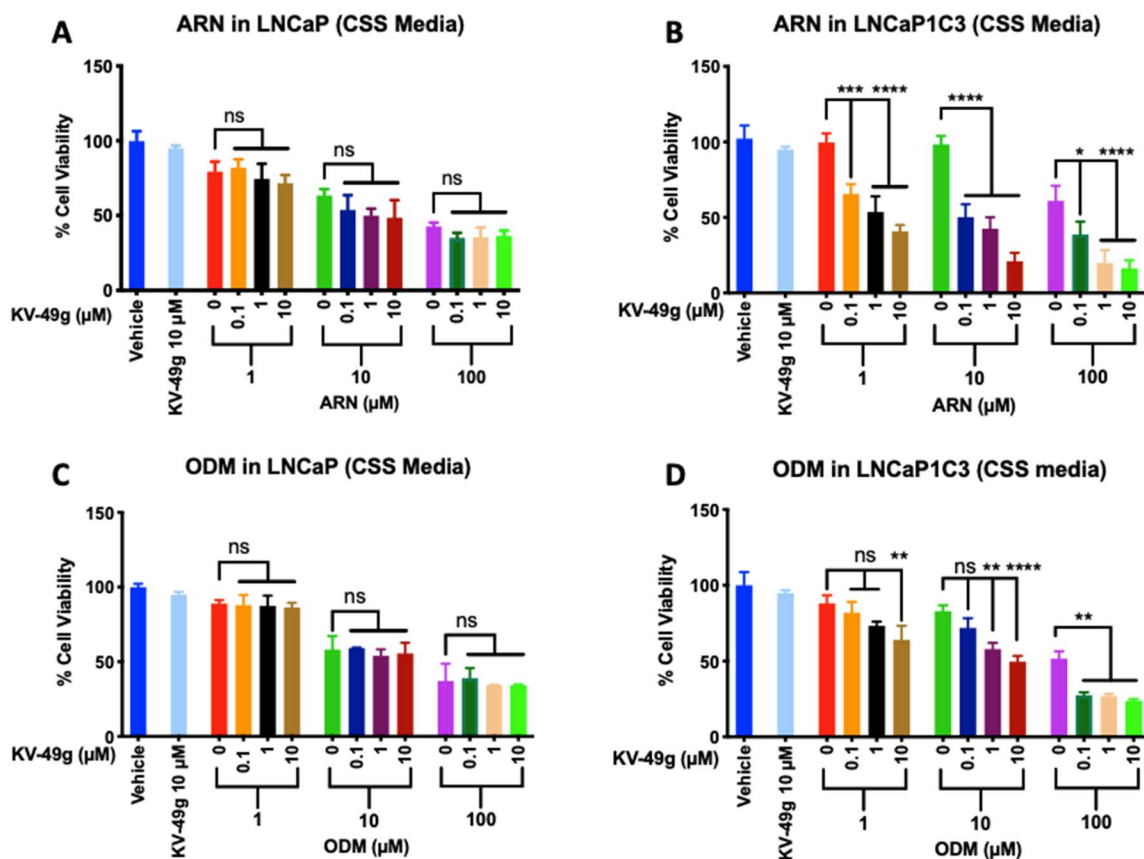


**Figure 15.** Combination effects of KV-49g and ARN or ODM.

KV-49g and ARN in A) LNCaP and B) LNCaP1C3 cells. KV-49g and ODM in C) LNCaP and D) LNCaP1C3 cells. One-way ANOVA; 95% Confidence Interval; \*,  $p < 0.05$ ; \*\*,  $p < 0.001$ ; \*\*\*,  $p < 0.0002$ ; \*\*\*\*,  $p < 0.0001$ ; ns = no significance.<sup>84</sup>

To further evaluate the synergistic effect, we screened the same combination treatment in 22Rv1 cells grown in CSS, which results in AKR1C3 expression levels similar to clinical samples. A remarkable synergistic effect was observed with both ARN and ODM (Figure 16A). Concentrations of KV-49g, as low as 0.1  $\mu$ M, were capable of potentiating ARN effect in 22Rv1 cells. Pretreatment with 1  $\mu$ M of KV-49g and just 10  $\mu$ M of ARN resulted in >60% loss of cell viability. The  $IC_{50}$  of ARN in this cell line is 203  $\mu$ M. Immunoblotting analysis revealed that treatment of 22Rv1 cells with 50  $\mu$ M of ARN alone resulted in induction of AKR1C3 by two-fold, further correlating expression of the enzyme to resistance. Almost no change in PSA expression was observed (Figure 16B). However, 24 hours pretreatment with just 1  $\mu$ M of KV-49g resulted in reduced AKR1C3 expression, with a remarkable five-fold decrease in PSA expression.

Likewise, the combination of KV-49g and ODM provided a significant potentiation effect, 0.1  $\mu$ M of KV-49g was sufficient to sensitive 22Rv1 cells to a 10  $\mu$ M concentration of ODM, with 1  $\mu$ M of KV-49g sufficient to sensitize the cell line to just 1  $\mu$ M of ODM (Figure 16C). Immunoblotting analysis revealed a three-fold increase in AKR1C3 expression upon exposure to 50  $\mu$ M of ODM, which was accompanied by overexpression of PSA (Figure 16D). Pretreatment of the cell line with KV-49g for 24 hours at concentrations as low as 0.1  $\mu$ M induced an approximate three-fold reduction in AKR1C3 expression which was accompanied by a marked reduction in PSA expression. Collectively, this data demonstrated that KV-49g, through inhibition of AKR1C3 activity, resensitizes 22Rv1 PCa cells to both ARN and ODM treatment and induces a marked loss of cell viability and reduction of PSA expression.

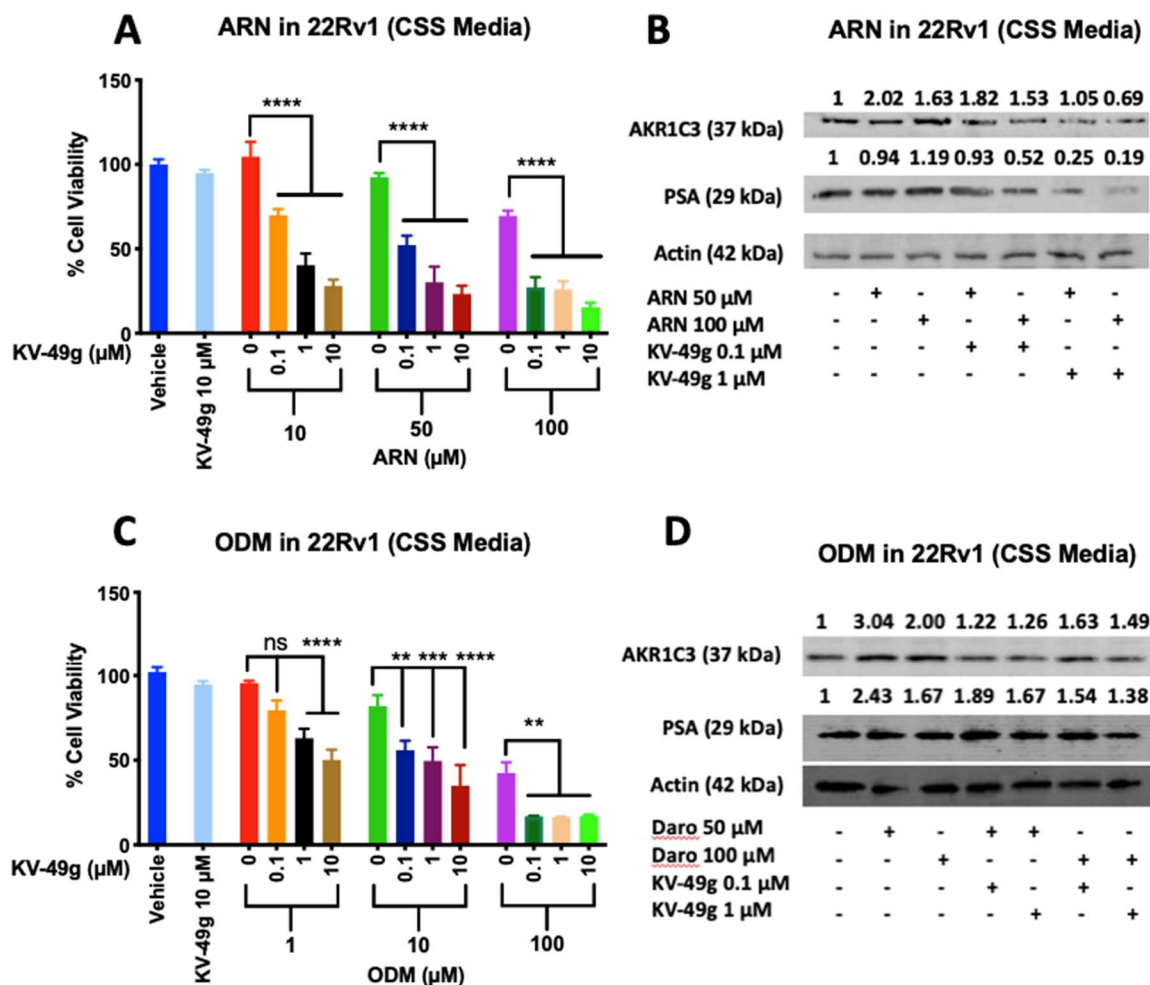


**Figure 16.** Combination of 24 hours pretreatment of KV-49g followed by 72 hours treatment with ARN or ODM in 22Rv1 cells (grown in CSS). A, C) cell viability. B, D) immunoblots of AKR1C3 and PSA expressions. One-way ANOVA; 95% Confidence Interval; \*\*,  $p < 0.001$ ; \*\*\*,  $p < 0.0002$ ; \*\*\*\*,  $p < 0.0001$ ; ns = no significance.<sup>84</sup>

The cyclooxygenase inhibitor INDO elicits AKR1C3 inhibition. However, it has lower potency and selectivity (AKR1C3  $IC_{50}$  = 2.3  $\mu$ M, 22-fold selectivity) vs KV-49g (AKR1C3  $IC_{50}$  = 70 nM, >2800-fold selectivity).<sup>161</sup> To directly compare the effect of both compounds to resensitize 22Rv1 cells (grown in CSS) to the effects of ARN or ODM, the effect of INDO alone was determined. No significant toxicity was observed until 100  $\mu$ M. In subsequent combination experiments, the clinically determined maximum blood concentration of ARN and ODM (12  $\mu$ M) was employed.<sup>84</sup> Gratifyingly, 24 hours pretreatment of KV-49g at just 0.1  $\mu$ M showed a significant effect in sensitizing 22Rv1 cells (CSS) to the action of both ARN and ODM (Figure 17A and 16C). A much lower potentiation effect was observed upon 24 hours pretreatment of INDO followed by ARN or ODM; 1  $\mu$ M of KV-49g was sufficient to induce 50% cell death when combined with 12  $\mu$ M ARN, while 1  $\mu$ M of INDO produced no statistically significant effect. Indeed, 10  $\mu$ M of INDO induced just 40% cell death when combined with 12  $\mu$ M of ARN. A similar effect was observed on AKR1C3 and PSA expression (Figure 17B and 16D). Pretreatment with 1  $\mu$ M of KV-49g and exposure to ARN resulted in the same reduction of PSA expression (50%) as the 10  $\mu$ M concentration of INDO. A combination of 24 hours pretreatment of KV-49g followed by exposure to ODM resulted in an even greater difference. A concentration of 1  $\mu$ M of KV-49g was more effective than 10  $\mu$ M of INDO to decrease PSA expression by 50% and 30%, respectively. This data shows that the more potent and selective AKR1C3 inhibitor, KV-49g, is more effective than the weaker, less selective INDO to resensitize 22Rv1 cells (CSS) to the cytotoxic action of both ARN and ODM.

Quantification of the degree of synergism in 22Rv1 cell lines (CSS) was performed using the Chou–Talalay method (Table in Figure 17).<sup>257</sup> Combination of KV-49g with either ARN or ODM resulted in high synergism and 126-fold or 75-fold dose-reduction indices (DRI), respectively. Combination treatment with INDO resulted in only 8-fold and 21-fold

DRI with ARN and ODM, respectively. Notably, combining KV-49g delivered IC<sub>50</sub> values for both ARN and ODM at or below the maximum concentration levels attainable in patients (12 µM).

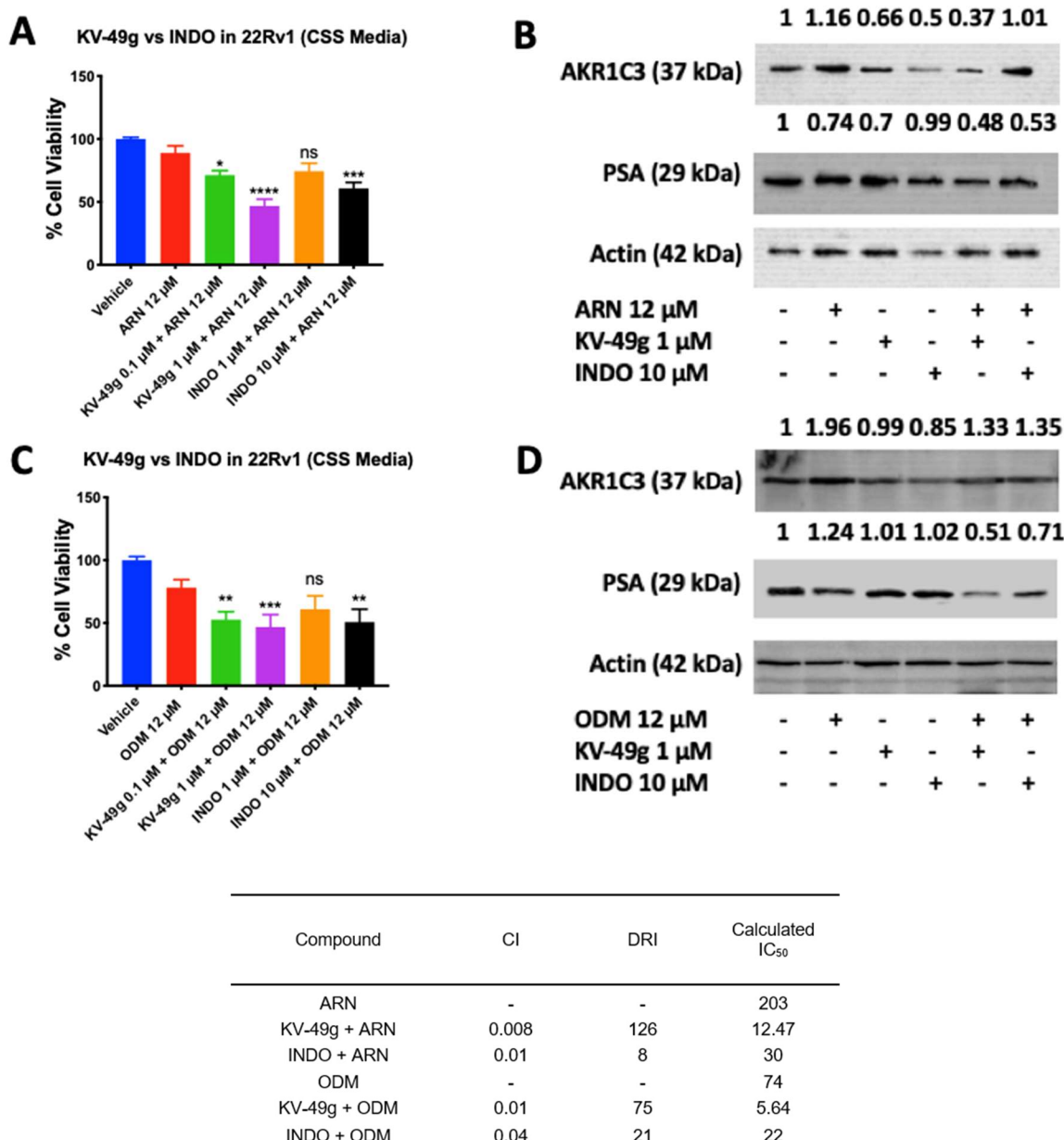


**Figure 17.** Combination of 24 hours pretreatment of KV-49g or INDO prior to 72 hours treatment with 12 µM of ARN or ODM in 22Rv1 cells (grown in CSS). A, C) cell viability. B, D) immunoblotting of AKR1C3 and PSA expression. Table represents calculated combination index (CI) and dose-reduction index (DRI) of treatment combinations in 22Rv1 cells grown in CSS media. One-way ANOVA; 95% Confidence Interval; \*,  $p < 0.05$ ; \*\*,  $p < 0.001$ ; \*\*\*,  $p < 0.0002$ ; \*\*\*\*,  $p < 0.0001$ ; ns = no significance.<sup>84</sup>

In summary, we report for the first time, to the best of our knowledge, AKR1C3 overexpression is a critical regulator of resistance to the newly approved AR antagonists ARN and ODM in CRPC. Inhibition of AKR1C3 via a potent and highly selective compound, KV-49g, resensitized PCa cells to the chemotherapeutic effect of both clinical agents, completely countering resistance. Thus, pharmacological inhibition of AKR1C3 is a promising target to counter drug-resistant PCa and KV-49g represents an advanced lead compound for pre-clinical evaluation.



## 2.4. CONCLUSION AND FUTURE DIRECTIONS

A preliminary SAR for prenyl side chain modification of the parent lead compound, KV-49g, was performed. Several other derivatives are currently under investigation to fully elucidate the SAR of the side chain. Scale-up synthesis for KV-49g was achieved (up to 25 % yield increase) and paved the way for synthesizing the bulk amount of the compound for *in vivo* PK studies. The metabolic stability and PK profile of KV-49g demonstrated 'drug-like' properties suitable for *in vivo* experiments. Dosing strategy for proof-of-principle studies in a PDX mouse model is currently being formulated by evaluating our lead compounds in a broad range of lymphoid patient-derived cells to determine the suitable malignancy for our lead compounds and defining a safe and effective dose. Lastly, the evaluation of both ARN and the structurally distinct ODM in inducing AKR1C3 expression in *in vitro* models of PCa was reported. This led to an AKR1C3-mediated resistance which can be countered by pretreatment with a potent and highly selective AKR1C3 inhibitor, KV-49g, sensitizing high AKR1C3 expressing PCa cell lines to the action of both chemotherapeutics with a concomitant reduction in expression of AKR1C3 and the biomarker PSA.

### **CHAPTER 3: DESIGN, SYNTHESIS AND EVALUATION OF ABAD INHIBITOR**

### 3.1. INTRODUCTION

The importance of the ABAD enzyme originates from its involvement in many physiological functions. It is considered essential for normal neuronal development and functioning of mitochondria,<sup>8, 262</sup> whereas any defects in its expression or function lead to disruptions in homeostasis. The loss of ABAD function in *HSD17B10* gene knock-out mice embryos results in mitochondrial dysfunction that leads to apoptosis and death in the early stages of embryogenesis, as shown in studies using mice and *Xenopus* embryos.<sup>263-265</sup> Other studies have shown that ABAD gene mutations and duplications lead to pathological phenotypes such as mental retardation.<sup>266</sup> This implicates that the balance of ABAD expression has an essential role in cell survival, which is independent of its catalytic activity.<sup>267</sup>

In AD, it has been shown that ABAD is upregulated in the brains of AD mice and AD patients.<sup>268, 269</sup> It has been suggested that the binding of A $\beta$  changes the enzyme's conformation, which in part exacerbates mitochondrial dysfunction induced by A $\beta$ . Thus, in an environment rich in A $\beta$ , the protective properties of ABAD appear to be negated. The involvement of ABAD in the metabolism of the potent human estrogen that has neuroprotective roles, 17 $\beta$ -estradiol, provides a possible link between ABAD's physiological functions and pathology of AD.<sup>270</sup> Furthermore, it was found that ABAD contributes to the metabolic stress-protective response by utilization of ketone bodies, especially  $\beta$ -hydroxybutyrate for energy production in an energy-deficient environment and can degrade aldehydes, such as 4-hydroxy-2-nonenal, which is a product of lipid peroxide metabolism and is highly toxic and capable of promoting neuronal death.<sup>271</sup> Several essential roles for ABAD have been linked to metabolic homeostasis related to energy metabolism and catabolism of isoleucine and branched-chain fatty acids.<sup>272</sup> Taken together, these findings indicate that ABAD plays a vital role in neuroprotection in AD, and

the formation of the A $\beta$ -ABAD interaction leads to an imbalance in neurosteroid levels, mitochondrial dysfunction, and neuronal death.<sup>24</sup> Elevated levels of ABAD in AD may be a feedback mechanism to restore the decreased level of enzyme activity that is apparent by its binding to intracellular A $\beta$ .<sup>273</sup> Perhaps ABAD confers a chain reaction role in AD where intracellular A $\beta$  binding blocks its enzymatic function, causing the accumulation of toxic metabolites controlled by ABAD, which leads to a compensation mechanism that elevates the expression of the enzyme. The overexpressed enzyme contributes to lowering neuroprotective estradiol levels, leading to insufficient expression of A $\beta$  clearing factors controlled by estradiol. Lack of adequate clearance of intracellular A $\beta$  then causes its accumulation and aggregation and increases binding to ABAD enzyme, and the process continues (Figure 18). Thus, disruption of the A $\beta$ -ABAD protein-protein interaction and restoring its physiological level, or inhibition of the overexpressed enzyme could lead to the resurrection of neuroprotective effects of ABAD. Based on these findings, human ABAD is considered a potential drug target for AD.<sup>24</sup> Inhibitors discovered so far were shown to benefit AD models, both *in vitro* and *in vivo*. These inhibitors can inhibit ABAD activity with an IC<sub>50</sub> ranging from low micromolar to nanomolar level.<sup>25, 220, 235, 237, 238, 240, 274,</sup>  
<sup>275</sup> These inhibitors provide a starting point for further development of novel and more effective compounds.

The development of small molecule inhibitors of ABAD is in the nascent stage and can be divided into four scaffolds; fused pyrazole compounds,<sup>235</sup> benzothiazolyl ureas,<sup>276</sup> steroidal inhibitors,<sup>274</sup> and L<sub>D</sub> loop hot spot mimetics (Figure 9).<sup>240</sup> The fused pyrazoles are the first identified compounds and possess the greatest potency among ABAD inhibitors, exemplified by AG18051 (IC<sub>50</sub> = 92 nM). However, AG18051 suffers from low solubility and poor predicted blood-brain barrier (BBB) penetration. The SAR of these compounds

has been largely underexplored, except for an *in silico* study that predicted modifications on the phenyl and/or azepane ring would improve potency.<sup>277</sup>

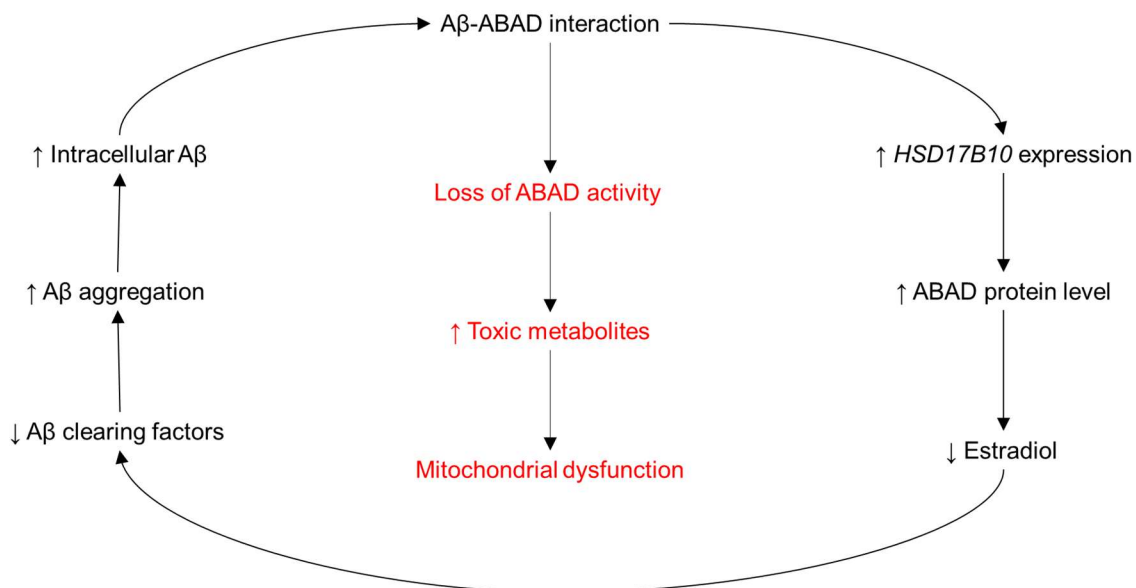


**Figure 18.** A $\beta$ -ABAD interaction pathology cascade.

A $\beta$  binds intracellularly to ABAD, thus it is inhibiting its enzymatic activity and causing a natural compensatory mechanism by increasing the expression of *17BHS10* gene and increased ABAD protein level. Higher level of enzyme causes increased degradation of estradiol, which modulates the expression of A $\beta$  clearing factors, resulting in accumulation of A $\beta$ . Furthermore, amyloid can enter into mitochondria, binds ABAD and the cascade is repeated.

The benzothiazolyl ureas are based on the frentizole scaffold ( $IC_{50} = 200 \mu M$ ), an FDA approved immunosuppressant.<sup>239</sup> The most potent compound from this class identified to date possesses an  $IC_{50} = 1.2 \mu M$ .<sup>276</sup> However, this type of compound has been previously shown to have low absorption, distribution, metabolism, and excretion (ADME) properties and low BBB permeability,<sup>278</sup> which is a crucial consideration for a CNS drug.<sup>279</sup> The steroidal compounds mimic the natural substrates of ABAD. The most potent compound from the steroidal inhibitors identified to date is the reversible inhibitor RM-532-46. The inhibitor was tested *in vitro* using a HEK-293 cell line stably overexpressing ABAD and

showed an  $IC_{50} = 0.55 \mu M$ . However, when tested in an isolated enzyme assay, the inhibitor showed an  $IC_{50}$  of  $985 \mu M$  and  $710 \mu M$  using radiolabeled allopregnanolone and estradiol, respectively. The steroidal inhibitor has also demonstrated activity towards type 3  $17\beta$ -HSD and was metabolically unstable in human liver microsomes, highlighting potential issues toward its translation into a drug.<sup>25</sup> The  $L_D$  loop hotspot mimics were identified through a virtual screening. The most potent inhibitor identified to date is VC15 ( $IC_{50} = 4.4 \mu M$ ).<sup>240</sup> These compounds are in early-stage development and have limited *in vivo* data. In addition to these compound classes, the natural product alkaloid Huperzine A (HupA), an over the counter nutrient that is clinically approved for the treatment of AD in China,<sup>280</sup> has recently been shown to possess ABAD inhibition activity.<sup>281</sup> Our program to identify novel ABAD inhibitors has chosen AG18501 as a hit molecule for SAR identification. No medicinal chemistry driven SAR studies have been conducted on the hit ABAD inhibitor AG18051 in this project's structural classes to the best of our knowledge. Only a limited structure-activity relationship has been reported for AG18051, hence no pharmacophore has been identified. The main goals of this chapter are as follows:

1. Develop a synthetic route for the hit molecule AG18051 and its analogues. We have encountered difficulty in synthesizing the hit molecules according to the initial patent application reports, which resulted in low yields of both target product and intermediates.<sup>237</sup> Developing an efficient, more straightforward synthetic route will provide access to a wide variety of structurally diverse AG18051 derivatives that can be analyzed in *in vitro* assays.
2. Evaluate the ABAD inhibition potency of novel compounds. Bioassay of derivatives in enzyme inhibition assays will establish their ABAD inhibition activity and identify potent compounds.

3. Evaluate the *in vitro* pharmacology of ABAD inhibition in rescuing A $\beta$ -induced mitochondrial dysfunction and ameliorate A $\beta$ -induced toxicity in an *in vitro* cellular model. It is thereby establishing the neuroprotective effect of ABAD inhibitors.

The experiments are collectively designed to evaluate, design, and synthesize AG18051 analogues to study the SAR towards ABAD activity to optimize potency and selectivity around the hit compound. This further establishes the basis for an AD drug discovery project.

## 3.2. MATERIALS AND METHODS

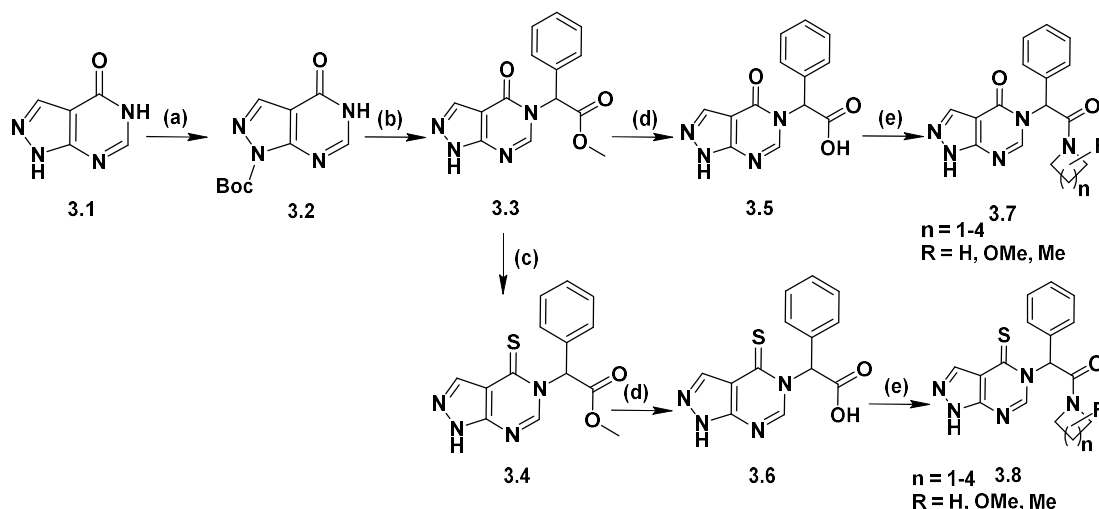
A detailed account of chemistry procedures and characterization ( $^1\text{H}$ ,  $^{13}\text{C}$ , NMR and HRMS) is provided in Chapter four. The following sections describe the experiments used throughout this dissertation pertaining to synthesis of AG18051 and its analogues, enzyme activity assay, cell culture, amyloid preparation, estradiol ELISA assay, cell viability assays,  $\text{IC}_{50}$  value determination, statistical analyses, and mitochondrial stress test.

### *Synthesis of AG18051 and its analogues*

An expedient synthetic route developed in our lab allowed rapid access to a wide variety of structurally diverse derivatives of AG18051 (Scheme 3). The initially reported synthetic route to access AG18051 and derivatives,<sup>237</sup> proved highly challenging in our hands, resulting in low yields of both target product and intermediates. Our developed synthetic scheme features rapid access to the amide bioisostere of AG18051 in just four-steps and a high overall yield (65%) compared with the original eight-step route. The addition of one step allows access to the original thioamide derivative. It is notable that the low yielding steps that drive down overall yield occur in the first two transformations and provide almost quantitative recovery of starting material. Commercially available allopurinol (**3.1**) undergoes chemoselective protection with di-*tert*-butyl dicarbonate to yield **3.2**, with its structure unequivocally assigned by HMBC  $^1\text{H}$ - $^{14}\text{N}$  NMR. Exposure of carbonate **3.2** to sodium hydride results in abstraction of a proton and electrophilic attack of a suitably substituted methyl  $\alpha$ -bromophenylacetate to afford methyl ester **3.3** with concomitant deprotection of Boc in almost quantitative yield. At this point, the synthetic route can branch to afford access to either amide or thioamide bioisosteres of the hit compound. Exposure of amide (**3.3**) to Lawesson's reagent afforded thioamide **3.4** in



moderate yield. Subsequent hydrolysis of **3.3** and **3.4** affords carboxylic acid **3.5** and **3.6**, respectively. Coupling of a suitably substituted nitrogen heterocycle employing benzotriazolyl-oxytris (dimethylamino) phosphonium hexafluorophosphate (BOP) afforded final compounds of types **3.7** and **3.8**.



**Scheme 3.** Synthesis of AG18051 and its analogues.

**Reagents and conditions:** (a) DIPEA, DMAP, (Boc)<sub>2</sub>O, THF, 90%; (b) NaH, LiBr, DMF, methyl  $\alpha$ -bromophenylacetate, 96%; (c) Lawesson's Reagent, PhMe, 67%; (d) NaOH, THF, quan.; (e) BOP, DIPEA, DMF, appropriately substituted amine 47-80%.

### **Enzyme Activity Assay: Measuring NADH Absorbance Change**

The enzyme activity screen for all compounds was performed in collaboration with the Frank Gunn-Moore lab at the University of St. Andrews. Purification of ABAD was performed according to the described conditions.<sup>282</sup> The kinetic parameters of the ABAD mediated reduction of acetoacetyl-CoA were measured using recombinant ABAD enzyme (0.02  $\mu$ g/mL, 740 pM), NADH (250  $\mu$ M) and a range of acetoacetyl-CoA concentrations (0 – 140  $\mu$ M). Solutions were prepared in assay buffer (10 mM HEPES buffer,  $\pm$  0.5 % (w/v) gelatin (porcine skin), pH 7.4 at 37 °C). Reaction progression was measured via a decrease in NADH absorbance at 340 nm using a SpectraMAX 250 spectrophotometer.

A reaction time of 800 s was employed yielding steady state conditions ( $R^2 > 0.9$ ). Non-linear regression analysis was performed using GraphPad Prism, utilising the Michaelis-Menten equation. The kinetic parameters of the ABAD mediated reduction of acetoacetyl-CoA were assessed with respect to the co-factor, NADH, using recombinant ABAD enzyme (0.02  $\mu\text{g/mL}$ , 740 pM), 120  $\mu\text{M}$  acetoacetyl-CoA and a range of NADH concentrations (0 – 600  $\mu\text{M}$ ). Experiments were performed as described for acetoacetyl-CoA above. A  $V_{\text{max}}$  value of  $10.64 \pm 0.42 \mu\text{mol min}^{-1} \text{mg}^{-1}$  and a  $K_m$  value of  $11.79 \pm 1.86 \mu\text{M}$  were calculated with respect to acetoacetyl-CoA. A concentration of 120  $\mu\text{M}$  acetoacetyl-CoA was selected for subsequent experiments. A  $V_{\text{max}}$  value of  $15.54 \pm 0.95 \mu\text{mol min}^{-1} \text{mg}^{-1}$  and a  $K_m$  value of  $99.84 \pm 21.34 \mu\text{M}$  were calculated with respect to NADH. A cofactor concentration of 250  $\mu\text{M}$  NADH was selected for subsequent experiments.<sup>283</sup>

Compound screening assay conditions consisted of ABAD enzyme (0.5  $\mu\text{g/mL}$ ), NADH (250  $\mu\text{M}$ ), acetoacetyl-CoA (120  $\mu\text{M}$ ) and a primary screen consisting of three concentrations of our synthesized compounds (1  $\mu\text{M}$ , 25  $\mu\text{M}$  and 100  $\mu\text{M}$ ; 1% DMSO (v/v)). Solutions were prepared in assay buffer (10 mM HEPES buffer, 0.5% (w/v)), pH 7.4 at 37 °C). Each compound was weighted in milligrams with maximal 0.1 mg deviation to prepare a 10 mM stock solution in DMSO. The DMSO stock solution was further diluted by 10 mM HEPES buffer solution to give a final assay concentration 25  $\mu\text{M}$  1% DMSO (v/v). Control solutions containing an equivalent concentration of DMSO (1% (v/v)) were also prepared and run concurrently. Reaction progression was measured via a decrease in NADH absorbance at 340 nm using a SpectraMAX M2e spectrophotometer. The reaction period was gated to yield steady state conditions ( $R^2 > 0.9$ ).

### ***Cell Culture***

The cell line SH-SY5Y (ATCC, catalog number CRL-2266) was cultured in DMEM/F12 media (Fisher Scientific, catalog number 10131035) supplemented with 10% fetal bovine serum (Corning, catalog number 35-010-CV), 1% penicillin–streptomycin (Corning, catalog number 30-002-CI) and maintained as monolayer cultures in a humidified atmosphere containing 5% CO<sub>2</sub> at 37 °C.<sup>284</sup> All cell lines were authenticated via short tandem repeat analysis and tested for mycoplasma using the MycoAlert mycoplasma detection kit as per the manufacturer's instructions (Texas cancer cell repository) in May 2017, showing no contamination. Where indicated, cells were also cultured in DMEM/low glucose media (Thermofisher scientific, catalog number SH3002101). All compounds were diluted to 20 mM solution in DMSO and were serially diluted in cell culture media for cell treatments to a final concentration range of 0.01 to 100 µM, maintaining the final DMSO concentration at less than 1%. Positive control compound HupA (Fisher Scientific, catalog number 507063) was serially diluted in a similar fashion as the synthesized compounds.

### ***Amyloid Preparation***

The peptide A $\beta$ <sub>1-42</sub>, referred to as “A $\beta$ ”, was obtained from rPeptide (catalog number A11662). The oligomers of A $\beta$  were prepared using an established method,<sup>285</sup> A $\beta$  peptide was resuspended in 0.5 mM NaOH at a concentration of 350 mM and stored at -80 °C. For use in cell cultures, the stock solution was incubated at 37 °C for 5–7 days. Before use, the peptide was diluted to 25 µM in DMEM/low glucose media.

### ***Estradiol ELISA assay***

SH-SY5Y cells were treated with compounds (24 hours), followed by A $\beta$  (72 hours) in a similar fashion to that employed in the cell viability assays, the cell culture medium

was collected, and cells were lysed using RIPA buffer and protease inhibitor cocktail, then proteins were quantified via BCA assay. The estradiol assay was performed according to the manufacturer's guidelines (Cayman, catalog number 501890). In brief, the plate was loaded with samples, along with the estradiol tracer and the specific antiserum to estradiol and incubated for one hour at room temperature. After five washing steps, Ellman's Reagent was added, and the plate developed for 60 minutes with gentle shaking at room temperature. The calculated estradiol concentration was normalized to the total protein content of the samples.

### ***Cell Viability Assays***

The SH-SY5Y cells were plated at a density of 50,000 cells/well in 96-well plates and allowed to adapt overnight in a humidified atmosphere containing 5% CO<sub>2</sub> at 37 °C. The cells were pretreated (24 hours) with the test compound and exchanged to a serum-free DMEM/low glucose media, prior to incubation with 25 µM of Aβ<sub>1-42</sub>. Cell viability was measured after 48 hours using the MTS assay (Promega, catalog number G3580) or the lactate dehydrogenase (LDH) cytotoxicity assay kit (Fisher Scientific, catalog number PI88954) according to the manufacturer's protocols.

### ***IC<sub>50</sub> Value Determination and Statistical Analyses***

*For enzyme assays*, the inhibitory potency for each compound was represented by IC<sub>50</sub> values and measured as described before.<sup>155, 157, 256</sup> The IC<sub>50</sub> values of AG18051 and its analogues in the isolated enzyme assays were determined by measuring the decrease in NADH absorbance at 340 nm. In the estradiol-based enzyme assay, compounds activity was measured by determining the amount of estradiol concentration. The IC<sub>50</sub> values of each compound was acquired from a single experiment with each inhibitor concentration run in triplicate and the statistical significance was calculated using

the Student *t* test. A *P* value of <0.05 was considered statistically significant. IC<sub>50</sub> values were calculated by using GraphPad prism software version 9.0.

### ***Mitochondrial Stress Test***

Cultured SH-SY5Y cells were plated at a density of 50,000 cells/well in 24-well assay plates (Seahorse Bioscience, catalog number 100850001) and allowed to adapt for 24 hours days prior to pretreatment (24 hours) with the test compound followed by incubation with 25  $\mu$ M of A $\beta$ <sub>1-42</sub>. After 48 hours, media was replaced with assay medium consisting of XF Base Medium (Seahorse Bioscience, catalog number 103575100) supplemented with 10 mM glucose, 10 mM pyruvic acid, and 1 mM L-glutamine. Subsequently, the analysis of mitochondrial oxygen consumption rate (OCR) was performed in a Seahorse Bioscience XFe 24 flux analyzer according to the manufacturer's instructions. The OCR values were obtained both during baseline (prior to addition of any Mito Stress Test substances), and after the addition of 1.5  $\mu$ M oligomycin, 2  $\mu$ M FCCP and 0.5  $\mu$ M rotenone + 0.5  $\mu$ M antimycin A, respectively. Prior to analysis, data were corrected by withdrawing non-mitochondrial respiration (measured after the injection of rotenone and antimycin A) from all measured OCR values. After the experiment, cells were lysed using RIPA buffer and protease inhibitor cocktail, then proteins were quantified via BCA assay. Results were normalized to protein concentration of each well to its OCR value.

### 3.3. RESULTS AND DISCUSSION

#### *Chemistry*

Given that the original synthetic route of the patent application describing AG18051 provided low yields of both target product and intermediates and was not applicable to access a wide variety of structurally diverse derivatives, we aimed to develop an alternative synthesis. We faced several difficulties in developing a synthetic route, and with optimizing several reaction conditions, we were able to overcome these challenges and obtain the desired compounds. In this section, the rationales for selecting reagents and optimizing reaction conditions are discussed. Moreover, proposed reasons for reaction failures are also discussed.

In protecting the amine of the pyrazole ring (Step (a) in Scheme 3), we faced difficulties in isolating the desired intermediate **3.2**. We utilized a reported method using triethylamine (TEA) as a base to deprotonate the amine in the pyrazole ring, which undergoes protection with di-*tert*-butyl dicarbonate to yield **3.2**.<sup>286</sup> However, in our hands, this reaction and many other conditions gave mixtures of different products that proved difficult to separate and purify the desired Boc-protected allopurinol, which was isolated in low yields (~10%). We then attempted using the Cbz group for protection. The treatment of **3.1** with benzylcarbamoylchloride (CbzCl) afforded the Cbz-protected allopurinol in 20% yield but only 70% pure. Since, the Boc protection method provided a pure compound and spares a reaction-step by combining the deprotection and methyl-bromophenylacetate coupling in one step, we then thought to optimize the reaction condition and purification method for the Boc-protected allopurinol.<sup>287</sup> We attempted the use of a different catalyst than 4-dimethylaminopyridine (DMAP). Using molecular iodine has drawn considerable attention lately as an inexpensive, non-toxic, nonmetallic, and readily available catalyst for effecting various organic transformations.<sup>288, 289</sup> The methodology described by

Viswanadham *et al.* employs solvent-free conditions and at room temperature. We have attempted this methodology in our synthesis and was found that **3.1** was insoluble, and the reaction did not proceed. We then tried to perform the Boc protection in H<sub>2</sub>O using a catalyst-free environment at room temperature utilizing a reported method by Chankeshwara and Chakrabort.<sup>290</sup> However, the solubility of **3.1** in water was very poor, and the reaction did not proceed. Taking these failures into perspective, the reaction conditions where we used TEA and DMAP was successful, although low yield, a product was isolated. Optimizing the conditions and purification process of the reaction was our alternative resolution. A summary of the failed attempts of the Boc-protected allopurinol is presented in Table 5. The product degradation during separation using chromatography on silica gel was our assumption for the purification's failure. After several modifications, the optimized reaction conditions that improved yield of our product were to use DIPEA, DMAP, and THF/reflux — overnight. These conditions must be followed by using 3% TEA in the mobile phase used for purification, which neutralizes the acidity of silica gel and affords **3.2**. Although the reaction yield was 40%, quantitative recovery of starting material allowed for subsequent further exposure to reaction conditions and sequential production of more of the targeted intermediate. Considering the recovery of starting material, the yield of the reaction was found to 90%.

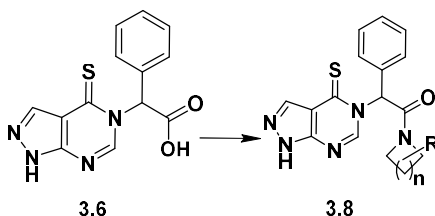
**Table 5.** Optimization of protection reaction conditions to synthesize an *N*-protected **3.1**.

REAGENTS	SOLVENT/CONDITION	NOTES
Boc* + TEA + DMAP	THF / Reflux — Overnight	Majority of product degraded during purification. Yield (~10%).
Boc + TEA + DMAP	THF / Reflux — 6 hours	No reaction
Boc + TEA + DMAP	THF / Reflux — 12 hours	No reaction
Boc + TEA + DMAP	THF / RT** — Overnight	Majority of product degraded during purification
Boc + TEA + DMAP	THF / 0 °C — Overnight	Majority of product degraded during purification
Boc + TEA + DMAP	PhMe / Reflux — Overnight	Majority of product degraded during purification
Boc + TEA + DMAP	PhMe / Reflux — 6 hours	No reaction
Boc + TEA + DMAP	PhMe / Reflux — 12 hours	No reaction
Cbz***	Dioxane-AcOH / RT — Overnight	20% product; 70% pure
Boc + I <sub>2</sub>	Solvent free / RT — Overnight	Poor solubility – no reaction
Boc	H <sub>2</sub> O / RT —Overnight	No solubility – no reaction
Boc + NaH + DMAP	THF / Reflux — Overnight	No reaction
Boc + NaH + DMAP	PhMe / Reflux — Overnight	No reaction
Boc + NaH + DMAP	DMF / Reflux — Overnight	No reaction
Boc + DIPEA + DMAP	THF / Reflux — Overnight	Majority of product degraded during purification. Yield (~15%).
Boc + DIPEA + DMAP	THF / Reflux — 6 hours	No reaction
Boc + DIPEA + DMAP	THF / Reflux — 12 hours	No reaction

\*Boc anhydride, \*\* room temperature, \*\*\*carboxybenzyl group,



In the final step of the synthesis of AG18051 derivatives. We found some challenges in finding a suitable amide-coupling reagent that will provide the final compounds (Scheme 4). We initially used BOP coupling reagent to synthesize AG18051. In the presence of DIPEA, deprotonation of the carboxylic acid group in **3.6** affords the carboxylate that attacks the electrophilic phosphorus atom in BOP. This electrophilic substitution leads to the formation of activated acyl-phosphonium species, with the elimination of a deprotonated *N*-hydroxybenzotriazole molecule (HOBt). The formed deprotonated HOBt attacks the carbon atom of the activated acid to produce a reactive benzotriazole ester, which finally undergoes aminolysis. The formation of a *N*-hydroxybenzotriazole ester activates towards the condensation with the amine moiety of the coupling partner.



**Scheme 4.** Amide-coupling step in the synthesis of AG18051 and its derivatives.

We found that BOP amide-coupling conditions were optimal to synthesis AG18501 and its amide bioisostere **3.7a**. Our attempts to synthesize other derivatives of AG18501 using BOP amide-coupling were unsuccessful. We then tried another coupling reagent named *N*'-ethyl-*N*'-(3-(dimethylamino)propyl) carbodiimide (EDC). The advantage of using EDC is that it is easily removed during workup as it is a water-soluble reagent. The mechanism of EDC with HOBt as a catalyst is similar to that of BOP. The use of EDC-HOBt coupling route was successfully used in the synthesis of all other compounds. Detailed reactions conditions for each of synthesized compounds are explained in Chapter

four. Interestingly, using EDC-HOBt amide-coupling route produced a loss in the chirality of the final compounds, yielding racemic mixtures final compounds. The synthesis of AG18051 and **3.7a** using EDC-HOBt amide-coupling route yielded an approximate of 1:1 ratio of the *R* and *S* chiral centers, while using the BOP amide-coupling maintained the chiral integrity of **3.6**. In a review paper by Dunetz *et al.*,<sup>291</sup> the use of BOP as an amide coupling reagent was noted to be favored over carbodiimide reagents such as EDC to avoid epimerization. As described in the 'Structure-Activity Relationship' section below, the  $\alpha$ -stereocenter of the final compounds was not required for activity, hence, an amide-coupling reagent that suppresses epimerization was superfluous.

### **Structure-Activity Relationship**

In collaboration with the Gunn-Moore group at the University of St. Andrews, we conducted ABAD inhibition assays using a developed screening method that measures the change in NADH absorbance upon treatment with our synthesized AG18051 derivatives. A modified screening assay was used from that reported in the literature,<sup>283</sup> in which kinetic readings were used to calculate the specific activity instead of an endpoint read.<sup>292</sup> A primary screen consisting of three concentrations of our synthesized compounds (1, 25 and 100  $\mu$ M) was employed to determine ABAD-specific activity relative to DMSO negative control. The calculated 3-point IC<sub>50</sub> for the compounds as a preliminary determination of compound potency was determined. The parent compound AG18051 was used as a positive control (Table 6). We first wished to investigate the effect of stereochemistry on ABAD inhibition activity. To this end, we synthesized the racemic of AG18051 derivative (**3.8a**). Racemate **3.8a** proved equipotent at 1 $\mu$ M concentration to parent AG18051. However, the racemate proved more active at the higher concentrations tested, 100  $\mu$ M concentration. Compound **3.8a** completely abrogated ABAD activity, whereas AG18051 resulted in only 66% ABAD inhibition. The addition of a methoxy

substituent to the 2-position of the azepane ring (**3.8b**) reduced inhibitory activity by approximately 6-fold compared with AG18051 (78% inhibition vs 92% inhibition at 1  $\mu$ M, respectively). Although at 100  $\mu$ M concentration, **3.8b** completely abrogated ABAD activity compared with just 66% inhibition with AG18051. Contraction of the seven-membered azepane ring to a six-membered piperidine bearing a 4-substituted methoxy group (**3.8b**) resulted in significantly reduced ABAD inhibition activity (30% inhibition at 1  $\mu$ M). Gratifyingly, when the substituent on the piperidine ring is changed to an alcohol (**3.8c**), a compound with more significant ABAD inhibition activity to the parent (98% inhibition activity at 1  $\mu$ M, at 100  $\mu$ M concentration complete abrogation of ABAD activity) is obtained. Thus, a hydrogen bond donating group at the 4-position of the piperidine ring is required for activity. When the alcohol substituent is moved to position 3 of the piperidine ring (**3.8d**), a more potent ABAD inhibitor is obtained (98.3% inhibition at 1  $\mu$ M), potentially indicating the formation of a stronger hydrogen bond by decreasing the distance between the donor and acceptor.

This data represents critical findings for the design of further inhibitors; azepane ring derivatives are not readily available and involve significant synthetic steps to generate. Whereas piperidine ring derivatives are much easier to synthesize and therefore would allow for greater exploration of chemical space around this compound fragment. Further contraction of the heterocyclic ring to a four-membered azetidine, retaining the alcohol substituent (**3.8h**), provided a compound with equipotent activity to the parent (96.5% inhibition at 1  $\mu$ M concentration). Both compounds **3.8d** and **3.8h** share a similar positioning of the alcohol group, being two carbons away from the nitrogen within the ring system. This would place the alcohol moiety in a similar spatial arrangement in both compounds, engendering greater binding. Replacement of the azepane ring of AG18051 with a morpholino ring (**3.8f**) provides a compound with 91.5% inhibition of ABAD at 1  $\mu$ M

concentration. Collectively this data shows that a large degree of lipophilicity at this fragment of the parent compound is not required for ABAD inhibition activity to the degree that was first reported for AG18051.

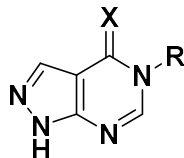
We were particularly interested in comparing activity between thioamide derivatives of the parent compound and amide bioisosteres based on molecular modeling data that did not predict a crucial role for the thioamide sulphur. As the amide bioisostere is an intermediate *en-route* to the thioamide derivatives, if ABAD inhibition activity could be retained, we could shorten the synthetic route to access allopurinol-based ABAD inhibitors more rapidly. The amide bioisostere of AG18051 (**3.7a**) proved to have similar inhibition activity to the parent compound when compared at 1  $\mu$ M (93.4% ABAD activity inhibited v 98% for AG18051). Interestingly, at the higher concentrations tested, compound **3.7a** was more potent than AG18051, especially at 100  $\mu$ M, indicating that the amide bioisostere may constitute active ABAD inhibitors. As with the thioamide, the amide bioisostere racemate (**rac-3.7a**) retained ABAD inhibition activity. The calculated  $IC_{50}$  for **3.7a** and **rac-3.7a** were 0.46 and 0.24  $\mu$ M, respectively. The 2-methoxy substituted azepane amide bioisostere (**3.7b**) showed attenuated activity (15% ABAD inhibition at 1  $\mu$ M) compared to the thioamide bioisostere (**3.8b**). The 4-methoxy substituted piperidine amide derivative (**3.7e**) showed equally attenuated ABAD inhibition activity as its thioamide counterpart (**3.8e**). The 3-hydroxy substituted piperidine amide bioisostere (**3.7d**) possesses attenuated ABAD inhibition activity at 1  $\mu$ M when compared with the thioamide derivative (**3.8d**), 60%, and 98.3% ABAD inhibition, respectively. Likewise, the hydroxy-azetidine amide bioisostere (**3.7h**) shows attenuated ABAD inhibition activity when compared to its thioamide counterpart (**3.8h**), 27% ABAD inhibition activity at 1  $\mu$ M and 96.5% at 1  $\mu$ M, respectively. This indicates that the thioamide moiety is a requirement for ABAD inhibition activity in the piperidine and azepane ring derivatives we have

synthesized, possibly forming part of the pharmacophore. This agrees with known ABAD inhibitors; a literature review indicates a thioamide moiety is common between ABAD inhibitor classes.

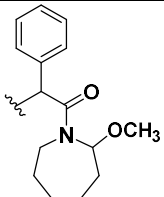
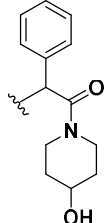
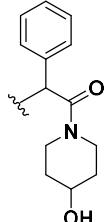
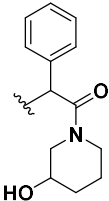
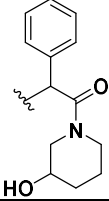
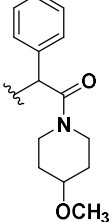
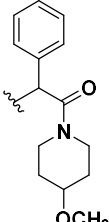
### ***Multiparameter Optimization Score***

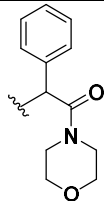
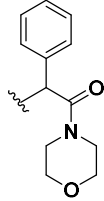
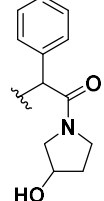
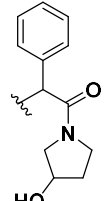
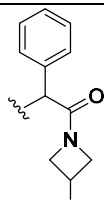
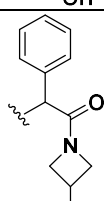
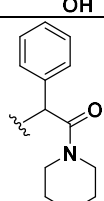
The CNS multiparameter optimization (MPO) score predicts the BBB penetrations of a molecule. Researchers at Pfizer developed this complex multivariate model to understand small molecules' physicochemical parameters that play a role in the BBB penetration.<sup>293</sup> They showed the importance of lipophilicity (clogP), distribution coefficient (clogD) calculated at pH 7.4, molecular weight (MW), topological polar surface area (TPSA), number of hydrogen bond donors (HBD), and most basic center ( $pK_a$ ). Understanding the effect of these parameters on a library of marketed drugs approved for treating CNS disorders.<sup>294</sup> Each individual parameter is assigned a value ranging from 0 to 1. Based on this algorithm, 74% of CNS drugs displayed MPO score  $\geq 4$ , suggesting that molecules displaying an MPO score  $\geq 4$  will likely penetrate the BBB. While this method holds drawbacks, such as the limited class of molecules analyzed, we intended to incorporate the MPO score as a representative measure of synthesized compounds' physicochemical parameters. Current drug discovery efforts are focused on nontraditional CNS targets; thus, a diverse library of molecules is required to derive a formula to predict BBB. Several studies presented a variety of other parameters that hold to be vital in the prediction of a small molecule's BBB penetration.<sup>295-297</sup> All our synthesized AG18501 derivatives have MPO score between 3.5 and 4, thus increasing the chances of the molecules to penetrate the BBB and reaching a therapeutic concentration in the brain.

**Table 6.** Assessing the activity of AG18051 derivatives by measuring the change in NADH absorbance in the presence of ABAD.



Compound	R	X	% ABAD activity remaining at:			3-point IC <sub>50</sub> (μM)	MPO score
			1 μM	25 μM	100 μM		
Vehicle	N/A <sup>1</sup>	N/A	100 ± 3.59	100 ± 20.67	100 ± 9.26	N/A	N/A
<b>AG18051</b>		S	1.96 ± 0.12	1.88 ± 0.45	34.03 ± 12.55	0.28	3.6
<b>(R)-3.7a</b>		O	6.60 ± 0.63	0.49 ± 0.79	0.51 ± 1.84	0.46	4.0
<b>(rac)-3.7a</b>		O	4.46 ± 6.69	1.39 ± 0.48	4.26 ± 1.43	0.24	4.0
<b>3.8a</b>		S	7.86 ± 6.69	1.39 ± 0.48	4.26 ± 1.43	0.73	3.6
<b>3.7b</b>		O	85.29 ± 1.34	71.62 ± 23.97	21.18 ± 6.23	44.2	3.6

<b>3.8b</b>		S	11.56 ± 0.31	11.16 ± 0.93	0.51 ± 4.50	0.7	3.5
<b>3.7c</b>		O	TBD <sup>2</sup>	TBD	TBD	TBD	3.7
<b>3.8c</b>		S	2.07 ± 1.08	8.10 ± 6.37	31.45 ± 14.39	0.2	3.6
<b>3.7d</b>		O	40.45 ± 0.75	18.59 ± 2.16	5.41 ± 1.40	0.73	3.7
<b>3.8d</b>		S	1.71 ± 0.35	-1.91 ± 1.87	-6.87 ± 3.61	0.24	3.6
<b>3.7e</b>		O	50.78 ± 0.30	32.54 ± 2.02	10.51 ± 0.38	46.2	3.6
<b>3.8e</b>		S	70.60 ± 9.99	22.67 ± 4.52	4.79 ± 0.02	3.54	3.5

<b>3.7f</b>		O	TBD	TBD	TBD	TBD	4.0
<b>3.8f</b>		S	8.56 ± 0.40	5.74 ± 0.46	-3.02 ± 0.54	0.25	4.0
<b>3.7g</b>		O	TBD	TBD	TBD	TBD	3.7
<b>3.8g</b>		S	TBD	TBD	TBD	TBD	4.0
<b>3.7h</b>		O	72.67 ± 2.56	33.68 ± 8.95	9.59 ± 0.30	5.6	3.7
<b>3.8h</b>		S	3.45 ± 0.33	20.42 ± 5.17	9.26 ± 2.64	0.66	4.0
<b>3.7i</b>		O	TBD	TBD	TBD	TBD	4.0

<sup>1</sup>NA, not applicable; <sup>2</sup>TBD, to be determined.



In closing, we have synthesized and identified several more potent ABAD inhibitors than the AG18051 hit compound. Importantly, we have replaced the difficult to access azepane ring system of the parent with piperidine and azetidine rings that are commercially and synthetically readily available. We expanded the SAR of this chemotype to understand the minimum pharmacophore (Figure 19). The two adjacent nitrogens of the pyrazole ring are required to bind to the NAD<sup>+</sup> co-factor within the ABAD active site. A thioamide is superior to the corresponding amide bioisostere, a common functionality in active ABAD inhibitors from the literature. The stereochemistry of the linking carbon is unimportant for activity. A number of ring systems can result in activity with both six- and four-membered rings providing active compounds. The five-membered ring system has been synthesized and is awaiting ABAD inhibition assay. A hydrogen bond donor appended to the piperidine ring system at either the 4- or 3- position increases activity. A two-carbon spacer between the heterocyclic nitrogen and hydrogen bond donor substituent seems to be essential for activity.

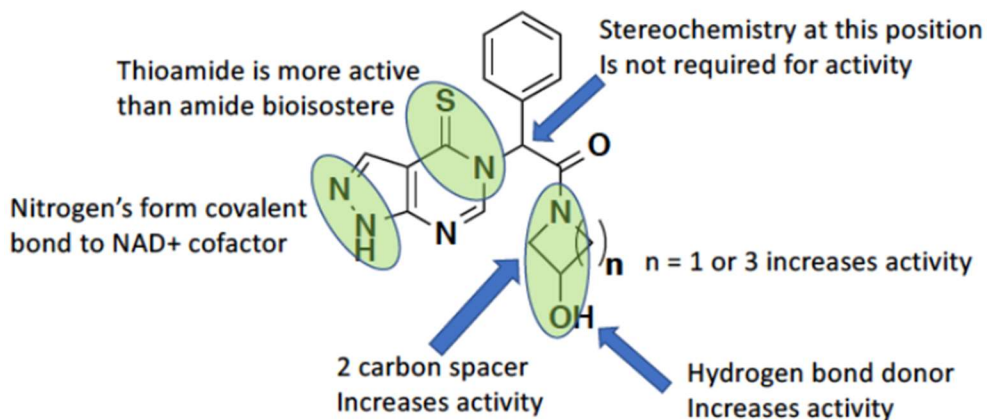


**Figure 19.** Activity map summarizing the minimum pharmacophore for ABAD inhibition.

### ***Estradiol-Based Enzyme Assay***

Due to the current worldwide pandemic, collaboration with the Gunn-Moore lab at the University of St. Andrews was halted and testing a full set of concentrations needed to determine a more accurate  $IC_{50}$  for our synthesized compounds was constrained. Thus, an alternative enzyme assay was employed to test the activity of the synthesized compounds. We decided to develop an in-house cell-based enzyme assay. In this assay, we used estradiol as a marker for activity instead of the difference in NADH absorbance. The hit compound AG18051 has been shown in a crystal structure with ABAD to form a covalent adduct with  $NAD^+$  cofactor in enzyme active site,<sup>235</sup> hence measuring the NADH absorbance may mislead compounds action. A comparison of the enzyme's forward and backward catalytic efficiencies indicates that at pH 7.4, estradiol conversion to estrone is about three times more favored than the backward reaction. Since the mitochondrial matrix is slightly more basic than that in the cytosol, the enzyme activity study on neurosteroid metabolism should be observed at pH 7.4. This also implies that using estradiol will test the reduction activity of ABAD, while the use of acetoacetyl-CoA tests for the oxidation activity. Thus, testing the function of the enzyme in conditions similar to that of the mitochondria.

To determine the toxicity of  $A\beta$  and ABAD's role in this process, we incubated human SH-SY5Y cell lines for 72 hours with  $A\beta$ , followed by measuring estradiol levels in the cell lysate. Similar to published literature,<sup>227</sup> we found that estradiol levels were significantly decreased after  $A\beta$  exposure (Figure 20A). To determine whether AG18051 affects  $A\beta$ -induced reduction of estradiol levels, we preincubated SH-SY5Y for 24 hours with 1  $\mu$ M AG18051 (Figure 20A). The ABAD inhibitor, AG18051, significantly maintained estradiol levels in the cells when compared to  $A\beta$ -only treatment (Figure 20A). Comparing the effect of AG18051 to that of HupA (Figure 20A), a clinically approved AD in China<sup>280</sup>

and has recently been shown to possess ABAD inhibition activity,<sup>281</sup> we tested the effect of the reported  $IC_{50}$  of HupA ( $10\text{ }\mu\text{M}$ )<sup>281</sup> treatment in the estradiol assay. We found  $1\text{ }\mu\text{M}$  of AG18051 to be more significant than HupA in protecting SH-SY5Y cells. This data shows that AG18051 is more potent than HupA in restoring estradiol level and ameliorating  $A\beta$ -induced toxicity. This suggests that AG18051 is neuroprotective and that it may exert its neuroprotective effect either by inhibiting ABAD and priming cells to become resistant to the impact of  $A\beta$  or via direct inhibition of the  $A\beta$ -ABAD interaction. In addition, employing the estradiol assay in testing the activity of the compounds in the presence of  $A\beta$  directly correlates the relation between  $A\beta$  and ABAD, thus more significant than the NADH absorbance enzyme assay in incorporating  $A\beta$ -ABAD interaction. To measure the effect of AG18051 alone in SH-SY5Y cell lines, we tested the increase of its dose in affecting estradiol levels (Figure 20B). Contrary to the previously reported reduction in estradiol levels and toxicity seen with concentrations higher than  $0.1\text{ }\mu\text{M}$ ,<sup>227</sup> no significant reduction in estradiol levels was observed. However, at  $100\text{ }\mu\text{M}$ , we found AG18051 to induce a 20% decrease in estradiol levels when compared to control. To evaluate the effect of the increase of AG18051 dose in maintaining estradiol levels reduced by  $A\beta$ , we tested AG18051 increasing concentrations in the presence of  $A\beta$  (Figure 20B). We found AG18051 to display a dose-response increase in estradiol levels. This suggests that  $A\beta$ -ABAD interaction may be inhibited by AG18051, as no significant change in estradiol levels was seen with AG18051 alone. While in the presence of  $A\beta$  and AG18051, the estradiol levels were restored. Alternatively, this may also suggest that  $A\beta$ -ABAD interaction leads to the enzyme's reduction activity, and as a feedback mechanism ABAD levels are increased leading to decreased estradiol levels. While in the presence of AG18051, inhibition of ABAD is achieved, and estradiol levels are maintained.

We began evaluating the effect of our synthesized compounds in the estradiol assay with a preliminary screening of 10 compounds (Table 7). The screening resulted in the identification of four compounds demonstrating more potency than the parent compound AG18051. These four compounds were found to have a hydrogen bond donor attached to position 3 or 4 in the six-membered ring, replacing the azepane. Further, the stereochemistry of the linking carbon is not required for activity. These results support our initial finding of the SAR from enzyme inhibition assay. This initial screening provided various potent compounds that can be used for further optimization in properties such as BBB penetration, *in vivo* metabolic stability, bioavailability, and others.

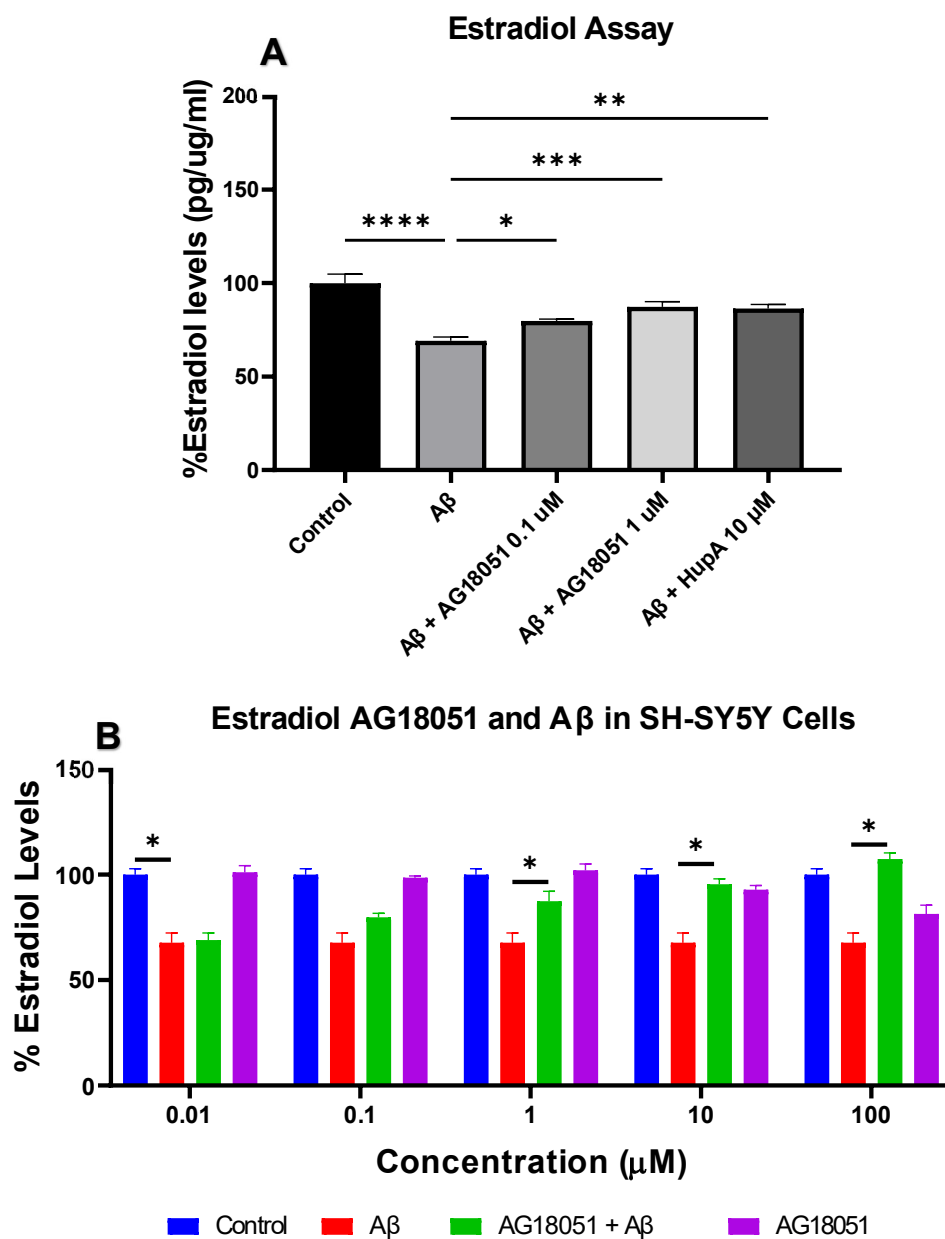
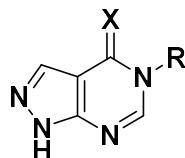


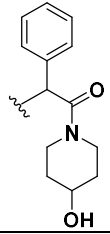
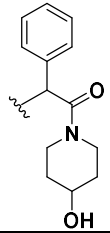
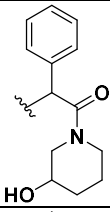
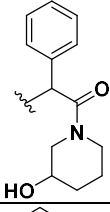
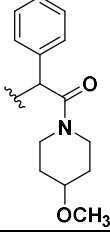
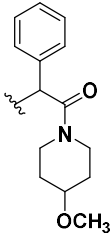
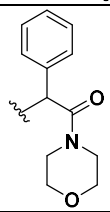
**Figure 20.** The effect of A $\beta$  and AG18051 on estradiol levels.

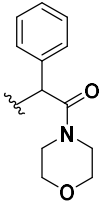
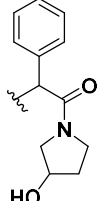
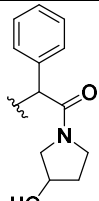
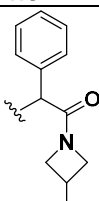
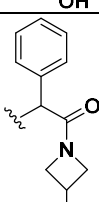
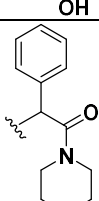
A) Estradiol levels in SH-SY5Y cells treated with A $\beta$  alone (72 hours) and with the pretreatment for 24 hours with AG18051 and HupA. B) Percentage of estradiol levels in SH-SY5Y cells treated with increasing concentration of AG18051 alone and in the presence of A $\beta$ . n=3,  $\pm$ SEM, A) One-way ANOVA; 95% Confidence Interval; \*,  $p < 0.02$  \*\*,  $p = 0.001$ ; \*\*\*,  $p = 0.0007$ ; \*\*\*\*,  $p < 0.0001$ . B) Two-way ANOVA; 95% Confidence Interval; \*,  $p < 0.03$ .

**Table 7.** Assessing the potency of AG18051 derivatives in ameliorating A $\beta$ -induced reduction in estradiol levels.



Compound	R	X	IC <sub>50</sub> (μM)
<b>AG18051</b>		S	1.224±0.050
<b>(R)-3.7a</b>		O	TBD <sup>1</sup>
<b>(rac)-3.7a</b>		O	1.093±0.064
<b>3.8a</b>		S	TBD
<b>3.7b</b>		O	TBD
<b>3.8b</b>		S	TBD

<b>3.7c</b>		<b>O</b>	<b>TBD</b>
<b>3.8c</b>		<b>S</b>	<b>TBD</b>
<b>3.7d</b>		O	0.707 $\pm$ 0.055
<b>3.8d</b>		S	0.732 $\pm$ 0.089
<b>3.7e</b>		O	0.735 $\pm$ 0.068
<b>3.8e</b>		S	0.653 $\pm$ 0.061
<b>3.7f</b>		O	2.484 $\pm$ 0.096

<b>3.8f</b>		S	3.574 $\pm$ 0.102
<b>3.7g</b>		O	TBD
<b>3.8g</b>		S	TBD
<b>3.7h</b>		O	TBD
<b>3.8h</b>		S	2.631 $\pm$ 0.042
<b>3.7i</b>		O	5.395 $\pm$ 0.111

<sup>1</sup>TBD; to be determined.



### ***Neuroprotective Activity of ABAD Inhibitors in Ameliorating A $\beta$ -Induced Toxicity***

We have established and optimized an assay to test the protective activity of our developed derivatives to ameliorate A $\beta$ -induced toxicity. Using human neuroblastoma SH-SY5Y 'neuron-like' cells, known to express ABAD.<sup>227</sup> We have developed robust conditions that result in reproducible loss of 65% cell viability upon treatment with 25  $\mu$ M A $\beta$  after 48-hour incubation (Figure 21A). AG18051 and its analog **3.8c** were screened for toxic effects in SH-SY5Y cell lines. Both compounds displayed no toxicity up to concentrations as high as 100  $\mu$ M (Figure 21B). Our initial screen of derivatives to ameliorate A $\beta$ -induced toxicity revealed AG18051 and the piperidine ring derivative with a hydroxyl group in position 4 (**3.8c**) to afford 79% and 82% protection of cell viability at 1  $\mu$ M concentration, respectively, when measured in the MTS assay (Figure 21C). While in the LDH assay, which measures the amount of LDH released by the cells in the media upon cell death, cells treated with A $\beta$  and either AG18051 or **3.8c** had a 2-fold reduction in the amount of LDH released when compared with cells treated with A $\beta$  only (Figure 21D). To compare the inhibition effect of our synthesized compound to that of HupA, we found 74% protection from A $\beta$ -induced toxicity in SH-SY5Y cells treated with HupA utilizing the MTS assay and a 1.5-fold reduction in the amount of LDH released when compared with cells treated with A $\beta$  only (Figure 21C and 21D). This data shows that 1  $\mu$ M of our synthesized compounds was more potent and effective than 10  $\mu$ M HupA in providing protection to SH-SY5Y cells from A $\beta$ -induced toxicity and reducing LDH release *in vitro*.

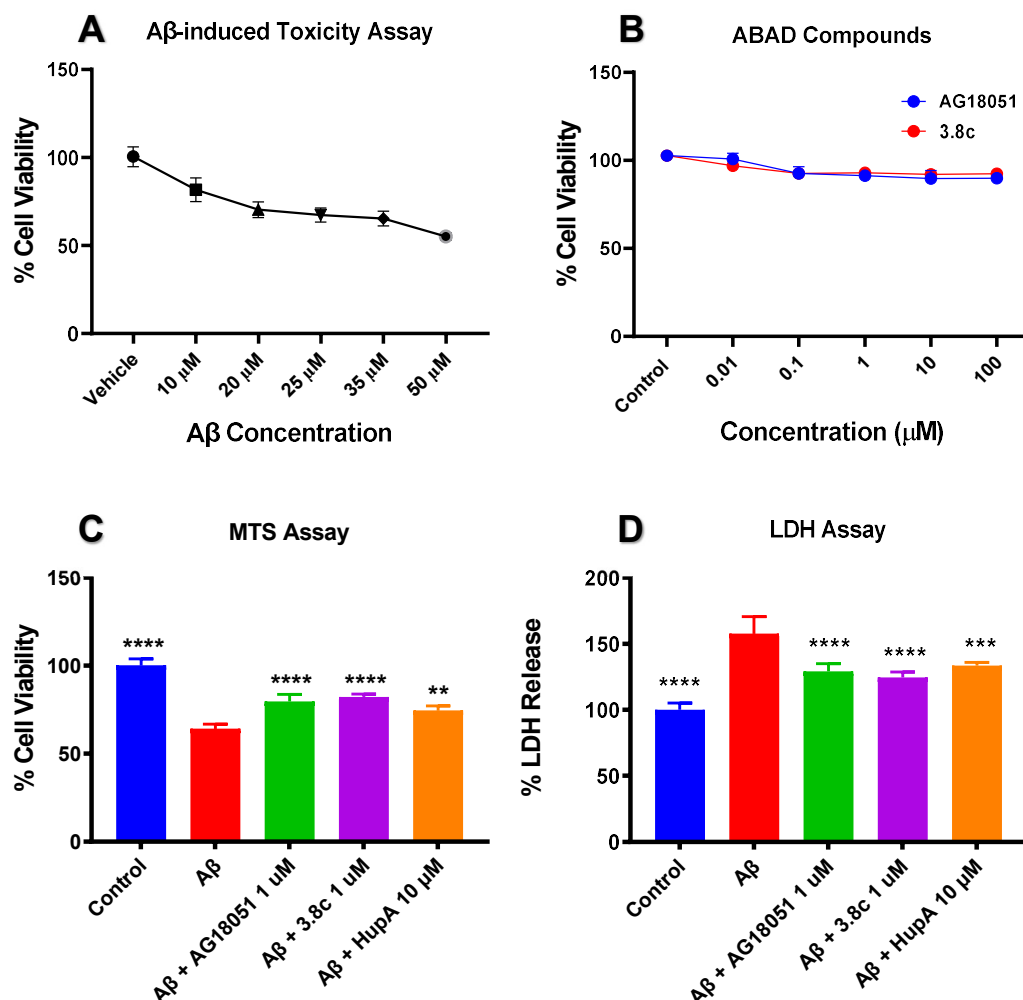


**Figure 21.** Neuroprotective effect of AG18051 and 3.8c in ameliorating A $\beta$ -induced toxicity in human SH-SY5Y 'neuron-like' cells.

Percentage of cell viability of SH-SY5Y cells with increasing concentrations of A) A $\beta$  and B) AG18051 and **3.8c**. SH-SY5Y cells were pretreated with ABAD inhibitor for 24 hrs. prior to incubation with 25  $\mu$ M A $\beta$  for 48 hrs. C) Percentage of cell viability measured by MTS assay. D) Percentage of Lactate dehydrogenase release.  $n=3$ ,  $\pm$ SEM, One-way ANOVA; 95% Confidence Interval; \*\*,  $p < 0.001$ ; \*\*\*,  $p < 0.0006$ ; \*\*\*\*,  $p < 0.0001$ .

### ***Neuroprotective ABAD Inhibitors Rescue A $\beta$ -Induced Mitochondrial Dysfunction in SH-SY5Y Cells***

Mitochondrial dysfunction is a hallmark of AD.<sup>215-217</sup> We determined the mitochondrial respiration of A $\beta$ -treated SH-SY5Y cells on a Seahorse extracellular flux analyzer (Figure 22A). Similar to previously reported literature showing distribution in mitochondrial functions,<sup>298, 299</sup> basal respiration in A $\beta$ -treated cells was significantly lower than control cells (67%; Figure 22B). This level was increased, but not significantly, by the treatment of SH-SY5Y cells with AG18501 (1  $\mu$ M) and restored 37% of the cell respiration reduced by A $\beta$ . While the respiration level was significantly increased by **3.8c** (1  $\mu$ M), restoring 46%. The positive control HupA (10  $\mu$ M) was also able to restore respiration levels by 46%. Similar effects were observed in proton leak, ATP production and maximal respiration measurements (Figure 22C, 22D and 22E). These findings are consistent with other reports of SH-SY5Y treated with A $\beta$  or overexpressing APP.<sup>300, 301</sup> Cells treated with A $\beta$  showed a significant reduction in proton leak, ATP production and maximal respiration, 55%, 60% and 50%, respectively, when compared to control. Treatments with AG18501 (1  $\mu$ M), **3.8c** (1  $\mu$ M) or HupA (10  $\mu$ M) were able to slightly restore this lost mitochondrial function induced by A $\beta$ .

This data shows that AG18051 or **3.8c** can successfully rescue A $\beta$ -induced mitochondrial dysfunction. Basal respiration, proton leak, ATP production and maximal respiration measurements were reduced with A $\beta$  treatment. These functions were restored with 1  $\mu$ M of either AG18051 or **3.8c**. A similar effect was observed with HupA, but with 10  $\mu$ M treatment. This data shows that our synthesized compound demonstrates to be more potent and effective in inhibiting ABAD than the clinically approved AD treatment in China, HupA.<sup>280</sup>

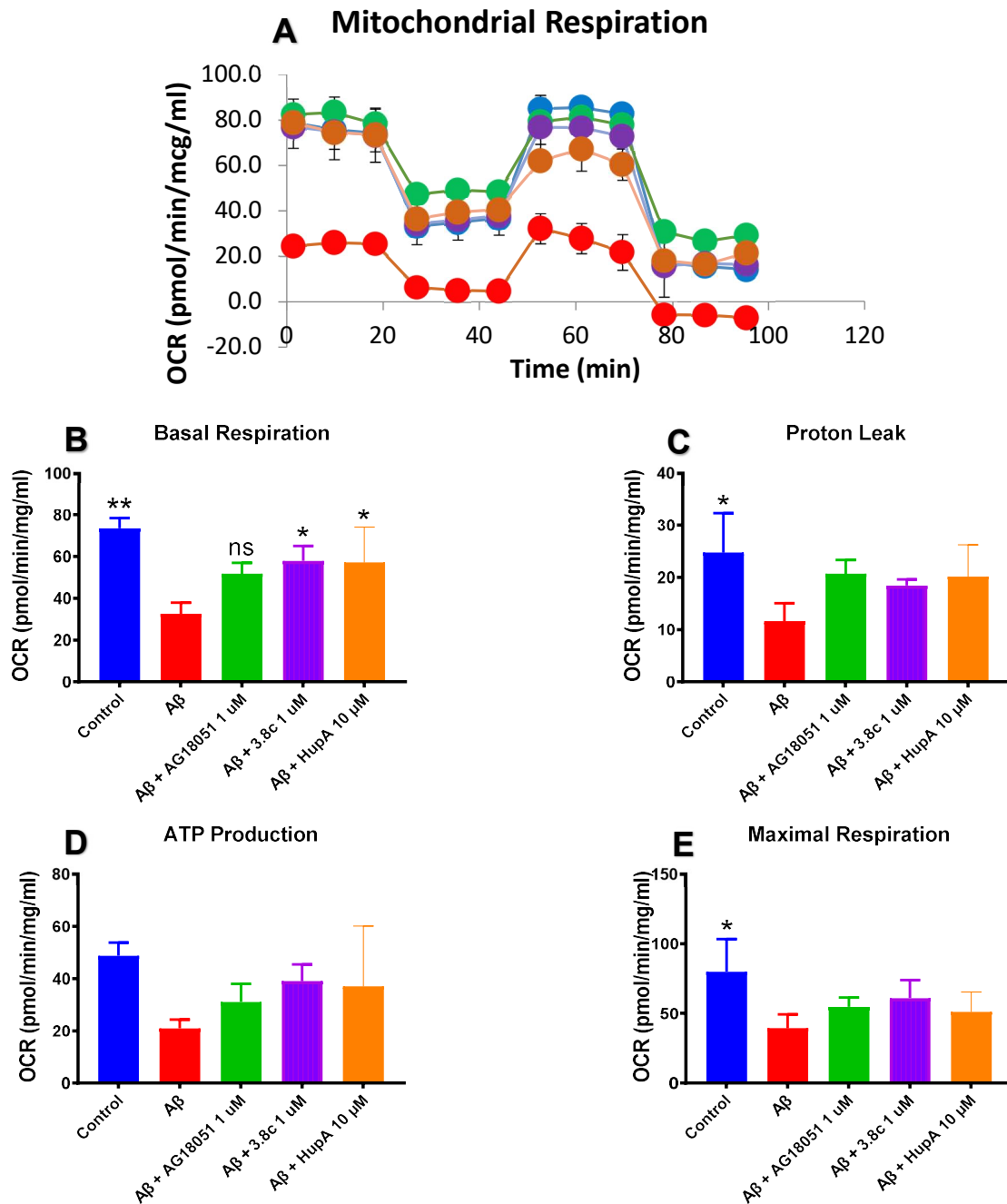


**Figure 22.** AG18051 and 3.8c rescue A $\beta$ -induced mitochondrial dysfunction. Human SH-SY5Y 'neuron-like' cells were pretreated with ABAD inhibitor for 24 hrs. prior to incubation with 25  $\mu$ M A $\beta$  for 48 hrs. A) Mitochondrial Respiration of SH-SY5Y cells (blue bar), A $\beta$ -treated SH-SY5Y cells (red bar), treated with 1  $\mu$ M AG18051 and A $\beta$  (green bar), 1  $\mu$ M 3.8c and A $\beta$  (purple bar) and 10  $\mu$ M HupA and A $\beta$  (orange bar) as determined by the mito stress test on a Seahorse extracellular flux analyzer. B) Quantification of Basal respiration. C) Proton leak. D) ATP production. n=3,  $\pm$ SD, One-way ANOVA; 95% Confidence Interval; \*,  $p$ = <0.04; \*\*,  $p$ = <0.001; \*\*\*\*,  $p$ = <0.0001.

### 3.4. CONCLUSION AND FUTURE DIRECTIONS

We have expanded the SAR of the AG18051 chemotype to understand the minimum pharmacophore required for ABAD inhibition. We have synthesized and identified a number of more potent ABAD inhibitors that replace the difficult to access azepane ring system of the parent with piperidine and azetidine rings that are commercially and synthetically readily available. A number of AG18051 analogs have been synthesized and is awaiting an ABAD inhibition assay that has been delayed due to the current pandemic. We have screened the AG18051 analogues in estradiol-based enzyme assay to establish a dose-response curve for compound activity in a more directly correlated A $\beta$ -ABAD *in vitro* model. We have also evaluated the neuroprotective effects of AG18051 and its derivative **3.8c** in ameliorating A $\beta$ -induced toxicity. Our synthesized compounds protect SH-SY5Y cells from A $\beta$ -induced toxicity by restoring estradiol levels, mitochondrial dysfunction and increasing cell viability.

Future work will aim to complete the SAR around the AG18051 chemotype to identify lead compounds that can be evaluated for their BBB penetration properties and efficacy in rescuing deteriorated phenotypic features in AD patient iPSC-derived neurons.

## **CHAPTER 4: CHARACTERIZATION OF SYNTHESIZED MOLECULES**

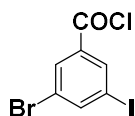
**General Chemistry procedures.**

All reactions were carried out in oven-dried glassware under positive nitrogen pressure unless otherwise noted. Reaction progress was monitored by thin-layer chromatography carried out on silica gel plates (2.5 cm × 7.5 cm, 200 μm thick, 60 F254) and visualized by using UV (254 nm) or by potassium permanganate and/or phosphomolybdic acid solution as indicator. Flash column chromatography was performed with silica gel (40–63 μm, 60 Å) using the mobile phase indicated. Commercial grade solvents and reagents were purchased from Fisher Scientific (Houston, TX) or Sigma-Aldrich (Milwaukee, WI) and were used without further purification. Anhydrous solvents were purchased from Across Organics and stored under an atmosphere of dry nitrogen over molecular sieves.

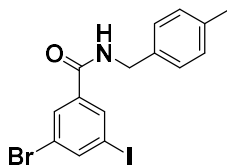
<sup>1</sup>H and <sup>13</sup>C NMR spectra were recorded in the indicated solvent on a Bruker 400 MHz Avance III HD spectrometer at 400 and 100 MHz for <sup>1</sup>H and <sup>13</sup>C, respectively. Multiplicities are indicated by s (single), d (doublet), dd (doublet of doublets), t (triplet), q (quartet), m (multiplet), and br (broad). Chemical shifts (δ) are reported in parts per million (ppm) and coupling constants (J), in hertz. High-resolution mass spectroscopy was performed on compounds included in chapter 2 using a Q Exactive HF Hybrid Quadrupole Orbitrap mass spectrometer conducted at the University of Nebraska Medical Center. While compounds included in chapter 3 was analyzed using a LC/ MS IT-TOF (Shimadzu), using an ESI source conducted at the University of Texas at Arlington and Shimadzu Center for Advanced Analytical Chemistry. High-pressure liquid chromatography (HPLC) was performed on compounds included in chapter 2 using an Agilent 1260 Infinity HPLC system, using Agilent ChemStation software with 215 ELSD detector with an Eclipse 216 plus (C8, 3.5 μM, 150 mm × 4.6 mm) column, while compounds included in chapter 3 was analyzed using Gilson HPLC system with 321 pumps and 155 UV/vis detector using

Trilution software v.2.1 with an ACE Equivalence 3 (C18, 3 mm, 4.6 mm × 150 mm) column. All samples were determined to possess >95% purity.

*General Procedure A. Methyl Ester Hydrolysis.* To a solution of appropriately substituted side chain in position 5 of methyl(*E*)-3-(3-((4-methylbenzyl)carbamoyl)phenyl)acrylate (1 equiv.) in THF (5 mL), 3N NaOH (1.5 equiv.) was added and the solution refluxed overnight. Upon completion, the solution was quenched using of 3N HCl (1.5 equiv.). The aqueous layer was extracted with EtOAc (2 x 75 mL), dried (Na<sub>2</sub>SO<sub>4</sub>), filtered and concentrated in vacuo to afford the final compound.



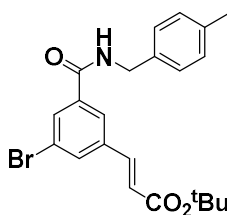
*3-bromo-5-iodobenzoyl chloride (2.2).* To a suspension of 3-bromo-5-iodobenzoic acid (**2.1**) (200 mg, 1.47 mmol) in toluene (10 mL) was added thionyl chloride (0.75 mL, 4.28 mmol). The reaction was stirred at reflux overnight. The reaction mixture was allowed to cool to room temperature and evaporated in vacuo to provide the title compound with 99% yield. R<sub>f</sub>: 0.42 (DCM/MeOH, 10:1). <sup>1</sup>H NMR (400 MHz; CDCl<sub>3</sub>): δ<sub>H</sub> 7.77 (1H, t, *J* = 1.6 Hz, ArCH), 7.93 – 7.94 (2H, m, ArCH).



*3-bromo-5-iodo-N-(4-methylbenzyl)benzamide (2.3).* To a suspension of 3-bromo-5-iodobenzoyl chloride (**2.2**) (200 mg, 1.47 mmol) in DCM (10 mL) was added DMAP (18 mg, 0.15 mmol), followed by addition of 4-methylbenzylamine (270 μL, 2.21 mmol) and NEt<sub>3</sub> (230 μL, 2.21 mmol). The mixture was stirred at reflux overnight. The reaction mixture was allowed to cool to room temperature, brine was added (75 mL) and the layers

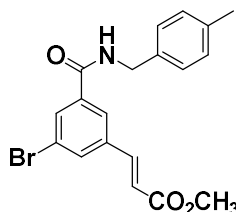


were separated. The organic layer was washed with water (3 x 75 mL), dried ( $\text{Na}_2\text{SO}_4$ ), filtered and concentrated in vacuo. The crude product was purified by column chromatography using hexane/EtOAc gradient (10:1, 4:1, 2:1) to provide the title compound as a yellow solid (99%).  $R_f$ : 0.62 (hexane:EtOAc, 4:1).  $^1\text{H}$  NMR (400 MHz;  $\text{CDCl}_3$ ):  $\delta_{\text{H}}$  2.37 (3H, s,  $\text{CH}_3$ ), 4.58 (2H, d,  $J = 5.5$  Hz,  $\text{CH}_2$ ), 7.18 (2H, d,  $J = 7.8$  Hz, ArCH), 7.24 (2H, d,  $J = 8.0$  Hz, ArCH), 7.87 (1H, t,  $J = 1.6$  Hz, ArCH), 7.98 (1H, t,  $J = 1.5$  Hz, ArCH), 8.02 (1H, t,  $J = 1.5$  Hz, ArCH).  $^{13}\text{C}$  NMR (100 MHz;  $\text{CDCl}_3$ ):  $\delta_{\text{C}}$  21.1, 44.2, 94.4, 123.2, 128.8, 129.5, 134.4, 134.6, 137.7, 142.4, 164.3.

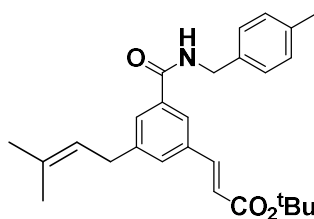


*Tert-butyl(E)-3-(3-bromo-5-((4-methylbenzyl)carbamoyl)phenyl)acrylate (2.4)*. To a solution of 3-bromo-5-iodo-*N*-(4-methylbenzyl)benzamide (**2.3**) (570 mg, 1.9 mmol) in dry toluene (8 mL), was added  $\text{PPh}_3$  (65.5 mg, 0.2 mmol) and  $\text{Pd}(\text{OAc})_2$  (60 mg, 0.1 mmol). *Tert*-butyl acrylate (370  $\mu\text{L}$ , 2.5 mmol) and  $\text{NEt}_3$  (420  $\mu\text{L}$ , 3.0 mmol) were added and the mixture was stirred at reflux overnight. The reaction was allowed to cool to room temperature and was washed with saturated aqueous  $\text{NH}_4\text{Cl}$  (75 mL) and brine (2 x 75 mL), layers were separated, and the organic layer was extracted with DCM, dried ( $\text{Na}_2\text{SO}_4$ ), filtered and concentrated in vacuo. Purification by column chromatography using hexane/EtOAc gradient (12:1, 9:1, 4:1) provided the title compound as a brown oil (64% brsm.).  $R_f$ : 0.3 (hexane:EtOAc, 4:1).  $^1\text{H}$  NMR (400 MHz;  $\text{CDCl}_3$ ):  $\delta_{\text{H}}$  1.55 (9H, s,  $(\text{CH}_3)_3$ ), 2.34 (3H, s,  $\text{CH}_3$ ), 3.37 (2H, d,  $J = 7.3$  Hz,  $\text{CH}_2$ ), 5.28 (1H, t,  $J = 7.3$  Hz, CH), 6.39 (1H, d,  $J = 15.9$  Hz, CH), 7.25 (2H, d,  $J = 8.0$  Hz, ArCH), 7.37 (2H, d,  $J = 7.8$  Hz, ArCH),

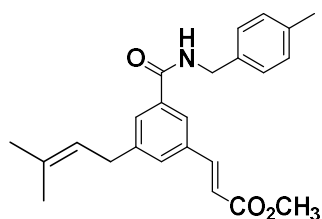
7.51 (1H, s, ArCH), 7.55 (1H, d,  $J = 16.0$  Hz, ArCH), 7.61 (1H, s, ArCH).  $^{13}\text{C}$  NMR (100 MHz;  $\text{CDCl}_3$ ):  $\delta_{\text{C}}$  17.9, 25.7, 28.1, 34.0, 35.6, 41.1, 80.6, 121.1, 121.9, 123.7, 126.6, 128.3, 128.7, 128.8, 130.6, 133.7, 135.0, 135.4, 138.8, 142.6, 143.1, 166.0, 167.1.



*Methyl(E)-3-(3-bromo-5-((4-methylbenzyl)carbamoyl)phenyl)acrylate (2.5)*: To a solution of 3-bromo-5-iodo-*N*-(4-methylbenzyl)benzamide (**2.3**) (570 mg, 1.9 mmol) in dry toluene (8 mL), was added  $\text{PPh}_3$  (65.5 mg, 0.2 mmol) and  $\text{Pd}(\text{OAc})_2$  (60 mg, 0.1 mmol). Methyl acrylate (240  $\mu\text{L}$ , 2.8 mmol) and  $\text{NEt}_3$  (420  $\mu\text{L}$ , 3.0 mmol) were added and the mixture was stirred at reflux overnight. The reaction was allowed to cool to room temperature and was washed with saturated aqueous  $\text{NH}_4\text{Cl}$  (75 mL) and brine (2 x 75 mL), layers were separated, and the organic layer was extracted with DCM, dried ( $\text{Na}_2\text{SO}_4$ ), filtered and concentrated in vacuo. Purification by column chromatography using hexane/EtOAc gradient (12:1, 9:1, 4:1) provided the title compound as a brown oil (84% brsm.).  $R_f$ : 0.3 (hexane:EtOAc, 4:1).  $^1\text{H}$  NMR (400 MHz;  $\text{CDCl}_3$ ):  $\delta_{\text{H}}$  2.34 (3H, s,  $\text{CH}_3$ ), 3.89 (3H, d, s,  $\text{CH}_3$ ), 4.55 (2H, d,  $J = 5.5$  Hz,  $\text{CH}_2$ ), 6.37 (1H, d,  $J = 15.9$  Hz, CH), 7.15 (2H, d,  $J = 7.8$  Hz, ArCH), 7.22 (2H, d,  $J = 8.0$  Hz, ArCH), 7.44 (1H, d,  $J = 15.9$  Hz, CH), 7.70 (1H, t,  $J = 1.4$  Hz, ArCH), 7.81 (1H, t,  $J = 1.2$  Hz, ArCH), 7.87 (1H, t,  $J = 1.6$  Hz, ArCH);  $^{13}\text{C}$  NMR (100 MHz;  $\text{CDCl}_3$ ):  $\delta_{\text{C}}$  21.1, 28.1, 44.0, 81.0, 122.8, 123.1, 125.1, 127.9, 129.4, 131.0, 133.1, 134.6, 136.8, 137.0, 137.4, 140.7, 165.4, 165.4.

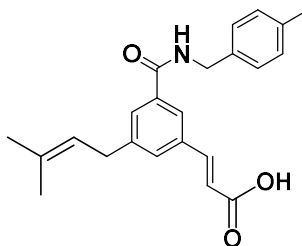


*Tert-butyl(E)-3-(3-((4-methylbenzyl)carbamoyl)-5-(3-methylbut-2-en-1-yl)phenyl)acrylate (2.6)*: To a solution of (**2.4**) (80 mg, 0.18 mmol) in dry DMF (2 mL), Cs<sub>2</sub>CO<sub>3</sub> (130 mg, 0.4 mmol), Pd(dppf)Cl<sub>2</sub> (8.5 mg, 0.01 mmol) were added and the flask was purged with nitrogen. Prenyl boronic acid pinacol ester (70  $\mu$ L, 0.3 mmol) was added and the mixture was stirred at 90 °C overnight. The reaction was allowed to cool and was filtered through a celite® pad with EtOAc. The solvent was evaporated in vacuo, re-dissolved in DCM and the residual DMF removed by washing with copious amounts of water in DCM, the organic phase was extracted, dried (Na<sub>2</sub>SO<sub>4</sub>), filtered, and concentrated. Purification by column chromatography (hexane:EtOAc = 10:1, 4:1, 2:1) provided the title compound as a transparent oil (66%). R<sub>f</sub>: 0.5 (hexane:EtOAc, 4:1). <sup>1</sup>H NMR (400 MHz; CDCl<sub>3</sub>):  $\delta_{\text{H}}$  1.55 (9H, s, (CH<sub>3</sub>)<sub>3</sub>), 1.72 (3H, s, CH<sub>3</sub>), 1.77 (3H, s, CH<sub>3</sub>), 2.34 (3H, s, CH<sub>3</sub>), 3.37 (2H, d,  $J$  = 7.3 Hz, CH<sub>2</sub>), 4.55 (2H, d,  $J$  = 5.5 Hz, CH<sub>2</sub>), 5.28 (1H, t,  $J$  = 7.3 Hz), 6.39 (1H, d,  $J$  = 15.9 Hz, CH), 7.25 – 7.37 (4H, m, ArCH), 7.41 (1H, s, ArCH), 7.51 (1H, s, ArCH), 7.55 (1H, d,  $J$  = 16.0 Hz, CH), 7.61 (1H, s, ArCH). <sup>13</sup>C NMR (100 MHz; CDCl<sub>3</sub>):  $\delta_{\text{C}}$  17.9, 25.7, 28.1, 34.0, 35.6, 41.1, 80.6, 121.1, 121.9, 123.7, 126.6, 128.3, 128.7, 128.8, 130.6, 133.7, 135.0, 135.4, 138.8, 142.6, 143.1, 166.0, 167.1.

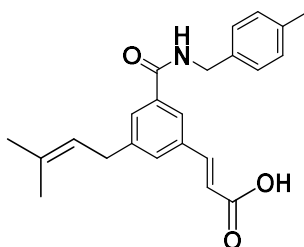


*Methyl(E)-3-(3-((4-methylbenzyl)carbamoyl)-5-(3-methylbut-2-en-1-yl)phenyl)*

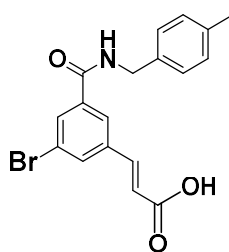
*acrylate (2.7)*: To a solution of (**2.5**) (80 mg, 0.18 mmol) in dry DMF (2 mL) was added Cs<sub>2</sub>CO<sub>3</sub> (130 mg, 0.4 mmol), Pd(dppf)Cl<sub>2</sub> (8.5 mg, 0.01 mmol) and the flask was purged with nitrogen. Prenyl boronic acid pinacol ester (70 µL, 0.3 mmol) was added and the mixture was stirred at 90 °C overnight. The reaction was allowed to cool and was filtered through a celite® pad with EtOAc. The solvent was evaporated in vacuo, re-dissolved in DCM and the residual DMF removed by washing with copious amounts of water in DCM, the organic phase was extracted, dried (Na<sub>2</sub>SO<sub>4</sub>), filtered, and concentrated. Purification by column chromatography (hexane:EtOAc = 10:1, 4:1, 2:1) provided the title compound as a transparent oil (73%). R<sub>f</sub>: 0.5 (hexane:EtOAc, 4:1). <sup>1</sup>H NMR (400 MHz; CDCl<sub>3</sub>): δ<sub>H</sub> 1.72 (3H, s, CH<sub>3</sub>), 1.77 (3H, s, CH<sub>3</sub>), 2.34 (3H, s, CH<sub>3</sub>), 3.37 (2H, d, *J* = 7.3 Hz, CH<sub>2</sub>), 3.89 (3H, d, s, CH<sub>3</sub>), 4.55 (2H, d, *J* = 5.5 Hz, CH<sub>2</sub>), 5.28 (1H, t, *J* = 7.3 Hz), 6.39 (1H, d, *J* = 15.9 Hz, CH), 7.25 – 7.37 (4H, m, ArCH), 7.41 (1H, s, ArCH), 7.51 (1H, s, ArCH), 7.55 (1H, d, *J* = 16.0 Hz, CH), 7.61 (1H, s, ArCH). <sup>13</sup>C NMR (100 MHz; CDCl<sub>3</sub>): δ<sub>C</sub> 17.9, 25.7, 28.1, 34.0, 35.6, 41.1, 80.6, 121.1, 121.9, 123.7, 126.6, 128.3, 128.7, 128.8, 130.6, 133.7, 135.0, 135.4, 138.8, 142.6, 143.1, 166.0, 167.1.



(*E*)-3-(3-((4-methylbenzyl)carbamoyl)-5-(3-methylbut-2-en-1-yl)phenyl) acrylic acid (**2.8**): To a solution of substituted *tert*-butyl intermediates (**2.6**) (60 mg, 0.14 mmol) in toluene, chromatography-grade silica gel (5 mL) was added and the mixture was refluxed with vigorous agitation overnight. Upon cooling, the reaction mixture was diluted with 10% methanol in DCM and filtered over a celite pad using 10% methanol in DCM as the solvent. The crude product was purified by column chromatography using DCM/MeOH gradient (20:1, 10:1) and a solvent was evaporated in vacuo to provide the final compound as a white solid (30%).  $R_f$ : 0.3 (DCM:MeOH 10:1).  $^1\text{H}$  NMR (400 MHz; MeOD):  $\delta_{\text{H}}$  1.72 (3H, s,  $\text{CH}_3$ ), 1.77 (3H, s,  $\text{CH}_3$ ), 2.34 (3H, s,  $\text{CH}_3$ ), 3.37 (2H, t,  $J = 6.9$  Hz,  $\text{CH}_2$ ), 4.55 (2H, d,  $J = 7.3$  Hz,  $\text{CH}_2$ ), 5.28 (1H, t,  $J = 7.3$  Hz), 6.39 (1H, d,  $J = 15.9$  Hz, CH), 7.15 (2H, d,  $J = 7.8$  Hz, ArCH), 7.24 (2H, d,  $J = 8.0$  Hz, ArCH), 7.41 (1H, s, ArCH), 7.51 (1H, s, ArCH), 7.55 (1H, d,  $J = 16.0$  Hz, CH), 7.61 (1H, s, ArCH).  $^{13}\text{C}$  NMR (100 MHz; MeOD):  $\delta_{\text{C}}$  17.9, 25.7, 28.1, 34.0, 35.6, 41.1, 80.6, 121.1, 121.9, 123.7, 126.6, 128.3, 128.7, 128.8, 130.6, 133.7, 135.0, 135.4, 138.8, 142.6, 143.1, 166.0, 167.1. HRMS (ESI): ( $m/z$ ):  $[\text{M} + \text{H}]^+$  calcd for  $\text{C}_{23}\text{H}_{25}\text{NO}_3$ , 364.1907; found, 364.1899.

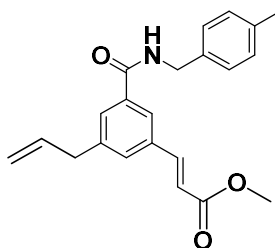


*(E)*-3-(3-((4-methylbenzyl)carbamoyl)-5-(3-methylbut-2-en-1-yl)phenyl) acrylic acid (**2.8**): Compound **2.6** (260 mg, 0.68 mmol) was hydrolyzed following the general procedure B. The solvent was evaporated in vacuo to provide the title compound as a white solid (95%).  $R_f$ : 0.3 (DCM:MeOH 10:1).  $^1\text{H}$  NMR (400 MHz; MeOD):  $\delta_{\text{H}}$  1.72 (3H, s,  $\text{CH}_3$ ), 1.77 (3H, s,  $\text{CH}_3$ ), 2.34 (3H, s,  $\text{CH}_3$ ), 3.37 (2H, t,  $J = 6.9$  Hz,  $\text{CH}_2$ ), 4.55 (2H, d,  $J = 7.3$  Hz,  $\text{CH}_2$ ), 5.28 (1H, t,  $J = 7.3$  Hz), 6.39 (1H, d,  $J = 15.9$  Hz, CH), 7.15 (2H, d,  $J = 7.8$  Hz, ArCH), 7.24 (2H, d,  $J = 8.0$  Hz, ArCH), 7.41 (1H, s, ArCH), 7.51 (1H, s, ArCH), 7.55 (1H, d,  $J = 16.0$  Hz, CH), 7.61 (1H, s, ArCH).  $^{13}\text{C}$  NMR (100 MHz; MeOD):  $\delta_{\text{C}}$  17.9, 25.7, 28.1, 34.0, 35.6, 41.1, 80.6, 121.1, 121.9, 123.7, 126.6, 128.3, 128.7, 128.8, 130.6, 133.7, 135.0, 135.4, 138.8, 142.6, 143.1, 166.0, 167.1. HRMS (ESI): ( $m/z$ ):  $[\text{M} + \text{H}]^+$  calcd for  $\text{C}_{23}\text{H}_{25}\text{NO}_3$ , 364.1907; found, 364.1899.

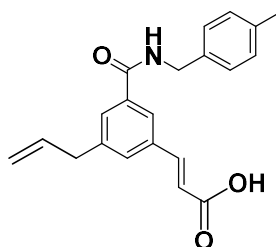


*(E)*-3-(3-bromo-5-((4-methylbenzyl)carbamoyl)phenyl) acrylic acid (**2.18**): Compound **2.5** (271 mg, 0.7 mmol) was hydrolyzed following the general procedure B. The solvent was evaporated in vacuo to provide the title compound as a white solid (95%).  $R_f$ : 0.4 (DCM:MeOH 10:1).  $^1\text{H}$  NMR (400 MHz; MeOD):  $\delta_{\text{H}}$  2.34 (3H, s,  $\text{CH}_3$ ), 4.55 (2H, d,  $J = 5.5$  Hz,  $\text{CH}_2$ ), 6.37 (1H, d,  $J = 15.9$  Hz, CH), 7.15 (2H, d,  $J = 7.8$  Hz, ArCH), 7.22 (2H,

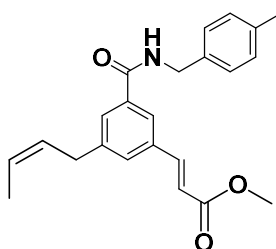
d,  $J = 8.0$  Hz, ArCH), 7.44 (1H, d,  $J = 15.9$  Hz, CH), 7.70 (1H, t,  $J = 1.4$  Hz, ArCH). 7.81 (1H, t,  $J = 1.2$  Hz, ArCH). 7.87 (1H, t,  $J = 1.6$  Hz, ArCH).  $^{13}\text{C}$  NMR (100 MHz; MeOD):  $\delta_{\text{C}}$  21.1, 28.1, 44.0, 81.0, 122.8, 123.1, 125.1, 127.9, 129.4, 131.0, 133.1, 134.6, 136.8, 137.0, 137.4, 140.7, 165.4, 165.4. HRMS (ESI): ( $m/z$ ):  $[\text{M} + \text{H}]^+$  calcd for  $\text{C}_{18}\text{H}_{16}\text{BrNO}_3$ , 375.2319; found, 375.2318.



*Methyl(E)-3-(3-allyl-5-((4-methylbenzyl)carbamoyl)phenyl)acrylate*: Following the procedure as described for **2.7** the title compound was obtained using allyl boronic acid pinacol ester as a transparent oil (70%). R<sub>f</sub>: 0.26 (hexane:EtOAc, 4:1).  $^1\text{H}$  NMR (400 MHz;  $\text{CDCl}_3$ ):  $\delta_{\text{H}}$  2.34 (3H, s,  $\text{CH}_3$ ), 2.43 (2H, d,  $J = 6.6$  Hz,  $\text{CH}_2$ ), 2.96 (2H, t,  $J = 6.9$  Hz,  $\text{CH}_2$ ), 3.89 (3H, d, s,  $\text{CH}_3$ ), 5.09 – 5.15 (2H, m,  $\text{CH}_2$ ), 5.89 – 5.99 (1H, m, CH), 6.40 (1H, d,  $J = 15.9$  Hz, CH), 7.25 – 7.30 (2H, m, ArCH), 7.34 – 7.38 (2H, m, ArCH), 7.44 (1H, s, ArCH), 7.52 (1H, s, ArCH), 7.56 (1H, d,  $J = 16.0$  Hz, CH), 7.63 (1H, s, ArCH).  $^{13}\text{C}$  NMR (100 MHz;  $\text{CDCl}_3$ ):  $\delta_{\text{C}}$  28.1, 35.6, 39.8, 41.7, 80.7, 116.9, 121.3, 126.6, 128.5, 128.7, 128.8, 129.6, 130.8, 135.2, 135.5, 136.2, 138.8, 141.3, 142.4, 165.9, 167.0.



*(E)*-3-(3-allyl-5-((4-methylbenzyl)carbamoyl)phenyl) acrylic acid (**2.19**): Following the general procedure A, the title compound, synthesized using **2.6**, was obtained as a white solid (77%).  $R_f$ : 0.26 (DCM:MeOH, 20:1).  $^1\text{H}$  NMR (400 MHz; MeOD):  $\delta_{\text{H}}$  2.34 (3H, s,  $\text{CH}_3$ ), 2.94 (2H, t,  $J = 7.1$  Hz,  $\text{CH}_2$ ), 3.48 (2H, d,  $J = 6.7$  Hz,  $\text{CH}_2$ ), 5.11–5.17 (2H, m,  $\text{CH}_2$ ), 5.96–6.06 (1H, m, CH), 6.55 (1H, d,  $J = 16.0$  Hz, CH), 7.15 (2H, d,  $J = 7.8$  Hz, ArCH), 7.24 (2H, d,  $J = 8.0$  Hz, ArCH), 7.59 (1H, s, ArCH), 7.66 (1H, s, ArCH), 7.70 (1H, s, ArCH), 7.82 (1H, d,  $J = 16.0$  Hz, CH).  $^{13}\text{C}$  NMR (100 MHz; MeOD):  $\delta_{\text{C}}$  35.0, 39.3, 41.2, 115.5, 124.0, 125.9, 127.6, 128.1, 128.5, 128.8, 129.4, 130.8, 134.9, 135.3, 136.5, 139.1, 141.5, 143.6, 168.1. HRMS (ESI): ( $m/z$ ):  $[\text{M} + \text{H}]^+$  calcd for  $\text{C}_{22}\text{H}_{23}\text{NO}_3$ , 350.1794; found, 350.1795.

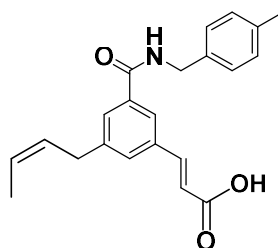


*Methyl(E)*-3-(3-((*Z*)-but-2-en-1-yl)-5-((4-methylbenzyl)carbamoyl)phenyl)acrylate:

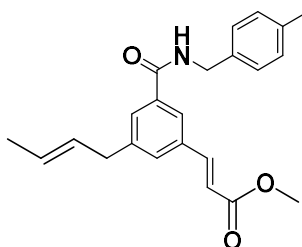
Following the procedure as described for **2.7** the title compound was obtained using *cis*-crotylboronic acid pinacol ester as a transparent oil (75%).  $R_f$ : 0.5 (hexane:EtOAc, 4:1).  $^1\text{H}$  NMR (400 MHz;  $\text{CDCl}_3$ ):  $\delta_{\text{H}}$  1.77 (3H, s,  $\text{CH}_3$ ), 2.34 (3H, s,  $\text{CH}_3$ ), 2.96 (2H, t,  $J = 6.9$  Hz,  $\text{CH}_2$ ), 3.76 (2H, d,  $J = 6.6$  Hz,  $\text{CH}_2$ ), 3.89 (3H, d, s,  $\text{CH}_3$ ), 5.09 – 5.15 (1H, m, CH), 5.89 – 5.99 (1H, m, CH), 6.40 (1H, d,  $J = 15.9$  Hz, CH), 7.25 – 7.30 (2H, m, ArCH), 7.34



– 7.38 (2H, m, ArCH), 7.44 (1H, s, ArCH), 7.52 (1H, s, ArCH), 7.56 (1H, d,  $J = 16.0$  Hz, CH), 7.63 (1H, s, ArCH).  $^{13}\text{C}$  NMR (100 MHz;  $\text{CDCl}_3$ ):  $\delta_{\text{C}}$  28.1, 35.6, 39.8, 41.7, 80.7, 116.9, 121.3, 126.6, 128.5, 128.7, 128.8, 129.6, 130.8, 135.2, 135.5, 136.2, 138.8, 141.3, 142.4, 165.9, 167.0.



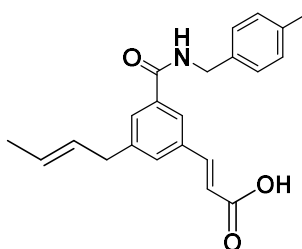
*(E)-3-(3-((Z)-but-2-en-1-yl)-5-((4-methylbenzyl)carbamoyl)phenyl) acrylic acid* (**2.20**): Following the general procedure A, the title compound, synthesized using **2.6**, was obtained as a white solid (87%).  $R_f$ : 0.26 (DCM:MeOH, 20:1).  $^1\text{H}$  NMR (400 MHz; MeOD):  $\delta_{\text{H}}$  1.77 (3H, s,  $\text{CH}_3$ ), 2.34 (3H, s,  $\text{CH}_3$ ), 2.96 (2H, t,  $J = 6.9$  Hz,  $\text{CH}_2$ ), 3.76 (2H, d,  $J = 6.6$  Hz,  $\text{CH}_2$ ), 5.09 – 5.15 (1H, m, CH), 5.89 – 5.99 (1H, m, CH), 6.40 (1H, d,  $J = 15.9$  Hz, CH), 7.25 – 7.30 (2H, m, ArCH), 7.34 – 7.38 (2H, m, ArCH), 7.44 (1H, s, ArCH), 7.52 (1H, s, ArCH), 7.56 (1H, d,  $J = 16.0$  Hz, CH), 7.63 (1H, s, ArCH).  $^{13}\text{C}$  NMR (100 MHz; MeOD):  $\delta_{\text{C}}$  28.1, 35.6, 39.8, 41.7, 80.7, 116.9, 121.3, 126.6, 128.5, 128.7, 128.8, 129.6, 130.8, 135.2, 135.5, 136.2, 138.8, 141.3, 142.4, 165.9, 167.0. HRMS (ESI): ( $m/z$ ):  $[\text{M} + \text{H}]^+$  calcd for  $\text{C}_{23}\text{H}_{25}\text{NO}_3$ , 363.4617; found, 363.4679.



*Methyl(E)-3-(3-((E)-but-2-en-1-yl)-5-((4-methylbenzyl)carbamoyl)phenyl)acrylate:*

Following the procedure as described for **2.7** the title compound was obtained using *trans*-crotylboronic acid pinacol ester as a transparent oil (75%). *R*<sub>f</sub>: 0.5 (hexane:EtOAc, 4:1).

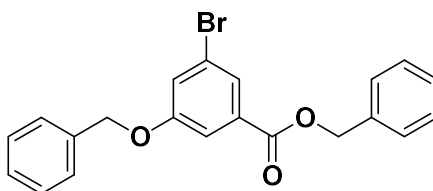
<sup>1</sup>H NMR (400 MHz; CDCl<sub>3</sub>): δ<sub>H</sub> 1.72 (3H, s, CH<sub>3</sub>), 2.34 (3H, s, CH<sub>3</sub>), 2.96 (2H, t, *J* = 6.9 Hz, CH<sub>2</sub>), 3.76 (2H, d, *J* = 6.6 Hz, CH<sub>2</sub>), 3.89 (3H, d, s, CH<sub>3</sub>), 5.09 – 5.15 (1H, m, CH), 5.89 – 5.99 (1H, m, CH), 6.40 (1H, d, *J* = 15.9 Hz, CH), 7.25 – 7.30 (2H, m, ArCH), 7.34 – 7.38 (2H, m, ArCH), 7.44 (1H, s, ArCH), 7.52 (1H, s, ArCH), 7.56 (1H, d, *J* = 16.0 Hz, CH), 7.63 (1H, s, ArCH). <sup>13</sup>C NMR (100 MHz; CDCl<sub>3</sub>): δ<sub>C</sub> 28.1, 35.6, 39.8, 41.7, 80.7, 116.9, 121.3, 126.6, 128.5, 128.7, 128.8, 129.6, 130.8, 135.2, 135.5, 136.2, 138.8, 141.3, 142.4, 165.9, 167.0.



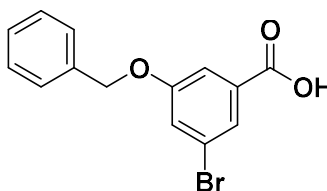
*(E)-3-(3-((E)-but-2-en-1-yl)-5-((4-methylbenzyl)carbamoyl)phenyl) acrylic acid*

**(2.21)**: Following the general procedure A, the title compound, synthesized using **2.6**, was obtained as a white solid (83%). *R*<sub>f</sub>: 0.26 (DCM:MeOH, 20:1). <sup>1</sup>H NMR (400 MHz; MeOD): δ<sub>H</sub> 1.72 (3H, s, CH<sub>3</sub>), 2.34 (3H, s, CH<sub>3</sub>), 2.97 (2H, t, *J* = 6.9 Hz, CH<sub>2</sub>), 3.77 (2H, d, *J* = 6.6 Hz, CH<sub>2</sub>), 5.09 – 5.15 (1H, m, CH), 5.89 – 5.99 (1H, m, CH), 6.40 (1H, d, *J* = 15.9 Hz, CH), 7.25 – 7.30 (2H, m, ArCH), 7.34 – 7.38 (2H, m, ArCH), 7.44 (1H, s, ArCH), 7.52 (1H, s,

ArCH), 7.56 (1H, d,  $J$  = 16.0 Hz, CH), 7.63 (1H, s, ArCH).  $^{13}\text{C}$  NMR (100 MHz; MeOD):  $\delta_{\text{C}}$  28.1, 35.6, 39.8, 41.7, 80.7, 116.9, 121.3, 126.6, 128.5, 128.7, 128.8, 129.6, 130.8, 135.2, 135.5, 136.2, 138.8, 141.3, 142.4, 165.9, 167.0. HRMS (ESI): ( $m/z$ ):  $[\text{M} + \text{H}]^+$  calcd for  $\text{C}_{23}\text{H}_{25}\text{NO}_3$ , 363.4694; found, 363.4695.

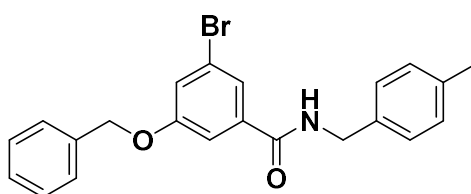


**Benzyl 3-(benzyloxy)-5-bromobenzoate (2.10a):** To a solution of 3-bromo-5-hydroxy benzoic acid (200 mg, 1 mmol) in DIPEA (0.4 mL, 2.4 mmol) was added benzyl bromide (0.2 mL, 2.2 mmol) and the solution was heated at 150 °C overnight. The solution was allowed to cool and extracted with EtOAc (2 x 75 mL), dried ( $\text{Na}_2\text{SO}_4$ ), filtered and concentrated. Purification by column chromatography (hexane:EtOAc = 10:1, 4:1, 2:1) provided the title compound as a transparent oil (80%).  $R_f$ : 0.6 (hexane:EtOAc, 4:1).  $^1\text{H}$  NMR (400 MHz;  $\text{CDCl}_3$ ):  $\delta_{\text{H}}$  5.11 (2H, s,  $\text{CH}_2$ ), 5.41 (2H, s,  $\text{CH}_2$ ), 7.34 – 7.51 (11H, m, ArCH), 7.68 (1H, q,  $J$  = 1.3 Hz, ArCH), 7.88 (1H, t,  $J$  = 1.4 Hz, ArCH).  $^{13}\text{C}$  NMR (100 MHz;  $\text{CDCl}_3$ ):  $\delta_{\text{C}}$  67.2, 70.5, 114.6, 122.8, 123.0, 125.2, 127.6, 128.3, 128.4, 128.7, 128.7, 128.8, 132.8, 135.6, 135.9, 159.3, 164.9.



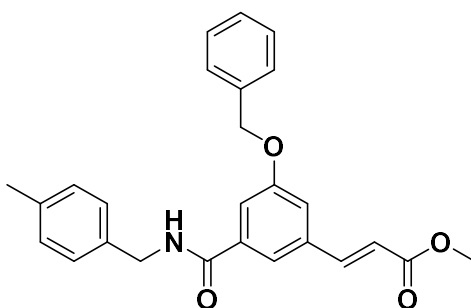
**3-(benzyloxy)-5-bromobenzoic acid (2.11a):** To a solution of benzyl 3-(benzyloxy)-5-bromobenzoate in MeOH (5 mL) was added 1M KOH (10 mL) and refluxed for 4 h. The pH of the solution was adjusted to 3 and extracted with EtOAc (2 x 75 mL), dried ( $\text{Na}_2\text{SO}_4$ ),

filtered and concentrated to provide the title compound as a white solid. (99%).  $R_f$ : 0.1 (hexane:EtOAc, 4:1).  $^1\text{H}$  NMR (400 MHz;  $\text{CDCl}_3$ ):  $\delta_{\text{H}}$  5.07 (2H, s,  $\text{CH}_2$ ), 7.29 – 7.43 (6H, m, ArCH), 7.57 (1H, q,  $J = 1.3$  Hz, ArCH), 7.71 (1H, t,  $J = 1.4$  Hz, ArCH).  $^{13}\text{C}$  NMR (100 MHz;  $\text{CDCl}_3$ ):  $\delta_{\text{C}}$  70.0, 114.4, 122.1, 124.6, 127.2, 127.7, 128.2, 133.4, 136.3, 159.5, 166.5.



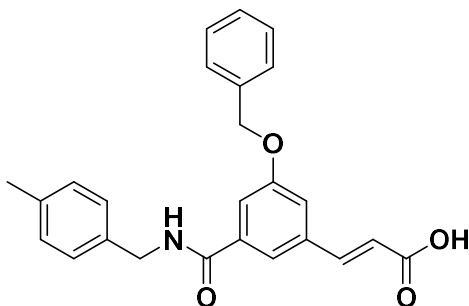
*3-(benzyloxy)-5-bromo-N-(4-methylbenzyl)benzamide (2.13a)*: To a solution of 3-(benzyloxy)-5-bromobenzoic acid (250 mg, 0.8 mmol) in dry toluene (7 mL) was added  $\text{SOCl}_2$  (220  $\mu\text{L}$ , 3 mmol) and the mixture was refluxed overnight. The reaction vessel was cooled to room temperature and the solvent was evaporated in vacuo. The resultant brown oil was used further without purification. To a solution of the acid chloride in DCM (10 mL) was added DMAP (26 mg, 0.2 mmol) and the flask was purged with nitrogen. 4-methylbenzylamine (250  $\mu\text{L}$ , 2 mmol) and  $\text{NEt}_3$  (350  $\mu\text{L}$ , 2.5 mmol) were added to the flask and the mixture was stirred at 70  $^\circ\text{C}$  overnight. The reaction mixture was cooled to room temperature, diluted with DCM, washed with a saturated aqueous  $\text{NaHCO}_3$  (40 mL), water (40 mL) and the organic phase was extracted with DCM, dried ( $\text{Na}_2\text{SO}_4$ ), filtered and concentrated. Purification by column chromatography (hexane:EtOAc = 10:1, 4:1) provided the title compound as a white solid (50%).  $R_f$ : 0.2 (hexane:EtOAc, 4:1).  $^1\text{H}$  NMR (400 MHz;  $\text{CDCl}_3$ ):  $\delta_{\text{H}}$  2.34 (3H, s,  $\text{CH}_3$ ), 2.92 (2H, t,  $J = 7.0$  Hz,  $\text{CH}_2$ ), 3.89 (3H, s,  $\text{CH}_3$ ), 5.03 (2H, s,  $\text{CH}_2$ ), 7.23 – 7.42 (12H, m, ArCH).  $^{13}\text{C}$  NMR (100 MHz;  $\text{CDCl}_3$ ):  $\delta_{\text{C}}$  35.6, 41.3,

70.4, 112.4, 121.2, 122.3, 122.9, 126.6, 127.5, 128.3, 128.7, 128.8, 128.8, 135.9, 137.5, 138.7, 159.5, 166.0.



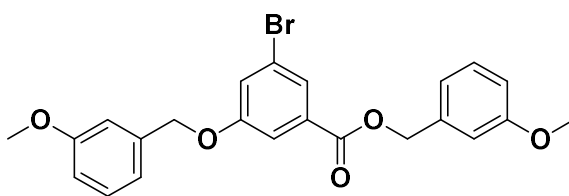
*Methyl(E)-3-(3-(benzyloxy)-5-((4-methylbenzyl)carbamoyl)phenyl)acrylate*

**(2.14a)**: To a solution of 3-(benzyloxy)-5-bromo-*N*-(4-methylbenzyl)benzamide (100 mg, 0.3 mmol) in dry DMF (1.5 mL), was added DABCO (4 mg, 0.03 mmol), Pd(OAc)<sub>2</sub> (4 mg, 0.015 mmol) and the flask was purged with nitrogen. methylacrylate (60  $\mu$ L, 0.4 mmol) and K<sub>2</sub>CO<sub>3</sub> (55 mg, 0.4 mmol) were added and the mixture was stirred at 120 °C for 18 h. The reaction was allowed to cool and washed with saturated aqueous NH<sub>4</sub>Cl (50 mL), brine (2 x 50 mL), extracted with DCM, dried (Na<sub>2</sub>SO<sub>4</sub>), filtered and concentrated. Purification by column chromatography (hexane:EtOAc = 9:1, 4:1, 2:1) provided the title compound as a white solid (22%). *R*<sub>f</sub>: 0.21 (hexane:EtOAc, 4:1). <sup>1</sup>H NMR (400 MHz; CDCl<sub>3</sub>):  $\delta_{\text{H}}$  2.34 (3H, s, CH<sub>3</sub>), 2.96 (2H, t, *J* = 7.0 Hz, CH<sub>2</sub>), 3.73 (2H, q, *J* = 6.0 Hz, CH<sub>2</sub>), 3.89 (3H, d, s, CH<sub>3</sub>), 6.37 (1H, d, *J* = 15.9 Hz, CH), 7.21 – 7.46 (11H, m, ArCH), 7.52 (1H, d, *J* = 15.9 Hz, CH). <sup>13</sup>C NMR (100 MHz; CDCl<sub>3</sub>):  $\delta_{\text{C}}$  28.1, 35.6, 41.1, 70.3, 80.8, 114.6, 117.2, 118.5, 121.7, 126.7, 127.5, 128.2, 128.6, 128.7, 128.8, 136.1, 136.3, 136.7, 142.2, 159.2, 165.8, 166.7.



*(E)*-3-(3-(benzyloxy)-5-((4-methylbenzyl)carbamoyl)phenyl) acrylic acid (**2.22**):

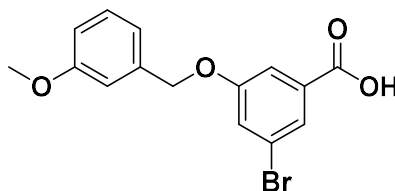
Following the general procedure A, the title compound, synthesized using **2.6**, was obtained as a white solid (65%).  $R_f$ : 0.26 (DCM:MeOH, 20:1).  $^1\text{H}$  NMR (400 MHz; MeOD):  $\delta_{\text{H}}$  2.34 (3H, s,  $\text{CH}_3$ ), 2.96 (2H, t,  $J = 7.0$  Hz,  $\text{CH}_2$ ), 3.73 (2H, q,  $J = 6.0$  Hz,  $\text{CH}_2$ ), 6.37 (1H, d,  $J = 15.9$  Hz, CH), 7.21 – 7.46 (11H, m, ArCH), 7.52 (1H, d,  $J = 15.9$  Hz, CH), 7.71 (1H, t,  $J = 1.4$  Hz, ArCH).  $^{13}\text{C}$  NMR (100 MHz; MeOD):  $\delta_{\text{C}}$  28.1, 35.6, 41.1, 70.3, 80.8, 114.6, 117.2, 118.5, 121.7, 126.7, 127.5, 128.2, 128.6, 128.7, 128.8, 136.1, 136.3, 136.7, 142.2, 159.2, 165.8, 166.7. HRMS (ESI): ( $m/z$ ):  $[\text{M} + \text{H}]^+$  calcd for  $\text{C}_{25}\text{H}_{23}\text{NO}_4$ , 424.1719; found, 424.1520.



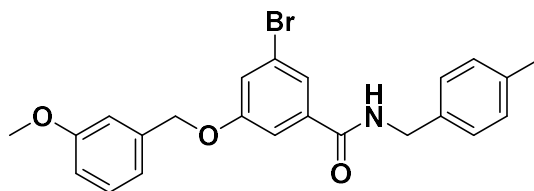
3-methoxybenzyl 3-bromo-5-((3-methoxybenzyl)oxy)benzoate (**2.10b**):

Following the procedure as described for benzyl 3-(benzyloxy)-5-bromobenzoate the title compound was obtained as a transparent oil (51%).  $^1\text{H}$  NMR (400 MHz;  $\text{CDCl}_3$ ):  $\delta_{\text{H}}$  3.84 (3H, s,  $\text{CH}_3$ ), 3.85 (3H, s,  $\text{CH}_3$ ), 5.07 (2H, s,  $\text{CH}_2$ ), 5.35 (2H, s,  $\text{CH}_2$ ), 6.90 – 7.05 (6H, m, ArCH), 7.30 – 7.36 (3H, m, ArCH), 7.63 (1H, q,  $J = 1.3$  Hz, ArCH), 7.83 (1H, t,  $J = 1.4$  Hz, ArCH).  $^{13}\text{C}$

NMR (100 MHz; CDCl<sub>3</sub>):  $\delta_C$  55.2, 67.0, 70.3, 112.9, 113.8, 113.8, 113.8, 114.6, 119.7, 120.4, 122.7, 123.0, 125.2, 129.7, 129.7, 132.7, 137.1, 137.4, 159.3, 159.8, 159.9, 164.9.

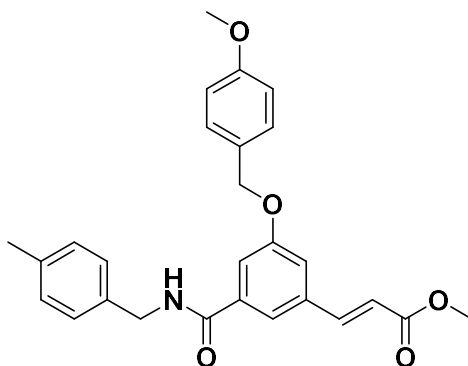


**3-bromo-5-((3-methoxybenzyl)oxy)benzoic acid (2.11b):** Following the procedure as described for 3-(benzyloxy)-5-bromobenzoic acid the title compound was obtained as a white solid (78%). R<sub>f</sub>: 0.1 (hexane:EtOAc, 4:1). <sup>1</sup>H NMR (400 MHz; CDCl<sub>3</sub>):  $\delta_H$  3.79 (3H, s, CH<sub>3</sub>), 5.09 (2H, s, CH<sub>2</sub>), 6.79 – 7.00 (4H, m, ArCH), 7.37 (1H, s, CH<sub>3</sub>), 7.58 (1H, s, CH<sub>3</sub>), 7.75 (1H, s, CH<sub>3</sub>). <sup>13</sup>C NMR (100 MHz; CDCl<sub>3</sub>):  $\delta_C$  63.7, 69.9, 114.4, 118.6, 119.3, 122.1, 122.1, 124.6, 128.9, 129.2, 133.6, 137.8, 142.9, 159.5, 166.5.



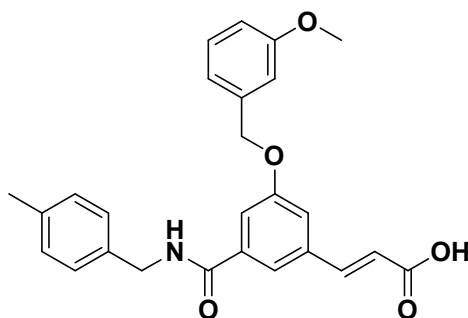
**3-bromo-5-((3-methoxybenzyl)oxy)-N-(4-methylbenzyl)benzamide (2.13b):**

Following the procedure as described for 3-(benzyloxy)-5-bromo-N-(4-methylbenzyl)benzamide the title compound was obtained as a white solid (60%). R<sub>f</sub>: 0.1 (hexane:EtOAc, 4:1). <sup>1</sup>H NMR (400 MHz; CDCl<sub>3</sub>):  $\delta_H$  2.34 (3H, s, CH<sub>3</sub>), 3.70 (2H, q, *J* = 6.0 Hz, CH<sub>2</sub>), 3.84 (3H, s, CH<sub>3</sub>), 5.04 (2H, s, CH<sub>2</sub>), 7.89 – 7.00 (2H, m, ArCH), 7.23 – 7.37 (9H, m, ArCH). <sup>13</sup>C NMR (100 MHz; CDCl<sub>3</sub>):  $\delta_C$  35.6, 41.3, 55.2, 70.3, 112.4, 112.9, 113.7, 119.6, 121.2, 122.2, 122.9, 126.6, 128.7, 128.8, 129.7, 137.4, 137.5, 138.7, 159.5, 159.8, 165.9.



*Methyl(E)-3-(3-((3-methoxybenzyl)oxy)-5-((4-methylbenzyl)carbamoyl)phenyl)*

*acrylate (2.14b)*: Following the procedure as described for methyl (*E*)-3-(3-(benzyloxy)-5-((4-methylbenzyl)carbamoyl)phenyl)acrylate the title compound was obtained as a white solid (20%). *R*<sub>f</sub>: 0.1 (hexane:EtOAc, 4:1). <sup>1</sup>H NMR (400 MHz; CDCl<sub>3</sub>): δ<sub>H</sub> 2.34 (3H, s, CH<sub>3</sub>), 2.96 (2H, t, *J* = 7.0 Hz, CH<sub>2</sub>), 3.72 (2H, q, *J* = 6.0 Hz, CH<sub>2</sub>), 3.84 (3H, s, CH<sub>3</sub>), 3.89 (3H, s, CH<sub>3</sub>), 6.37 (1H, d, *J* = 15.9 Hz, CH), 7.20 – 7.38 (11H, m, ArCH), 7.52 (1H, d, *J* = 15.9 Hz, CH). <sup>13</sup>C NMR (100 MHz; CDCl<sub>3</sub>): δ<sub>C</sub> 28.1, 35.6, 41.1, 55.2, 70.1, 80.8, 112.9, 113.7, 114.7, 117.1, 118.5, 119.6, 121.7, 126.7, 128.7, 128.7, 128.8, 129.7, 136.3, 136.7, 137.7, 138.7, 142.2, 159.8, 165.8, 166.7.

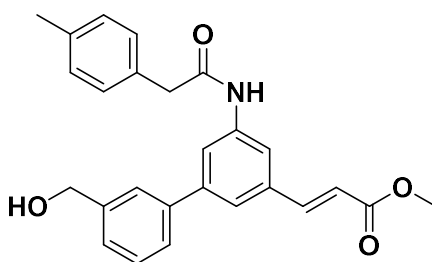


*(E)-3-(3-((3-methoxybenzyl)oxy)-5-((4-methylbenzyl)carbamoyl)phenyl) acrylic*

*acid (2.23)*: Following the general procedure A, the title compound, synthesized using **2.6**, was obtained as a white solid (63%). *R*<sub>f</sub>: 0.26 (DCM:MeOH, 20:1). <sup>1</sup>H NMR (400 MHz; MeOD): δ<sub>H</sub> 2.34 (3H, s, CH<sub>3</sub>), 2.96 (2H, t, *J* = 7.0 Hz, CH<sub>2</sub>), 3.72 (2H, q, *J* = 6.0 Hz, CH<sub>2</sub>),

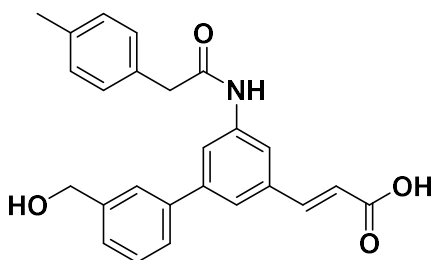


3.84 (3H, s, CH<sub>3</sub>), 6.37 (1H, d,  $J$  = 15.9 Hz, CH), 7.20 – 7.38 (11H, m, ArCH), 7.52 (1H, d,  $J$  = 15.9 Hz, CH). <sup>13</sup>C NMR (100 MHz; MeOD):  $\delta_c$  28.1, 35.6, 41.1, 55.2, 70.1, 80.8, 112.9, 113.7, 114.7, 117.1, 118.5, 119.6, 121.7, 126.7, 128.7, 128.7, 128.8, 129.7, 136.3, 136.7, 137.7, 138.7, 142.2, 159.8, 165.8, 166.7. HRMS (ESI): ( $m/z$ ): [M + H]<sup>+</sup> calcd for C<sub>26</sub>H<sub>25</sub>NO<sub>5</sub>, 454.1625; found, 454.1630.



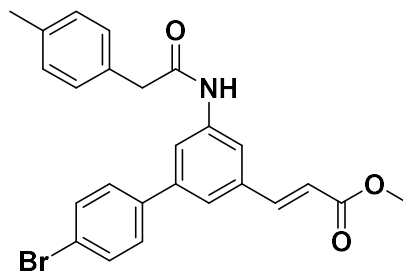
*Methyl(E)-3-(3'-(hydroxymethyl)-5-(2-(p-tolyl)acetamido)-[1,1'-biphenyl]-3-yl)*

*acrylate*: Following the procedure as described for **2.7** the title compound was obtained using (3-(4,4,5,5-tetramethyl-1,3,2-dioxaborolan-2-yl)phenyl)methanol as a transparent oil (75%). R<sub>f</sub>: 0.3 (hexane:EtOAc, 4:1). <sup>1</sup>H NMR (400 MHz; CDCl<sub>3</sub>):  $\delta_H$  2.34 (3H, s, CH<sub>3</sub>), 2.64 (2H, t,  $J$  = 7.4 Hz, CH<sub>2</sub>), 3.89 (3H, s, CH<sub>3</sub>), 4.68 (2H, s, CH<sub>2</sub>), 6.35 (1H, d,  $J$  = 15.9 Hz, CH), 7.19 – 7.50 (9H, m, ArCH), 7.56 (1H, s, CH), 7.59 (1H, s, ArCH), 8.08 (1H, s, ArCH). <sup>13</sup>C NMR (100 MHz; CDCl<sub>3</sub>):  $\delta_c$  28.2, 31.4, 39.0, 64.9, 80.8, 120.3, 120.9, 122.5, 125.6, 126.1, 126.3, 128.3, 128.6, 128.6, 128.9, 129.2, 135.6, 138.7, 140.1, 140.5, 141.5, 142.1, 143.1, 166.3, 171.2.



*(E)-3-(3'-(hydroxymethyl)-5-(2-(p-tolyl)acetamido)-[1,1'-biphenyl]-3-yl) acrylic acid*

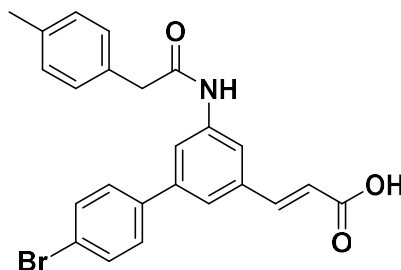
**(2.24)**: Following the general procedure A, the title compound, synthesized using **2.6**, was obtained as a white solid (73%).  $R_f$ : 0.26 (DCM:MeOH, 20:1).  $^1\text{H}$  NMR (400 MHz; MeOD):  $\delta_{\text{H}}$  2.44 (3H, s,  $\text{CH}_3$ ), 2.72 (2H, t,  $J = 7.3$  Hz,  $\text{CH}_2$ ), 6.54 (1H, d,  $J = 15.8$  Hz, CH), 7.17–7.22 (1H, m, ArCH), 7.28–7.29 (3H, m, ArCH), 7.37–7.39 (1H, m, ArCH), 7.44 (1H, t,  $J = 7.5$  Hz, ArCH), 7.53–7.56 (2H, m, ArCH), 7.64 (1H, s, ArCH), 7.70 (1H, d,  $J = 16.0$  Hz, CH), 7.78 (1H, s, ArCH), 7.85 (1H, s, ArCH).  $^{13}\text{C}$  NMR (100 MHz; MeOD):  $\delta_{\text{C}}$  31.3, 38.5, 63.7, 117.5, 120.1, 122.2, 125.2, 125.5, 125.8, 126.0, 128.0, 128.1, 128.6, 135.5, 139.5, 140.0, 140.7, 142.1, 142.4, 144.5, 172.5. ESI-HRMS ( $m/z$ ):  $[\text{M} + \text{H}]^+$  calcd for  $\text{C}_{25}\text{H}_{23}\text{NO}_4$ , 402.1700; found, 402.1701.



*Methyl(E)-3-(4'-bromo-5-(2-(p-tolyl)acetamido)-[1,1'-biphenyl]-3-yl)acrylate:*

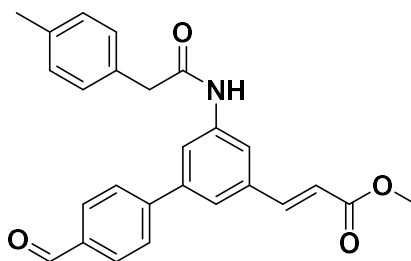
Following the procedure as described for **2.7** the title compound was obtained using 2-(4-bromophenyl)-4,4,5,5-tetramethyl-1,3,2-dioxaborolane as a transparent oil (78%).  $R_f$ : 0.32 (hexane:EtOAc, 4:1).  $^1\text{H}$  NMR (400 MHz;  $\text{CDCl}_3$ ):  $\delta_{\text{H}}$  2.34 (3H, s,  $\text{CH}_3$ ), 2.64 (2H, t,  $J = 7.4$

Hz, CH<sub>2</sub>), 3.89 (3H, s, CH<sub>3</sub>), 6.35 (1H, d,  $J$  = 15.9 Hz, CH), 7.19 – 7.50 (8H, m, ArCH), 7.56 (1H, s, ArCH), 7.59 (1H, s, ArCH), 7.64 (1H, s, ArCH), 8.08 (1H, s, ArCH). <sup>13</sup>C NMR (100 MHz; CDCl<sub>3</sub>): δ<sub>C</sub> 28.2, 31.4, 39.0, 64.9, 80.8, 120.3, 120.9, 122.5, 125.6, 126.1, 126.3, 128.9, 129.2, 135.6, 138.7, 140.1, 140.5, 141.5, 142.1, 143.1, 166.3, 171.2.



*(E)-3-(4'-bromo-5-(2-(p-tolyl)acetamido)-[1,1'-biphenyl]-3-yl) acrylic acid (2.25):*

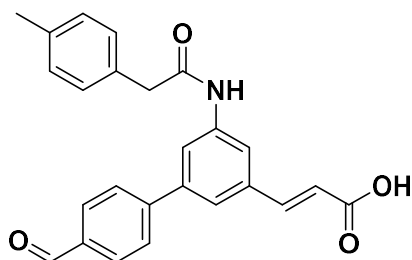
Following the general procedure A, the title compound, synthesized using **2.6**, was obtained as a white solid (72%). R<sub>f</sub>: 0.29 (DCM:MeOH, 20:1). <sup>1</sup>H NMR (400 MHz; MeOD): δ<sub>H</sub> 2.34 (3H, s, CH<sub>3</sub>), 2.64 (2H, t,  $J$  = 7.4 Hz, CH<sub>2</sub>), 6.35 (1H, d,  $J$  = 15.9 Hz, CH), 7.19 – 7.50 (8H, m, ArCH), 7.56 (1H, s, ArCH), 7.59 (1H, s, ArCH), 7.79 (1H, s, ArCH), 8.08 (1H, s, ArCH). <sup>13</sup>C NMR (100 MHz; MeOD): δ<sub>C</sub> 28.2, 31.4, 39.0, 64.9, 80.8, 120.3, 120.9, 122.5, 125.6, 126.1, 126.3, 128.9, 129.2, 135.6, 138.7, 140.1, 140.5, 141.5, 142.1, 143.1, 166.3, 171.2. ESI-HRMS (m/z): [M + H]<sup>+</sup> calcd for C<sub>24</sub>H<sub>20</sub>BrNO<sub>3</sub>, 451.0617; found, 451.0681.



*Methyl(E)-3-(4'-formyl-5-(2-(p-tolyl)acetamido)-[1,1'-biphenyl]-3-yl)acrylate:*

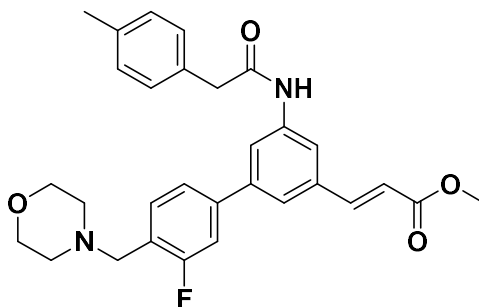
Following the procedure as described for **2.7** the title compound was obtained using 4-

(4,4,5,5-tetramethyl-1,3,2-dioxaborolan-2-yl)benzaldehyde as a white solid (78%).  $R_f$ : 0.25 (hexane:EtOAc, 4:1).  $^1\text{H}$  NMR (400 MHz;  $\text{CDCl}_3$ ):  $\delta_{\text{H}}$  2.34 (3H, s,  $\text{CH}_3$ ), 2.64 (2H, t,  $J$  = 7.4 Hz,  $\text{CH}_2$ ), 3.89 (3H, s,  $\text{CH}_3$ ), 6.35 (1H, d,  $J$  = 15.9 Hz, CH), 7.19 – 7.50 (8H, m, ArCH), 7.56 (1H, s, ArCH), 7.59 (1H, s, CH), 7.79 (1H, s, ArCH), 8.08 (1H, s, ArCH), 8.89 (1H, s, CH).  $^{13}\text{C}$  NMR (100 MHz;  $\text{CDCl}_3$ ):  $\delta_{\text{C}}$  28.2, 31.4, 39.0, 64.9, 80.8, 120.3, 120.9, 122.5, 125.6, 126.1, 126.3, 128.9, 129.2, 135.6, 138.7, 140.1, 140.5, 141.5, 142.1, 143.1, 166.3, 181.2.

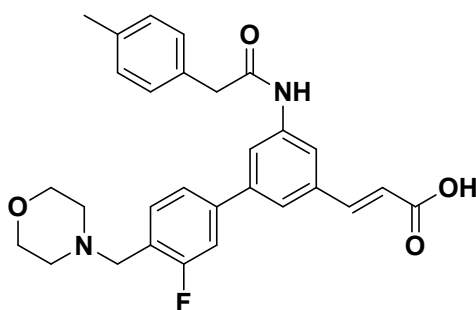


*(E)-3-(4'-formyl-5-(2-(p-tolyl)acetamido)-[1,1'-biphenyl]-3-yl) acrylic acid (2.26):*

Following the general procedure A, the title compound, synthesized using **2.6**, was obtained as a white solid (77%).  $R_f$ : 0.29 (DCM:MeOH, 20:1).  $^1\text{H}$  NMR (400 MHz; MeOD):  $\delta_{\text{H}}$  2.41 (3H, s,  $\text{CH}_3$ ), 2.69 (2H, t,  $J$  = 7.4 Hz,  $\text{CH}_2$ ), 6.34 (1H, d,  $J$  = 15.9 Hz, CH), 7.29 – 7.60 (8H, m, ArCH), 7.66 (1H, s, ArCH), 7.69 (1H, s, CH), 7.79 (1H, s, ArCH), 8.28 (1H, s, ArCH), 8.99 (1H, s, CH).  $^{13}\text{C}$  NMR (100 MHz; MeOD):  $\delta_{\text{C}}$  28.2, 31.4, 39.0, 64.9, 80.8, 120.3, 120.9, 122.5, 125.6, 126.1, 126.3, 128.9, 129.2, 135.6, 138.7, 140.1, 140.5, 141.5, 142.1, 143.1, 166.3, 181.2. ESI-HRMS ( $m/z$ ):  $[\text{M} + \text{H}]^+$  calcd for  $\text{C}_{25}\text{H}_{21}\text{NO}_4$ , 400.0379; found, 400.0381.

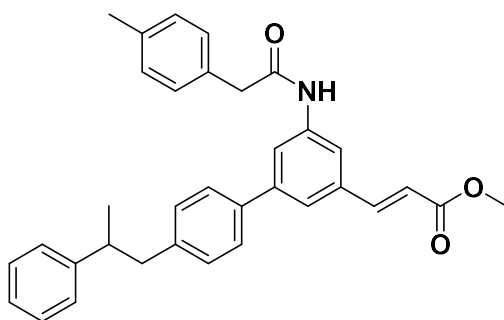


*Methyl(E)-3-(3'-fluoro-4'-(morpholinomethyl)-5-(2-(p-tolyl)acetamido)-[1,1'-biphenyl]-3-yl)acrylate*: Following the procedure as described for **2.7** the title compound was obtained using 4-(2-methyl-4-(4,4,5,5-tetramethyl-1,3,2-dioxaborolan-2-yl)benzyl)morpholine as a yellow solid (78%).  $R_f$ : 0.27 (hexane:EtOAc, 4:1).  $^1\text{H}$  NMR (400 MHz;  $\text{CDCl}_3$ ):  $\delta_{\text{H}}$  2.32 (3H, s,  $\text{CH}_3$ ), 2.64 (2H, t,  $J = 7.4$  Hz,  $\text{CH}_2$ ), 3.68 – 3.87 (8H, m,  $\text{CH}_2$ ), 3.89 (3H, s,  $\text{CH}_3$ ), 4.58 (2H, t,  $J = 7.4$  Hz,  $\text{CH}_2$ ), 6.65 (1H, d,  $J = 15.9$  Hz, CH), 7.15 – 7.28 (4H, m, ArCH), 7.50 – 7.76 (5H, m, ArCH and CH), 8.02 (1H, s, ArCH), 8.08 (1H, s, ArCH), 8.89 (1H, s, CH).  $^{13}\text{C}$  NMR (100 MHz;  $\text{CDCl}_3$ ):  $\delta_{\text{C}}$  28.2, 31.4, 39.0, 64.9, 80.8, 120.3, 120.9, 122.5, 125.6, 126.1, 126.3, 128.9, 129.2, 135.6, 138.7, 140.1, 140.5, 141.5, 142.1, 143.1, 166.3, 181.2.



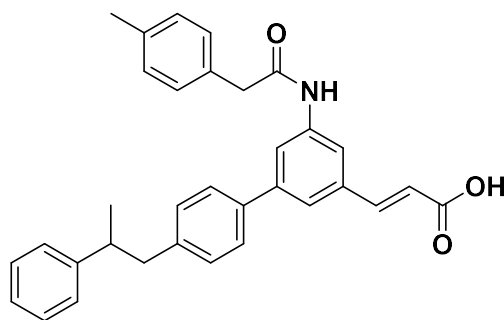
*(E)-3-(3'-fluoro-4'-(morpholinomethyl)-5-(2-(p-tolyl)acetamido)-[1,1'-biphenyl]-3-yl)acrylic acid (2.27)*: Following the general procedure A, the title compound, synthesized using **2.6**, was obtained as a yellow solid (60%).  $R_f$ : 0.29 (DCM:MeOH, 20:1).  $^1\text{H}$  NMR (400 MHz; MeOD):  $\delta_{\text{H}}$  2.32 (3H, s,  $\text{CH}_3$ ), 2.64 (2H, t,  $J = 7.4$  Hz,  $\text{CH}_2$ ), 3.68 – 3.87 (8H, m,

CH<sub>2</sub>), 4.58 (2H, t,  $J = 7.4$  Hz, CH<sub>2</sub>), 6.65 (1H, d,  $J = 15.9$  Hz, CH), 7.15 – 7.28 (4H, m, ArCH), 7.50 – 7.76 (5H, m, ArCH and CH), 8.02 (1H, s, ArCH), 8.08 (1H, s, ArCH), 8.89 (1H, s, CH). <sup>13</sup>C NMR (100 MHz; MeOD):  $\delta_c$  28.2, 31.4, 39.0, 64.9, 80.8, 120.3, 120.9, 122.5, 125.6, 126.1, 126.3, 128.9, 129.2, 135.6, 138.7, 140.1, 140.5, 141.5, 142.1, 143.1, 166.3, 181.2. ESI-HRMS ( $m/z$ ):  $[M + H]^+$  calcd for C<sub>29</sub>H<sub>29</sub>N<sub>2</sub>O<sub>4</sub>, 489.2179; found, 489.2138.



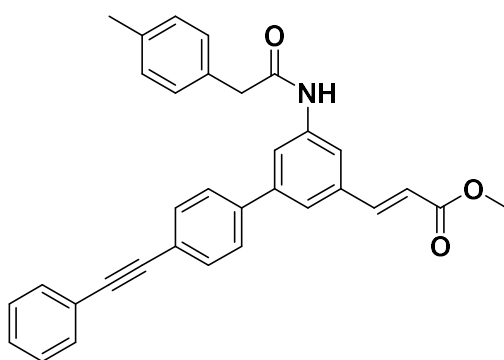
*Methyl(E)-3-(4'-(2-phenylpropyl)-5-(2-(p-tolyl)acetamido)-[1,1'-biphenyl]-3-*

*yl)acrylate*: Following the procedure as described for **2.7** the title compound was obtained using 4,4,5,5-tetramethyl-2-(4-(phenylethynyl)phenyl)-1,3,2-dioxaborolane as a transparent oil (82%).  $R_f$ : 0.37 (hexane:EtOAc, 4:1). <sup>1</sup>H NMR (400 MHz; CDCl<sub>3</sub>):  $\delta_H$  1.20 (3H, s, CH<sub>3</sub>), 1.28 – 1.32 (2H, m,  $J = 7.4$  Hz, CH<sub>2</sub>), 1.40 (1H, d,  $J = 7.4$  Hz, CH), 2.39 (3H, s, CH<sub>3</sub>), 3.89 (3H, s, CH<sub>3</sub>), 4.64 (2H, d,  $J = 7.4$  Hz, CH<sub>2</sub>), 6.54 (1H, s, CH), 7.19 – 7.28 (7H, m, ArCH), 7.50 – 7.76 (7H, m, ArCH and CH), 7.02 (1H, s, ArCH), 7.08 (1H, s, ArCH), 7.89 (1H, s, ArCH). <sup>13</sup>C NMR (100 MHz; CDCl<sub>3</sub>):  $\delta_c$  29.2, 33.4, 36.0, 61.9, 87.8, 127.3, 128.9, 132.5, 135.6, 136.1, 136.3, 138.9, 139.2, 145.6, 148.7, 150.1, 150.5, 151.5, 152.1, 153.1, 163.3, 180.2.



*(E)-3-(4'-(2-phenylpropyl)-5-(2-(p-tolyl)acetamido)-[1,1'-biphenyl]-3-yl) acrylic acid*

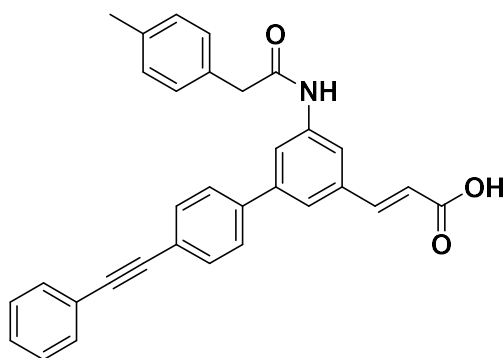
**(2.28):** Following the general procedure A, the title compound, synthesized using **2.6**, was obtained as a yellow solid (57%).  $R_f$ : 0.29 (DCM:MeOH, 20:1).  $^1\text{H}$  NMR (400 MHz; MeOD):  $\delta_{\text{H}}$  1.18 (3H, s,  $\text{CH}_3$ ), 1.26 – 1.30 (2H, m,  $J = 7.4$  Hz,  $\text{CH}_2$ ), 1.38 (1H, d,  $J = 7.4$  Hz, CH), 2.37 (3H, s,  $\text{CH}_3$ ), 3.87 (3H, s,  $\text{CH}_3$ ), 4.62 (2H, d,  $J = 7.4$  Hz,  $\text{CH}_2$ ), 6.52 (1H, s, CH), 7.17 – 7.26 (7H, m, ArCH), 7.48 – 7.74 (7H, m, ArCH and CH), 7.02 (1H, s, ArCH), 7.08 (1H, s, ArCH), 7.89 (1H, s, ArCH).  $^{13}\text{C}$  NMR (100 MHz; MeOD):  $\delta_{\text{C}}$  29.2, 33.4, 36.0, 61.9, 87.8, 127.3, 128.9, 132.5, 135.6, 136.1, 136.3, 138.9, 139.2, 145.6, 148.7, 150.1, 150.5, 151.5, 152.1, 153.1, 163.3, 180.2. ESI-HRMS ( $m/z$ ):  $[\text{M} + \text{H}]^+$  calcd for  $\text{C}_{27}\text{H}_{27}\text{NO}_3$ , 490.2319; found, 490.2188.



*Methyl(E)-3-(4'-(phenylethynyl)-5-(2-(p-tolyl)acetamido)-[1,1'-biphenyl]-3-*

*yl)acrylate:* Following the procedure as described for **2.7** the title compound was obtained using 4,4,5,5-tetramethyl-2-(4-(1-phenylethyl)phenyl)-1,3,2-dioxaborolane as a transparent oil (72%).  $R_f$ : 0.37 (hexane:EtOAc, 4:1).  $^1\text{H}$  NMR (400 MHz;  $\text{CDCl}_3$ ):  $\delta_{\text{H}}$  2.32

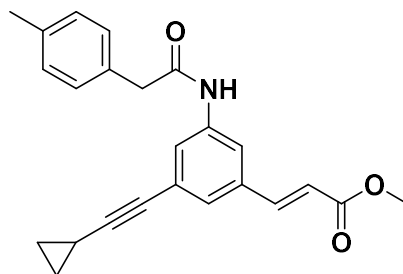
(3H, s, CH<sub>3</sub>), 3.89 (3H, s, CH<sub>3</sub>), 4.64 (2H, d,  $J$  = 7.4 Hz, CH<sub>2</sub>), 6.54 (1H, s, CH), 7.15 (2H, d,  $J$  = 7.8 Hz, ArCH), 7.24 (2H, d,  $J$  = 8.0 Hz, ArCH), 7.28 – 7.39 (5H, m, ArCH), 7.53 – 7.54 (4H, m, CH), 7.63 (1H, s, ArCH), 7.83 (1H, s, ArCH), 7.98 (1H, s, ArCH), 8.01 (1H, s, ArCH). <sup>13</sup>C NMR (100 MHz; CDCl<sub>3</sub>): δ<sub>C</sub> 63.7, 69.9, 114.4, 118.6, 119.3, 122.1, 122.1, 124.6, 128.9, 129.2, 133.6, 137.8, 142.9, 159.5, 166.5.



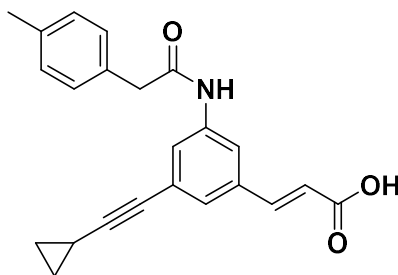
*(E)-3-(4'-(phenylethynyl)-5-(2-(p-tolyl)acetamido)-[1,1'-biphenyl]-3-yl) acrylic acid*

**(2.29):** Following the general procedure A, the title compound, synthesized using **2.6**, was obtained as a yellow solid (72%). R<sub>f</sub>: 0.27 (DCM:MeOH, 20:1). <sup>1</sup>H NMR (400 MHz; MeOD): δ<sub>H</sub> 2.32 (3H, s, CH<sub>3</sub>), 4.64 (2H, d,  $J$  = 7.4 Hz, CH<sub>2</sub>), 6.54 (1H, s, CH), 7.15 (2H, d,  $J$  = 7.8 Hz, ArCH), 7.24 (2H, d,  $J$  = 8.0 Hz, ArCH), 7.28 – 7.39 (5H, m, ArCH), 7.53 – 7.54 (4H, m, ArCH), 7.63 (1H, s, CH), 7.83 (1H, s, ArCH), 7.98 (1H, s, ArCH), 8.01 (1H, s, ArCH), <sup>13</sup>C NMR (100 MHz; MeOD): δ<sub>C</sub> 63.7, 69.9, 114.4, 118.6, 119.3, 122.1, 122.1, 124.6, 128.9, 129.2, 133.6, 137.8, 142.9, 159.5, 166.5. ESI-HRMS ( $m/z$ ): [M + H]<sup>+</sup> calcd for C<sub>27</sub>H<sub>23</sub>NO<sub>3</sub>, 419.1919; found, 419.1928.



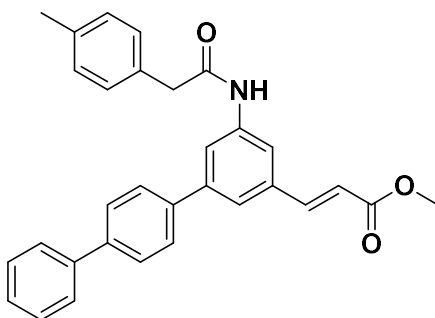


*Methyl(E)-3-(4'-(cyclopropylethynyl)-5-(2-(p-tolyl)acetamido)-[1,1'-biphenyl]-3-yl)acrylate*: Following the procedure as described for **2.7** the title compound was obtained using 2-(4-(cyclopropylethynyl)phenyl)-4,4,5,5-tetramethyl-1,3,2-dioxaborolane as a transparent oil (79%).  $R_f$ : 0.32 (hexane:EtOAc, 4:1).  $^1\text{H}$  NMR (400 MHz;  $\text{CDCl}_3$ ):  $\delta_H$  0.89 (2H, m,  $J = 7.4$  Hz,  $\text{CH}_2$ ), 1.28 (3H, s,  $J = 7.4$  Hz,  $\text{CH}_2$  and CH), 2.32 (3H, s,  $\text{CH}_3$ ), 3.89 (3H, s,  $\text{CH}_3$ ), 4.64 (2H, d,  $J = 7.4$  Hz,  $\text{CH}_2$ ), 6.54 (1H, s, CH), 7.15 – 7.22 (2H, d,  $J = 7.8$  Hz, ArCH), 7.34 (2H, d,  $J = 8.0$  Hz, ArCH), 7.56 (1H, d,  $J = 8.0$ , CH), 7.73 (1H, s, ArCH), 7.83 (1H, s, ArCH), 7.98 (1H, d,  $J = 8.0$ , ArCH).  $^{13}\text{C}$  NMR (100 MHz;  $\text{CDCl}_3$ ):  $\delta_C$  16.5, 24.4, 33.4, 42.4, 119.3, 119.3, 120.7, 122.0, 123.8, 128.7, 128.8, 130.7, 133.1, 134.8, 134.9, 138.1, 143.3, 143.8, 148.1, 168.2.

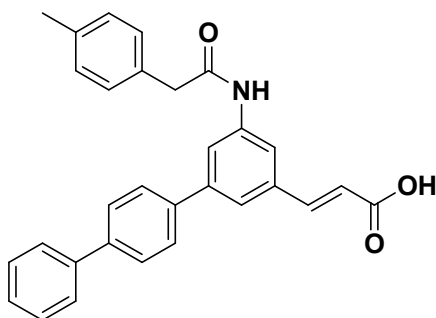


*(E)-3-(4'-(cyclopropylethynyl)-5-(2-(p-tolyl)acetamido)-[1,1'-biphenyl]-3-yl)acrylic acid (2.30)*: Following the general procedure A, the title compound, synthesized using **2.6**, was obtained as a white solid (71%).  $R_f$ : 0.29 (DCM:MeOH, 20:1).  $^1\text{H}$  NMR (400 MHz; MeOD):  $\delta_H$  0.89 (2H, m,  $J = 7.4$  Hz,  $\text{CH}_2$ ), 1.28 (3H, s,  $J = 7.4$  Hz,  $\text{CH}_2$  and CH), 2.32 (3H, s,  $\text{CH}_3$ ), 4.64 (2H, d,  $J = 7.4$  Hz,  $\text{CH}_2$ ), 6.54 (1H, s, CH), 7.15 (2H, d,  $J = 7.8$  Hz, ArCH),

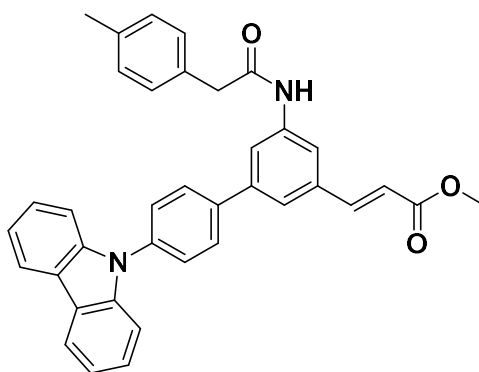
7.24 (2H, d,  $J = 8.0$  Hz, ArCH), 7.56 (1H, d,  $J = 8.0$ , CH), 7.78 (1H, s, ArCH), 7.83 (1H, s, ArCH), 7.98 (1H, d,  $J = 8.0$ , ArCH).  $^{13}\text{C}$  NMR (100 MHz; MeOD):  $\delta_{\text{C}}$  16.5, 24.4, 33.4, 42.4, 119.3, 119.3, 120.7, 122.0, 123.8, 128.7, 128.8, 130.7, 133.1, 134.8, 134.9, 138.1, 143.3, 143.8, 148.1, 168.2. ESI-HRMS ( $m/z$ ):  $[\text{M} + \text{H}]^+$  calcd for  $\text{C}_{29}\text{H}_{23}\text{NO}_3$ , 436.1979; found, 436.1991.



*Methyl(E)-3-(5-(2-(p-tolyl)acetamido)-[1,1':4',1''-terphenyl]-3-yl)acrylate*: Following the procedure as described for **2.7** the title compound was obtained using 2-([1,1'-biphenyl]-4-yl)-4,4,5,5-tetramethyl-1,3,2-dioxaborolane as a transparent oil (74%).  $R_f$ : 0.30 (hexane:EtOAc, 4:1).  $^1\text{H}$  NMR (400 MHz;  $\text{CDCl}_3$ ):  $\delta_{\text{H}}$  2.32 (3H, s,  $\text{CH}_3$ ), 3.89 (3H, s,  $\text{CH}_3$ ), 4.49 (2H, s,  $\text{CH}_2$ ), 6.26 (1H, d,  $J = 16.00$  Hz, CH), 7.14-7.21 (8H, m, ArCH), 7.38-7.50 (6H, m, ArCH and CH), 7.74 (1H, s, CH), 7.88 (1H, s, CH).  $^{13}\text{C}$  NMR (100 MHz;  $\text{CDCl}_3$ ):  $\delta_{\text{C}}$  18.23, 41.41, 118.00, 123.04, 124.90, 125.62, 126.00, 126.22, 127.22, 128.11, 128.39, 128.71, 130.64, 132.95, 133.32, 133.98, 135.00, 137.29, 139.28, 139.61, 141.07, 141.09.

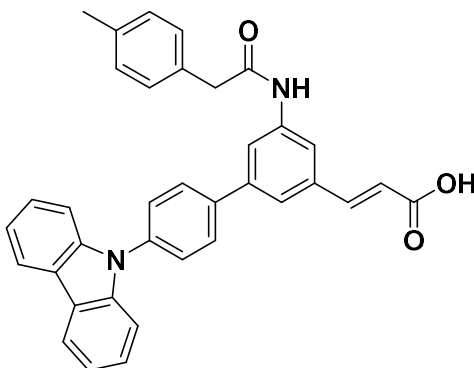


*(E)*-3-(4'-(cyclopropylethynyl)-5-(2-(*p*-tolyl)acetamido)-[1,1'-biphenyl]-3-yl)acrylic acid (**2.31**): Following the general procedure A, the title compound, synthesized using **2.6**, was obtained as a white solid (71%).  $R_f$ : 0.29 (DCM:MeOH, 20:1).  $^1\text{H}$  NMR (400 MHz; MeOD):  $\delta_{\text{H}}$  2.32 (3H, s,  $\text{CH}_3$ ), 4.49 (2H, s,  $\text{CH}_2$ ), 6.26 (1H, d,  $J = 16.00$  Hz, CH), 7.14-7.21 (8H, m, ArCH), 7.38-7.50 (6H, m, ArCH and CH), 7.74 (1H, s, CH), 7.88 (1H, s, CH).  $^{13}\text{C}$  NMR (100 MHz; MeOD):  $\delta_{\text{C}}$  18.23, 41.41, 118.00, 123.04, 124.90, 125.62, 126.00, 126.22, 127.22, 128.11, 128.39, 128.71, 130.64, 132.95, 133.32, 133.98, 135.00, 137.29, 139.28, 139.61, 141.07, 141.09. ESI-HRMS ( $m/z$ ):  $[\text{M} + \text{H}]^+$  calcd for  $\text{C}_{30}\text{H}_{25}\text{NO}_3$ , 448.1979; found, 448.1991.

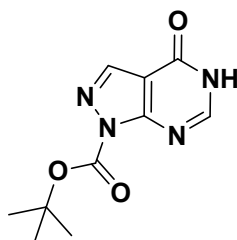


Methyl(*E*)-3-(4'-(9H-carbazol-9-yl)-5-(2-(*p*-tolyl)acetamido)-[1,1'-biphenyl]-3-yl)acrylate: Following the procedure as described for **2.7** the title compound was obtained using 2-(4-(9H-fluoren-9-yl)phenyl)-4,4,5,5-tetramethyl-1,3,2-dioxaborolane as a

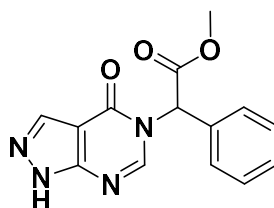
transparent oil (74%).  $R_f$ : 0.37 (hexane:EtOAc, 4:1).  $^1\text{H}$  NMR (400 MHz;  $\text{CDCl}_3$ ):  $\delta_{\text{H}}$  2.32 (3H, s,  $\text{CH}_3$ ), 3.89 (3H, s,  $\text{CH}_3$ ), 4.49 (2H, s,  $\text{CH}_2$ ), 6.26 (1H, d,  $J = 16.00$  Hz, CH), 7.14-7.21 (7H, m, ArCH), 7.38-7.62 (10H, m, ArCH), 7.74 (1H, s, CH), 7.88 (1H, s, ArCH), 8.17 (1H, s, ArCH).  $^{13}\text{C}$  NMR (100 MHz;  $\text{CDCl}_3$ ):  $\delta_{\text{C}}$  18.23, 41.41, 118.00, 123.04, 124.90, 125.62, 126.00, 126.22, 127.22, 128.11, 128.39, 128.71, 130.64, 132.95, 133.32, 133.98, 135.00, 137.29, 139.28, 139.61, 141.07, 141.09.



*(E)*-3-(4'-(9H-carbazol-9-yl)-5-(2-(*p*-tolyl)acetamido)-[1,1'-biphenyl]-3-yl)acrylic acid (**2.32**): Following the general procedure A, the title compound, synthesized using **2.6**, was obtained as a white solid (71%).  $R_f$ : 0.39 (DCM:MeOH, 20:1).  $^1\text{H}$  NMR (400 MHz; MeOD):  $\delta_{\text{H}}$  2.32 (3H, s,  $\text{CH}_3$ ), 4.49 (2H, s,  $\text{CH}_2$ ), 6.26 (1H, d,  $J = 16.00$  Hz, CH), 7.14-7.21 (7H, m, ArCH), 7.38-7.62 (10H, m, ArCH), 7.74 (1H, s, CH), 7.88 (1H, s, ArCH), 8.17 (1H, s, ArCH).  $^{13}\text{C}$  NMR (100 MHz; MeOD):  $\delta_{\text{C}}$  18.23, 41.41, 118.00, 123.04, 124.90, 125.62, 126.00, 126.22, 127.22, 128.11, 128.39, 128.71, 130.64, 132.95, 133.32, 133.98, 135.00, 137.29, 139.28, 139.61, 141.07, 141.09. ESI-HRMS ( $m/z$ ):  $[\text{M} + \text{H}]^+$  calcd for  $\text{C}_{36}\text{H}_{28}\text{N}_2\text{O}_3$ , 537.2197; found, 537.2188.

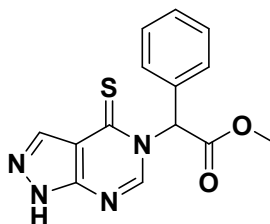


*Tert-butyl 4-oxo-4,5-dihydro-1H-pyrazolo[3,4-d]pyrimidine-1-carboxylate (3.2):* To a suspension of 1,5-dihydro-4H-pyrazolo[3,4-d]pyrimidin-4-one (200 mg, 1.47 mmol,) in THF (10 mL), DIPEA (0.75 mL, 4.28 mmol), DMAP (17.5 mg, 0.14 mmol) and di-*tert*-butyl dicarbonate (641 mg, 2.94 mmol) were added. The reaction was stirred at refluxed conditions overnight. The reaction mixture was allowed to cool to room temperature, and water (30 mL) was added slowly with stirring resulting in a white solid. The mixture was extracted with EtOAc (3 × 50 mL). The organic layer was separated and dried (Na<sub>2</sub>SO<sub>4</sub>), filtered and evaporated in vacuo. Purification by column chromatography using DCM/MeOH gradient with 3% TEA (20:1, 10:1) provided the title compound (90% brsm.). R<sub>f</sub>: 0.42 (DCM:MeOH,10:1). <sup>1</sup>H NMR (400 MHz, MeOD) δ<sub>H</sub> 1.65 (9H, s, (CH<sub>3</sub>)<sub>3</sub>), 8.23, (1H, s, ArCH), 8.44 (1H, s, ArCH). <sup>13</sup>C NMR (100 MHz, MeOD) δ<sub>C</sub> 27.97, 76.73, 76.73, 87.04, 108.97, 138.05, 147.14, 155.25.

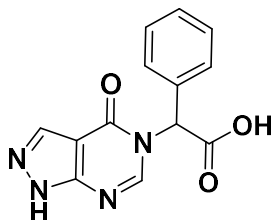


*Methyl-2-(4-oxo-1,4-dihydro-5H-pyrazolo[3,4-d]pyrimidin-5-yl)-2-phenylacetate (3.3):* To a solution of *tert*-butyl 4-oxo-4,5-dihydro-1H-pyrazolo[3,4-d]pyrimidine-1-carboxylate (**3.2**) (200 mg, 0.85 mmol) in DMF (4 mL), sodium hydride (42 mg, 1.02 mmol) and lithium bromide (149 mg, 1.7 mmol) were added. The solution was stirred for 30 minutes at room temperature. Methyl bromophenylacetate (136 μL, 0.85 mmol) was

added and the reaction was stirred at room temperature for 4 hours. Water (30 mL) was added to the reaction mixture and was extracted with EtOAc (3 × 50 mL). The organic layer was separated and dried (Na<sub>2</sub>SO<sub>4</sub>), filtered and evaporated in vacuo. Purification by column chromatography using hexane/EtOAc gradient (3:1, 2:1, 1:1) provided the title compound (96%). R<sub>f</sub>: 0.18 (hexane:EtOAc, 1:1). <sup>1</sup>H NMR (400 MHz, CDCl<sub>3</sub>) δ<sub>H</sub> ppm 3.86 (3H, s, CH<sub>3</sub>), 6.83 (1H, s, CH), 7.33-7.38 (2H, m, ArCH), 7.41-7.48 (3H, m, ArCH), 7.92 (1H, s, ArCH), 8.22 (1H, s, ArCH). <sup>13</sup>C NMR (100 MHz, CDCl<sub>3</sub>) δ<sub>C</sub> 30.32, 35.62, 52.31, 59.85, 128.97, 129.26, 129.30, 133.21, 148.26, 163.50, 169.50.

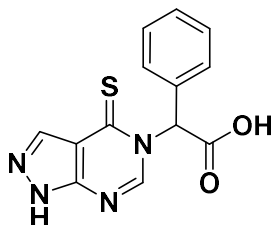


*Methyl-2-phenyl-2-(4-thioxo-1,4-dihydro-5H-pyrazolo[3,4-d]pyrimidin-5-yl)acetate (3.4)*: To a solution of methyl-2-(4-oxo-1,4-dihydro-5H-pyrazolo[3,4-d]pyrimidin-5-yl)-2-phenylacetate (**3.3**) (300 mg, 1.05 mmol) in toluene (10 mL), Lawesson's Reagent (848.4 mg, 2.10 mmol) was added. The reaction mixture was stirred and refluxed for 2 hours. The reaction mixture was allowed to cool to room temperature, and water (30 mL) was added slowly with stirring to provide a yellow solid. The mixture was extracted with EtOAc (3 × 50 mL), the organic layer was separated and dried (Na<sub>2</sub>SO<sub>4</sub>), filtered, and evaporated in vacuo. Purification by column chromatography using DCM/MeOH gradient (20:1, 10:1) provided the title compound (67%). R<sub>f</sub>: 0.32 (DCM:MeOH, 10:1). <sup>1</sup>H NMR (400 MHz, CDCl<sub>3</sub>) δ<sub>H</sub> ppm 3.86 (3H, s, CH<sub>3</sub>), 7.33 - 7.38 (2H, m, ArCH), 7.43 - 7.47 (3H, m, ArCH), 7.99 (1H, s, CH), 8.07 (1H, s, ArCH), 8.35 (1H, s, ArCH). <sup>13</sup>C NMR (100 MHz, CDCl<sub>3</sub>) δ<sub>C</sub> 53.44, 63.43, 117.70, 128.95, 129.89, 133.51, 139.06, 146.28, 148.34, 169.17, 181.25.



2-(4-oxo-1,4-dihydro-5H-pyrazolo[3,4-d]pyrimidin-5-yl)-2-phenylacetic acid (**3.5**):

To a solution of methyl-2-(4-oxo-1,4-dihydro-5H-pyrazolo[3,4-d]pyrimidin-5-yl)-2-phenylacetate (**3.3**) (240mg, 0.85 mmol) in THF (5mL), NaOH (0.25N, 6.75 mL, 1.69 mmol) was added. The reaction mixture was stirred at room temperature (without nitrogen pressure) for 2 hours and then quenched using HCl (0.25N, 6.75 mL, 1.69 mmol). The solution was air-dried at room temperature to afford the title compound (96%).  $^1\text{H}$  NMR (400 MHz, MeOD)  $\delta_{\text{H}}$  6.65 (1H, s, CH), 7.26 - 7.37 (5H, m, ArCH), 7.73 (1H, s, ArCH), 8.07 (1H, s, ArCH).  $^{13}\text{C}$  NMR (100 MHz, MeOD)  $\delta_{\text{C}}$  60.82, 127.76, 128.57, 128.97, 138.33, 145.72, 174.00.



2-phenyl-2-(4-thioxo-1,4-dihydro-5H-pyrazolo[3,4-d]pyrimidin-5-yl)acetic acid

(**3.6**): To a solution of methyl-2-phenyl-2-(4-thioxo-1,4-dihydro-5H-pyrazolo[3,4-d]pyrimidin-5-yl)acetate (**3.4**) (240 mg, 0.8 mmol) in THF (5mL) NaOH (0.25N, 6.75 mL, 1.69 mmol) was added. The reaction mixture was stirred at room temperature (without nitrogen pressure) for 2 hours and then quenched using HCl (0.25N, 6.75 mL, 1.69 mmol). The solution was air-dried at room temperature to afford the title compound (96%).  $^1\text{H}$  NMR (400 MHz,  $\text{CDCl}_3$ )  $\delta_{\text{H}}$  7.33 - 7.38 (2H, m, ArCH), 7.43 - 7.47 (3H, m, ArCH), 7.99

(1H, s, CH), 8.07 (1H, s, ArCH), 8.35 (1H, s, ArCH).  $^{13}\text{C}$  NMR (100 MHz,  $\text{CDCl}_3$ )  $\delta_{\text{C}}$  67.43, 119.70, 128.85, 129.87, 133.41, 139.76, 146.18, 148.74, 169.87, 181.35.

*General Synthetic Procedure B.* To a solution of 2-(4-oxo-1,4-dihydro-5H-pyrazolo[3,4-d]pyrimidin-5-yl)-2-phenylacetic acid (**3.5**) (200 mg, 0.74 mmol) in DMF (5 mL), (Benzotriazol-1-yloxy)tris(dimethylamino)phosphonium hexafluorophosphate (392 mg, 0.88 mmol), DIPEA (260  $\mu\text{L}$ , 1.48 mmol) and the respective substituted amine (0.74 mmol). The reaction mixture was stirred at room temperature overnight. Water (40 mL) was added to the reaction mixture and was extracted with EtOAc (3  $\times$  50 mL). The organic layer was separated and dried ( $\text{Na}_2\text{SO}_4$ ), filtered, and evaporated in vacuo. Purification by column chromatography using DCM/MeOH gradient (20:1, 10:1) provided the title compound.

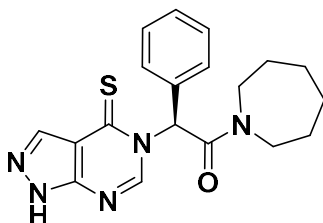
*General Synthetic Procedure C.* To a solution of 2-phenyl-2-(4-thioxo-1,4-dihydro-5H-pyrazolo[3,4-d]pyrimidin-5-yl)acetic acid (**3.6**) (200, 0.74 mmol) in DMF (5 mL), (Benzotriazol-1-yloxy)tris(dimethylamino)phosphonium hexafluorophosphate (370 mg, 0.84 mmol), DIPEA (245  $\mu\text{L}$ , 1.4 mmol) were added and the respective substituted amine (0.7 mmol). The reaction mixture was stirred at room temperature overnight. Water was added to the reaction mixture and was extracted with EtOAc (3  $\times$  50 mL). The organic layer was separated and dried ( $\text{Na}_2\text{SO}_4$ ), filtered, and evaporated in vacuo. Purification by column chromatography using DCM/MeOH gradient (20:1, 10:1) provided the title compound.

*General Synthetic Procedure D.* To a solution of 2-(4-oxo-1,4-dihydro-5H-pyrazolo[3,4-d]pyrimidin-5-yl)-2-phenylacetic acid (**3.5**) (200 mg, 0.74 mmol) in DMF (5 mL), *N'*-ethyl-*N'*-(3-(dimethylamino)propyl) carbodiimide (209 mg, 1.10 mmol), HOBt (55 mg, 0.36 mmol), 4-Methylmorpholine (246  $\mu\text{L}$ , 2.22 mmol) and the respective substituted amine (0.74 mmol). The reaction mixture was stirred at room temperature overnight. Water



(40 mL) was added to the reaction mixture and was extracted with EtOAc (3 × 50 mL). The organic layer was separated and dried (Na<sub>2</sub>SO<sub>4</sub>), filtered, and evaporated in vacuo. Purification by column chromatography using DCM/MeOH gradient (20:1, 10:1) provided the title compound.

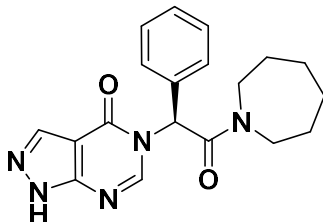
*General Synthetic Procedure E.* To a solution of 2-phenyl-2-(4-thioxo-1,4-dihydro-5H-pyrazolo[3,4-d]pyrimidin-5-yl)acetic acid (**3.6**) (200, 0.74 mmol) in DMF (5 mL), *N*-ethyl-*N'*-(3-(dimethylamino)propyl) carbodiimide (209 mg, 1.10 mmol), HOBT (55 mg, 0.36 mmol), 4-Methylmorpholine (246 µL, 2.22 mmol) and the respective substituted amine (0.74 mmol). The reaction mixture was stirred at room temperature overnight. Water was added to the reaction mixture and was extracted with EtOAc (3 × 50 mL). The organic layer was separated and dried (Na<sub>2</sub>SO<sub>4</sub>), filtered, and evaporated in vacuo. Purification by column chromatography using DCM/MeOH gradient (20:1, 10:1) provided the title compound.



(*S*)-1-(azepan-1-yl)-2-phenyl-2-(4-thioxo-1,4-dihydro-5H-pyrazolo[3,4-d]pyrimidin-5-yl)ethan-1-one (**AG18051**): According to the general procedure C, the title compound was obtained as a yellow solid (62%). *R*<sub>f</sub>: 0.3 (DCM:MeOH,10:1). <sup>1</sup>H NMR (400 MHz, MeOD) δ<sub>H</sub> 1.18 (1H, br. s., CH), 1.45 - 1.67 (7H, m, CH), 1.93 (1H, br. s., CH), 3.23 - 3.31 (1H, m, CH), 3.37 - 3.46 (1H, m, CH), 3.62 (1H, dt, *J* = 14.18, 5.62 Hz, CH), 3.76 (1H, ddd, *J* = 13.75, 7.15, 4.03 Hz, CH), 7.27 - 7.34 (2H, m, ArCH), 7.35 - 7.43 (3H, m, ArCH), 7.98 (1H, s, ArCH), 8.24 (1H, s, ArCH), 8.29 (1H, s, ArCH). <sup>13</sup>C NMR (100 MHz, MeOD) δ<sub>C</sub>

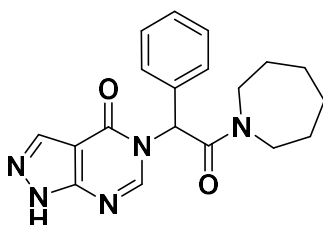
26.52, 27.32, 27.65, 28.43, 46.62, 48.18, 61.46, 129.10, 129.91, 134.29, 149.92, 166.63.

ESI-HRMS (m/z):  $[M + H]^+$  calcd for  $C_{19}H_{21}N_5OS$ , 368.1521; found, 368.1535.



*(S)*-5-(2-(azepan-1-yl)-2-oxo-1-phenylethyl)-1,5-dihydro-4H-pyrazolo[3,4-

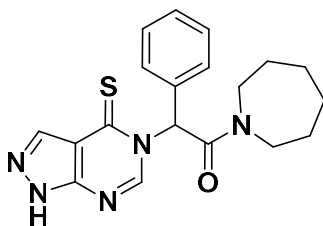
*d*]pyrimidin-4-one (**(R)-3.7a**): According to the general procedure B, the title compound was obtained as a white solid (57%).  $R_f$ : 0.3 (DCM:MeOH,10:1).  $^1H$  NMR (400 MHz, MeOD)  $\delta_H$  1.38 - 1.48 (1H, m, CH), 1.53 - 1.83 (6H, m, CH), 1.87 - 1.98 (1H, m, CH), 3.28 - 3.37 (1H, m, CH), 3.39 - 3.48 (1H, m, CH), 3.63 (1H, dt,  $J$  = 14.49, 5.35 Hz, CH), 3.82 (1H, ddd,  $J$  = 13.57, 7.09, 4.77 Hz, CH), 7.06 (1H, s, CH) 7.41 - 7.47 (2H, m, ArCH), 7.51-7.58 (3H, m, ArCH), 7.72 (1H, s, ArCH), 8.26 (1H, s, ArCH).  $^{13}C$  NMR (100 MHz, MeOD)  $\delta_C$  14.20, 21.06, 26.60, 28.57, 46.85, 56.24, 60.43, 129.00, 129.18, 129.83, 133.88, 150.14, 157.14, 167.28. ESI- HRMS (m/z):  $[M + H]^+$  calcd for  $C_{19}H_{21}N_5O_2$ , 352.1751; found, 352.1756.



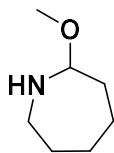
5-(2-(azepan-1-yl)-2-oxo-1-phenylethyl)-1,5-dihydro-4H-pyrazolo[3,4-*d*]pyrimidin-

4-one (**rac-3.7a**): According to the general procedure D, the title compound was obtained as a white solid (64%).  $R_f$ : 0.3 (DCM:MeOH,10:1).  $^1H$  NMR (400 MHz, MeOD)  $\delta_H$  1.26 - 1.38 (1H, m, CH), 1.41 - 1.67 (5H, m, CH), 1.70 - 1.93 (2H, m, CH), 3.11 - 3.24 (1H, m, CH), 3.27 - 3.39 (1H, m, CH), 3.53 (1H, dt,  $J$  = 14.37, 5.04 Hz, CH), 3.72 - 3.86 (1H, m,

CH), 6.75 (1H, d,  $J = 7.4$ , CH), 7.25 - 7.47 (5H, m, ArCH), 7.78-7.90 (1H, m, MeOD), 8.02 - 8.16 (1H, m, ArCH).  $^{13}\text{C}$  NMR (100 MHz, MeOD)  $\delta_{\text{C}}$  29.90, 30.03, 30.47, 39.60, 39.81, 42.82, 55.86, 111.41, 116.74, 126.82, 129.05, 129.98, 133.46, 133.46, 136.04, 150.07, 165.86. ESI- HRMS ( $m/z$ ):  $[\text{M} + \text{H}]^+$  calcd for  $\text{C}_{19}\text{H}_{21}\text{N}_5\text{O}_2$ , 352.1751; found, 352.1757.

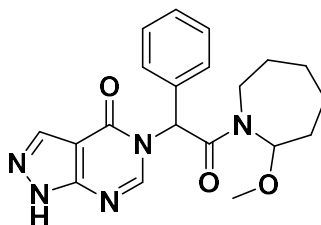


**1-(azepan-1-yl)-2-phenyl-2-(4-thioxo-1,4-dihydro-5H-pyrazolo[3,4-d]pyrimidin-5-yl)ethan-1-one (3.8a):** According to the general procedure E, the title compound was obtained as a yellow solid (72 %).  $R_f$ : 0.3 (DCM:MeOH,10:1).  $^1\text{H}$  NMR (400 MHz, MeOD)  $\delta_{\text{H}}$  1.31 - 1.41 (1H, m, CH), 1.47 - 1.65 (6H, m, CH), 1.81 - 1.91 (1H, m, CH), 3.17 - 3.25 (1H, m, CH), 3.34 (1H, ddd,  $J = 13.69, 7.58, 4.40$  Hz, CH), 3.48 - 3.56 (1H, m, CH), 3.74 - 3.82 (1H, m, CH), 7.07 (1H, m, CH), 7.08 - 7.12 (2H, m, ArCH), 7.33 (3H, dd,  $J = 8.44, 5.01$  Hz, ArCH) 7.82 - 7.88 (1H, m, ArCH) 8.08 - 8.14 (1H, m, ArCH).  $^{13}\text{C}$  NMR (100 MHz, MeOD)  $\delta_{\text{C}}$  26.60, 26.86, 27.35, 28.60, 29.72, 46.92, 48.14, 116.91, 117.13, 131.20, 150.12, 167.03. ESI-HRMS ( $m/z$ ):  $[\text{M} + \text{H}]^+$  calcd for  $\text{C}_{19}\text{H}_{21}\text{N}_5\text{OS}$ , 368.1521; found, 368.1576.

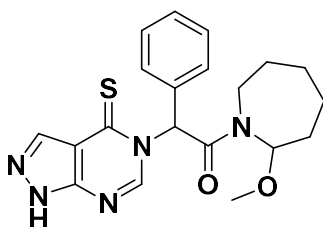


**2-methoxyazepane:** A solution of 1-Aza-2-methoxy-1-cycloheptene (690  $\mu\text{L}$ , 4.70 mmol) and Pd/C (22 mg, 0.2 mmol) in methanol (10 mL) was stirred under hydrogen gas (80 psi) in a mini-autoclave overnight at room temperature. The reaction mixture was filtered using Celite® bed, washed with methanol, and the solvent was evaporated in

vacuo to afford the title compound (92%).  $^1\text{H}$  NMR (400 MHz,  $\text{CDCl}_3$ )  $\delta_{\text{H}}$  1.25 – 1.55 (8H, m, CH), 2.21 – 2.30 (2H, m, CH), 3.33 (3H, s,  $\text{CH}_3$ ), 4.65 (1H, t,  $J = 7.34$  Hz, CH).

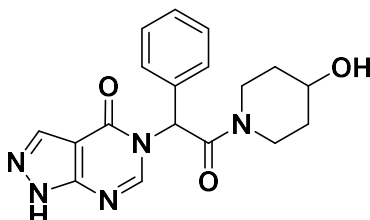


**5-(2-(2-methoxyazepan-1-yl)-2-oxo-1-phenylethyl)-1,5-dihydro-4H-pyrazolo[3,4-d]pyrimidin-4-one (3.7b):** According to the general procedure D, the title compound was obtained as a white solid (59%).  $R_f$ : 0.2 (DCM/MeOH,10:1).  $^1\text{H}$  NMR (400 MHz, MeOD)  $\delta_{\text{H}}$  1.16 - 1.30 (2H, m, CH), 1.43 - 1.58 (4H, m, CH), 2.21 (2H, t,  $J = 7.34$  Hz, CH), 3.28 (2H, td,  $J = 13.08, 7.09$  Hz, CH), 3.57 (3H, s,  $\text{CH}_3$ ), 6.53 (1H, d,  $J = 4.16$  Hz, CH), 6.74 (1H, s, CH), 7.28 - 7.39 (5H, m, ArCH), 7.99 (1H, s, ArCH), 8.08 (1H, s, ArCH).  $^{13}\text{C}$  NMR (100 MHz, MeOD)  $\delta_{\text{C}}$  24.28, 26.23, 28.86, 33.76, 39.88, 51.57, 58.60, 128.89, 129.65, 134.63, 149.37, 157.38, 167.47, 174.08. ESI-HRMS ( $m/z$ ):  $[\text{M} + \text{H}]^+$  calcd for  $\text{C}_{20}\text{H}_{23}\text{N}_5\text{O}_3$ , 368.1521; found, 382.1475.

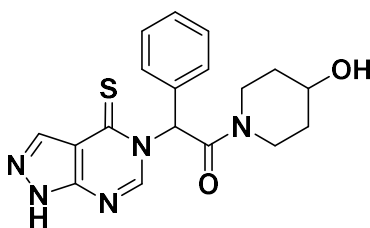


**1-(2-methoxyazepan-1-yl)-2-phenyl-2-(4-thioxo-1,4-dihydro-5H-pyrazolo[3,4-d]pyrimidin-5-yl)ethan-1-one (3.8b).** According to the general procedure E, the title compound was obtained as a yellow solid (64%).  $R_f$ : 0.2 (DCM:MeOH,10:1).  $^1\text{H}$  NMR (400 MHz, MeOD)  $\delta_{\text{H}}$  1.25 (3H, d,  $J = 7.34$  Hz, CH), 1.49 (4H, td,  $J = 15.41, 8.07$  Hz, CH), 2.21 (2H, t,  $J = 7.46$  Hz, CH), 3.18 (1H, d,  $J = 6.85$  Hz, CH), 3.53 (3H, s,  $\text{CH}_3$ ), 6.65 (1H, s,

CH), 7.30 - 7.41 (5H, m, ArCH), 7.74 (1H, s, ArCH), 8.09 (1H, br. s, ArCH).  $^{13}\text{C}$  NMR (100 MHz, MeOD)  $\delta_{\text{C}}$  24.18, 25.98, 28.41, 33.25, 39.17, 50.57, 128.82, 129.08, 129.27, 174.39. ESI-HRMS (m/z):  $[\text{M} + \text{H}]^+$  calcd for  $\text{C}_{20}\text{H}_{23}\text{N}_5\text{O}_2\text{S}$ , 398.1121; found, 398.1177.

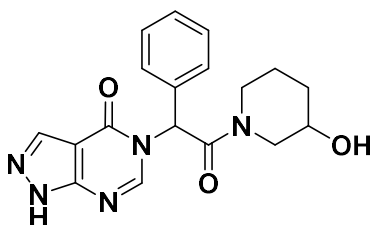


*5-(2-(4-hydroxypiperidin-1-yl)-2-oxo-1-phenylethyl)-1,5-dihydro-4H-pyrazolo[3,4-d]pyrimidin-4-one (3.7c)*: According to the general procedure D, the title compound was obtained as a white solid (72%).  $R_f$ : 0.2 (DCM:MeOH,10:1).  $^1\text{H}$  NMR (400 MHz, MeOD)  $\delta_{\text{H}}$  1.35 (2H, s, CH), 1.60 - 1.69 (1H, m, CH), 1.72 - 1.83 (1H, m, CH), 2.99 - 3.09 (1H, m, CH), 3.23 - 3.30 (1H, m, CH), 3.53 - 3.63 (1H, m, CH), 3.72 (1H, dt,  $J = 7.64, 3.88$  Hz, CH), 3.96 - 4.10 (1H, m, CH), 7.05 (1H, d,  $J = 6.85$  Hz, CH), 7.29 - 7.36 (2H, m, ArCH), 7.38 - 7.48 (3H, m, ArCH), 7.56 - 7.61 (1H, m, ArCH), 8.09 (1H, d,  $J = 3.42$  Hz, ArCH).  $^{13}\text{C}$  NMR (100 MHz, MeOD)  $\delta_{\text{C}}$  29.70, 30.13, 30.58, 30.67, 30.94, 39.62, 39.84, 42.66, 55.86, 61.32, 74.52, 129.00, 129.99, 133.84, 134.06, 149.68, 165.21. ESI-HRMS (m/z):  $[\text{M} + \text{H}]^+$  calcd for  $\text{C}_{18}\text{H}_{19}\text{N}_5\text{O}_3$ , 354.1521; found, 354.1544.

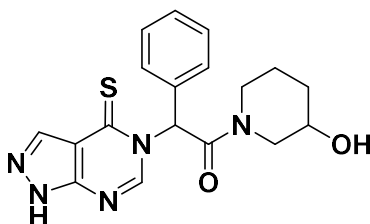


*1-(4-hydroxypiperidin-1-yl)-2-phenyl-2-(4-thioxo-1,4-dihydro-5H-pyrazolo[3,4-d]pyrimidin-5-yl)ethan-1-one (3.8c)*: According to the general procedure E, the title compound was obtained as a yellow solid (70%).  $R_f$ : 0.2 (DCM:MeOH,10:1).  $^1\text{H}$  NMR (400 MHz, MeOD)  $\delta_{\text{H}}$  1.40 - 2.00 (4H, m, CH), 2.82 - 3.03 (1H, m, CH), 3.21 - 3.33 (1H, m, CH),

3.37 - 3.47 (1H, m, CH), 3.53 - 3.71 (1H, m, CH), 3.73 - 3.90 (1H, m, CH), 7.27 - 7.32 (2H, m, ArCH), 7.33 - 7.41 (3H, m, ArCH), 7.88 - 7.97 (1H, m, CH), 8.17 - 8.26 (1H, m, ArCH), 8.28 - 8.39 (1H, m, ArCH).  $^{13}\text{C}$  NMR (100 MHz, MeOD)  $\delta_{\text{C}}$  22.84, 29.38, 33.14, 33.32, 40.02, 42.90, 65.99, 116.53, 116.75, 131.49, 131.67, 131.76, 162.18, 164.65, 166.35. ESI- HRMS (m/z):  $[\text{M} + \text{H}]^+$  calcd for  $\text{C}_{18}\text{H}_{19}\text{N}_5\text{O}_2\text{S}$ , 370.1352; found, 370.1341.

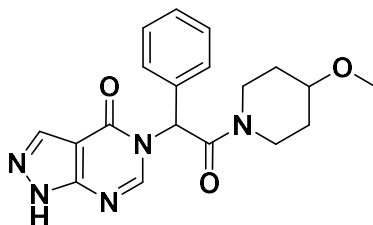


*5-(2-(3-hydroxypiperidin-1-yl)-2-oxo-1-phenylethyl)-1,5-dihydro-4H-pyrazolo[3,4-d]pyrimidin-4-one (3.7d)*: According to the general procedure D, the title compound was obtained as a white solid (52%).  $R_f$ : 0.2 (DCM:MeOH,10:1).  $^1\text{H}$  NMR (400 MHz, MeOD)  $\delta_{\text{H}}$  1.28 - 1.55 (1H, m, CH), 1.64 - 1.88 (2H, m, CH), 2.54 - 2.87 (1H, m, CH), 3.02 - 3.17 (1H, m, CH), 3.43 - 3.66 (2H, m, CH), 3.67 - 3.93 (1H, m, CH), 4.17 - 4.29 (1H, m, CH), 7.02 - 7.12 (1H, m, CH), 7.27 - 7.47 (5H, m, ArCH), 7.53 - 7.65 (1H, m, ArCH), 8.09 (1H, br. s., ArCH).  $^{13}\text{C}$  NMR (100 MHz, MeOD)  $\delta_{\text{C}}$  22.44, 22.90, 31.72, 32.10, 42.77, 45.42, 48.93, 57.36, 57.38, 65.42, 66.18, 129.28, 129.70, 132.90, 133.18, 133.49, 166.98. ESI- HRMS (m/z):  $[\text{M} + \text{H}]^+$  calcd for  $\text{C}_{18}\text{H}_{19}\text{N}_5\text{O}_3$ , 354.1435; found, 354.1544.

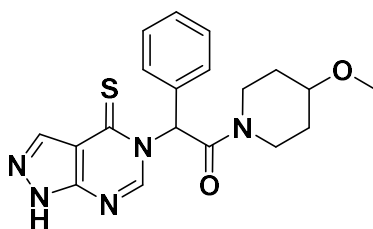


*1-(3-hydroxypiperidin-1-yl)-2-phenyl-2-(4-thioxo-1,4-dihydro-5H-pyrazolo[3,4-d]pyrimidin-5-yl)ethan-1-one (3.8d)*: According to the general procedure E, the title compound was obtained as a yellow solid (52%).  $R_f$ : 0.2 (DCM:MeOH,10:1).  $^1\text{H}$  NMR (400

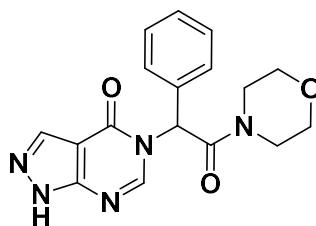
MHz, MeOD)  $\delta_{\text{H}}$  1.36 - 1.99 (4H, m, CH), 2.81 (1H, s, CH), 3.22 - 3.37 (1H, m, CH), 3.40 - 3.55 (1H, m, CH), 3.56 - 3.73 (1H, m, CH), 3.73 - 3.87 (1H, m, CH), 7.22 - 7.29 (2H, m, ArCH), 7.30 - 7.39 (3H, m, ArCH), 7.86 - 7.94 (1H, m, CH), 8.15 - 8.23 (1H, m, ArCH), 8.25 - 8.35 (1H, m, ArCH).  $^{13}\text{C}$  NMR (100 MHz, MeOD)  $\delta_{\text{C}}$  22.49, 22.67, 29.30, 42.84, 45.45, 45.85, 48.92, 65.18, 65.37, 129.69, 129.77, 130.93, 130.99, 132.49, 166.48. ESI-HRMS (m/z):  $[\text{M} + \text{H}]^+$  calcd for  $\text{C}_{18}\text{H}_{19}\text{N}_5\text{O}_2\text{S}$ , 370.1355; found, 370.1324.



*5-(2-(4-methoxypiperidin-1-yl)-2-oxo-1-phenylethyl)-1,5-dihydro-4H-pyrazolo[3,4-d]pyrimidin-4-one (3.7e)*: According to the general procedure D, the title compound was obtained as a white solid (42%).  $R_f$ : 0.2 (DCM:MeOH,10:1).  $^1\text{H}$  NMR (400 MHz, MeOD)  $\delta_{\text{H}}$  1.26 (1H, d,  $J = 9.78$  Hz, CH), 1.34 - 1.43 (1H, m, CH), 1.50 - 1.67 (1H, m, CH), 1.69 - 1.85 (1H, m, CH), 3.05 - 3.16 (1H, m, CH), 3.25 (3H, s,  $\text{CH}_3$ ), 3.27 - 3.63 (3H, m, CH), 3.72 - 3.86 (1H, m, CH), 7.15 (1H, d,  $J = 6.85$  Hz, CH), 7.30 (2H, td,  $J = 6.79, 1.83$  Hz, ArCH), 7.34 - 7.41 (3H, m, ArCH), 7.80 (1H, d,  $J = 10.76$  Hz, ArCH), 8.08 (1H, d,  $J = 1.22$  Hz, ArCH).  $^{13}\text{C}$  NMR (100 MHz, MeOD)  $\delta_{\text{C}}$  26.61, 26.90, 27.37, 28.59, 46.87, 48.09, 56.30, 129.01, 129.17, 129.89, 148.68, 150.40, 167.14, 169.54. ESI-HRMS (m/z):  $[\text{M} + \text{H}]^+$  calcd for  $\text{C}_{19}\text{H}_{21}\text{N}_5\text{O}_3$ , 368.1755; found, 368.1702.

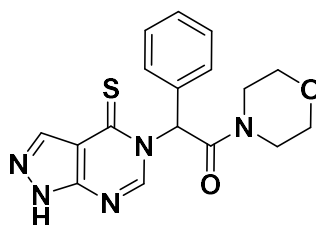


(*S*)-1-(4-methoxypiperidin-1-yl)-2-phenyl-2-(4-thioxo-1,4-dihydro-5H-pyrazolo[3,4-d]pyrimidin-5-yl)ethan-1-one (**3.8e**): According to the general procedure E, the title compound was obtained as a yellow solid (47%). *R*<sub>f</sub>: 0.2 (DCM:MeOH,10:1). <sup>1</sup>H NMR (400 MHz, MeOD) δ<sub>H</sub> 1.23 - 1.33 (1H, m, CH), 1.35 - 1.44 (1H, m, CH), 1.50 - 1.86 (2H, m, CH), 3.06 - 3.16 (1H, m, CH), 3.25 (3H, s, CH<sub>3</sub>), 3.27 - 3.64 (3H, m, CH), 3.72 - 3.87 (1H, m, CH), 7.12 - 7.18 (1H, m, CH), 7.26 - 7.33 (2H, m, ArCH), 7.35 - 7.45 (3H, m, ArCH), 7.78 (1H, m, ArCH), 8.07 - 8.13 (1H, m, ArCH). <sup>13</sup>C NMR (100 MHz, MeOD) δ<sub>C</sub> 29.92, 30.40, 30.51, 39.58, 39.77, 55.76, 55.87, 56.20, 129.04, 129.98, 136.31, 150.17, 157.37, 165.81. ESI-HRMS (*m/z*): [M + H]<sup>+</sup> calcd for C<sub>19</sub>H<sub>21</sub>N<sub>5</sub>O<sub>2</sub>S, 384.1465; found, 384.1479.

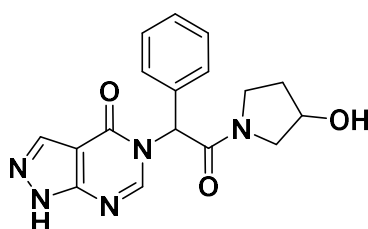


5-(2-morpholino-2-oxo-1-phenylethyl)-1,5-dihydro-4H-pyrazolo[3,4-d]pyrimidin-4-one (**3.7f**): According to the general procedure D, the title compound was obtained as a white solid (46%). *R*<sub>f</sub>: 0.2 (DCM:MeOH,10:1). <sup>1</sup>H NMR (400 MHz, MeOD) δ<sub>H</sub> 3.20 - 3.28 (1H, m, CH), 3.29 - 3.36 (1H, m, CH), 3.51 (1H, ddd, *J* = 13.02, 6.66, 3.06 Hz, CH), 3.57 - 3.75 (5H, m, CH), 7.11 (1H, s, CH), 7.30 - 7.35 (2H, m, ArCH), 7.37 - 7.45 (3H, m, ArCH), 7.79 - 7.79 (1H, m, ArCH), 8.11 (1H, s, CH). <sup>13</sup>C NMR (100 MHz, MeOD) δ<sub>C</sub> 29.71, 42.95, 46.17, 55.97, 66.23, 66.71, 129.03, 130.07, 150.00, 166.28. ESI-HRMS (*m/z*): [M + H]<sup>+</sup> calcd for C<sub>17</sub>H<sub>17</sub>N<sub>5</sub>O<sub>3</sub>, 340.1346; found, 340.1389.

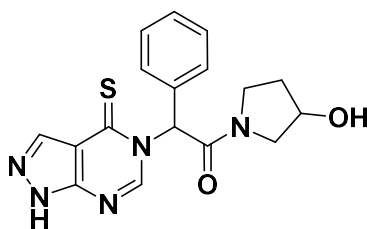




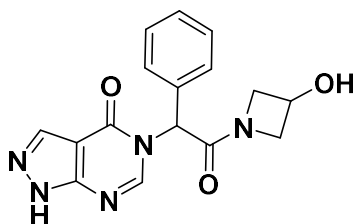
*1-morpholino-2-phenyl-2-(4-thioxo-1,4-dihydro-5H-pyrazolo[3,4-d]pyrimidin-5-yl)ethan-1-one (3.8f)*: According to the general procedure E, the title compound was obtained as a yellow solid (52%).  $R_f$ : 0.2 (DCM:MeOH,10:1).  $^1\text{H}$  NMR (400 MHz, MeOD)  $\delta_{\text{H}}$  3.29 (1H, ddd,  $J$  = 13.27, 6.79, 2.93 Hz, CH), 3.42 (1H, ddd,  $J$  = 11.55, 6.05, 2.93 Hz, CH), 3.56 - 3.75 (6H, m, CH), 7.27 - 7.35 (2H, m, ArCH), 7.37 - 7.46 (3H, m, ArCH), 7.89 - 7.97 (1H, m, CH), 8.22 - 8.27 (1H, m, ArCH), 8.28 (1H, s, CH).  $^{13}\text{C}$  NMR (100 MHz, MeOD)  $\delta_{\text{C}}$  30.97, 43.01, 46.17, 47.25, 61.17, 66.40, 66.76, 129.05, 130.13, 133.43, 149.49, 165.69, 180.93. ESI-HRMS ( $m/z$ ):  $[\text{M} + \text{H}]^+$  calcd for  $\text{C}_{17}\text{H}_{17}\text{N}_5\text{O}_2\text{S}$ , 384.1465; found, 356.1168.



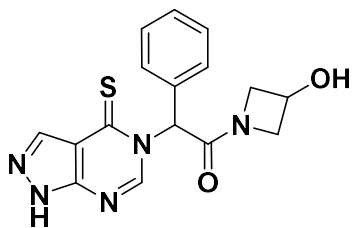
*5-(2-(3-hydroxypyrrolidin-1-yl)-2-oxo-1-phenylethyl)-1,5-dihydro-4H-pyrazolo[3,4-d]pyrimidin-4-one (3.7g)*: According to the general procedure D, the title compound was obtained as a white solid (22%).  $R_f$ : 0.2 (DCM:MeOH,10:1).  $^1\text{H}$  NMR (400 MHz, MeOD)  $\delta_{\text{H}}$  1.89 - 2.21 (2H, m, CH), 3.11 - 3.29 (1H, m, CH), 3.62 (3H, br. s., CH), 3.88 - 3.97 (1H, m, CH), 4.36 - 4.50 (1H, m, CH), 6.86 - 7.03 (1H, m, CH), 7.43 - 7.48 (2H, m, ArCH), 7.49 - 7.56 (3H, m, ArCH), 7.74 - 7.81 (2H, m, CH).  $^{13}\text{C}$  NMR (100 MHz, MeOD)  $\delta_{\text{C}}$  14.20, 21.06, 26.60, 28.57, 46.85, 48.09, 56.24, 60.43, 129.18, 129.83, 133.88, 150.14, 157.47, 167.28. ESI-HRMS ( $m/z$ ):  $[\text{M} + \text{H}]^+$  calcd for  $\text{C}_{17}\text{H}_{17}\text{N}_5\text{O}_3$ , 340.1365; found, 340.1391.



*1-(3-hydroxypyrrolidin-1-yl)-2-phenyl-2-(4-thioxo-1,4-dihydro-5H-pyrazolo[3,4-d]pyrimidin-5-yl)ethan-1-one (3.8g)*: According to the general procedure E, the title compound was obtained as a yellow solid (24%).  $R_f$ : 0.2 (DCM:MeOH,10:1).  $^1\text{H}$  NMR (400 MHz, MeOD)  $\delta_{\text{H}}$  1.79 - 2.02 (2H, m, CH), 3.06 (1H, d,  $J$  = 10.76 Hz, CH), 3.44 - 3.74 (2H, m, CH), 3.86 - 3.99 (1H, m, CH), 4.26 - 4.40 (1H, m, CH), 7.30 (2H, d,  $J$  = 7.58 Hz, ArCH), 7.37 - 7.46 (3H, m, ArCH), 7.63 (1H, d,  $J$  = 8.31 Hz, CH), 7.75 - 7.86 (1H, m, ArCH), 7.92 - 7.96 (1H, m, ArCH), 8.18 (1H, br. s., NH).  $^{13}\text{C}$  NMR (100 MHz, MeOD)  $\delta_{\text{C}}$  22.83, 31.85, 31.99, 33.50, 44.07, 62.80, 63.09, 68.40, 70.08, 126.88, 128.87, 129.00, 129.73, 129.76, 166.30. ESI-HRMS ( $m/z$ ):  $[\text{M} + \text{H}]^+$  calcd for  $\text{C}_{17}\text{H}_{17}\text{N}_5\text{O}_2\text{S}$ , 356.1115; found, 356.1182.



*(S)-5-(2-(3-hydroxyazetidin-1-yl)-2-oxo-1-phenylethyl)-1,5-dihydro-4H-pyrazolo[3,4-d]pyrimidin-4-one (3.7h)*: According to the D, the title compound was obtained as a white solid (44%).  $R_f$ : 0.2 (DCM:MeOH,10:1).  $^1\text{H}$  NMR (400 MHz, MeOD)  $\delta_{\text{H}}$  ppm 3.49 (1H, d,  $J$  = 5.62 Hz, CH), 3.78 (1H, dd,  $J$  = 18.71, 10.88 Hz, CH), 3.91 - 4.33 (2H, m, CH), 4.43 (1H, br. s., CH), 6.58- 6.67 (1H, m, CH), 7.32 - 7.53 (5H, m, ArCH), 7.61 - 7.68 (1H, m, ArCH), 7.78 (1H, d,  $J$  = 8.31 Hz, ArCH).  $^{13}\text{C}$  NMR (100 MHz, MeOD)  $\delta_{\text{C}}$  29.33, 33.13, 33.33, 40.04, 42.86, 43.00, 65.90, 66.01, 129.84, 130.86, 131.02, 135.70. ESI-HRMS ( $m/z$ ):  $[\text{M} + \text{H}]^+$  calcd for  $\text{C}_{16}\text{H}_{15}\text{N}_5\text{O}_3$ , 326.1265; found, 326.1244.



(*S*)-1-(3-hydroxyazetidin-1-yl)-2-phenyl-2-(4-thioxo-1,4-dihydro-5H-pyrazolo[3,4-*d*]pyrimidin-5-yl)ethan-1-one (**3.8h**). According to the general procedure E, the title compound was obtained as a yellow solid (34%).  $R_f$ : 0.2 (DCM:MeOH,10:1).  $^1\text{H}$  NMR (400 MHz, MeOD)  $\delta_{\text{H}}$  3.73 - 3.87 (1H, m, CH), 3.93 - 4.23 (2H, m, CH), 4.24 - 4.45 (1H m,), 4.53 - 4.62 (1H, m, CH), 4.65 - 4.79 (1H, m, CH), 7.29 - 7.44 (5H, m, ArCH), 7.71 - 7.77 (1H, m, CH), 7.80 - 7.94 (1H, m, ArCH), 8.21 (1H, d,  $J$  = 17.61 Hz, ArCH).  $^{13}\text{C}$  NMR (100 MHz, MeOD)  $\delta_{\text{C}}$  18.90, 58.40, 60.09, 60.80, 61.60, 62.66, 111.96, 116.02, 126.82, 128.51, 128.90, 128.95, 129.93, 162.41, 167.06. ESI-HRMS ( $m/z$ ):  $[\text{M} + \text{H}]^+$  calcd for  $\text{C}_{16}\text{H}_{15}\text{N}_5\text{O}_2\text{S}$ , 342.1066; found, 342.1011.

## REFERENCES

1. Jornvall, H.; Danielsson, O.; Hjelmqvist, L.; Persson, B.; Shafqat, J., The alcohol dehydrogenase system. *Adv. Exp. Med. Biol.* **1995**, 372, 281-294.
2. Day, J. M.; Tutill, H. J.; Purohit, A.; Reed, M. J., Design and validation of specific inhibitors of 17beta-hydroxysteroid dehydrogenases for therapeutic application in breast and prostate cancer, and in endometriosis. *Endocr. Relat. Cancer* **2008**, 15, 665-692.
3. Mindnich, R.; Moller, G.; Adamski, J., The role of 17 beta-hydroxysteroid dehydrogenases. *Mol. Cell Endocrinol.* **2004**, 218, 7-20.
4. Penning, T. M.; Burczynski, M. E.; Jez, J. M.; Hung, C. F.; Lin, H. K.; Ma, H.; Moore, M.; Palackal, N.; Ratnam, K., Human 3alpha-hydroxysteroid dehydrogenase isoforms (AKR1C1-AKR1C4) of the aldo-keto reductase superfamily: functional plasticity and tissue distribution reveals roles in the inactivation and formation of male and female sex hormones. *Biochem. J.* **2000**, 351, 67-77.
5. Markus, M.; Husen, B.; Leenders, F.; Seedorf, U.; Jungblut, P. W.; Hall, P. H.; Adamski, J., Peroxisomes contain an enzyme with 17 beta-estradiol dehydrogenase, fatty acid hydratase/dehydrogenase, and sterol carrier activity. *Ann. N. Y. Acad. Sci.* **1996**, 804, 691-693.
6. Moon, Y. A.; Horton, J. D., Identification of two mammalian reductases involved in the two-carbon fatty acyl elongation cascade. *J. Biol. Chem.* **2003**, 278, 7335-7343.
7. Krazeisen, A.; Breitling, R.; Imai, K.; Fritz, S.; Moller, G.; Adamski, J., Determination of cDNA, gene structure and chromosomal localization of the novel human 17beta-hydroxysteroid dehydrogenase type 7(1). *FEBS Lett.* **1999**, 460, 373-379.
8. Shafqat, N.; Marschall, H. U.; Filling, C.; Nordling, E.; Wu, X. Q.; Bjork, L.; Thyberg, J.; Martensson, E.; Salim, S.; Jornvall, H.; Oppermann, U., Expanded substrate screenings of human and Drosophila type 10 17beta-hydroxysteroid dehydrogenases (HSDs) reveal multiple specificities in bile acid and steroid hormone metabolism: characterization of multifunctional 3alpha/7alpha/7beta/17beta/20beta/21-HSD. *Biochem. J.* **2003**, 376, 49-60.
9. Zhang, M.; Chen, W.; Smith, S. M.; Napoli, J. L., Molecular characterization of a mouse short chain dehydrogenase/reductase active with all-trans-retinol in intact cells, mRDH1. *J. Biol. Chem.* **2001**, 276, 44083-44090.
10. He, X. Y.; Isaacs, C.; Yang, S. Y., Roles of Mitochondrial 17beta-Hydroxysteroid Dehydrogenase Type 10 in Alzheimer's Disease. *J. Alzheimers Dis.* **2018**, 62, 665-673.
11. Hilborn, E.; Stal, O.; Jansson, A., Estrogen and androgen-converting enzymes 17beta-hydroxysteroid dehydrogenase and their involvement in cancer: with a special focus on 17beta-hydroxysteroid dehydrogenase type 1, 2, and breast cancer. *Oncotarget* **2017**, 8, 30552-30562.
12. Andersson, S.; Moghrabi, N., Physiology and molecular genetics of 17 beta-hydroxysteroid dehydrogenases. *Steroids* **1997**, 62, 143-147.
13. Karageorgi, S.; McGrath, M.; Lee, I. M.; Buring, J.; Kraft, P.; De Vivo, I., Polymorphisms in genes hydroxysteroid-dehydrogenase-17b type 2 and type 4 and endometrial cancer risk. *Gynecol. Oncol.* **2011**, 121, 54-58.

14. Day, J. M.; Foster, P. A.; Tutill, H. J.; Schmidlin, F.; Sharland, C. M.; Hargrave, J. D.; Vicker, N.; Potter, B. V.; Reed, M. J.; Purohit, A., STX2171, a 17beta-hydroxysteroid dehydrogenase type 3 inhibitor, is efficacious in vivo in a novel hormone-dependent prostate cancer model. *Endocr. Relat. Cancer* **2013**, *20*, 53-64.
15. Pierce, S. B.; Walsh, T.; Chisholm, K. M.; Lee, M. K.; Thornton, A. M.; Fiumara, A.; Opitz, J. M.; Levy-Lahad, E.; Klevit, R. E.; King, M. C., Mutations in the DBP-deficiency protein HSD17B4 cause ovarian dysgenesis, hearing loss, and ataxia of Perrault Syndrome. *Am. J. Hum. Genet.* **2010**, *87*, 282-288.
16. Beesley, J.; Jordan, S. J.; Spurdle, A. B.; Song, H.; Ramus, S. J.; Kjaer, S. K.; Hogdall, E.; DiCioccio, R. A.; McGuire, V.; Whittemore, A. S.; Gayther, S. A.; Pharoah, P. D.; Webb, P. M.; Chenevix-Trench, G.; Australian Ovarian Cancer Study, G.; Australian Cancer, S.; Australian Breast Cancer Family, S., Association between single-nucleotide polymorphisms in hormone metabolism and DNA repair genes and epithelial ovarian cancer: results from two Australian studies and an additional validation set. *Cancer Epidemiol. Biomarkers Prev.* **2007**, *16*, 2557-2565.
17. Byrns, M. C.; Penning, T. M., Type 5 17beta-hydroxysteroid dehydrogenase/prostaglandin F synthase (AKR1C3): role in breast cancer and inhibition by non-steroidal anti-inflammatory drug analogs. *Chem. Biol. Interact.* **2009**, *178*, 221-227.
18. Adeniji, A. O.; Chen, M.; Penning, T. M., AKR1C3 as a target in castrate resistant prostate cancer. *J. Steroid Biochem. Mol. Biol.* **2013**, *137*, 136-149.
19. Moradi Manesh, D.; El-Hoss, J.; Evans, K.; Richmond, J.; Toscan, C. E.; Bracken, L. S.; Hedrick, A.; Sutton, R.; Marshall, G. M.; Wilson, W. R.; Kurmasheva, R. T.; Billups, C.; Houghton, P. J.; Smith, M. A.; Carol, H.; Lock, R. B., AKR1C3 is a biomarker of sensitivity to PR-104 in preclinical models of T-cell acute lymphoblastic leukemia. *Blood* **2015**, *126*, 1193-1202.
20. Biswas, M. G.; Russell, D. W., Expression cloning and characterization of oxidative 17beta- and 3alpha-hydroxysteroid dehydrogenases from rat and human prostate. *J. Biol. Chem.* **1997**, *272*, 15959-15966.
21. Song, D.; Liu, G.; Luu-The, V.; Zhao, D.; Wang, L.; Zhang, H.; Xueling, G.; Li, S.; Desy, L.; Labrie, F.; Pelletier, G., Expression of aromatase and 17beta-hydroxysteroid dehydrogenase types 1, 7 and 12 in breast cancer. An immunocytochemical study. *J. Steroid Biochem. Mol. Biol.* **2006**, *101*, 136-44.
22. Maxwell, M. M.; Nearing, J.; Aziz, N., Ke 6 gene. Sequence and organization and aberrant regulation in murine polycystic kidney disease. *J. Biol. Chem.* **1995**, *270*, 25213-25219.
23. Skorczyk-Werner, A.; Pawlowski, P.; Michalczyk, M.; Warowicka, A.; Wawrocka, A.; Wicher, K.; Bakunowicz-Lazarczyk, A.; Krawczynski, M. R., Fundus albipunctatus: review of the literature and report of a novel RDH5 gene mutation affecting the invariant tyrosine (p.Tyr175Phe). *J. Appl. Genet.* **2015**, *56*, 317-327.
24. Morsy, A.; Trippier, P. C., Amyloid-binding alcohol dehydrogenase (ABAD) inhibitors for the treatment of Alzheimer's disease. *J. Med. Chem.* **2019**, *62*, 4252-4264.

25. Ayan, D.; Maltais, R.; Poirier, D., Identification of a 17beta-hydroxysteroid dehydrogenase type 10 steroidal inhibitor: a tool to investigate the role of type 10 in Alzheimer's disease and prostate cancer. *ChemMedChem* **2012**, *7*, 1181-1184.
26. Rotinen, M.; Villar, J.; Celay, J.; Serrano, I.; Notario, V.; Encio, I., Transcriptional regulation of type 11 17beta-hydroxysteroid dehydrogenase expression in prostate cancer cells. *Mol. Cell Endocrinol.* **2011**, *339*, 45-53.
27. Szajnik, M.; Szczepanski, M. J.; Elishaev, E.; Visus, C.; Lenzner, D.; Zabel, M.; Glura, M.; DeLeo, A. B.; Whiteside, T. L., 17beta Hydroxysteroid dehydrogenase type 12 (HSD17B12) is a marker of poor prognosis in ovarian carcinoma. *Gynecol. Oncol.* **2012**, *127*, 587-594.
28. Ma, Y.; Belyaeva, O. V.; Brown, P. M.; Fujita, K.; Valles, K.; Karki, S.; de Boer, Y. S.; Koh, C.; Chen, Y.; Du, X.; Handelman, S. K.; Chen, V.; Speliotes, E. K.; Nestlerode, C.; Thomas, E.; Kleiner, D. E.; Zmuda, J. M.; Sanyal, A. J.; Kedishvili, N. Y.; Liang, T. J.; Rotman, Y., 17-Beta Hydroxysteroid Dehydrogenase 13 Is a Hepatic Retinol Dehydrogenase Associated With Histological Features of Nonalcoholic Fatty Liver Disease. *Hepatology* **2019**, *69*, 1504-1519.
29. Jansson, A. K.; Gunnarsson, C.; Cohen, M.; Sivik, T.; Stal, O., 17beta-hydroxysteroid dehydrogenase 14 affects estradiol levels in breast cancer cells and is a prognostic marker in estrogen receptor-positive breast cancer. *Cancer Res.* **2006**, *66*, 11471-11477.
30. Xie, Y. A.; Lee, W.; Cai, C.; Gambin, T.; Noupou, K.; Sujirakul, T.; Ayuso, C.; Jhangiani, S.; Muzny, D.; Boerwinkle, E.; Gibbs, R.; Greenstein, V. C.; Lupski, J. R.; Tsang, S. H.; Allikmets, R., New syndrome with retinitis pigmentosa is caused by nonsense mutations in retinol dehydrogenase RDH11. *Hum. Mol. Genet.* **2014**, *23*, 5774-5780.
31. Housman, G.; Byler, S.; Heerboth, S.; Lapinska, K.; Longacre, M.; Snyder, N.; Sarkar, S., Drug resistance in cancer: an overview. *Cancers (Basel)* **2014**, *6*, 1769-1792.
32. Gottesman, M. M., Mechanisms of cancer drug resistance. *Annu. Rev. Med.* **2002**, *53*, 615-627.
33. Siegel, R. L.; Miller, K. D.; Jemal, A., Cancer statistics, 2020. *CA Cancer J. Clin.* **2020**, *70*, 7-30.
34. Aragon-Ching, J. B.; Williams, K. M.; Gulley, J. L., Impact of androgen-deprivation therapy on the immune system: implications for combination therapy of prostate cancer. *Front. Biosci.* **2007**, *12*, 4957-4971.
35. Chen, R. C.; Rumble, R. B.; Loblaw, D. A.; Finelli, A.; Ehdaie, B.; Cooperberg, M. R.; Morgan, S. C.; Tyldesley, S.; Haluschak, J. J.; Tan, W.; Justman, S.; Jain, S., Active Surveillance for the Management of Localized Prostate Cancer (Cancer Care Ontario Guideline): American Society of Clinical Oncology Clinical Practice Guideline Endorsement. *J. Clin. Oncol.* **2016**, *34*, 2182-2190.
36. Gandaglia, G.; Abdollah, F.; Schiffmann, J.; Trudeau, V.; Shariat, S. F.; Kim, S. P.; Perrotte, P.; Montorsi, F.; Briganti, A.; Trinh, Q. D.; Karakiewicz, P. I.; Sun, M., Distribution of metastatic sites in patients with prostate cancer: A population-based analysis. *Prostate* **2014**, *74*, 210-216.

37. Sharifi, N.; Gulley, J. L.; Dahut, W. L., Androgen deprivation therapy for prostate cancer. *JAMA* **2005**, *294*, 238-244.
38. Paich, K.; Dunn, R.; Skolarus, T.; Montie, J.; Hollenbeck, B.; Palapattu, G.; Wood, D., Jr.; Mitchell, S.; Hola, V.; Erickson, K.; Shifferd, J.; Wittmann, D., Preparing patients and partners for recovery from the side effects of prostate cancer surgery: a group approach. *Urology* **2016**, *88*, 36-42.
39. Stephenson, A. J.; Scardino, P. T.; Kattan, M. W.; Pisansky, T. M.; Slawin, K. M.; Klein, E. A.; Anscher, M. S.; Michalski, J. M.; Sandler, H. M.; Lin, D. W.; Forman, J. D.; Zelefsky, M. J.; Kestin, L. L.; Roehrborn, C. G.; Catton, C. N.; DeWeese, T. L.; Liauw, S. L.; Valicenti, R. K.; Kuban, D. A.; Pollack, A., Predicting the outcome of salvage radiation therapy for recurrent prostate cancer after radical prostatectomy. *J. Clin. Oncol.* **2007**, *25*, 2035-2041.
40. Tilbrook, A. J.; Clarke, I. J., Negative feedback regulation of the secretion and actions of gonadotropin-releasing hormone in males. *Biol. Reprod.* **2001**, *64*, 735-742.
41. Crawford, E. D., Hormonal therapy in prostate cancer: historical approaches. *Rev. Urol.* **2004**, *6 Suppl 7*, S3-S11.
42. Labrie, F.; Belanger, A.; Luu-The, V.; Labrie, C.; Simard, J.; Cusan, L.; Gomez, J.; Candas, B., Gonadotropin-releasing hormone agonists in the treatment of prostate cancer. *Endocr. Rev.* **2005**, *26*, 361-379.
43. Lepor, H.; Shore, N. D., LHRH agonists for the treatment of prostate cancer: 2012. *Rev. Urol.* **2012**, *14*, 1-12.
44. Perachino, M.; Cavalli, V.; Bravi, F., Testosterone levels in patients with metastatic prostate cancer treated with luteinizing hormone-releasing hormone therapy: prognostic significance? *BJU Int.* **2010**, *105*, 648-651.
45. Goodman, O. B., Jr., Is there a role for LHRH antagonists in prostate cancer? *Oncology* **2009**, *23*, 632-635.
46. Dellis, A.; Papatsoris, A., Therapeutic outcomes of the LHRH antagonists. *Expert Rev. Pharmacoecon. Outcomes Res.* **2017**, *17*, 481-488.
47. Ozono, S.; Tsukamoto, T.; Naito, S.; Horie, S.; Ohashi, Y.; Uemura, H.; Yokomizo, Y.; Fukasawa, S.; Kusuoka, H.; Akazawa, R.; Saito, M.; Akaza, H., Efficacy and safety of 3-month dosing regimen of degarelix in Japanese subjects with prostate cancer: A phase III study. *Cancer Sci.* **2018**, *109*, 1920-1929.
48. Ozono, S.; Tsukamoto, T.; Naito, S.; Ohashi, Y.; Ueda, T.; Nishiyama, T.; Maeda, H.; Kusuoka, H.; Akazawa, R.; Ito, M.; Akaza, H., Efficacy and safety of a 3-month dosing regimen of degarelix in Japanese patients with prostate cancer: a phase II maintenance-dose-finding study. *Jpn. J. Clin. Oncol.* **2017**, *47*, 438-446.
49. You, D.; Chung, B. H.; Lee, S. E.; Kim, C. S., Efficacy and safety of degarelix in Korean patients with prostate cancer requiring androgen deprivation therapy: Open-label multicenter phase III study. *Prostate Int.* **2015**, *3*, 22-26.
50. Sun, Y.; Xie, L.; Xu, T.; Jakobsen, J. S.; Han, W.; Sorensen, P. S.; Wang, X., Efficacy and safety of degarelix in patients with prostate cancer: Results from a phase III study in China. *Asian J. Urol.* **2020**, *7*, 301-308.

51. Shore, N. D.; Saad, F.; Cookson, M. S.; George, D. J.; Saltzstein, D. R.; Tutrone, R.; Akaza, H.; Bossi, A.; van Veenhuyzen, D. F.; Selby, B.; Fan, X.; Kang, V.; Walling, J.; Tombal, B.; Investigators, H. S., Oral relugolix for androgen-deprivation therapy in advanced prostate cancer. *N. Engl. J. Med.* **2020**, *382*, 2187-2196.
52. Slater, H., Phase 3 HERO trial finds relugolix to be superior to leuprolide in prostate cancer. *Oncology* **2020**, *34*, 252.
53. Lv, J.; Lin, J., Relugolix as a promising novel oral GnRH antagonist for prostate cancer treatment. *Asian J. Androl.* **2020**.
54. Sachdev, S.; Zhang, H.; Hussain, M., Relugolix: early promise for a novel oral androgen deprivation therapy with radiation therapy for prostate cancer. *Eur. Urol.* **2020**, *78*, 193-194.
55. Magee, D. E.; Singal, R. K., Androgen deprivation therapy: indications, methods of utilization, side effects and their management. *Can. J. Urol.* **2020**, *27*, 11-16.
56. Balk, S. P.; Ko, Y. J.; Bubley, G. J., Biology of prostate-specific antigen. *J. Clin. Oncol.* **2003**, *21*, 383-391.
57. Hotte, S. J.; Saad, F., Current management of castrate-resistant prostate cancer. *Curr. Oncol.* **2010**, *17 Suppl 2*, S72-79.
58. Halabi, S.; Lin, C. Y.; Kelly, W. K.; Fizazi, K. S.; Moul, J. W.; Kaplan, E. B.; Morris, M. J.; Small, E. J., Updated prognostic model for predicting overall survival in first-line chemotherapy for patients with metastatic castration-resistant prostate cancer. *J. Clin. Oncol.* **2014**, *32*, 671-677.
59. Gregory, C. W.; He, B.; Johnson, R. T.; Ford, O. H.; Mohler, J. L.; French, F. S.; Wilson, E. M., A mechanism for androgen receptor-mediated prostate cancer recurrence after androgen deprivation therapy. *Cancer Res.* **2001**, *61*, 4315-4319.
60. El-Amm, J.; Aragon-Ching, J. B., The current landscape of treatment in non-metastatic castration-resistant prostate cancer. *Clin. Med. Insights Oncol.* **2019**, *13*, 1179554919833927.
61. Fizazi, K.; Scher, H. I.; Molina, A.; Logothetis, C. J.; Chi, K. N.; Jones, R. J.; Staffurth, J. N.; North, S.; Vogelzang, N. J.; Saad, F.; Mainwaring, P.; Harland, S.; Goodman, O. B., Jr.; Sternberg, C. N.; Li, J. H.; Kheoh, T.; Haqq, C. M.; de Bono, J. S.; Investigators, C.-A.-. Abiraterone acetate for treatment of metastatic castration-resistant prostate cancer: final overall survival analysis of the COU-AA-301 randomised, double-blind, placebo-controlled phase 3 study. *Lancet Oncol.* **2012**, *13*, 983-992.
62. Fernandez-Cancio, M.; Camats, N.; Fluck, C. E.; Zalewski, A.; Dick, B.; Frey, B. M.; Monne, R.; Toran, N.; Audi, L.; Pandey, A. V., Mechanism of the dual activities of human CYP17A1 and binding to anti-prostate cancer drug abiraterone revealed by a novel V366M mutation causing 17,20 lyase deficiency. *Pharmaceuticals (Basel)* **2018**, *11*.
63. Attard, G.; Reid, A. H.; Yap, T. A.; Raynaud, F.; Dowsett, M.; Settatree, S.; Barrett, M.; Parker, C.; Martins, V.; Folkerd, E.; Clark, J.; Cooper, C. S.; Kaye, S. B.; Dearnaley, D.; Lee, G.; de Bono, J. S., Phase I clinical trial of a selective inhibitor of CYP17, abiraterone acetate, confirms that castration-resistant prostate cancer commonly remains hormone driven. *J. Clin. Oncol.* **2008**, *26*, 4563-4571.



64. Berruti, A.; Pia, A.; Terzolo, M., Abiraterone and increased survival in metastatic prostate cancer. *N. Engl. J. Med.* **2011**, *365*, 766.
65. James, N. D.; de Bono, J. S.; Spears, M. R.; Clarke, N. W.; Mason, M. D.; Dearnaley, D. P.; Ritchie, A. W. S.; Amos, C. L.; Gilson, C.; Jones, R. J.; Matheson, D.; Millman, R.; Attard, G.; Chowdhury, S.; Cross, W. R.; Gillessen, S.; Parker, C. C.; Russell, J. M.; Berthold, D. R.; Brawley, C.; Adab, F.; Aung, S.; Birtle, A. J.; Bowen, J.; Brock, S.; Chakraborti, P.; Ferguson, C.; Gale, J.; Gray, E.; Hingorani, M.; Hoskin, P. J.; Lester, J. F.; Malik, Z. I.; McKinna, F.; McPhail, N.; Money-Kyrle, J.; O'Sullivan, J.; Parikh, O.; Protheroe, A.; Robinson, A.; Srihari, N. N.; Thomas, C.; Wagstaff, J.; Wylie, J.; Zarkar, A.; Parmar, M. K. B.; Sydes, M. R.; Investigators, S., Abiraterone for prostate cancer not previously treated with hormone therapy. *N. Engl. J. Med.* **2017**, *377*, 338-351.
66. Keizman, D.; Huang, P.; Carducci, M. A.; Eisenberger, M. A., Contemporary experience with ketoconazole in patients with metastatic castration-resistant prostate cancer: clinical factors associated with PSA response and disease progression. *Prostate* **2012**, *72*, 461-467.
67. Eichenberger, T.; Trachtenberg, J., Effects of high-dose ketoconazole in patients with androgen-independent prostatic cancer. *Am. J. Clin. Oncol.* **1988**, *11 Suppl 2*, S104-107.
68. Pont, A., Long-term experience with high dose ketoconazole therapy in patients with stage D2 prostatic carcinoma. *J. Urol.* **1987**, *137*, 902-904.
69. Nakabayashi, M.; Oh, W. K.; Jacobus, S.; Regan, M. M.; Taplin, M. E.; Kantoff, P. W.; Rosenberg, J. E., Activity of ketoconazole after taxane-based chemotherapy in castration-resistant prostate cancer. *BJU Int.* **2010**, *105*, 1392-1396.
70. Small, E. J.; Halabi, S.; Dawson, N. A.; Stadler, W. M.; Rini, B. I.; Picus, J.; Gable, P.; Torti, F. M.; Kaplan, E.; Vogelzang, N. J., Antiandrogen withdrawal alone or in combination with ketoconazole in androgen-independent prostate cancer patients: a phase III trial (CALGB 9583). *J. Clin. Oncol.* **2004**, *22*, 1025-1033.
71. Pond, G. R.; Armstrong, A. J.; Galsky, M. D.; Wood, B. A.; Leopold, L.; Sonpavde, G., Efficacy of docetaxel-based chemotherapy following ketoconazole in metastatic castration-resistant prostate cancer: implications for prior therapy in clinical trials. *Urol. Oncol.* **2013**, *31*, 1457-1463.
72. Taplin, M. E.; Regan, M. M.; Ko, Y. J.; Bubley, G. J.; Duggan, S. E.; Werner, L.; Beer, T. M.; Ryan, C. W.; Mathew, P.; Tu, S. M.; Denmeade, S. R.; Oh, W. K.; Sartor, O.; Mantzoros, C. S.; Rittmaster, R.; Kantoff, P. W.; Balk, S. P., Phase II study of androgen synthesis inhibition with ketoconazole, hydrocortisone, and dutasteride in asymptomatic castration-resistant prostate cancer. *Clin. Cancer Res.* **2009**, *15*, 7099-7105.
73. Francini, E.; Petrioli, R.; Roviello, G., No clear evidence of a clinical benefit of a sequential therapy regimen with abiraterone acetate and enzalutamide. *Expert Rev. Anticancer Ther.* **2014**, *14*, 1135-1140.
74. Kokal, M.; Mirzakhani, K.; Pungsrinont, T.; Baniahmad, A., Mechanisms of androgen receptor agonist- and antagonist-mediated cellular senescence in prostate cancer. *Cancers* **2020**, *12*.

75. Scher, H. I.; Beer, T. M.; Higano, C. S.; Anand, A.; Taplin, M. E.; Efstathiou, E.; Rathkopf, D.; Shelkey, J.; Yu, E. Y.; Alumkal, J.; Hung, D.; Hirmand, M.; Seely, L.; Morris, M. J.; Danila, D. C.; Humm, J.; Larson, S.; Fleisher, M.; Sawyers, C. L.; Prostate Cancer Foundation/Department of Defense Prostate Cancer Clinical Trials, C., Antitumour activity of MDV3100 in castration-resistant prostate cancer: a phase 1-2 study. *Lancet* **2010**, *375*, 1437-1446.
76. Foster, W. R.; Car, B. D.; Shi, H.; Levesque, P. C.; Obermeier, M. T.; Gan, J.; Arezzo, J. C.; Powlin, S. S.; Dinchuk, J. E.; Balog, A.; Salvati, M. E.; Attar, R. M.; Gottardis, M. M., Drug safety is a barrier to the discovery and development of new androgen receptor antagonists. *Prostate* **2011**, *71*, 480-488.
77. Liu, C.; Lou, W.; Zhu, Y.; Yang, J. C.; Nadiminty, N.; Gaikwad, N. W.; Evans, C. P.; Gao, A. C., Intracrine androgens and AKR1C3 activation confer resistance to enzalutamide in prostate cancer. *Cancer Res.* **2015**, *75*, 1413-1422.
78. Liu, C.; Armstrong, C. M.; Lou, W.; Lombard, A.; Evans, C. P.; Gao, A. C., Inhibition of AKR1C3 activation overcomes resistance to abiraterone in advanced prostate cancer. *Mol. Cancer Ther.* **2017**, *16*, 35-44.
79. Verma, K.; Gupta, N.; Zang, T.; Wangtrakuldee, P.; Srivastava, S. K.; Penning, T. M.; Trippier, P. C., AKR1C3 inhibitor KV-37 exhibits antineoplastic effects and potentiates enzalutamide in combination therapy in prostate adenocarcinoma cells. *Mol. Cancer. Ther.* **2018**, *17*, 1833-1845.
80. Dellis, A. E.; Papatsoris, A. G., Perspectives on the current and emerging chemical androgen receptor antagonists for the treatment of prostate cancer. *Expert Opin. Pharmacother.* **2019**, *20*, 163-172.
81. Smith, M. R.; Saad, F.; Chowdhury, S.; Oudard, S.; Hadaschik, B. A.; Graff, J. N.; Olmos, D.; Mainwaring, P. N.; Lee, J. Y.; Uemura, H.; Lopez-Gitlitz, A.; Trudel, G. C.; Espina, B. M.; Shu, Y.; Park, Y. C.; Rackoff, W. R.; Yu, M. K.; Small, E. J., Apalutamide treatment and metastasis-free survival in prostate cancer. *N. Engl. J. Med.* **2018**, *378*, 1408-1418.
82. Koshkin, V. S.; Small, E. J., Apalutamide in the treatment of castrate-resistant prostate cancer: evidence from clinical trials. *Ther. Adv. Urol.* **2018**, *10*, 445-454.
83. Fizazi, K.; Smith, M. R.; Tombal, B., Clinical development of darolutamide: A novel androgen receptor antagonist for the treatment of prostate cancer. *Clin. Genitourin. Cancer* **2018**, *16*, 332-340.
84. Morsy, A.; Trippier, P. C., Reversal of apalutamide and darolutamide aldo-keto reductase 1C3-mediated resistance by a small molecule inhibitor. *ACS Chem. Biol.* **2020**, *15*, 646-650.
85. Fizazi, K.; Shore, N.; Tammela, T. L.; Ulys, A.; Vjaters, E.; Polyakov, S.; Jievaltas, M.; Luz, M.; Alekseev, B.; Kuss, I.; Kappeler, C.; Snapir, A.; Sarapohja, T.; Smith, M. R., Darolutamide in nonmetastatic, castration-resistant prostate cancer. *N. Engl. J. Med.* **2019**, *380*, 1235-1246.

86. Girolimetti, G.; Perrone, A. M.; Santini, D.; Barbieri, E.; Guerra, F.; Ferrari, S.; Zamagni, C.; De Iaco, P.; Gasparre, G.; Turchetti, D., BRCA-associated ovarian cancer: from molecular genetics to risk management. *Biomed. Res. Int.* **2014**, *2014*, 787143.
87. Abida, W.; Armenia, J.; Gopalan, A.; Brennan, R.; Walsh, M.; Barron, D.; Danila, D.; Rathkopf, D.; Morris, M.; Slovin, S.; McLaughlin, B.; Curtis, K.; Hyman, D. M.; Durack, J. C.; Solomon, S. B.; Arcila, M. E.; Zehir, A.; Syed, A.; Gao, J.; Chakravarty, D.; Vargas, H. A.; Robson, M. E.; Joseph, V.; Offit, K.; Donoghue, M. T. A.; Abeshouse, A. A.; Kundra, R.; Heins, Z. J.; Penson, A. V.; Harris, C.; Taylor, B. S.; Ladanyi, M.; Mandelker, D.; Zhang, L.; Reuter, V. E.; Kantoff, P. W.; Solit, D. B.; Berger, M. F.; Sawyers, C. L.; Schultz, N.; Scher, H. I., Prospective genomic profiling of prostate cancer across disease states reveals germline and somatic alterations that may affect clinical decision making. *JCO Precis. Oncol.* **2017**, *2017*.
88. Javle, M.; Curtin, N. J., The role of PARP in DNA repair and its therapeutic exploitation. *Br. J. Cancer* **2011**, *105*, 1114-1122.
89. Gunderson, C. C.; Moore, K. N., BRCAAnalysis CDx as a companion diagnostic tool for Lynparza. *Expert. Rev. Mol. Diagn.* **2015**, *15*, 1111-1116.
90. Ford, L.; Wolford, J. E.; Brown, S. M.; Randall, L. M., A profile on the FoundationFocus CDxBRCA tests. *Expert Rev. Mol. Diagn.* **2020**, *20*, 285-292.
91. Syed, Y. Y., Rucaparib: First global approval. *Drugs* **2017**, *77*, 585-592.
92. Abida, W.; Patnaik, A.; Campbell, D.; Shapiro, J.; Bryce, A. H.; McDermott, R.; Sautois, B.; Vogelzang, N. J.; Bambury, R. M.; Voog, E.; Zhang, J.; Piulats, J. M.; Ryan, C. J.; Merseburger, A. S.; Daugaard, G.; Heidenreich, A.; Fizazi, K.; Higano, C. S.; Krieger, L. E.; Sternberg, C. N.; Watkins, S. P.; Despain, D.; Simmons, A. D.; Loehr, A.; Dowson, M.; Golsorkhi, T.; Chowdhury, S.; investigators, T., Rucaparib in men with metastatic castration-resistant prostate cancer harboring a BRCA1 or BRCA2 gene alteration. *J. Clin. Oncol.* **2020**, *38*, 3763-3772.
93. Hussain, M.; Mateo, J.; Fizazi, K.; Saad, F.; Shore, N.; Sandhu, S.; Chi, K. N.; Sartor, O.; Agarwal, N.; Olmos, D.; Thiery-Vuillemin, A.; Twardowski, P.; Roubaud, G.; Ozguroglu, M.; Kang, J.; Burgents, J.; Gresty, C.; Corcoran, C.; Adelman, C. A.; de Bono, J.; Investigators, P. R. T., Survival with olaparib in metastatic castration-resistant prostate cancer. *N. Engl. J. Med.* **2020**, *383* (24), 2345-2357.
94. Tannock, I. F.; Osoba, D.; Stockler, M. R.; Ernst, D. S.; Neville, A. J.; Moore, M. J.; Armitage, G. R.; Wilson, J. J.; Venner, P. M.; Coppin, C. M.; Murphy, K. C., Chemotherapy with mitoxantrone plus prednisone or prednisone alone for symptomatic hormone-resistant prostate cancer: a Canadian randomized trial with palliative end points. *J. Clin. Oncol.* **1996**, *14*, 1756-1764.
95. Kantoff, P. W.; Halabi, S.; Conaway, M.; Picus, J.; Kirshner, J.; Hars, V.; Trump, D.; Winer, E. P.; Vogelzang, N. J., Hydrocortisone with or without mitoxantrone in men with hormone-refractory prostate cancer: results of the cancer and leukemia group B 9182 study. *J. Clin. Oncol.* **1999**, *17*, 2506-2513.
96. Cornford, P.; van den Bergh, R. C. N.; Briers, E.; Van den Broeck, T.; Cumberbatch, M. G.; De Santis, M.; Fanti, S.; Fossati, N.; Gandaglia, G.; Gillessen, S.; Grivas, N.;

Grummet, J.; Henry, A. M.; der Kwast, T. H. V.; Lam, T. B.; Lardas, M.; Liew, M.; Mason, M. D.; Moris, L.; Oprea-Lager, D. E.; der Poel, H. G. V.; Rouviere, O.; Schoots, I. G.; Tilki, D.; Wiegel, T.; Willemse, P. M.; Mottet, N., EAU-EANM-ESTRO-ESUR-SIOG guidelines on prostate cancer. Part II-2020 update: treatment of relapsing and metastatic prostate cancer. *Eur. Urol.* **2021**, *79*, 263-282.

97. Teo, M. Y.; Rathkopf, D. E.; Kantoff, P., Treatment of advanced prostate cancer. *Annu. Rev. Med.* **2019**, *70*, 479-499.

98. Shore, N. D.; Morgans, A. K.; Ryan, C. J., Resetting the bar of castration resistance - understanding androgen dynamics in therapy resistance and treatment choice in prostate cancer. *Clin. Genitourin. Cancer* **2020**.

99. Petrylak, D. P.; Tangen, C. M.; Hussain, M. H.; Lara, P. N., Jr.; Jones, J. A.; Taplin, M. E.; Burch, P. A.; Berry, D.; Moinpour, C.; Kohli, M.; Benson, M. C.; Small, E. J.; Raghavan, D.; Crawford, E. D., Docetaxel and estramustine compared with mitoxantrone and prednisone for advanced refractory prostate cancer. *N. Engl. J. Med.* **2004**, *351*, 1513-1520.

100. Tannock, I. F.; de Wit, R.; Berry, W. R.; Horti, J.; Pluzanska, A.; Chi, K. N.; Oudard, S.; Theodore, C.; James, N. D.; Turesson, I.; Rosenthal, M. A.; Eisenberger, M. A.; Investigators, T. A. X., Docetaxel plus prednisone or mitoxantrone plus prednisone for advanced prostate cancer. *N. Engl. J. Med.* **2004**, *351*, 1502-1512.

101. Oudard, S., TROPIC: Phase III trial of cabazitaxel for the treatment of metastatic castration-resistant prostate cancer. *Future Oncol.* **2011**, *7*, 497-506.

102. Westgeest, H. M.; Kuppen, M. C. P.; van den Eertwegh, A. J. M.; de Wit, R.; Coenen, J.; van den Berg, H. P. P.; Mehra, N.; van Oort, I. M.; Fossion, L.; Hendriks, M. P.; Bloemendal, H. J.; van de Luijngaarden, A. C. M.; Ten Bokkel Huinink, D.; van den Bergh, A.; van den Bosch, J.; Polee, M. B.; Weijl, N.; Bergman, A. M.; Uyl-de Groot, C. A.; Gerritsen, W. R., Second-line cabazitaxel treatment in castration-resistant prostate cancer clinical trials compared to standard of care in CAPRI: Observational study in the netherlands. *Clin. Genitourin. Cancer* **2019**, *17*, e946-e956.

103. de Wit, R.; de Bono, J.; Sternberg, C. N.; Fizazi, K.; Tombal, B.; Wulfing, C.; Kramer, G.; Eymard, J. C.; Bamias, A.; Carles, J.; Iacovelli, R.; Melichar, B.; Sverrisdottir, A.; Theodore, C.; Feyerabend, S.; Helissey, C.; Ozatilgan, A.; Geffriaud-Ricouard, C.; Castellano, D.; Investigators, C., Cabazitaxel versus abiraterone or enzalutamide in metastatic prostate cancer. *N. Engl. J. Med.* **2019**, *381*, 2506-2518.

104. Teply, B. A.; Hauke, R. J., Chemotherapy options in castration-resistant prostate cancer. *Indian J. Urol.* **2016**, *32*, 262-270.

105. Kantoff, P. W.; Higano, C. S.; Shore, N. D.; Berger, E. R.; Small, E. J.; Penson, D. F.; Redfern, C. H.; Ferrari, A. C.; Dreicer, R.; Sims, R. B.; Xu, Y.; Frohlich, M. W.; Schellhammer, P. F.; Investigators, I. S., Sipuleucel-T immunotherapy for castration-resistant prostate cancer. *N. Engl. J. Med.* **2010**, *363*, 411-422.

106. Burch, P. A.; Breen, J. K.; Buckner, J. C.; Gastineau, D. A.; Kaur, J. A.; Laus, R. L.; Padley, D. J.; Peshwa, M. V.; Pitot, H. C.; Richardson, R. L.; Smits, B. J.; Sopapan, P.; Strang, G.; Valone, F. H.; Vuk-Pavlovic, S., Priming tissue-specific cellular immunity in a

phase I trial of autologous dendritic cells for prostate cancer. *Clin. Cancer Res.* **2000**, *6*, 2175-2182.

107. Murphy, G.; Tjoa, B.; Ragde, H.; Kenny, G.; Boynton, A., Phase I clinical trial: T-cell therapy for prostate cancer using autologous dendritic cells pulsed with HLA-A0201-specific peptides from prostate-specific membrane antigen. *Prostate* **1996**, *29*, 371-380.

108. Small, E. J.; Fratesi, P.; Reese, D. M.; Strang, G.; Laus, R.; Peshwa, M. V.; Valone, F. H., Immunotherapy of hormone-refractory prostate cancer with antigen-loaded dendritic cells. *J. Clin. Oncol.* **2000**, *18*, 3894-903.

109. Risk, M.; Corman, J. M., The role of immunotherapy in prostate cancer: an overview of current approaches in development. *Rev. Urol.* **2009**, *11*, 16-27.

110. Bok, R. A., Treatment of prostate cancer: therapeutic potential of targeted immunotherapy with APC8015. *Ther. Clin. Risk Manag.* **2008**, *4*, 79-85.

111. Higano, C. S.; Schellhammer, P. F.; Small, E. J.; Burch, P. A.; Nemunaitis, J.; Yuh, L.; Provost, N.; Frohlich, M. W., Integrated data from 2 randomized, double-blind, placebo-controlled, phase 3 trials of active cellular immunotherapy with sipuleucel-T in advanced prostate cancer. *Cancer* **2009**, *115*, 3670-3679.

112. Small, E. J.; Schellhammer, P. F.; Higano, C. S.; Redfern, C. H.; Nemunaitis, J. J.; Valone, F. H.; Verjee, S. S.; Jones, L. A.; Hershsberg, R. M., Placebo-controlled phase III trial of immunologic therapy with sipuleucel-T (APC8015) in patients with metastatic, asymptomatic hormone refractory prostate cancer. *J. Clin. Oncol.* **2006**, *24*, 3089-3094.

113. Ascierto, P. A.; Kalos, M.; Schaer, D. A.; Callahan, M. K.; Wolchok, J. D., Biomarkers for immunostimulatory monoclonal antibodies in combination strategies for melanoma and other tumor types. *Clin. Cancer Res.* **2013**, *19*, 1009-1020.

114. Mamalis, A.; Garcha, M.; Jagdeo, J., Targeting the PD-1 pathway: a promising future for the treatment of melanoma. *Arch. Dermatol. Res.* **2014**, *306*, 511-519.

115. Tang, P. A.; Heng, D. Y., Programmed death 1 pathway inhibition in metastatic renal cell cancer and prostate cancer. *Curr. Oncol. Rep.* **2013**, *15*, 98-104.

116. Raedler, L. A., Keytruda (Pembrolizumab): First PD-1 inhibitor approved for previously treated unresectable or metastatic melanoma. *Am. Health Drug Benefits* **2015**, *8*, 96-100.

117. Lemery, S.; Keegan, P.; Pazdur, R., First FDA approval agnostic of cancer site - when a biomarker defines the indication. *N. Engl. J. Med.* **2017**, *377*, 1409-1412.

118. Marcus, L.; Lemery, S. J.; Keegan, P.; Pazdur, R., FDA approval summary: Pembrolizumab for the treatment of microsatellite instability-high solid tumors. *Clin. Cancer Res.* **2019**, *25*, 3753-3758.

119. Heidegger, I.; Necchi, A.; Pircher, A.; Tsaur, I.; Marra, G.; Kasivisvanathan, V.; Kretschmer, A.; Mathieu, R.; Ceci, F.; van den Bergh, R. C. N.; Thibault, C.; Tilki, D.; Valerio, M.; Surcel, C.; Gandaglia, G.; Party, E.-Y. P. C. W., A systematic review of the emerging role of immune checkpoint inhibitors in metastatic castration-resistant prostate cancer: Will combination strategies improve efficacy? *Eur. Urol. Oncol.* **2020**.

120. Petrioli, R.; Francini, E.; Laera, L.; Fiaschi, A. I.; Ponchietti, R.; Roviello, G., Role of chemotherapy in the treatment of metastatic castration-resistant prostate cancer

patients who have progressed after abiraterone acetate. *Cancer Chemother. Pharmacol.* **2015**, *76*, 439-445.

121. Jin, Y.; Penning, T. M., Aldo-keto reductases and bioactivation/detoxication. *Annu. Rev. Pharmacol. Toxicol.* **2007**, *47*, 263-292.

122. Penning, T. M., The aldo-keto reductases (AKRs): Overview. *Chem. Biol. Interact.* **2015**, *234*, 236-246.

123. Penning, T. M.; Wangtrakuldee, P.; Auchus, R. J., Structural and functional biology of aldo-keto reductase steroid-transforming enzymes. *Endocr. Rev.* **2019**, *40*, 447-475.

124. Lin, H. K.; Jez, J. M.; Schlegel, B. P.; Peehl, D. M.; Pachter, J. A.; Penning, T. M., Expression and characterization of recombinant type 2 3 alpha-hydroxysteroid dehydrogenase (HSD) from human prostate: demonstration of bifunctional 3 alpha/17 beta-HSD activity and cellular distribution. *Mol. Endocrinol.* **1997**, *11*, 1971-1984.

125. Byrns, M. C.; Jin, Y.; Penning, T. M., Inhibitors of type 5 17beta-hydroxysteroid dehydrogenase (AKR1C3): overview and structural insights. *J. Steroid Biochem. Mol. Biol.* **2011**, *125*, 95-104.

126. Rizner, T. L.; Smuc, T.; Ruprecht, R.; Sinkovec, J.; Penning, T. M., AKR1C1 and AKR1C3 may determine progesterone and estrogen ratios in endometrial cancer. *Mol. Cell. Endocrinol.* **2006**, *248*, 126-135.

127. Smuc, T.; Hevir, N.; Ribic-Pucelj, M.; Husen, B.; Thole, H.; Rizner, T. L., Disturbed estrogen and progesterone action in ovarian endometriosis. *Mol. Cell. Endocrinol.* **2009**, *301*, 59-64.

128. Suzuki-Yamamoto, T.; Nishizawa, M.; Fukui, M.; Okuda-Ashitaka, E.; Nakajima, T.; Ito, S.; Watanabe, K., cDNA cloning, expression and characterization of human prostaglandin F synthase. *FEBS Lett.* **1999**, *462*, 335-340.

129. Matsuura, K.; Shiraishi, H.; Hara, A.; Sato, K.; Deyashiki, Y.; Ninomiya, M.; Sakai, S., Identification of a principal mRNA species for human 3alpha-hydroxysteroid dehydrogenase isoform (AKR1C3) that exhibits high prostaglandin D2 11-ketoreductase activity. *J. Biochem.* **1998**, *124*, 940-946.

130. Birtwistle, J.; Hayden, R. E.; Khanim, F. L.; Green, R. M.; Pearce, C.; Davies, N. J.; Wake, N.; Schrewe, H.; Ride, J. P.; Chipman, J. K.; Bunce, C. M., The aldo-keto reductase AKR1C3 contributes to 7,12-dimethylbenz(a)anthracene-3,4-dihydrodiol mediated oxidative DNA damage in myeloid cells: implications for leukemogenesis. *Mutat. Res.* **2009**, *662*, 67-74.

131. Steckelbroeck, S.; Jin, Y.; Gopishetty, S.; Oyesanmi, B.; Penning, T. M., Human cytosolic 3alpha-hydroxysteroid dehydrogenases of the aldo-keto reductase superfamily display significant 3beta-hydroxysteroid dehydrogenase activity: implications for steroid hormone metabolism and action. *J. Biol. Chem.* **2004**, *279*, 10784-10795.

132. Guerini, V.; Sau, D.; Scaccianoce, E.; Rusmini, P.; Ciana, P.; Maggi, A.; Martini, P. G.; Katzenellenbogen, B. S.; Martini, L.; Motta, M.; Poletti, A., The androgen derivative 5alpha-androstane-3beta,17beta-diol inhibits prostate cancer cell migration through activation of the estrogen receptor beta subtype. *Cancer Res.* **2005**, *65*, 5445-5453.

133. Stayrook, K. R.; Rogers, P. M.; Savkur, R. S.; Wang, Y.; Su, C.; Varga, G.; Bu, X.; Wei, T.; Nagpal, S.; Liu, X. S.; Burris, T. P., Regulation of human 3 alpha-hydroxysteroid dehydrogenase (AKR1C4) expression by the liver X receptor alpha. *Mol. Pharmacol.* **2008**, *73*, 607-612.
134. Ji, Q.; Chang, L.; VanDenBerg, D.; Stanczyk, F. Z.; Stolz, A., Selective reduction of AKR1C2 in prostate cancer and its role in DHT metabolism. *Prostate* **2003**, *54*, 275-289.
135. Penning, T. M., Androgen biosynthesis in castration-resistant prostate cancer. *Endocr. Relat. Cancer* **2014**, *21* (4), T67-78.
136. Byrns, M. C.; Steckelbroeck, S.; Penning, T. M., An indomethacin analogue, N-(4-chlorobenzoyl)-melatonin, is a selective inhibitor of aldo-keto reductase 1C3 (type 2 3alpha-HSD, type 5 17beta-HSD, and prostaglandin F synthase), a potential target for the treatment of hormone dependent and hormone independent malignancies. *Biochem. Pharmacol.* **2008**, *75*, 484-493.
137. Hamid, A. R.; Pfeiffer, M. J.; Verhaegh, G. W.; Schaafsma, E.; Brandt, A.; Sweep, F. C.; Sedelaar, J. P.; Schalken, J. A., Aldo-keto reductase family 1 member C3 (AKR1C3) is a biomarker and therapeutic target for castration-resistant prostate cancer. *Mol. Med.* **2013**, *18*, 1449-1455.
138. Yepuru, M.; Wu, Z.; Kulkarni, A.; Yin, F.; Barrett, C. M.; Kim, J.; Steiner, M. S.; Miller, D. D.; Dalton, J. T.; Narayanan, R., Steroidogenic enzyme AKR1C3 is a novel androgen receptor-selective coactivator that promotes prostate cancer growth. *Clin. Cancer Res.* **2013**, *19*, 5613-5625.
139. Stanbrough, M.; Bubley, G. J.; Ross, K.; Golub, T. R.; Rubin, M. A.; Penning, T. M.; Febbo, P. G.; Balk, S. P., Increased expression of genes converting adrenal androgens to testosterone in androgen-independent prostate cancer. *Cancer Res.* **2006**, *66*, 2815-2825.
140. Tian, Y.; Zhao, L.; Zhang, H.; Liu, X.; Zhao, L.; Zhao, X.; Li, Y.; Li, J., AKR1C3 overexpression may serve as a promising biomarker for prostate cancer progression. *Diagn. Pathol.* **2014**, *9*, 42.
141. Wang, B.; Gu, Y.; Hui, K.; Huang, J.; Xu, S.; Wu, S.; Li, L.; Fan, J.; Wang, X.; Hsieh, J. T.; He, D.; Wu, K., AKR1C3, a crucial androgenic enzyme in prostate cancer, promotes epithelial-mesenchymal transition and metastasis through activating ERK signaling. *Urol. Oncol.* **2018**, *36*, 472 e11-472 e20.
142. Pan, C.-x.; Lara, P.; Evans, C. P.; Parikh, M.; White, R. d. V.; Dall'era, M.; Liu, C.; Robles, D.; Gao, A., A phase Ib/II trial of indomethacin and enzalutamide to treat castration-resistant prostate cancer (CRPC). *J. Clin. Oncol.* **2018**, *36*, TPS394-TPS394.
143. Byrns, M. C.; Mindnich, R.; Duan, L.; Penning, T. M., Overexpression of aldo-keto reductase 1C3 (AKR1C3) in LNCaP cells diverts androgen metabolism towards testosterone resulting in resistance to the 5alpha-reductase inhibitor finasteride. *J. Steroid Biochem. Mol. Biol.* **2012**, *130*, 7-15.
144. Komoto, J.; Yamada, T.; Watanabe, K.; Takusagawa, F., Crystal structure of human prostaglandin F synthase (AKR1C3). *Biochemistry* **2004**, *43*, 2188-2198.

145. Sun, S. Q.; Gu, X.; Gao, X. S.; Li, Y.; Yu, H.; Xiong, W.; Yu, H.; Wang, W.; Li, Y.; Teng, Y.; Zhou, D., Overexpression of AKR1C3 significantly enhances human prostate cancer cells resistance to radiation. *Oncotarget* **2016**, 7 (30), 48050-48058.
146. Sales, K. J.; Milne, S. A.; Williams, A. R.; Anderson, R. A.; Jabbour, H. N., Expression, localization, and signaling of prostaglandin F2 alpha receptor in human endometrial adenocarcinoma: regulation of proliferation by activation of the epidermal growth factor receptor and mitogen-activated protein kinase signaling pathways. *J. Clin. Endocrinol. Metab.* **2004**, 89, 986-993.
147. Desmond, J. C.; Mountford, J. C.; Drayson, M. T.; Walker, E. A.; Hewison, M.; Ride, J. P.; Luong, Q. T.; Hayden, R. E.; Vanin, E. F.; Bunce, C. M., The aldo-keto reductase AKR1C3 is a novel suppressor of cell differentiation that provides a plausible target for the non-cyclooxygenase-dependent antineoplastic actions of nonsteroidal anti-inflammatory drugs. *Cancer Res.* **2003**, 63, 505-512.
148. Hofman, J.; Malcekova, B.; Skarka, A.; Novotna, E.; Wsol, V., Anthracycline resistance mediated by reductive metabolism in cancer cells: the role of aldo-keto reductase 1C3. *Toxicol. Appl. Pharmacol.* **2014**, 278, 238-248.
149. Heibein, A. D.; Guo, B.; Sprowl, J. A.; Maclean, D. A.; Parissenti, A. M., Role of aldo-keto reductases and other doxorubicin pharmacokinetic genes in doxorubicin resistance, DNA binding, and subcellular localization. *BMC Cancer* **2012**, 12, 381.
150. Tavares, T. S.; Hofman, J.; Lekesova, A.; Zelazkova, J.; Wsol, V., Olaparib Synergizes the Anticancer Activity of Daunorubicin via Interaction with AKR1C3. *Cancers (Basel)* **2020**, 12 (11).
151. Liu, Y.; He, S.; Chen, Y.; Liu, Y.; Feng, F.; Liu, W.; Guo, Q.; Zhao, L.; Sun, H., Overview of AKR1C3: Inhibitor achievements and disease insights. *J. Med. Chem.* **2020**, 63, 11305-11329.
152. Penning, T. M., Aldo-Keto Reductase (AKR) 1C3 inhibitors: a patent review. *Expert Opin. Ther. Pat.* **2017**, 27, 1329-1340.
153. Skarydova, L.; Zivna, L.; Xiong, G.; Maser, E.; Wsol, V., AKR1C3 as a potential target for the inhibitory effect of dietary flavonoids. *Chem. Biol. Interact.* **2009**, 178, 138-144.
154. Davies, N. J.; Hayden, R. E.; Simpson, P. J.; Birtwistle, J.; Mayer, K.; Ride, J. P.; Bunce, C. M., AKR1C isoforms represent a novel cellular target for jasmonates alongside their mitochondrial-mediated effects. *Cancer Res.* **2009**, 69, 4769-4775.
155. Liedtke, A. J.; Adeniji, A. O.; Chen, M.; Byrns, M. C.; Jin, Y.; Christianson, D. W.; Marnett, L. J.; Penning, T. M., Development of potent and selective indomethacin analogues for the inhibition of AKR1C3 (Type 5 17beta-hydroxysteroid dehydrogenase/prostaglandin F synthase) in castrate-resistant prostate cancer. *J. Med. Chem.* **2013**, 56, 2429-2446.
156. Khanim, F.; Davies, N.; Velica, P.; Hayden, R.; Ride, J.; Pararasa, C.; Chong, M. G.; Gunther, U.; Veerapen, N.; Winn, P.; Farmer, R.; Trivier, E.; Rigoreau, L.; Drayson, M.; Bunce, C., Selective AKR1C3 inhibitors do not recapitulate the anti-leukaemic



activities of the pan-AKR1C inhibitor medroxyprogesterone acetate. *Br. J. Cancer* **2014**, *110*, 1506-1516.

157. Adeniji, A.; Uddin, M. J.; Zang, T.; Tamae, D.; Wangtrakuldee, P.; Marnett, L. J.; Penning, T. M., Discovery of (R)-2-(6-Methoxynaphthalen-2-yl)butanoic Acid as a Potent and Selective Aldo-keto Reductase 1C3 Inhibitor. *J. Med. Chem.* **2016**, *59*, 7431-7444.

158. Lorient, Y.; Fizazi, K.; Jones, R. J.; Van den Brande, J.; Molife, R. L.; Omlin, A.; James, N. D.; Baskin-Bey, E.; Heeringa, M.; Baron, B.; Holtkamp, G. M.; Ouatas, T.; De Bono, J. S., Safety, tolerability and anti-tumour activity of the androgen biosynthesis inhibitor ASP9521 in patients with metastatic castration-resistant prostate cancer: multi-centre phase I/II study. *Invest. New Drugs* **2014**, *32*, 995-1004.

159. Endo, S.; Oguri, H.; Segawa, J.; Kawai, M.; Hu, D.; Xia, S.; Okada, T.; Irie, K.; Fujii, S.; Gouda, H.; Iguchi, K.; Matsukawa, T.; Fujimoto, N.; Nakayama, T.; Toyooka, N.; Matsunaga, T.; Ikari, A., Development of novel AKR1C3 inhibitors as new potential treatment for castration-resistant prostate cancer. *J. Med. Chem.* **2020**, *63*, 10396-10411.

160. Endo, S.; Matsunaga, T.; Kanamori, A.; Otsuji, Y.; Nagai, H.; Sundaram, K.; El-Kabbani, O.; Toyooka, N.; Ohta, S.; Hara, A., Selective inhibition of human type-5 17beta-hydroxysteroid dehydrogenase (AKR1C3) by baccharin, a component of Brazilian propolis. *J. Nat. Prod.* **2012**, *75*, 716-721.

161. Verma, K.; Zang, T.; Penning, T. M.; Trippier, P. C., Potent and highly selective aldo-keto reductase 1C3 (AKR1C3) inhibitors act as chemotherapeutic potentiators in acute myeloid leukemia and T-Cell acute lymphoblastic leukemia. *J. Med. Chem.* **2019**, *62*, 3590-3616.

162. Lovering, A. L.; Ride, J. P.; Bunce, C. M.; Desmond, J. C.; Cummings, S. M.; White, S. A., Crystal structures of prostaglandin D(2) 11-ketoreductase (AKR1C3) in complex with the nonsteroidal anti-inflammatory drugs flufenamic acid and indomethacin. *Cancer Res.* **2004**, *64*, 1802-1810.

163. Komoto, J.; Yamada, T.; Watanabe, K.; Woodward, D. F.; Takusagawa, F., Prostaglandin F2alpha formation from prostaglandin H2 by prostaglandin F synthase (PGFS): crystal structure of PGFS containing bimatoprost. *Biochemistry* **2006**, *45*, 1987-1996.

164. Qiu, W.; Zhou, M.; Mazumdar, M.; Azzi, A.; Ghanmi, D.; Luu-The, V.; Labrie, F.; Lin, S. X., Structure-based inhibitor design for an enzyme that binds different steroids: a potent inhibitor for human type 5 17beta-hydroxysteroid dehydrogenase. *J. Biol. Chem.* **2007**, *282*, 8368-8379.

165. Wierenga, R. K., The TIM-barrel fold: a versatile framework for efficient enzymes. *FEBS Lett.* **2001**, *492*, 193-198.

166. Zhao, Y.; Zheng, X.; Zhang, H.; Zhai, J.; Zhang, L.; Li, C.; Zeng, K.; Chen, Y.; Li, Q.; Hu, X., In vitro inhibition of AKR1Cs by sulphonylureas and the structural basis. *Chem. Biol. Interact.* **2015**, *240*, 310-325.

167. 2020 Alzheimer's disease facts and figures. *Alzheimers Dement.* **2020**.

168. Morsy, A.; Trippier, P. C., Current and emerging pharmacological targets for the treatment of Alzheimer's disease. *J. Alzheimers Dis.* **2019**, *72*, S145-S176.

169. Koulakoff, A.; Mei, X.; Orellana, J. A.; Saez, J. C.; Giaume, C., Glial connexin expression and function in the context of Alzheimer's disease. *Biochim. Biophys. Acta.* **2012**, *1818*, 2048-2057.
170. Yi, C.; Koulakoff, A.; Giaume, C., Astroglial connexins as a therapeutic target for Alzheimer's disease. *Curr. Pharm. Des.* **2017**, *23*, 4958-4968.
171. Bateman, R. J.; Xiong, C.; Benzinger, T. L.; Fagan, A. M.; Goate, A.; Fox, N. C.; Marcus, D. S.; Cairns, N. J.; Xie, X.; Blazey, T. M.; Holtzman, D. M.; Santacruz, A.; Buckles, V.; Oliver, A.; Moulder, K.; Aisen, P. S.; Ghetti, B.; Klunk, W. E.; McDade, E.; Martins, R. N.; Masters, C. L.; Mayeux, R.; Ringman, J. M.; Rossor, M. N.; Schofield, P. R.; Sperling, R. A.; Salloway, S.; Morris, J. C., Clinical and biomarker changes in dominantly inherited Alzheimer's disease. *N. Engl. J. Med.* **2012**, *367*, 795-804.
172. Goldgaber, D.; Lerman, M. I.; McBride, O. W.; Saffiotti, U.; Gajdusek, D. C., Characterization and chromosomal localization of a cDNA encoding brain amyloid of Alzheimer's disease. *Science* **1987**, *235*, 877-880.
173. Kang, J.; Lemaire, H. G.; Unterbeck, A.; Salbaum, J. M.; Masters, C. L.; Grzeschik, K. H.; Multhaup, G.; Beyreuther, K.; Muller-Hill, B., The precursor of Alzheimer's disease amyloid A4 protein resembles a cell-surface receptor. *Nature* **1987**, *325*, 733-736.
174. Tanzi, R. E.; St George-Hyslop, P. H.; Haines, J. L.; Polinsky, R. J.; Nee, L.; Foncin, J. F.; Neve, R. L.; McClatchey, A. I.; Conneally, P. M.; Gusella, J. F., The genetic defect in familial Alzheimer's disease is not tightly linked to the amyloid beta-protein gene. *Nature* **1987**, *329*, 156-157.
175. Zhao, L. N.; Long, H.; Mu, Y.; Chew, L. Y., The toxicity of amyloid beta oligomers. *Int. J. Mol. Sci.* **2012**, *13*, 7303-7327.
176. Mucke, L.; Selkoe, D. J., Neurotoxicity of amyloid beta-protein: synaptic and network dysfunction. *Cold Spring Harb Perspect Med* **2012**, *2*, a006338.
177. Mietelska-Porowska, A.; Wasik, U.; Goras, M.; Filipek, A.; Niewiadomska, G., Tau protein modifications and interactions: their role in function and dysfunction. *Int. J. Mol. Sci.* **2014**, *15*, 4671-4713.
178. Kimura, T.; Ishiguro, K.; Hisanaga, S., Physiological and pathological phosphorylation of tau by Cdk5. *Front. Mol. Neurosci.* **2014**, *7*, 65.
179. Aschenbrenner, A. J.; Gordon, B. A.; Benzinger, T. L. S.; Morris, J. C.; Hassenstab, J. J., Influence of tau PET, amyloid PET, and hippocampal volume on cognition in Alzheimer disease. *Neurology* **2018**, *91*, e859-e866.
180. Heneka, M. T.; Carson, M. J.; El Khoury, J.; Landreth, G. E.; Brosseon, F.; Feinstein, D. L.; Jacobs, A. H.; Wyss-Coray, T.; Vitorica, J.; Ransohoff, R. M.; Herrup, K.; Frautschy, S. A.; Finsen, B.; Brown, G. C.; Verkhratsky, A.; Yamanaka, K.; Koistinaho, J.; Latz, E.; Halle, A.; Petzold, G. C.; Town, T.; Morgan, D.; Shinohara, M. L.; Perry, V. H.; Holmes, C.; Bazan, N. G.; Brooks, D. J.; Hunot, S.; Joseph, B.; Deigendesch, N.; Garaschuk, O.; Boddeke, E.; Dinarello, C. A.; Breitner, J. C.; Cole, G. M.; Golenbock, D. T.; Kummer, M. P., Neuroinflammation in Alzheimer's disease. *Lancet Neurol.* **2015**, *14*, 388-405.

181. Bronzuoli, M. R.; Iacomino, A.; Steardo, L.; Scuderi, C., Targeting neuroinflammation in Alzheimer's disease. *J. Inflamm. Res.* **2016**, *9*, 199-208.
182. De Strooper, B.; Vassar, R.; Golde, T., The secretases: enzymes with therapeutic potential in Alzheimer disease. *Nat. Rev. Neurol.* **2010**, *6*, 99-107.
183. Weiner, H. L.; Frenkel, D., Immunology and immunotherapy of Alzheimer's disease. *Nat. Rev. Immunol.* **2006**, *6*, 404-416.
184. Kandimalla, R.; Reddy, P. H., Therapeutics of neurotransmitters in Alzheimer's disease. *J. Alzheimers Dis.* **2017**, *57*, 1049-1069.
185. Yin, H.; Flynn, A. D., Drugging membrane protein interactions. *Annu. Rev. Biomed. Eng.* **2016**, *18*, 51-76.
186. Mroczo, B.; Groblewska, M.; Litman-Zawadzka, A.; Kornhuber, J.; Lewczuk, P., Cellular receptors of amyloid beta oligomers (AbetaOs) in Alzheimer's disease. *Int. J. Mol. Sci.* **2018**, *19*.
187. Borger, E.; Aitken, L.; Muirhead, K. E.; Allen, Z. E.; Ainge, J. A.; Conway, S. J.; Gunn-Moore, F. J., Mitochondrial beta-amyloid in Alzheimer's disease. *Biochem. Soc. Trans.* **2011**, *39*, 868-873.
188. Sameem, B.; Saeedi, M.; Mahdavi, M.; Shafiee, A., A review on tacrine-based scaffolds as multi-target drugs (MTDLs) for Alzheimer's disease. *Eur. J. Med. Chem.* **2017**, *128*, 332-345.
189. Rogers, S. L.; Farlow, M. R.; Doody, R. S.; Mohs, R.; Friedhoff, L. T., A 24-week, double-blind, placebo-controlled trial of donepezil in patients with Alzheimer's disease. *Neurology* **1998**, *50*, 136-145.
190. Rösler, M.; Anand, R.; Cicin-Sain, A.; Gauthier, S.; Agid, Y.; Dal-Bianco, P.; Stähelin, H. B.; Hartman, R.; M., G., Efficacy and safety of rivastigmine in patients with Alzheimer's disease: international randomised controlled trial. *BMJ* **1999**, *318*, 633-640.
191. Tariot, P. N.; Solomon, P. R.; Morris, J. C.; Kershaw, P.; Lilienfeld, S.; Ding, C., A 5-month, randomized, placebo-controlled trial of galantamine in AD. *Neurology* **2000**, *54* (12), 2269-2276.
192. Massoud, F.; Gauthier, S., Update on the pharmacological treatment of Alzheimer's disease. *Curr. Neuropharmacol.* **2010**, *8*, 69-80.
193. Hansen, R. A.; Gartlehner, G.; Webb, A. P.; Morgan, L. C.; Moore, C. G.; Jonas, D. E., Efficacy and safety of donepezil, galantamine, and rivastigmine for the treatment of Alzheimer's disease: a systematic review and meta-analysis. *Clin. Interv. Aging* **2008**, *3*, 211-225.
194. Mucha, L.; Shaohung, S.; Cuffel, B.; McRae, T.; Mark, T. L.; Del Valle, M., Comparison of cholinesterase inhibitor utilization patterns and associated health care costs in Alzheimer's disease. *J. Manag. Care Pharm.* **2008**, *14*, 451-461.
195. Wattmo, C.; Wallin, A. K.; Londos, E.; Minthon, L., Predictors of long-term cognitive outcome in Alzheimer's disease. *Alzheimers Res. Ther.* **2011**, *3*, 23.
196. Wattmo, C.; Wallin, A. K.; Londos, E.; Minthon, L., Risk factors for nursing home placement in Alzheimer's disease: a longitudinal study of cognition, ADL, service utilization, and cholinesterase inhibitor treatment. *Gerontologist* **2011**, *51*, 17-27.

197. Gilling, K. E.; Jatzke, C.; Hechenberger, M.; Parsons, C. G., Potency, voltage-dependency, agonist concentration-dependency, blocking kinetics and partial untrapping of the uncompetitive N-methyl-D-aspartate (NMDA) channel blocker memantine at human NMDA (GluN1/GluN2A) receptors. *Neuropharmacology* **2009**, *56*, 866-875.
198. Alberdi, E.; Sanchez-Gomez, M. V.; Cavaliere, F.; Perez-Samartin, A.; Zugaza, J. L.; Trullas, R.; Domercq, M.; Matute, C., Amyloid beta oligomers induce Ca<sup>2+</sup> dysregulation and neuronal death through activation of ionotropic glutamate receptors. *Cell Calcium* **2010**, *47*, 264-272.
199. Reisberg, B.; Doody, R.; Stoffler, A.; Schmitt, F.; Ferris, S.; Mobius, H. J.; Memantine Study, G., Memantine in moderate-to-severe Alzheimer's disease. *N. Engl. J. Med.* **2003**, *348*, 1333-1341.
200. Winblad, B.; Poritis, N., Memantine in severe dementia: results of the 9M-Best Study (Benefit and efficacy in severely demented patients during treatment with memantine). *Int. J. Geriatr. Psychiatry* **1999**, *14*, 135-146.
201. Tariot, P. N.; Farlow, M. R.; Grossberg, G. T.; Graham, S. M.; McDonald, S.; Gergel, I.; Memantine Study, G., Memantine treatment in patients with moderate to severe Alzheimer disease already receiving donepezil: a randomized controlled trial. *JAMA* **2004**, *291*, 317-324.
202. Kishi, T.; Matsunaga, S.; Oya, K.; Nomura, I.; Ikuta, T.; Iwata, N., Memantine for Alzheimer's disease: An updated systematic review and meta-analysis. *J. Alzheimers Dis.* **2017**, *60*, 401-425.
203. Howard, R.; McShane, R.; Lindesay, J.; Ritchie, C.; Baldwin, A.; Barber, R.; Burns, A.; Denning, T.; Findlay, D.; Holmes, C.; Jones, R.; Jones, R.; McKeith, I.; Macharouthu, A.; O'Brien, J.; Sheehan, B.; Juszczak, E.; Katona, C.; Hills, R.; Knapp, M.; Ballard, C.; Brown, R. G.; Banerjee, S.; Adams, J.; Johnson, T.; Bentham, P.; Phillips, P. P., Nursing home placement in the donepezil and memantine in moderate to severe Alzheimer's disease (DOMINO-AD) trial: secondary and post-hoc analyses. *Lancet Neurol.* **2015**, *14*, 1171-1181.
204. Porsteinsson, A. P.; Grossberg, G. T.; Mintzer, J.; Olin, J. T.; Memantine, M. E. M. D. S. G., Memantine treatment in patients with mild to moderate Alzheimer's disease already receiving a cholinesterase inhibitor: a randomized, double-blind, placebo-controlled trial. *Curr Alzheimer Res* **2008**, *5* (1), 83-9.
205. Lopez, O. L.; Becker, J. T.; Wahed, A. S.; Saxton, J.; Sweet, R. A.; Wolk, D. A.; Klunk, W.; Dekosky, S. T., Long-term effects of the concomitant use of memantine with cholinesterase inhibition in Alzheimer disease. *J. Neurol. Neurosurg. Psychiatry* **2009**, *80*, 600-607.
206. Cummings, J.; Lee, G.; Ritter, A.; Sabbagh, M.; Zhong, K., Alzheimer's disease drug development pipeline: 2020. *Alzheimers Dement. (N Y)* **2020**, *6*, e12050.
207. Xia, W., Gamma-secretase and its modulators: Twenty years and beyond. *Neurosci. Lett.* **2019**, *701*, 162-169.

208. Ceyzeriat, K.; Zilli, T.; Millet, P.; Frisoni, G. B.; Garibotto, V.; Tournier, B. B., Learning from the Past: A Review of clinical trials targeting amyloid, tau and neuroinflammation in Alzheimer's disease. *Curr. Alzheimer Res.* **2020**, *17*, 112-125.
209. Frisoni, G. B.; Boccardi, M.; Barkhof, F.; Blennow, K.; Cappa, S.; Chiotis, K.; Démonet, J.; Garibotto, V.; Giannakopoulos, P.; Gietl, A.; Hansson, O.; Herholz, K.; Jack, C. R.; Nobili, F.; Nordberg, A.; Snyder, H. M.; Ten Kate, M.; Varrone, A.; Albanese, E.; Becker, S.; Bossuyt, P.; Carrillo, M. C.; Cerami, C.; Dubois, B.; Gallo, V.; Giacobini, E.; Gold, G.; Hurst, S.; Lönneborg, A.; Lovblad, K.; Mattsson, N.; Molinuevo, J.; Monsch, A. U.; Mosimann, U.; Padovani, A.; Picco, A.; Porteri, C.; Ratib, O.; Saint-Aubert, L.; Scerri, C.; Scheltens, P.; Schott, J. M.; Sonni, I.; Teipel, S.; Vineis, P.; Visser, P. J.; Yasui, Y.; Winblad, B., Strategic roadmap for an early diagnosis of alzheimer's disease based on biomarkers. *Lancet Neurol.* **2017**, *16* (8), 661-676.
210. Olsson, B.; Lautner, R.; Andreasson, U.; Ohrfelt, A.; Portelius, E.; Bjerke, M.; Holtta, M.; Rosen, C.; Olsson, C.; Strobel, G.; Wu, E.; Dakin, K.; Petzold, M.; Blennow, K.; Zetterberg, H., CSF and blood biomarkers for the diagnosis of Alzheimer's disease: a systematic review and meta-analysis. *Lancet Neurol.* **2016**, *15*, 673-684.
211. Zetterberg, H.; Blennow, K., Cerebrospinal fluid biomarkers for Alzheimer's disease: more to come? *J. Alzheimers Dis.* **2013**, *33 Suppl 1*, S361-369.
212. Mantzavinos, V.; Alexiou, A., Biomarkers for alzheimer's disease diagnosis. *Curr. Alzheimer Res.* **2017**, *14*, 1149-1154.
213. Cummings, J., Disease modification and Neuroprotection in neurodegenerative disorders. *Transl Neurodegener* **2017**, *6*, 25.
214. Cummings, J.; Fox, N., Defining disease modifying therapy for Alzheimer's disease. *J. Prev. Alzheimers Dis.* **2017**, *4*, 109-115.
215. Manczak, M.; Anekonda, T. S.; Henson, E.; Park, B. S.; Quinn, J.; Reddy, P. H., Mitochondria are a direct site of A $\beta$  accumulation in alzheimer's disease neurons: implications for free radical generation and oxidative damage in disease progression. *Hum. Mol. Genet.* **2006**, *15*, 1437-1449.
216. Gouras, G. K.; Tsai, J.; Naslund, J.; Vincent, B.; Edgar, M.; Checler, F.; Greenfield, J. P.; Haroutunian, V.; Buxbaum, J. D.; Xu, H.; Greengard, P.; Relkin, N. R., Intraneuronal Abeta42 accumulation in human brain. *Am. J. Pathol.* **2000**, *156*, 15-20.
217. LaFerla, F. M.; Green, K. N.; Oddo, S., Intracellular amyloid-beta in Alzheimer's disease. *Nat. Rev. Neurosci.* **2007**, *8*, 499-509.
218. Venkitaramani, D. V.; Chin, J.; Netzer, W. J.; Gouras, G. K.; Lesne, S.; Malinow, R.; Lombroso, P. J., Beta-amyloid modulation of synaptic transmission and plasticity. *J. Neurosci.* **2007**, *27*, 11832-11837.
219. Yan, S. D.; Fu, J.; Soto, C.; Chen, X.; Zhu, H.; Al-Mohanna, F.; Collison, K.; Zhu, A.; Stern, E.; Saido, T.; Tohyama, M.; Ogawa, S.; Roherk, A.; Stern, D., An intracellular protein that binds amyloid- $\beta$  peptide and mediates neurotoxicity in alzheimer's disease. *Nature* **1997**, *389*, 689-695.
220. Lustbader, J. W.; Cirilli, M.; Lin, C.; Xu, H. W.; Takuma, K.; Wang, N.; Caspersen, C.; Chen, X.; Pollak, S.; Chaney, M.; Trinchese, F.; Liu, S.; Gunn-Moore, F. J.; Lue, L. F.;

Walker, D. G.; Kuppusamy, P.; Zewier, Z. L.; Arancio, O.; Stern, D.; Yan, S. S.; H., W., ABAD directly Links A $\beta$  to mitochondrial toxicity in alzheimer's disease. *Science* **2004**, *304*, 448-452.

221. Yang, S. Y.; He, X. Y.; Schulz, H., Multiple functions of type 10 17 $\beta$ -hydroxysteroid dehydrogenase. *Trends Endocrinol. Metab.* **2005**, *16*, 167-175.

222. Yang, S. Y.; He, X. Y.; Schulz, H., 3-Hydroxyacyl-CoA dehydrogenase and short chain 3-hydroxyacyl-CoA dehydrogenase in human health and disease. *FEBS J.* **2005**, *272*, 4874-4883.

223. Ofman, R.; Ruiter, J. P. N.; Feenstra, M.; Duran, M.; Poll-The, B. T.; Zschocke, J.; Ensenauer, R.; Lehnert, W.; Sass, J. O.; Sperl, W.; Wanders, R. J. A., 2-Methyl-3-hydroxybutyryl-CoA dehydrogenase deficiency is caused by mutations in the HADH2 gene. *Am. J. Hum. Genet.* **2003**, *72*, 1300-1307.

224. He, X.; Yang, Y.; Peehl, D. M.; Lauderdale, A.; Schulz, H.; Yang, S. Y., Oxidative 3 $\alpha$ -hydroxysteroid dehydrogenase activity of human type 10 17 $\beta$ -hydroxysteroid dehydrogenase. *J. Steroid Biochem. Mol. Biol.* **2003**, *87*, 191-198.

225. Ivell, R.; Balvers, M.; Anand, R. J.; Paust, H. J.; McKinnell, C.; Sharpe, R., Differentiation-dependent expression of 17 $\beta$ -hydroxysteroid dehydrogenase, type 10, in the rodent testis: effect of aging in Leydig cells. *Endocrinology* **2003**, *144*, 3130-3137.

226. Grimm, A.; Lim, Y. A.; Mensah-Nyagan, A. G.; Gotz, J.; Eckert, A., Alzheimer's disease, oestrogen and mitochondria: an ambiguous relationship. *Mol. Neurobiol.* **2012**, *46*, 151-160.

227. Lim, Y. A.; Grimm, A.; Giese, M.; Mensah-Nyagan, A. G.; Villafranca, J. E.; Ittner, L. M.; Eckert, A.; Gotz, J., Inhibition of the mitochondrial enzyme ABAD restores the amyloid- $\beta$ -mediated deregulation of estradiol. *PLoS One* **2011**, *6* (12), e28887.

228. Podcasy, J. L.; Epperson, C. N., Considering sex and gender in Alzheimer disease and other dementias. *Dialogues Clin. Neurosci.* **2016**, *18*, 437-446.

229. Takuma, K.; Yao, J.; Huang, J.; Xu, H.; Chen, X.; Luddy, J.; Trillat, A. C.; Stern, D. M.; Arancio, O.; Yan, S. S., ABAD enhances A $\beta$ -induced cell stress via mitochondrial dysfunction. *FASEB J.* **2005**, *19*, 597-598.

230. Yao, J.; Taylor, M.; Davey, F.; Ren, Y.; Aiton, J.; Coote, P.; Fang, F.; Chen, J. X.; Yan, S. D.; Gunn-Moore, F. J., Interaction of amyloid binding alcohol dehydrogenase/A $\beta$  mediates up-regulation of peroxiredoxin II in the brains of alzheimer's disease patients and a transgenic alzheimer's disease mouse model. *Mol. Cell Neurosci.* **2007**, *35*, 377-382.

231. Kjaerulff, O.; Brodin, L.; Jung, A., The structure and function of endophilin proteins. *Cell Biochem. Biophys.* **2011**, *60*, 137-154.

232. Ren, Y.; Xu, H. W.; Davey, F.; Taylor, M.; Aiton, J.; Coote, P.; Fang, F.; Yao, J.; Chen, D.; Chen, J. X.; Yan, S. D.; Gunn-Moore, F. J., Endophilin I expression is increased in the brains of alzheimer disease patients. *J. Biol. Chem.* **2008**, *283*, 5685-5691.

233. Yan, S. D.; Fu, J.; Soto, C.; Chen, X.; Zhu, H.; Al-Mohanna, F.; Collison, K.; Zhu, A.; Stern, E.; Saido, T.; Tohyama, M.; Ogawa, S.; Roher, A.; Stern, D., An intracellular protein that binds amyloid-beta peptide and mediates neurotoxicity in Alzheimer's disease. *Nature* **1997**, *389*, 689-695.

234. Yao, J.; Du, H.; Yan, S.; Fang, F.; Wang, C.; Lue, L. F.; Guo, L.; Chen, D.; Stern, D. M.; Gunn Moore, F. J.; Xi Chen, J.; Arancio, O.; Yan, S. S., Inhibition of amyloid- $\beta$  (A $\beta$ ) peptide-binding alcohol dehydrogenase-A $\beta$  interaction reduces A $\beta$  accumulation and improves mitochondrial function in a mouse model of alzheimer's disease. *J. Neurosci.* **2011**, *31* (6), 2313-2320.
235. Kissinger, C. R.; Rejto, P. A.; Pelletier, L. A.; Thomson, J. A.; Showalter, R. E.; Abreo, M. A.; Agree, C. S.; Margosiak, S.; Meng, J. J.; Aust, R. M.; Vanderpool, D.; Li, B.; Tempczyk-Russell, A.; Villafranca, J. E., Crystal structure of human ABAD/HSD10 with a bound inhibitor: implications for design of Alzheimer's disease therapeutics. *J. Mol. Biol.* **2004**, *342* (3), 943-952.
236. Marques, A. T.; Fernandes, P. A.; Ramos, M. J., ABAD: A Potential Therapeutic Target for A $\beta$ -Induced Mitochondrial Dysfunction in Alzheimers Disease. *Mini-Reviews in Medicinal Chemistry* **2009**, *9*, 1002 - 1008.
237. Abreo, M. A.; Meng, J. J.; Agree, C. S. Fused pyrazole compounds, pharmaceutical compositions, and methods for modulating or inhibiting ERAB or HADH2 activity. U.S. Patent 6,964,957 B2, 2005.
238. Benek, O.; Hroch, L.; Aitken, L.; Gunn-Moore, F.; Vinklarova, L.; Kuca, K.; Perez, D. I.; Perez, C.; Martinez, A.; Fisar, Z.; Musilek, K., 1-(Benzo[d]thiazol-2-yl)-3-phenylureas as dual inhibitors of casein kinase 1 and ABAD enzymes for treatment of neurodegenerative disorders. *J. Enzyme Inhib. Med. Chem.* **2018**, *33*, 665-670.
239. Xie, Y.; Deng, S.; Chen, Z.; Yan, S.; Landry, D. W., Identification of small-molecule inhibitors of the A $\beta$ -ABAD interaction. *Bioorg. Med. Chem. Lett.* **2006**, *16*, 4657-4660.
240. Viswanath, A. N. I.; Kim, T.; Jung, S. Y.; Lim, S. M.; Pae, A. N., In silico-designed novel non-peptidic ABAD LD hot spot mimetics reverse A $\beta$ -induced mitochondrial impairments in vitro. *Chem. Biol. Drug Des.* **2017**, *90*, 1041-1055.
241. Chen, X.; Yan, S. D., Mitochondrial A $\beta$ : a potential cause of metabolic dysfunction in alzheimer's disease. *IUBMB Life* **2006**, *58*, 686-694.
242. Yan, Y.; Liu, Y.; Sorci, M.; Belfort, G.; Lustbader, J. W.; Yan, S. S.; C., W., Surface plasmon resonance and nuclear magnetic resonance studies of ABAD-A $\beta$  interaction. *Biochemistry* **2007**, *46*, 1724-1731.
243. Marques, A. T.; Fernandes, P. A.; Ramos, M. J., Molecular dynamics simulations of the amyloid-beta binding alcohol dehydrogenase (ABAD) enzyme. *Bioorg. Med. Chem.* **2008**, *16*, 9511-9518.
244. Powell, A. J.; Read, J. A.; Banfield, M. J.; Gunn-Moore, F.; Yan, S. D.; Lustbader, J.; Stern, A. R.; Stern, D. M.; Brady, R. L., Recognition of structurally diverse substrates by type II 3-hydroxyacyl-CoA dehydrogenase (HADH II)/amyloid- $\beta$  binding alcohol dehydrogenase (ABAD). *J. Mol. Biol.* **2000**, *303*, 311-327.
245. Bauman, D. R.; Rudnick, S. I.; Szewczuk, L. M.; Jin, Y.; Gopishetty, S.; Penning, T. M., Development of nonsteroidal anti-inflammatory drug analogs and steroid carboxylates selective for human aldo-keto reductase isoforms: potential antineoplastic agents that work independently of cyclooxygenase isozymes. *Mol. Pharmacol.* **2005**, *67*, 60-68.

246. Pippione, A. C.; Carnovale, I. M.; Bonanni, D.; Sini, M.; Goyal, P.; Marini, E.; Pors, K.; Adinolfi, S.; Zonari, D.; Festuccia, C.; Wahlgren, W. Y.; Friemann, R.; Bagnati, R.; Boschi, D.; Oliaro-Bosso, S.; Lolli, M. L., Potent and selective aldo-keto reductase 1C3 (AKR1C3) inhibitors based on the benzoisoxazole moiety: application of a bioisosteric scaffold hopping approach to flufenamic acid. *Eur. J. Med. Chem.* **2018**, *150*, 930-945.
247. Pippione, A. C.; Giraudo, A.; Bonanni, D.; Carnovale, I. M.; Marini, E.; Cena, C.; Costale, A.; Zonari, D.; Pors, K.; Sadiq, M.; Boschi, D.; Oliaro-Bosso, S.; Lolli, M. L., Hydroxytriazole derivatives as potent and selective aldo-keto reductase 1C3 (AKR1C3) inhibitors discovered by bioisosteric scaffold hopping approach. *Eur. J. Med. Chem.* **2017**, *139*, 936-946.
248. Lolli, M. L.; Carnovale, I. M.; Pippione, A. C.; Wahlgren, W. Y.; Bonanni, D.; Marini, E.; Zonari, D.; Gallicchio, M.; Boscaro, V.; Goyal, P.; Friemann, R.; Rolando, B.; Bagnati, R.; Adinolfi, S.; Oliaro-Bosso, S.; Boschi, D., Bioisosteres of Indomethacin as Inhibitors of Aldo-Keto Reductase 1C3. *ACS Med. Chem. Lett.* **2019**, *10*, 437-443.
249. Kikuchi, A.; Furutani, T.; Azami, H.; Watanabe, K.; Niimi, T.; Kamiyama, Y.; Kuromitsu, S.; Baskin-Bey, E.; Heeringa, M.; Ouatas, T.; Enjo, K., In vitro and in vivo characterisation of ASP9521: a novel, selective, orally bioavailable inhibitor of 17 $\beta$ -hydroxysteroid dehydrogenase type 5 (17 $\beta$ HSD5; AKR1C3). *Invest. New Drugs* **2014**, *32*, 860-870.
250. Rizner, T. L.; Penning, T. M., Aldo-keto reductase 1C3-Assessment as a new target for the treatment of endometriosis. *Pharmacol. Res.* **2020**, *152*, 104446.
251. Verma, K.; Zang, T.; Gupta, N.; Penning, T. M.; Trippier, P. C., Selective AKR1C3 Inhibitors Potentiate Chemotherapeutic Activity in Multiple Acute Myeloid Leukemia (AML) Cell Lines. *ACS Med. Chem. Lett.* **2016**, *7*, 774-779.
252. Endo, S.; Hu, D.; Matsunaga, T.; Otsuji, Y.; El-Kabbani, O.; Kandeel, M.; Ikari, A.; Hara, A.; Kitade, Y.; Toyooka, N., Synthesis of non-prenyl analogues of baccharin as selective and potent inhibitors for aldo-keto reductase 1C3. *Bioorg. Med. Chem.* **2014**, *22*, 5220-5333.
253. Heck, R., Palladium-Catalyzed Vinylation of Organic Halides. *Org. React.* **1982**, *27*, 345-390.
254. Miyaura, N.; Yamada, K.; Suzuki, A., A new stereospecific cross-coupling by the palladium-catalyzed reaction of 1-alkenylboranes with 1-alkenyl or 1-alkynyl halides. *Tetrahedron Lett.* **1979**, *20*, 3437-3440.
255. Theodorou, V.; Skobridis, K.; Tzakosb, A. G.; Ragoussisc, V., A simple method for the alkaline hydrolysis of esters. *Tetrahedron Lett.* **2007**, *48*, 8230-8233.
256. Adeniji, A. O.; Twenter, B. M.; Byrns, M. C.; Jin, Y.; Chen, M.; Winkler, J. D.; Penning, T. M., Development of potent and selective inhibitors of aldo-keto reductase 1C3 (type 5 17 $\beta$ -hydroxysteroid dehydrogenase) based on N-phenyl-aminobenzoates and their structure-activity relationships. *J. Med. Chem.* **2012**, *55*, 2311-2323.
257. Chou, T. C., Drug combination studies and their synergy quantification using the Chou-Talalay method. *Cancer Res.* **2010**, *70*, 440-446.



258. Chou, T. C., Theoretical basis, experimental design, and computerized simulation of synergism and antagonism in drug combination studies. *Pharmacol. Rev.* **2006**, *58*, 621-681.
259. Zang, T.; Verma, K.; Chen, M.; Jin, Y.; Trippier, P. C.; Penning, T. M., Screening baccharin analogs as selective inhibitors against type 5 17beta-hydroxysteroid dehydrogenase (AKR1C3). *Chem. Biol. Interact.* **2015**, *234*, 339-348.
260. Jernberg, E.; Thysell, E.; Bovinder Ylitalo, E.; Rudolfsson, S.; Crnalic, S.; Widmark, A.; Bergh, A.; Wikstrom, P., Characterization of prostate cancer bone metastases according to expression levels of steroidogenic enzymes and androgen receptor splice variants. *PLoS One* **2013**, *8*, e77407.
261. Rathkopf, D. E.; Smith, M. R.; Ryan, C. J.; Berry, W. R.; Shore, N. D.; Liu, G.; Higano, C. S.; Alumkal, J. J.; Hauke, R.; Tutrone, R. F.; Saleh, M.; Chow Maneval, E.; Thomas, S.; Ricci, D. S.; Yu, M. K.; de Boer, C. J.; Trinh, A.; Kheoh, T.; Bandekar, R.; Scher, H. I.; Antonarakis, E. S., Androgen receptor mutations in patients with castration-resistant prostate cancer treated with apalutamide. *Ann. Oncol.* **2017**, *28*, 2264-2271.
262. Vilardo, E.; Rossmanith, W., The amyloid-beta-SDR5C1(ABAD) interaction does not mediate a specific inhibition of mitochondrial RNase P. *PLoS One* **2013**, *8*, e65609.
263. Carlson, E. A.; Marquez, R. T.; Du, F.; Wang, Y.; Xu, L.; Yan, S. S., Overexpression of 17beta-hydroxysteroid dehydrogenase type 10 increases pheochromocytoma cell growth and resistance to cell death. *BMC Cancer* **2015**, *15*, 166.
264. Rauschenberger, K.; Scholer, K.; Sass, J. O.; Sauer, S.; Djuric, Z.; Rumig, C.; Wolf, N. I.; Okun, J. G.; Kolker, S.; Schwarz, H.; Fischer, C.; Grziwa, B.; Runz, H.; Numann, A.; Shafqat, N.; Kavanagh, K. L.; Hammerling, G.; Wanders, R. J.; Shield, J. P.; Wendel, U.; Stern, D.; Nawroth, P.; Hoffmann, G. F.; Bartram, C. R.; Arnold, B.; Bierhaus, A.; Oppermann, U.; Steinbeisser, H.; Zschocke, J., A non-enzymatic function of 17beta-hydroxysteroid dehydrogenase type 10 is required for mitochondrial integrity and cell survival. *EMBO Mol. Med.* **2010**, *2*, 51-62.
265. Zschocke, J., HSD10 disease: clinical consequences of mutations in the HSD17B10 gene. *J. Inherit. Metab. Dis.* **2012**, *35*, 81-89.
266. Froyen, G.; Corbett, M.; Vandewalle, J.; Jarvela, I.; Lawrence, O.; Meldrum, C.; Bauters, M.; Govaerts, K.; Vandeleur, L.; Van Esch, H.; Chelly, J.; Sanlaville, D.; van Bokhoven, H.; Ropers, H. H.; Laumonnier, F.; Ranieri, E.; Schwartz, C. E.; Abidi, F.; Tarpey, P. S.; Futreal, P. A.; Whibley, A.; Raymond, F. L.; Stratton, M. R.; Fryns, J. P.; Scott, R.; Peippo, M.; Sipponen, M.; Partington, M.; Mowat, D.; Field, M.; Hackett, A.; Marynen, P.; Turner, G.; Gecz, J., Submicroscopic duplications of the hydroxysteroid dehydrogenase HSD17B10 and the E3 ubiquitin ligase HUWE1 are associated with mental retardation. *Am. J. Hum. Genet.* **2008**, *82*, 432-443.
267. Deutschmann, A. J.; Amberger, A.; Zavadil, C.; Steinbeisser, H.; Mayr, J. A.; Feichtinger, R. G.; Oerum, S.; Yue, W. W.; Zschocke, J., Mutation or knock-down of 17beta-hydroxysteroid dehydrogenase type 10 cause loss of MRPP1 and impaired processing of mitochondrial heavy strand transcripts. *Hum. Mol. Genet.* **2014**, *23*, 3618-3628.

268. Yan, S. D.; Stern, D. M., Mitochondrial dysfunction and Alzheimer's disease: role of amyloid-beta peptide alcohol dehydrogenase (ABAD). *Int. J. Exp. Pathol.* **2005**, *86*, 161-171.
269. Kristofikova, Z.; Bockova, M.; Hegnerova, K.; Bartos, A.; Klaschka, J.; Ricny, J.; Ripova, D.; Homola, J., Enhanced levels of mitochondrial enzyme 17beta-hydroxysteroid dehydrogenase type 10 in patients with Alzheimer disease and multiple sclerosis. *Mol. Biosyst.* **2009**, *5* (10), 1174-1179.
270. Yang, S. Y.; He, X. Y.; Isaacs, C.; Dobkin, C.; Miller, D.; Philipp, M., Roles of 17beta-hydroxysteroid dehydrogenase type 10 in neurodegenerative disorders. *J. Steroid Biochem. Mol. Biol.* **2014**, *143*, 460-472.
271. Kruman, II; Mattson, M. P., Pivotal role of mitochondrial calcium uptake in neural cell apoptosis and necrosis. *J. Neurochem.* **1999**, *72*, 529-540.
272. He, X. Y.; Yang, S. Y., Roles of type 10 17beta-hydroxysteroid dehydrogenase in intracrinology and metabolism of isoleucine and fatty acids. *Endocr. Metab. Immune Disord. Drug Targets* **2006**, *6*, 95-102.
273. Yang, S. Y.; He, X. Y.; Miller, D., Hydroxysteroid (17beta) dehydrogenase X in human health and disease. *Mol. Cell Endocrinol.* **2011**, *343*, 1-6.
274. Boutin, S.; Roy, J.; Maltais, R.; Alata, W.; Calon, F.; Poirier, D., Identification of steroidal derivatives inhibiting the transformations of allopregnanolone and estradiol by 17 $\beta$ -hydroxysteroid dehydrogenase type 10. *Bioorg. Med. Chem. Lett.* **2018**, *28*, 3554-3559.
275. Valasani, K. R.; Sun, Q.; Hu, G.; Li, J.; Du, F.; Guo, Y.; Carlson, E. A.; Gan, X.; Yan, S. S., Identification of human ABAD inhibitors for rescuing A $\beta$ -mediated mitochondrial dysfunction. *Curr. Alzheimer Res.* **2014**, *11* (2), 128-136.
276. Schmidt, M.; Benek, O.; Vinklarova, L.; Hrabanova, M.; Zemanova, L.; Chribek, M.; Kralova, V.; Hroch, L.; Dolezal, R.; Lycka, A.; Prchal, L.; Jun, D.; Aitken, L.; Gunn-Moore, F.; Kuca, K.; Musilek, K., Benzothiazolyl Ureas are Low Micromolar and Uncompetitive Inhibitors of 17beta-HSD10 with Implications to Alzheimer's Disease Treatment. *Int. J. Mol. Sci.* **2020**, *21* (6).
277. Marques, A. T.; Antunes, A.; Fernandes, P. A.; Ramos, M. J., Computational optimization of AG18051 inhibitor for amyloid- $\beta$  binding alcohol dehydrogenase enzyme. *Int. J. Quantum Chem.* **2008**, *108* (11), 1982-1991.
278. Valasani, K. R.; Hu, G.; Chaney, M. O.; Yan, S. S., Structure-based design and synthesis of benzothiazole phosphonate analogues with inhibitors of human ABAD-A $\beta$  for treatment of alzheimer's disease. *Chem. Biol. Drug Des.* **2013**, *81* (2), 238-249.
279. Trippier, P. C., Selecting good 'drug-like' properties to optimize small molecule blood-brain barrier penetration. *Curr Med Chem* **2016**, *23*, 1392-1407.
280. Zhang, H. Y., New insights into huperzine A for the treatment of Alzheimer's disease. *Acta. Pharmacol. Sin.* **2012**, *33* (9), 1170-1175.
281. Xiao, X.; Chen, Q.; Zhu, X.; Wang, Y., ABAD/17beta-HSD10 reduction contributes to the protective mechanism of huperzine a on the cerebral mitochondrial function in APP/PS1 mice. *Neurobiol. Aging* **2019**, *81*, 77-87.

282. Jimonet, P.; Audiau, F.; Barreau, M.; Blanchard, J. C.; Boireau, A.; Bour, Y.; Coleno, M. A.; Doble, A.; Doerflinger, G.; Huu, C. D.; Donat, M. H.; Duchesne, J. M.; Ganil, P.; Gueremy, C.; Honor, E.; Just, B.; Kerphirique, R.; Gontier, S.; Hubert, P.; Laduron, P. M.; Le Blevec, J.; Meunier, M.; Miquet, J. M.; Nemecek, C.; Mignani, S., Riluzole series. Synthesis and in vivo "antiglutamate" activity of 6-substituted-2-benzothiazolamines and 3-substituted-2-imino-benzothiazolines. *J. Med. Chem.* **1999**, *42*, 2828-2843.
283. Aitken, L.; Baillie, G.; Pannifer, A.; Morrison, A.; Jones, P. S.; Smith, T. K.; McElroy, S. P.; Gunn-Moore, F. J., In vitro assay development and HTS of small-molecule human ABAD/17beta-HSD10 inhibitors as therapeutics in Alzheimer's disease. *SLAS Discov.* **2017**, *22*, 676-685.
284. Kovalevich, J.; Langford, D., Considerations for the use of SH-SY5Y neuroblastoma cells in neurobiology. *Methods Mol. Biol.* **2013**, *1078*, 9-21.
285. Takahashi, R. H.; Almeida, C. G.; Kearney, P. F.; Yu, F.; Lin, M. T.; Milner, T. A.; Gouras, G. K., Oligomerization of Alzheimer's beta-amyloid within processes and synapses of cultured neurons and brain. *J. Neurosci.* **2004**, *24*, 3592-3599.
286. Xie, H.; Zeng, L.; Zeng, S.; Lu, X.; Zhang, G.; Zhao, X.; Cheng, N.; Tu, Z.; Li, Z.; Xu, H.; Yang, L.; Zhang, X.; Huang, M.; Zhao, J.; Hu, W., Novel pyrrolopyrimidine analogues as potent dipeptidyl peptidase IV inhibitors based on pharmacokinetic property-driven optimization. *Eur. J. Med. Chem.* **2012**, *52*, 205-212.
287. Sajiki, H., Development of a novel type of Pd/C-catalyzed chemoselective hydrogenation using a nitrogen catalyst poison. *Yakugaku Zasshi* **2000**, *120*, 1091-1103.
288. Viswanadham, B.; Mahomed, A. S.; Friedrich, H. B.; Singh, S., Efficient and expeditious chemoselective BOC protection of amines in catalyst and solvent-free media. *Res. Chem. Intermed.* **2016**, *43*, 1355-1363.
289. Pavan Kumar, G.; Rambabu, D.; Basaveswara Rao, M. V.; Pal, M., Iodine-mediated neutral and selective *N*-Boc deprotection. *J. Chem.* **2013**, *2013*, 916960.
290. Chankeshwara, S. V.; Chakraborti, A. K., Catalyst-free chemoselective *N*-tert-butyloxycarbonylation of amines in water. *Org. Lett.* **2006**, *8*, 3259-3262.
291. Dunetz, J. R.; Magano, J.; Weisenburger, G. A., Large-scale applications of amide coupling reagents for the synthesis of pharmaceuticals. *Org. Process Res. Dev.* **2016**, *20*, 140-177.
292. Hroch, L.; Benek, O.; Guest, P.; Aitken, L.; Soukup, O.; Janockova, J.; Musil, K.; Dohnal, V.; Dolezal, R.; Kuca, K.; Smith, T. K.; Gunn-Moore, F.; Musilek, K., Design, synthesis and in vitro evaluation of benzothiazole-based ureas as potential ABAD/17β-HSD10 modulators for alzheimer's disease treatment. *Bioorg. Med. Chem. Lett.* **2016**, *26* (15), 3675-3678.
293. Wager, T. T.; Hou, X.; Verhoest, P. R.; Villalobos, A., Moving beyond rules: the development of a central nervous system multiparameter optimization (CNS MPO) approach to enable alignment of druglike properties. *ACS Chem. Neurosci.* **2010**, *1*, 435-449.

294. Wager, T. T.; Hou, X.; Verhoest, P. R.; Villalobos, A., Central nervous system multiparameter optimization desirability: application in drug discovery. *ACS Chem. Neurosci.* **2016**, *7*, 767-775.
295. Gupta, M.; Lee, H. J.; Barden, C. J.; Weaver, D. F., The blood-brain barrier (BBB) score. *J. Med. Chem.* **2019**, *62*, 9824-9836.
296. Ghose, A. K.; Ott, G. R.; Hudkins, R. L., Technically extended multiparameter optimization (TEMPO): an advanced robust scoring scheme to calculate central nervous system druggability and monitor lead optimization. *ACS Chem. Neurosci.* **2017**, *8*, 147-154.
297. Patel, N. C., Methods to optimize CNS exposure of drug candidates. *Bioorg. Med. Chem. Lett.* **2020**, *30*, 127503.
298. Rhein, V.; Baysang, G.; Rao, S.; Meier, F.; Bonert, A.; Muller-Spahn, F.; Eckert, A., Amyloid-beta leads to impaired cellular respiration, energy production and mitochondrial electron chain complex activities in human neuroblastoma cells. *Cell Mol. Neurobiol.* **2009**, *29*, 1063-1071.
299. Gray, N. E.; Sampath, H.; Zweig, J. A.; Quinn, J. F.; Soumyanath, A., Centella asiatica attenuates amyloid-beta-induced oxidative stress and mitochondrial dysfunction. *J. Alzheimers Dis.* **2015**, *45*, 933-946.
300. Kuhla, B.; Loske, C.; Garcia De Arriba, S.; Schinzel, R.; Huber, J.; Munch, G., Differential effects of "Advanced glycation endproducts" and beta-amyloid peptide on glucose utilization and ATP levels in the neuronal cell line SH-SY5Y. *J. Neural Transm. (Vienna)* **2004**, *111*, 427-439.
301. Ye, X.; Tai, W.; Bao, X.; Chen, X.; Zhang, D., FLZ inhibited gamma-secretase selectively and decreased Abeta mitochondrial production in APP-SH-SY5Y cells. *Naunyn Schmiedeberg Arch. Pharmacol.* **2014**, *387* (1), 75-85.